Circumferentially adhesive bonded glass panes for bracing steel frames in facades

Please check the document version of this publication:

Circumferentially Adhesive Bonded Glass Panes for Bracing Steel Frames in Façades

Edwin M.P. Huveners

Circumferentially Adhesive Bonded Glass Panes for Bracing Steel Frames in Façades

PROEFSCHRIFT

ter verkrijging van de graad van doctor aan de
Technische Universiteit Eindhoven, op gezag van de
rector magnificus, prof.dr.ir. C.J. van Duijn, voor een
commissie aangewezen door het College voor
Promoties in het openbaar te verdedigen
op donderdag 3 december 2009 om 16.00 uur

door

Edwin Michel Pierre Huveners

geboren te Maastricht

Acknowledgements

Circumferentially Adhesive Bonded Glass Panes for Bracing Steel Frames in Façades

Summary

Contemporary architecture desires large glass surfaces in the building envelop with a minimum of non transparent members such as steel braces needed for the stability of a building. Glass panes have the capacity to resist in-plane loads and can replace the steel braces of a one-storey building. The vertical stability system of a building is a primary structural component and has to comply with strength (safety) and building stiffness (serviceability). A circumferentially adhesive bonded joint is a suitable connection to introduce in-plane loads into the glass pane. For the research three joint types have been defined. Joint type 1 is a flexible adhesive bonded joint (polyurethane) across the full thickness of the glass pane. Joint type 2 is a two-sided stiff adhesive bonded joint (epoxy) along the edges of the glass pane. Joint type 3 is a one-sided stiff adhesive bonded joint (epoxy) along the edges of the glass pane. The steel frame, the single annealed glass pane and one of the three joint types form the system which is only subjected to a horizontally concentrated in-plane load at the top of the system. The objective of the research is to get more insight in the structural behaviour of these systems and to set-up mechanical models and possibly design rules. The research methodology consisted of experiments, finite element simulations and parametric studies.

The experiments were carried out with square glass pane sizes of 1.0 m with nominal glass pane thickness of 12 mm. Systems with joint type 1 had a very small in-plane stiffness of the system, a glass-steel contact at large horizontal in-plane displacements at the top of the system and a good residual capacity, namely large horizontal in-plane displacements at the top of the system with increasing horizontal in-plane load. Systems with joint type 2 had much larger in-plane stiffness of the system than systems with joint type 1. The residual capacity was very good, because the horizontal in-plane load kept increasing after the first and following glass cracks. Systems with joint type 3 had slightly smaller in-plane stiffness of the system than systems with joint type 2. The residual capacity after the first glass breakage was very poor.

One finite element model for systems with joint types 1 to 3 was developed and calibrated with experiments. The results of the finite element simulations matched well with the results of experiments till the onset of the first crack in the glass pane or till the glass-steel contact for systems with joint type 1.

The parametric studies only focused on the variation of the thickness, the width and the height of the glass pane. For systems with joint type 1, the in-plane stiffness of the system depends on the width-height ratio of the glass pane and the stiffness of the adhesive bonded joint. Systems with the rectangular glass panes have two glass-steel contacts at increasing horizontal in-plane displacements at the top of the system. Besides the stiffness criterion for vertical stability systems of buildings the normal strain rate and the shear strain rate can also be a criterion. For systems with joint type 2 and 3, the in-plane stiffness of the system is determined by the width-height ratio and the thickness of the glass pane. The maximum principle (tension) stress in the glass pane rapidly increases at the vicinity of the corners in which the 'tension diagonal' is

anchored, caused by the difference in in-plane displacements between the stiff adhesive bonded joint and the bolted connection between the outside beam and the beadwork of the steel frame. Moreover, for systems with joint type 3, the eccentric load transfer between the steel frame and the glass pane results in bending of the glass pane.

The mechanical models for systems with joint type 1 well predict the in-plane stiffness of the system, the largest maximum principle (tension) stress in the glass pane and the maximum normal and shear stresses in the adhesive bonded joint. The criteria were the limitation of the horizontal in-plane displacement at the top of the system or the limitation of the strain rates of the adhesive bonded joint. For the residual capacity, the mechanical models also predict well the horizontal in-plane load and the horizontal in-plane displacement at the top of the system at the first glass-steel contact. For systems with joint type 2 and 3, no mechanical models were developed, because the very stiff adhesive bonded joint and the very small in-plane displacements of the bolted connection between the outside beam and the beadwork of the steel frame resulted in a complex stress distribution along the edges of the glass pane as well as in the adhesive bonded joint. A range of several shear stiffnesses of the adhesive bonded joint has been presented which has a positive influence on the distribution of the principle stresses in the glass pane as well as the normal stresses and shear stresses in the adhesive bonded joint without losing of the in-plane stiffness of the system.

Glass panes as bracing elements in steel frames have a great potential. For systems with joint type 1, all glass panes have to be structurally bonded to the steel frame of the façade to guarantee the stability of the building because of the small in-plane stiffness. The residual capacity is good, because the horizontal in-plane load increases at overloading. Furthermore, the large horizontal in-plane displacements of the building visually warn for overloading. For systems with joint types 2 and 3, few bays in the façade are sufficient to guarantee the stability of the building by the larger in-plane stiffness. However, systems with joint type 2 produced the best results for a transparent vertical stability system for buildings because of the residual capacity at overloading. The applied epoxy adhesive behaved too stiff and therefore, it is recommended a range of several shear stiffnesses for the adhesive bonded joint for systems with joint type 2 which more favourably loads the glass pane as well as the adhesive bonded joint without a reduction of the in-plane stiffness of the system.

Samenvatting

De hedendaagse architectuur vraagt om grote glazen oppervlakten in de gevels van gebouwen met zo min mogelijk niet transparante onderdelen zoals stalen schoren die nodig zijn voor het stabiliseren van een gebouw. Glazen platen hebben de capaciteit om weerstand te bieden tegen vlakbelastingen en kunnen de stalen schoren vervangen van een eenlaagsgebouw. De verticale stabiliteitsvoorziening van een gebouw is een primair constructieonderdeel en moet voldoen aan sterkte (veiligheid) en aan stijfheid (bruikbaarheid). Een lijmnaad langs alle randen van de glazen plaat is een geschikte verbindingsmethode om vlakbelastingen in te leiden in de glazen plaat. Voor het onderzoek zijn drie lijmnaadtypen gedefinieerd. Lijmnaadtype 1 is een flexibele lijmnaad (polyurethaan) over de volledige dikte van de glazen plaat. Lijmnaadtype 2 is een tweezijdige stijve lijmnaad (epoxy) langs de randen van de glazen plaat. Lijmnaadtype 3 is een enkelzijdige lijmnaad (epoxy) langs de randen van de glazen plaat. Het stalen raamwerk, de ongeharde enkele glazen plaat en een van de drie lijmnaadtypen vormen het systeem dat alleen belast wordt door een geconcentreerde horizontale belasting in het vlak aan de bovenkant van het stalen raamwerk. De doelstelling van het onderzoek is om meer inzicht te krijgen in het constructieve gedrag van deze systemen en het opstellen van mechanicamodellen en mogelijk ontwerpregels. De onderzoeksmethodologie bestond uit experimenten, eindige elementensimulaties en een parameterstudie.

De experimenten werden uitgevoerd op systemen met vierkante glazen platen van 1,0 m en met een nominale glasdikte van 12 mm. Systemen met lijmnaadtype 1 hadden een zeer kleine in het vlakstijfheid van het systeem, een glas-staal contact bij grotere horizontale in het vlakverplaatsingen aan de bovenkant van het systeem en een goede restcapaciteit, namelijk grote horizontale in het vlakverplaatsingen aan de bovenkant van het systeem met toenemende horizontale in het vlakbelasting. Systemen met lijmnaadtype 2 hadden een veel hogere in het vlakstijfheid van het systeem dan systemen met lijmnaadtype 1. De restcapaciteit was zeer goed, omdat de horizontale in het vlakbelasting bleef toenemen na de eerste en daarop volgende scheuren in de glazen plaat. Systemen met lijmnaadtype 3 hadden een iets kleinere in het vlakstijfheid van het systeem dan systemen met lijmnaadtype 2. De restcapaciteit na de eerste scheur in de glazen plaat was nihil.

Een eindig elementenmodel voor systemen met lijmnaadtype 1 tot en met 3 werd ontwikkeld en gekalibreerd met experimenten. De resultaten van de eindige elementensimulaties kwamen goed overeen met de resultaten van experimenten tot de eerste scheur in de glazen plaat of tot het glas-staal contact voor systemen met lijmnaadtype 1.

De parameterstudie concentreerde zich op het variëren van de nominale dikte, de breedte en de hoogte van de glazen plaat. Voor systemen met lijmnaadtype 1, de in het vlakstijfheid van het systeem wordt bepaald door de breedte-hoogte verhouding van de glazen plaat en de stijfheid van de lijmnaad. Systemen met rechthoekige glazen platen hebben twee glas-staal contacten bij toenemende horizontale in het vlakverplaatsingen aan de bovenkant van het systeem. Naast het stijfheidcriterium voor de verticale stabiliteitsvoorzieningen van gebouwen kunnen de normaal- en schuifrekken in de lijmnaad ook maatgevend zijn.

Voor systemen met lijmnaadtype 2 en 3 wordt de in het vlakstijfheid van het systeem bepaald door de breedte-hoogte verhouding en de dikte van de glazen plaat. Maatgevend zijn de snel toenemende hoofdtrekspanningen in de glazen plaat die zich bevinden aan de uiteinde van de "trekdiagonaal". Dit wordt veroorzaakt door het verschil in in het vlakverplaatsingen tussen de stijve lijmnaad en de niet schuifvaste boutverbinding tussen de buitenste balk en het lijstwerk van het stalen raamwerk. Bovendien geldt voor systemen met lijmnaadtype 3 dat de excentrische belastingsoverdracht tussen het stalen raamwerk en de glazen plaat leidt tot een buigend moment in de glazen plaat.

De mechanicamodellen voor systemen met lijmnaadtype 1 voorspellen goed de in het vlakstijfheid van het systeem, de grootste hoofd(trek)spanning in de glazen plaat en de grootste normaal- en schuifspanningen in de lijmnaad. De criteria waren het limiteren van de horizontale in het vlakverplaatsing aan de bovenkant van het systeem of het limiteren van de rekken van de lijmnaad. Voor de restcapaciteit voorspellen de mechanicamodellen goed de horizontale in het vlakverplaatsing aan de bovenkant van het systeem en de horizontale in het vlakbelasting bij het eerste glas-staal contact. Voor systemen met lijmnaadtype 2 en 3 zijn er geen mechanicamodellen ontwikkeld, omdat de zeer stijve lijmnaad en de niet schuifvaste boutverbinding tussen de buitenste balk en het lijstwerk leiden tot een complexe spanningsverdeling zowel langs de randen van de glazen plaat als in de lijmnaad van het stalen raamwerk. Een range van verschillende schuifstijfheden van de lijmnaad wordt aangedragen welke een positieve invloed heeft op de verdeling van zowel de hoofdspanningen in de glazen plaat als de normaal- en schuifspanningen in de lijmnaad zonder dat het ten koste gaat van de in het vlakstijfheid van het systeem.

Glazen platen als schorend element in stalen raamwerken zijn mogelijk. Voor systemen met lijmnaadtype 1, moeten alle glazen platen in de façade constructief worden verbonden aan het stalen raamwerk om de stabiliteit van het gebouw te garanderen vanwege de geringe in het vlak stijfheid. De restcapaciteit is goed vanwege de toenemende horizontale in het vlakbelasting bij overbelasting. De zichtbare grote horizontale in het vlakverplaatsingen van het gebouw waarschuwen tijdig voor overbelasting. Voor systemen met lijmnaadtype 2 en 3, zijn enkele rijen in de façade voldoende om de stabiliteit van het gebouw te garanderen vanwege de hoge in het vlakstijfheid. Echter, systemen met lijmnaadtype 2 in dit onderzoek geven de beste resultaten als transparante stabiliteitvoorziening voor gebouwen, vanwege de zeer goede restcapaciteit bij overbelasting. De toegepaste epoxylijm gedraagt zich echter te stijf en daarom wordt er aanbevolen een range met verschillende schuifstijfheden van de lijmnaad voor systemen met lijmnaadtype 2 die zowel de glazen plaat als de lijmnaad gunstiger belasten met behoud van de in het vlakstijfheid.

Notations and abbreviations

Abbreviations

LBC read Left Bottom Corner
LTC read Left Top Corner
RBC read Right Bottom Corner
RTC read Right Top Corner

Notations

Latin capital letters

E_a Young's modulus of adhesive [N/mm²]
E_g Young's modulus of glass [N/mm²]
E_s Young's modulus of steel [N/mm²]
$F_{h;crit}$ critical plate buckling load at the RTC of the system [kN] (see figure 5.4)
F_h horizontal in-plane load at the RTC of the system [kN] (see figure 1.13)
$F_{h;1}$ horizontal in-plane load at the RTC of the system at first glass-steel contact for systems with joint type 1 [kN] (see figure 5.2)
$F_{h;2}$ horizontal in-plane load at the RTC of the system at second glass-steel contact for systems with joint type 1 [kN] (see figure 5.2)
$F_{h;lim}$ horizontal in-plane load at limited horizontal in-plane displacement at the RTC of the system for systems with joint type 1 [kN] (see figure 3.8)
G_a shear modulus of adhesive [N/mm²]
K_{1-4} discrete normal springs 1 to 4 in y-direction [kN/mm] (see figure 6.4)
K_{7-10} discrete normal springs 7 to 10 in x-direction [kN/mm](se figure 6.4)
K_{5-6} discrete shear springs 5 and 6 in y-direction [kN/mm] (see figure 6.4)
K_{11-12} discrete shear springs 11 and 12 in x-direction [kN/mm] (see figure 6.4)
K_s horizontal in-plane stiffness of the system [kN/mm] (see figure 1.13)
$K_{s;lim}$ horizontal in-plane stiffness of the system at limited horizontal in-plane displacement for systems with joint type 1 [kN/mm]
$K_{y;RBC}$ vertical normal stiffness at the RBC of the system [kN/mm] (see figure 4.1)
K_φ in-plane rotation stiffness [kN/rad] (see equation 6.11)
$K_{\varphi;1}$ in-plane rotation stiffness at first glass-steel contact [kN/rad] (see equation 6.23)

Latin lower case letters

$f_{g;k}$ characteristic value for the ultimate flexural tension strength of annealed float glass [N/mm²]
$f_{mt;u;rep}$ representative value for the ultimate flexural tension strength of glass [N/mm²]
h_{gr} groove height [mm] (see figure 3.2)
h_g glass pane height [mm]
h_s system height [mm] (see figure 3.2)
$k_{j;\xi}$ continuous normal stiffness of the adhesive bonded joint [N/mm³] (see figure 4.8)

$k_{j;\eta}$	continuous shear stiffness of the adhesive bonded joint in longitudinal direction [N/mm³] (see figure 4.8)
$k_{j;\zeta}$	continuous shear stiffness of the adhesive bonded joint in transversal direction [N/mm³] (see figure 4.8)
$k_{b;\xi}$	simulated continuous normal stiffness of the bolted connection between the outside beam and the beadwork [N/mm³] (see figure 4.8)
$k_{b;\eta}$	simulated continuous shear stiffness of the bolted connection between the outside beam and the beadwork [N/mm³] (see figure 4.8)
$k_{T;\xi}$	simulated continuous normal stiffness of the lateral support (Teflon) between the glass pane and the beadwork for systems with joint type 1 [N/mm³] (see figure 4.8)
$k_{T;\eta}$	simulated continuous shear stiffness in longitudinal direction of the lateral support (Teflon) between the glass pane and the beadwork for systems with joint type 1 [N/mm³] (see figure 4.8)
$k_{T;\zeta}$	simulated continuous shear stiffness in transversal direction of the lateral support (Teflon) between the glass pane and the beadwork for systems with joint type 1 [N/mm³] (see figure 4.8)
l_{gr}	groove length [mm]
l_j	joint length [mm] (see figure 4.8)
t_f	thickness of the steel frame [mm] (see figure 6.3)
t_g	glass thickness [mm]
$t_{g;n}$	nominal glass thickness [mm]
t_j	joint thickness [mm] (see figure 4.8)
u_{RTC}	horizontal in-plane displacement at the RTC of the system [mm] (see figure 1.13)
$u_{RTC;s}$	actually horizontal in-plane displacement at the RTC of the system [mm] (see section 3.5.1)
$u_{RTC;1}$	horizontal in-plane displacement at the RTC of the system at first glass-steel contact for systems with joint type 1 [mm] (see figure 5.2)
$u_{RTC;2}$	horizontal in-plane displacement at the RTC of the system at second glass-steel contact for systems with joint type 1 [mm] (see figure 5.2)
$u_{RTC;lim}$	limited horizontal in-plane displacement at the RTC of the system for systems with joint type 1 [mm] (see figure 3.8)
$u_{j;\xi;rel}$	relative horizontal in-plane displacement in normal direction of the adhesive bonded joint [mm] (see figures 5.8 and 5.13)
$u_{j;\eta;rel}$	relative horizontal in-plane displacement in longitudinal direction of the adhesive bonded joint [mm] (see figures 5.8 and 5.13)
$u_{j;\zeta;rel}$	relative horizontal in-plane displacement in transversal direction of the adhesive bonded joint [mm] (see figure 5.13)
v	velocity of the displacement control [mm/min]
$v_{j;\xi;rel}$	relative vertical in-plane displacement in normal direction of the adhesive bonded joint [mm] (see figures 5.8 and 5.13)
$v_{j;\eta;rel}$	relative vertical in-plane displacement in longitudinal direction of the adhesive bonded joint [mm] (see figures 5.8 and 5.13)
$v_{j;\zeta;rel}$	relative vertical in-plane displacement in transversal direction of the adhesive bonded joint [mm] (see figure 5.13)
w_{centre}	out-of-plane displacement at the centre of the glass pane [mm]
w_g	glass pane width [mm]
w_{gr}	groove width [mm] (see figure 3.2)
w_j	joint width [mm] (see figure 4.8)
$w_{j;\xi;rel}$	relative horizontal out-of-plane displacement in normal direction of the adhesive

| | bonded joint [mm] (see figure 5.13) |
| w_s | system width [mm] (see figure 3.2) |

Greek lower case letters

β	ratio between the horizontal in-plane displacement at the RTC of the system and the system height [-] (see figure 6.3)
φ	in-plane rotation of the glass pane [-] (see figure 6.3)
θ	angle between the horizontal axis and the direction of the maximum principle stress [°]
$\varepsilon_{0°}$	horizontally measured strain [-](see figure 3.7)
$\varepsilon_{45°}$	measured strain at an angle of 45° [-](see figure 3.7)
$\varepsilon_{90°}$	vertically measured strain [-](see figure 3.7)
ν_a	Poisson's ratio of adhesive [-]
ν_g	Poisson's ratio of glass [-]
$\sigma_{g;1}$	maximum principle stress in the glass pane [N/mm²]
$\sigma_{g;2}$	minimum principle stress in the glass pane [N/mm²]
$\sigma_{j;x;x}$	normal stress in the adhesive bonded joint in x-axis [N/mm²] (see figure 5.8)
$\sigma_{j;x;y}$	normal stress in the adhesive bonded joint in y-axis [N/mm²] (see figure 5.8)
$\sigma_{j;x;z}$	normal stress in the adhesive bonded joint in z-axis [N/mm²] (see figure 5.13)
$\tau_{j;\eta;x}$	shear stress in longitudinal direction of the adhesive bonded joint in x-axis [N/mm²] (see figures 4.8 and 5.13)
$\tau_{j;\eta;y}$	shear stress in longitudinal direction of the adhesive bonded joint in y-axis [N/mm²] (see figures 4.8 and 5.13)
$\tau_{j;\varsigma;x}$	shear stress in transversal direction of the adhesive bonded joint in x-axis [N/mm²] (see figure 5.13)
$\tau_{j;\varsigma;y}$	shear stress in transversal direction of the adhesive bonded joint in y-axis [N/mm²] (see figure 5.13)

x

Contents

1 Introduction

This chapter introduces the topic of this thesis: the use of the in-plane capacity of circumferentially adhesive bonded rectangular glass panes for bracing steel frames in façades. Section 1.1 discusses the development of the material glass as building material. Section 1.2 classifies the structural elements of a building. Section 1.3 explains the terms out-of-plane loaded and in-plane loaded structures and the accompanying connections. The problem definition and objective of this research is described in section 1.4. Finally, the methodology and the outline of this thesis are given in section 1.5.

1.1   Glass as building material

Glass made by nature or artificially, has been known by human for several millennia. Glass as building material entered upon the Romans [Hess 2004]. They were able to manufacture flat sheets of found glass of about one square metre which was applied as infill element in window frames. After the fall of the Roman Empire, much knowledge was lost, including the manufacturing process of flat glass. The manufacturing of flat glass restarted during the Renaissance. To increase the optical quality of found glass, the glass sheet was polished and mirror glass was introduced. This process was expensive.

In the 19th century, the advent of the industrialization also influenced the production of flat glass. The former green house Crystal Palace was a product of the industrialization and was presented at the World Fair in London in 1851. The building was built up of repeated cast-iron members and small glass sheets in the building envelope (80,000 square metres). Glass sheets became standard mass products with acceptable quality. Drawn sheet glass made its appearance in Belgium and the USA in 1913 [Hess 2004]. The molten glass was drawn vertically through rollers and was gradually cooled down. The production was a continuous process resulting in glass panes with a width of 2.3 m and a variety of thicknesses. The drawing process was world-wide the common manufacturing method for flat glass till 1959. In that year, Pilkington introduced a completely new manufacturing process for producing glass panes with exceptional good quality: float glass. This process rapidly replaced almost all other flat glass techniques world-wide. Float glass is today's glass used in buildings, transportation industry and other branches. The main application of a glass pane is as transparent infill element at tertiary structural level (section 1.2) in the building envelope which is predominately loaded by out-of-plane loads (section 1.3.2). However, glass panes also have the capacity to resist in-plane loads (section 1.3.3) and can take over the structural function of steel braces in a steel frame for the stabilization of one-storey buildings. In the case, the glass pane belongs to the primary structural level (section 1.2).

1.2 Classification of structural elements of buildings

Structural elements in buildings can be classified according to their importance as load bearing element. In this thesis, three structural levels are distinguished, namely the primary, secondary and tertiary structural level (figure 1.1). The primary structural level has to comply with safety (strength and stability) and serviceability (limited displacements) of the entire or part of the building. The secondary and tertiary structural levels only have to comply with the strength and the limited displacement at element level.
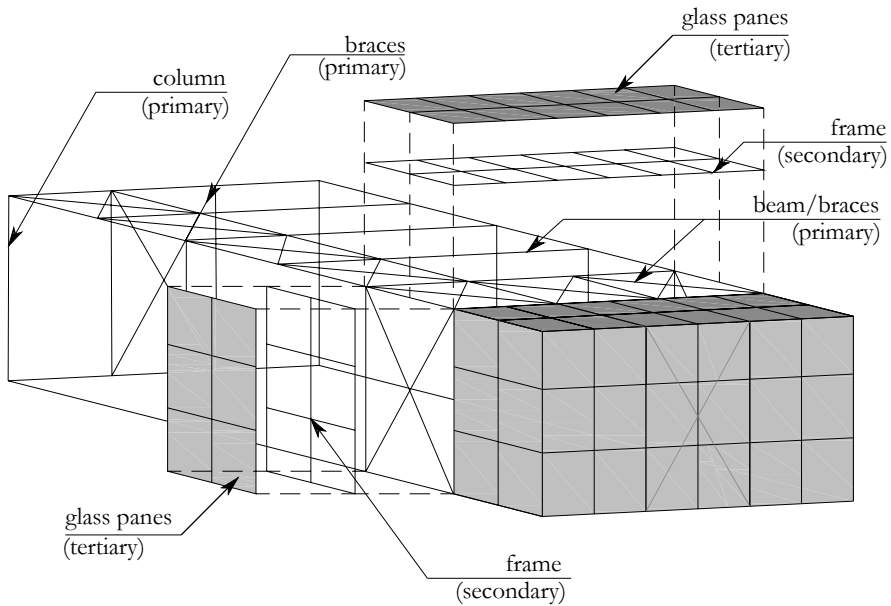
Figure 1.1:   Classification of the importance of the structural elements in buildings

Structural elements belonging to the primary structural level support and stabilize the building. Primary structural elements are e.g. columns, bearing walls, rigid frames, vertically and horizontally braced frames, and shear walls. Failure of one of these elements may lead to collapsing of the entire building. The structural elements belonging to the secondary structural level support a part of the building e.g. the framework of the façade and transfer the loads to the primary structure. Failure of the secondary structure does not lead to collapsing of the entire building, but only locally. Structural elements belonging to the tertiary structural level are e.g. façade claddings such as glass panes. Failure of the tertiary structure is restricted to element level without consequences for the building.

1.3   Loads on glass panes

1.3.1   Load definition

Figure 1.2 shows a vertically installed glass pane in an orthogonal co-ordinate system at element level used in the thesis. The glass pane width (w_g) and height (h_g) form the xy-plane and the glass thickness (t_g) is directed in z-direction. The glass pane width and height are always larger than the glass thickness. The direction of the mechanical loads on the glass pane can be defined with respect to the co-ordinate system. The out-of-plane loads (p_z) act perpendicularly to the xy-plane and the in-plane loads (q_x, q_y, q_{xy}, q_{yx}) act in the xy-plane.
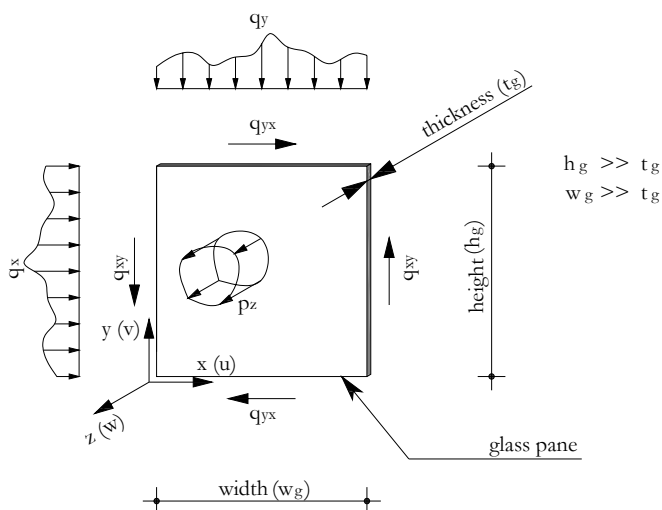
Figure 1.2:   Definition of loads on vertically installed glass pane

1.3.2   Out-of-plane loads

The main application of a glass pane is as transparent infill element in the building envelope such as in windows, curtain walls, structural sealant glazing (section 2.4.2) and double skin façades and belongs to the tertiary structural level (section 1.2). The design of a glass pane starts with the proper choice of the glass type which determines the desirable crack pattern regulated by the European standard EN 12600 [EN 12600 2003] or the Dutch standard NEN 3569 [NEN 3569 2001]. These standards also deal with laminated glass panes. Glass panes under an angle with the horizontal plane between 0° and 80° have to be laminated for safety reasons, because after failure of a glass pane the interlayer keeps the glass shards together to protect people from injury by falling glass. The glass pane is only subjected to out-of-plane loads such as dead weight, wind load, snow load and cavity pressure in case of insulated double glass units. The out-of-plane loads are established in structural standards and completed with glass standards (section 2.4). The usability of the glass standards is restricted to the common application of glass panes in the building envelope, namely as an infill element at tertiary level,

e.g. as shown in figures 1.3 and 1.4. The glass pane can move freely (within certain limits) in-plane and therefore it can not transfer in-plane loads to the surrounding structure.

Figure 1.3: Glass panes as tertiary structural elements in a roof structure (King Fischer BCC, Amsterdam, The Netherlands)

Figure 1.4: Glass panes as tertiary structural elements in a façade structure (assurance company Atradius, Amsterdam, The Netherlands)

1.3.3 In-plane loads

The previous section described the out-of-plane loads acting on glass panes. Actually, the glass pane is loaded by the out-of-plane component of the acting load. The in-plane component of the acting load is neglected such as the dead weight of vertically installed glass panes and the in-plane component of non-vertically installed glass panes. These in-plane loads are carried by two setting blocks placed between the bottom edge of the glass pane and the bottom transom (figure 1.11). A plate with small thickness in comparison to its size and subjected to an out-of-

plane load has large out-of-plane displacements. This results in in-plane compression stresses along the perimeter and in-plane tension stresses in the diagonals of the glass pane, the so-called membrane stresses [Vallabhan 1983, Szilard 2004]. Membrane stresses, as a result of large out-of-plane displacements of the glass pane, have favourable influences on the stress distribution by bending, because the portion of bending stresses gets smaller [Hess 2004]. However, in-plane loaded glass pane is consciously loaded in-plane to contribute as a structural element. These glass panes need another approach than the out-of-plane loaded glass panes and they belong rather to the secondary or primary structural level than the tertiary structural level. They can withstand large in-plane loads with small stresses and small in-plane displacements. A drawback is the stability of the unsupported compression zone of a slender glass pane which limits the bearing capacity of the structural element e.g. buckling of columns, lateral torsional buckling of beams or fins and plate buckling (section 2.5). Finally, whatever the positioning of the glass pane is, the element always has to be laminated for the coherence of the broken glass pane needed for residual capacity (section 2.5). For in-plane loaded glass structures no standards are available. Nevertheless, many contemporary in-plane loaded glass structures have been realized by the knowledge and experience of the structural designer.

The first use of in-plane loaded glass panes in building structures dates back to the beginning of the 19th century. The origin was the development of large spans built up of slender iron profiles provided with infill elements of glass panes connected by putty. The glass panes stiffened the slender iron intentionally or unintentionally [Schober et al. 2004]. These iron-glass structures were mostly confined to coverings for e.g. markets and railway stations. One of the first iron-glass domes was the ribbed dome of the Bourse du Commerce in Paris (France) and was built in 1811 [Schober et al. 2004]. The ribs gave the dome bending stiffness and the glass panes stiffened the entire dome. The single glass panes were circumferentially connected by putty to the cast-iron members. The gardener John Claudius Loudon (1783-1843) experienced with the construction of glass green houses in London in 1817-1818 [Weller et al. 2006a]. The structure was built up of very slender cast-iron frames (height of the frame was roughly 50 mm) with a spacing of roughly 200 mm. The structure clearly had no braces or stiffening members which is usual in today's structures (figures 1.1 and 1.9). The glass panes stiffened the structure for stability reasons and also transferred vertical loads. The greenhouses in the 19th century e.g. Bicton Garden built in 1838 in Dervin (UK) [Wellershoff 2006, Hagl 2006] (figure 1.10), Crystal Palace built in 1851 in London (UK) [Schober et al. 2004] and Kibble Palace built in 1873 in Glasgow (UK) [Schober et al. 2004] are examples of iron-glass structures. Most of these buildings endure the ravages of time and can still be admired nowadays. These structures were realized without any well-founded calculation of the load distribution. The calculation for the curved iron-glass structures, namely theory of shells, was published for the first time in 1928 [Weller et al. 2006a]. The glass panes in windows of e.g. houses, offices and factories were single glass panes. These glass panes also were connected with putty to the timber or steel frame till the introduction of the insulated double glass in the seventies of the 20th century. The single glass pane had a bracing effect on the timber or steel frame and transferred in-plane loads, because the connections between the transom and mullion of the timber or steel frame were less stiff than thought.

A tendency of the last decades is using glass panes for the benefit of transparency in linear supporting structures such as fins and beams to support glass panes in façades and roofs respectively (figure 1.5). These linear supporting structures have been successfully applied on a large scale. The span of glass beams is restricted to approximately 6 metre, because of the maximum standard size of the glass panes (section 2.1). The span can be enlarged with e.g.

composed beams built up of a laminated glass web and two timber flanges [Kreher et al. 2004]. The glass beams and fins are loaded in-plane by shear, tension, compression and bending. Glass columns (figure 1.6) have been realized at small scale. The glass columns are predominately loaded by normal compression loads, and fail under overloading without warning. To increase the transparency of the building envelope, glass panes are used as compression elements as substitution of the compression members in spatial grid structures [Weller 2007b] and in grid shells [Schober 2004] (figure 1.7). Glass panes also stabilize the spatial structure (retaining its form). These panes are loaded out-of-plane (bending) as well as in-plane (shear and compression). Other applications of in-plane loaded glass panes are stacked glass panes, vertically loaded glass e.g. a roof [Dubois 2007], lateral support for preventing of laterally torsional buckling of beams [Bergmeister et al. 2007] and preventing of buckling of slender-steel columns (not applied yet).
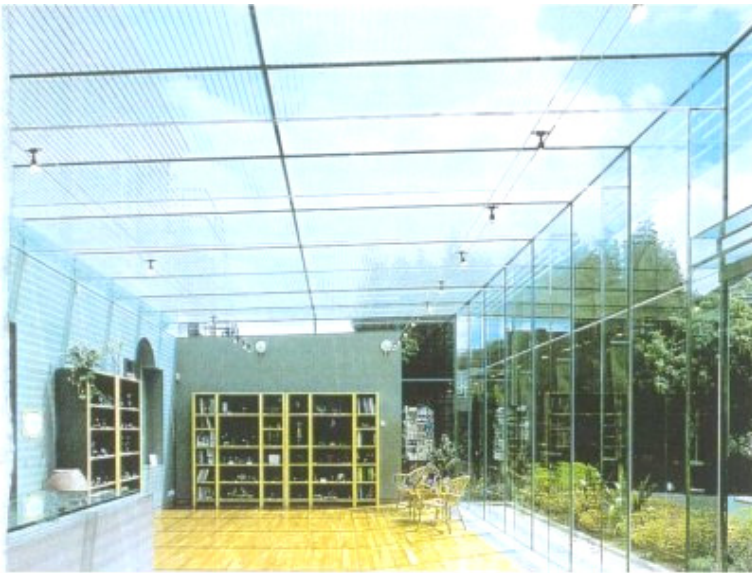
Figure 1.5:   Glass portal frame in Broadfield House, glass museum, Kingswinford, West Lands, UK (1994)

Glass panes also have the capacity to stabilize a building (figure 1.8). However, fully glass buildings, stabilized by glass panes, are still rare. The common structures to withstand the horizontal loads are shear walls, braced frames or frames with rigid column-beam connections. These stabilizing elements have to fulfil safety and serviceability belonging to the primary structural level. These stabilized structures are integrated in the architectural design and are mostly not visual anymore. One-storey buildings with glass façades are often designed with steel braces behind the glass façade to ensure the stability of the building, which often conflicts with the desired transparency (figure 1.9). A solution can be found by deleting the steel braces and using the secondary and tertiary structure, namely the frame and the glass panes of the façade to stabilize the building. In that case the façade is loaded in-plane as well as out-of-plane. The idea to use glass panes as stiffened elements for buildings is not new. The few drawn up 19th century buildings in this section are examples of structural collaboration between the very slender iron structure and the small single glass panes in the building

envelope. The glass panes were bonded to the iron frame by putty. These hybrid structures appear to be much lighter than many today's structures and this is what architects really want.

Figure 1.6:   Glass columns in Town hall, Saint Germain-en-Laye, France (1996)

Figure 1.7:   Glass roof of the Maximilian museum, Augsburg, Germany (2000)

Figure 1.8:   *Interior of the glass cube of the Apple Store, New York, USA (2006)*

Finally, the transportation industry also uses the in-plane stiffness of glass in vehicles. The windscreens of motor cars are structurally bonded with high modulus polyurethane adhesives to the car body [Wellershoff et al. 2005]. The bonded windscreen stiffens the car body significantly e.g. the torsional stiffness increases up to 40% by using polyurethane joint in stead of the former rubber gasket technology [Born 2005].

Figure 1.9:   *Steel braces behind glass façade of a residential building, Arnhem, The Netherlands*

Figure 1.10:   Palm House, Bicton Garden, Devin, UK

1.3.4   Connections

The connection types for out-of-plane loaded glass panes can be divided into two types, namely linear bearings and point bearings (figure 1.11) [Siebert 2004]. Both types have to resist the positive (e.g. wind suction) as well as the negative (e.g. wind pressure) out-of-plane loads whereby the glass pane can move freely in-plane. Furthermore, setting blocks are used to carry the in-plane loads of non-horizontally installed glass panes. The linear bearings support the glass pane two, three or four-sided. The glass pane is fixed by a flexible material such as neoprene at both sides of the edges. The structural sealant glazing (SSG) is a one-sided silicone joint. The structural performance mainly concerns resistance to wind suction [Schober et al. 2004]. Point bearings can be divided into fixing clamps and point fixed supports. The fixing clamps are locally placed along the glass pane edges or at the corners. The glass pane is placed between adjustable clips provided with an elastic material and these clips exert a pressure on the glass pane. The setting blocks also carry the in-plane load of non-horizontally installed glass panes. The point fixed supports are positioned in the glass pane in the vicinity of the glass edges. These supports consist of fixings, bolted or adhesive bonded. The in-plane load is transferred to the supporting structure through the bolt by bending and shear.

linear bearings   clamps (1)   point fixed

point bearings (2)

setting blocks

silicone (SSG)   adhesive bonded joint

putty   neoprene   nylon

nylon

neoprene

setting blocks   nylon
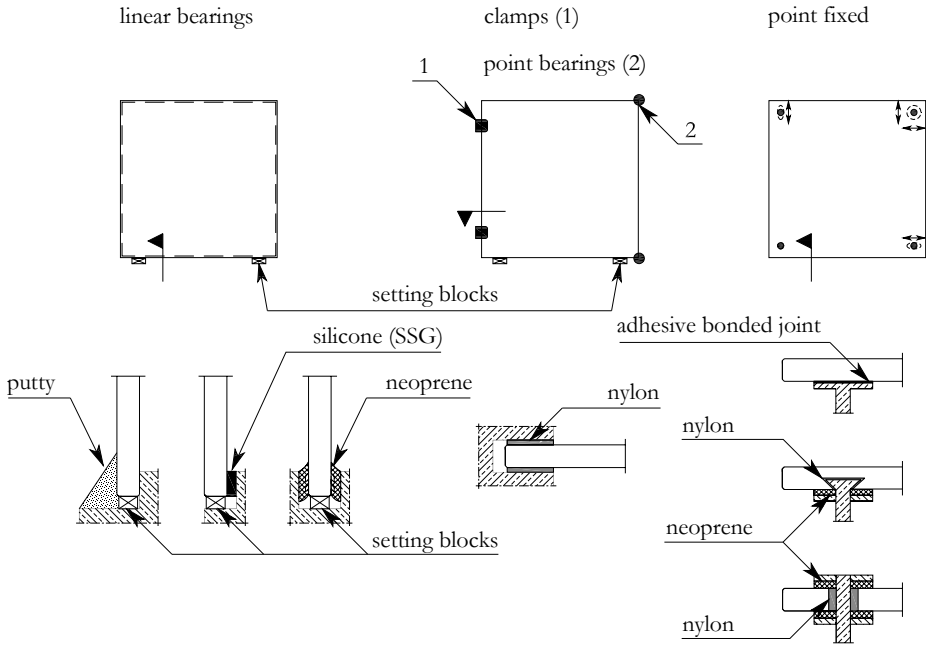
Figure 1.11:   Connection types for out-of-plane loaded glass panes

The connection types described above are not designed to transfer in-plane loads. However, the outmoded putty is a connection type which is able to transfer in-plane loads (section 1.3.3). Figure 1.12 gives two connection types along the glass pane edges to activate the in-plane capacity of a glass pane, namely a discrete joint (left) such as synthetic setting blocks and a continuous joint (right). A suitable continuous joint for glass is the adhesive bonded joint [Bos et al. 2007, Wellershoff et al. 2007]. This joint gradually introduces the load into the glass pane and forms a thin interlayer to prevent direct glass-steel contact.

frame   frame

glass pane   continuous connection

discrete connection   glass pane
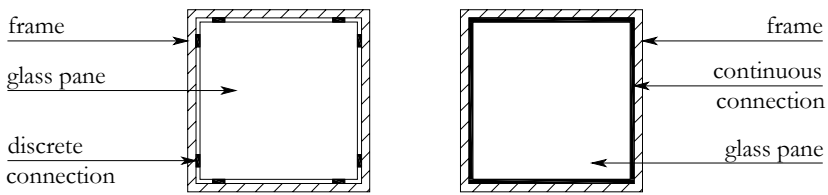
Figure 1.12:   Two connection types along the glass pane edges to activate the glass pane in-plane

1.4 Problem definition and objective

Standardization of out-of-plane loaded glass panes has been in progress to extend the field of application for the common use of glass in buildings on tertiary structural level. On the other hand, glass structures which are structurally loaded in-plane are not regulated in standards and no first step has been taken towards standardization of in-plane loaded glass panes. However, a clear tendency can be observed to use glass as secondary structural element and even in the future as primary structural element. Some glass structures, such as fins and beams, were successfully realized by the actual knowledge about glass and joining techniques, gained experience and common sense of the structural engineer. Nevertheless, a structural design without standards and guidelines is a serious obstacle to obtain approval from the local authorities. And therefore, glass structures at primary structural level, such as columns and diaphragms, were realized sporadically, because the insight into the structural behaviour is absented.

The problem statement is formulated as follows: no design rules are available in literature and standards for circumferentially adhesive bonded rectangular glass panes in steel frames acting as a vertical stability system for e.g. one-storey buildings. So, the strength (safety) and the in-plane stiffness (serviceability) of vertical stability systems can not be predicted.

The objectives of the research are by means of a system, an isolated rectangular steel frame provided with a circumferentially adhesive bonded single glass pane:
• to get more insight into the structural behaviour;
• to set-up mechanical models and possibly design rules for the prediction of the strength and the in-plane stiffness of the system.

1.5 Methodology and outline thesis

Figure 1.13 shows a one-storey building stabilized by one or more bays in the façade. The bays form the transparent vertical stability systems of the building. The number of bays depends on the strength (safety), the in-plane stiffness (serviceability), the redundancy in case of emergency and the dimensions of the building. The vertical loads (q_y) are directly transferred by the steel beams in the roof and the steel columns to the foundation. The steel beams and the steel columns are hinge connected. This connection type is an economical fastening technique as well as construction method. The horizontal loads acting on the building such as wind loads are transferred to the horizontal stability system in the roof which transfers the horizontal loads via the vertical stability systems of the building to the foundation. The vertical stability systems of the building are placed in the façade by means of circumferentially adhesive bonded rectangular glass panes in steel frameworks. One rectangular glass pane, the circumferential adhesive bonded joint and the encircling steel frame is isolated from the bay and is defined as 'the system' and is subject of the research.

q_y

braced structure

hinge connection

q_x

$F_{qx} + F_{px}$

roof

beam

column

p_x

F_{px}

foundation

y

z

x

$F_{v;qy}$ $F_{v;qy}$ $F_{v;qy}$ $F_{v;qy}$
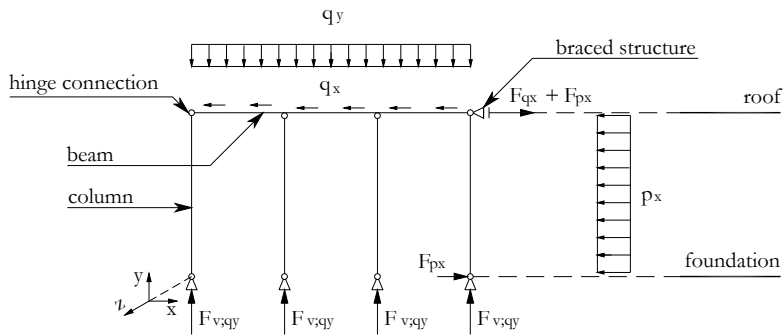
bearing structure for transferring vertical loads (primary structure)

bay

$F_h = F_{qx} + F_{px}$

roof

transom

glass pane

building height

mullion

adhesive bonded joint

hinge connection

foundation

F_h

$F_{v;Fh}$ $F_{v;Fh}$
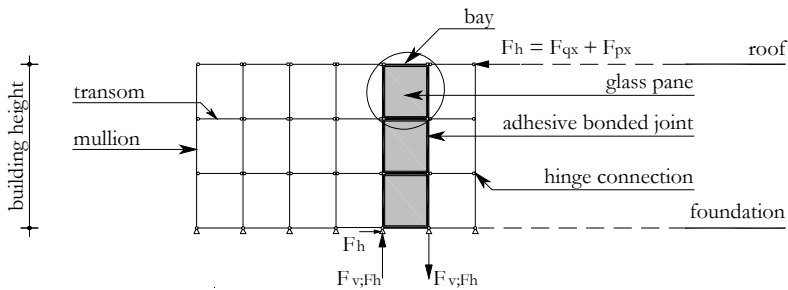
vertical stability system of the building for transferring horizontal loads (primary structure)

$EI = \infty$

load introduction

F_h (u_{RTC} / K_s)

single glass pane

circumferentially

h_s

adhesive bonded joint

infinite stiff steel frame

with hinged connections

y (v)

z (w)

x (u)

w_s
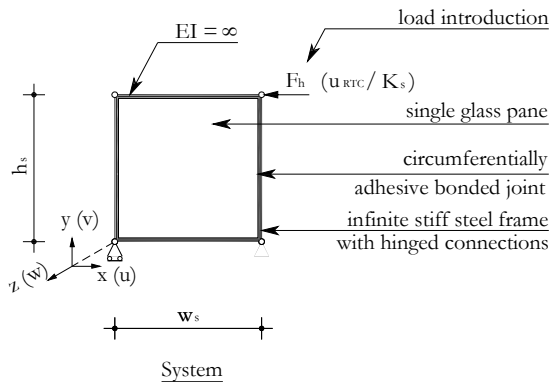
System

Figure 1.13:   Façade structure (top and middle) with selected system for the research in this thesis (bottom)

The investigated system is built up of a single glass pane, a steel frame and a circumferential adhesive bonded joint. The transoms and the mullions of the steel frame are hinge connected, being a good approximation of the actual connection between the mullions and the transoms in the façade. In this research, the transoms and mullions are infinite stiff. The steel frame is needed to spread the concentrated loads at the load introduction and at the supports (section

3.3.1). The glass pane is four-sided linearly supported in the weakest direction (z-axis) and is circumferentially adhesive bonded to the steel frame with one of the three defined joint types which will be discussed in section 3.3.3. The mid-plane of the glass pane lines up with the centre of the outside beam of the steel frame (figure 3.2). The applied glass type is annealed float glass which will be discussed in section 3.3.2. A horizontal in-plane load (F_h) with a short term load is introduced at the right side of the top transom. The out-of-plane load is beyond the scope of the research. The results of the limited tests will be analyzed and will be used to calibrate the finite element models. The calibrated finite element models will be used for the parametric studies to extend the limited tests. Finally, mechanical models will be developed.

Figure 1.14 schematically presents the outline of the thesis in a flow chart. After this introductory chapter a literature overview is given in chapter 2. This chapter gives the state of the art of glass as structural material and the relevant research projects.

Chapter 3 describes the test set-up and discusses the results of the experiments. The system is built up of a steel frame, a single glass pane and one of the three defined adhesive bonded joints (joint types 1 to 3). The measurements are the in-plane and out-of-plane displacements by means of displacement gauges, the horizontal in-plane load by means of a load cell, the in-plane load transfer through the glass pane by means of strain gauges and the crack initiation and propagation in the glass pane by means of high-speed shootings.

Chapter 4 deals with finite element simulations for systems with joint types 1 to 3. Characteristic of the finite element model is that it contains all parts to simulate systems with joint types 1 to 3. This finite element model is usable to the onset of the first crack or the first glass-steel contact.

Chapter 5 describes parametric studies for systems with joint types 1 to 3 by means of finite element models. Parametric studies focus on three nominal glass thicknesses and six glass pane sizes. The nominal glass thicknesses are 4 mm, 8 mm and 12 mm and the glass pane sizes are 1.0 m x 1.0 m, 1.5 m x 1.5 m, 1.0 m x 1.5 m, 1.5 m x 3.0 m, 1.5 m x 1.0 m and 3.0 m x 1.0 m.

Chapter 6 only gives the mechanical models for systems with joint type 1. The mechanical models predict the in-plane stiffness of the system, the horizontal in-plane load, the horizontal in-plane displacement at the RTC of the system, the maximum normal stress and shear stress in the adhesive bonded joint and the largest maximum principle stress in the glass pane. At the first glass-steel contact, the mechanical models predict the horizontal in-plane displacement at the RTC of the system and the horizontal in-plane load.

Chapter 7 presents an overall discussion for systems with joint types 1 to 3. For systems with joint types 2 and 3, a range of shear stiffnesses for the adhesive bonded joint which has a positive influence on the stress distribution in the glass pane and in the adhesive bonded joint is proposed. Finally, it ends with the conclusions for systems with joint types 1 to 3 and the recommendations for further research in this field.
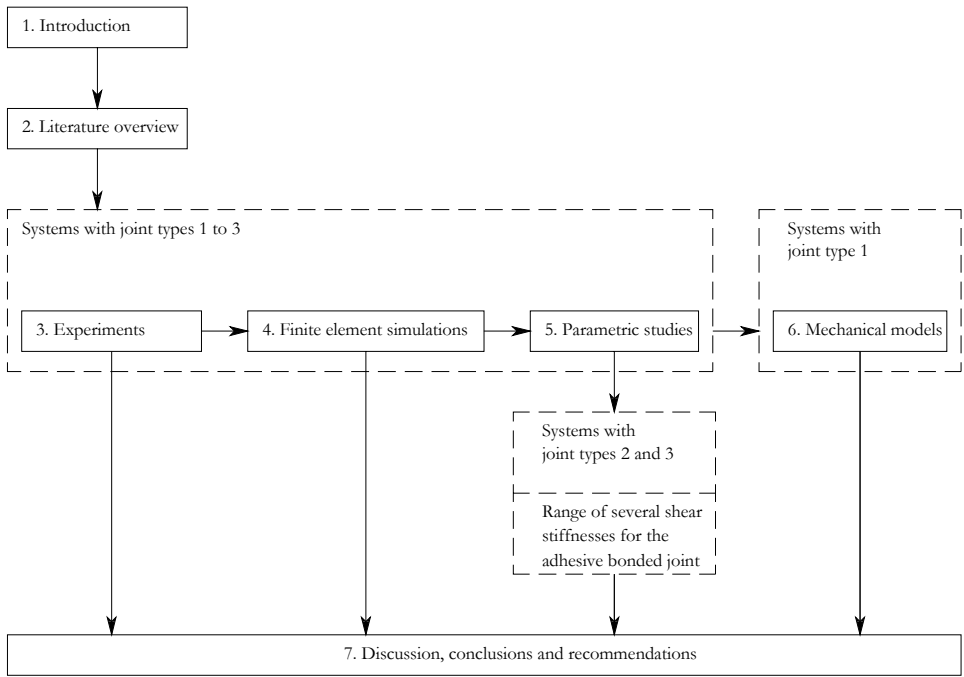
Figure 1.14:   Flow chart of the thesis

2   Literature review

This chapter summarizes relevant literature about the structural application of glass in buildings. Section 2.1 deals with the production of float glass. Section 2.2 discusses the chemical and mechanical properties of glass. Section 2.3 deals with glass types, glass units and residual capacity. Section 2.4 discusses the current requirements for glass application and adhesive bonded joints. Section 2.5 discusses research projects of in-plane loaded glass structures. The chapter ends with conclusions in section 2.6.

2.1   Production of float glass

Several manufacturing processes (section 1.1) are available to produce glass panes such as drawing, blowing, pressing, casting, rolling, extracting and floating. The floating process is the most common and economical production process of flat glass and it accounts for 90% of today's flat glass production worldwide [Haldimann et al. 2008]. Float glass production was introduced commercially by Pilkington in 1959. The production of float glass (figure 2.1) is a continuous process without major disruptions and it is operational for several years. The mix of raw materials provided with cullet (recycled broken glass from the cutting section) is melted in a furnace at a temperature of approximately 1500 ºC. Then the molten glass with a temperature of approximately 1100 ºC flows into an enclosed box with a bath of molten tin. An inert atmosphere consisting of hydrogen and nitrogen is created in the enclosed box to prevent oxidation of the molten tin. Tin has a high specific weight in comparison to glass. The melting point of tin is one of the lowest of any metals (T_m = 232 ºC) and the boiling point of tin is 2270 ºC. The molten glass floats over the molten tin and forms a smooth and plan parallel glass ribbon with an equilibrium thickness of roughly 6 to 7 mm determined by the surface tension of glass on tin. The thickness of the glass ribbon lies between 2 to 25 mm and is controlled by the speed of the rollers of the annealing lehr. Thinner glass ribbons are realised by stretching the natural flow. Thicker glass ribbons are realised by restraining the natural flow by means of fenders. Then the glass ribbon with a temperature of roughly 600 ºC enters on the rollers of the annealing lehr in which the glass ribbon gradually cools down under controlled conditions to prevent residual stresses. The glass ribbon leaves the annealing lehr with a temperature of roughly 100 ºC followed by an automatically optical check for visual defects and imperfections which are removed during cutting. The glass ribbon is finally cut into the standard size of 3.12 m x 6.00 m.

As a consequence of the float process, float glass has a current direction and different glass faces. The glass face which had contact with the molten tin is called the tin side of the glass pane. This side contains some diffusion of tin atoms in the glass face. The tin side can be detected by ultraviolet radiation which bluish fluorescence. The other side is called the atmospheric side of the glass pane.
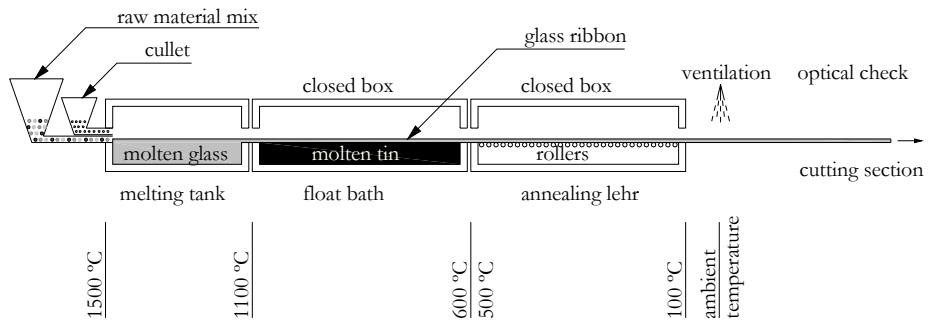
Figure 2.1:   Schematic representation of the float glass production process

2.2   Material properties

2.2.1   Chemical properties

The glass commonly used in buildings is standard soda lime silica glass [Haldimann 2006]. The chemical ingredients include silica sand, lime (calcium oxide), soda and several additives (table 2.1). Borosilicate glass has another glass compounding and is used for special applications in buildings e.g. heat resistance glazing [Haldimann et al. 2008]. Borosilicate glass has larger resistance to change of temperature and acids than soda lime silica glass. The chemical ingredients of borosilicate glass include silica sand, boron-oxide, soda and several additives (table 2.1). All chemical compounding of glass also has some contaminations [Haldimann et al. 2008]. Small amounts of iron oxides give the glass its characteristic green colour. The additions of small amounts of metal oxides e.g. iron oxide, cobalt oxide or titanium oxide colour the glass mass (body tinting). The strong reduction of iron oxide (Fe_2O_3) makes glass less green or even colourless. The glass used in this research is standard soda lime silica glass.

At molecule-level, soda lime silica glass has a three dimensional network consisting of oxygen tetrahedra which surround the silica atoms (figure 2.2, right) [Zachariasen 1932]. The tetrahedra are joined by primary chemical (covalent) bonds. Some of these tetrahedra are broken up by OH- groups and Na+ ions of the soda additive (figure 2.2, left). The tetrahedra network has an irregular geometrical network and therefore glass is an amorphous material. The lack of a crystal lattice prevents any plastic like behaviour. The strong primary chemical bonds can not redistribute. This bond can deform elastically or fracture [Veer 2007]. For fracture, the occurring tension stress has to exceed the theoretically molecular cohesion strength of the silicon-oxygen bond of about 20000 N/mm² according to [Doremus 1982] or 32000 N/mm² (Orowan stress) according to [Haldimann et al. 2008].

Glass is chemically an inorganic product of fusion which is cooled down to a rigid state without crystallization [Wigginton 1996, Hess 2004]. The prevention of crystallization is the consequence of the glass formers in the liquid which make many bonds between the molecules during cooling down. This results in complex chains which prevent the sudden transition from an unarranged to an arranged structure. In other words: the liquid has become too viscous.

The velocity of cooling down in the vicinity of the glass transition temperature (T_g) plays an important role in preventing crystals and a material becoming glassy. Every material has a so-called critical cooling velocity which prevents the growth of crystals. The critical cooling velocity of soda lime silica glass is low. The term glass transition temperature is a 'central point' of a zone in which a material gradually transfers from a liquid state to a vitreous state and vice versa. The glass transition temperature of soda lime silica glass is roughly 530 ºC [Haldimann et al. 2008]. During the cooling phase of the molten glass the viscosity (toughness of a liquid) constantly increases. At glass transition temperature the molten glass starts solidifying with a viscosity of 10^{14} Pa·s which gradually increases to 10^{20} Pa·s at room temperature. The solidification of glass is thus no crystallization, but a frozen state of the molecules and for that reason glass is transparent. Furthermore, glass is an inert (inactive reaction) material which makes glass a durable building material.

Table 2.1: *Chemical compounding of standard soda lime silica glass [EN 572-1:2004] and borosilicate glass [EN 1748-1-1:2004]*

Ingredients		Soda lime silica glass [%]	Borosilicate glass [%]
Silica sand	SiO_2	69-74	70-87
Calcium oxide (lime)	CaO	5-14	--
Soda	Na_2O	10-16	0-8
Boron oxide	B_2O_3	--	7-15
Potassium oxide	K_2O	--	0-8
Magnesia	MgO	0-6	--
Alumina	Al_2O_3	0-3	0-8
Others		0-5	0-8
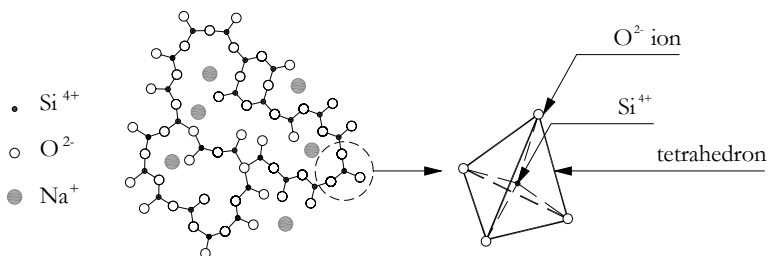
Figure 2.2: *Two-dimensional representation of the three-dimensional SiO_4 network of sodium lime silica glass (left) and an enlarged view of a SiO_4 tetrahedron (right)*

2.2.2 Mechanical properties

Glass is a perfect linear elastic and isotropic material without plastic behaviour i.e. it fails brittle without warning at a local peak stress exceeding the tension strength of glass [Schuler et al. 2004]. Moreover, the strength of glass is an indistinct material property. The intrinsic tension strength of perfect glass has a range between 6000 N/mm² and 10000 N/mm² and the intrinsic compression strength is much higher [Haldimann 2006]. These intrinsic strengths are not applicable for dimensioning glass panes and glass structures in buildings. The strength of the glass pane depends on the integrity of the surfaces and edge damages [Hess 2004]. The presence of many micro as well as macro flaws in the glass faces as the result of the cooling process (section 2.1), the surface damages at treatments and surface damages during service life limits the tension strength of the glass pane significantly. On the other hand, the compression and tension stresses in the core of the glass pane and the compression stresses in the glass faces are no criterion for failure of glass [Haldiman et al. 2008].

New glass has comparatively small surface damages. The surface damages in the tin side are slightly more than in the atmospheric side of the glass, because of the transport rollers in the annealing lehr (section 2.1) [Sedlacek et al. 1999]. Pre-damaging of the tin side and the atmospheric side is a method to make both glass faces identical for research [Güsgen 1998]. The flaw depths (*a*) of new glass vary between 16 µm to 36 µm [Fink 2000]. Treatments of new glass such as cutting and drilling [Maniatis et al. 2004] are the cause of more and deeper surface damages. During service life the number of surface damages increases, but the flaw depth is difficult to quantify. The flaw depth of 48 years-old glass was measured and the maximum flaw depth was 61 µm [Fink 2000]. However, larger flaw depths can not be excluded during service life. Hitting with a hard object gives flaw depths of roughly 100 µm [Fink 2000]. An approximation of the obsolescence of glass can be carried out with pre-damaging of the glass surfaces. However, the pre-damaged glass face is not the reproduction of the real surface damages during service life [Fink 2000]. A brittle material can be indented by another hard material. The microscopic particles of a hard material indent the glass surface which initiates fracture e.g. direct glass-to-metal contact. The glass pane can even be indented by micron-sized quartz particles in an air flow [Vuolio 2003].

The principle of fracture of glass is briefly discussed. A comprehensive explanation is given by [Haldimann et al. 2008]. Linear elastic fracture mechanics (quasi static fracture mechanics) is a good model for describing the brittle fracture of glass. The crack is modelled as an ideal flaw in the plane with a defined geometry. Figure 2.3 at the left shows a piece of glass with a surface flaw subjected to a uniformly distributed tension stress (σ_t). The flaw depth (*a*) is very small in comparison to the glass thickness. The surface flaws are the point of interest for structural glass.

A slot, a notch or a hole in a metal plate tends to reduce the tension strength more than the obtained tension stress from the reduction in load-bearing cross-sectional area [Inglis 1913]. A uniformly distributed tension stress (σ_t) which acts perpendicular to the longest diameter (2d) of an elliptical discontinuity results in an increase of the tension stress near the tip (σ_{tip}) of the elliptical discontinuity. An approximation for the tension stress near the tip is given in equation 2.1 in which *d* is the smallest diameter of the elliptical discontinuity and ϱ is the radius of curvature of the crack tip (figure 2.3, right). A sharp radius of curvature of the crack tip with even a small uniformly distributed tension stress can approach the molecular bond strength.

$$\sigma_{tip} = 2\sigma_t \sqrt{\frac{d}{\rho}} \qquad\qquad \text{[Equation 2.1]}$$

The theoretical molecular cohesion strength of the silicon-oxygen bond is very large (section 2.2.1), but the practical tension strength of annealed float glass is considerably smaller. Griffith [Griffith 1920] explained the difference between the theoretical molecular cohesion strength and the practical strength of annealed float glass. The fracture initiates from pre-existing flaws (Griffith flaws) on the surface which severely weaken brittle solids, because they cause high tension stress concentrations. Griffith's model with a static crack as a reversible thermodynamic system was based on Inglis' work and carried out experiments on glass specimens. Equation 2.2 gives the total free energy (U_T) in a system in which U_M is the mechanical energy and U_S is the free energy expended in creating of new cracks. The mechanical energy results in crack extension and the free energy resists crack extension. The total free energy in the system is minimized in which the crack just has an equilibrium state at the moment of crack extension. This resulted in equation 2.3 (known as the Griffith energy balance concept) in which the failure stress (σ_f) is predicted in which E_g is the Young's modulus of glass, γ_g is the fracture surface energy of glass and l_c is the crack length.

$$U_T = U_M + U_s \qquad\qquad \text{[Equation 2.2]}$$

$$\sigma_f = \sqrt{\frac{2E_g\gamma_g}{\pi l_c}} \qquad\qquad \text{[Equation 2.3]}$$

Griffith energy balance concept was extended by Irwin [Irwin 1957] by the fracture toughness (brittleness of a material). He introduced the stress intensity factor (K), which represents the elastic stress intensity near the crack tip, and is given in equation 2.4 in which Y is the geometry factor and a is the crack size i.e. the crack depth or the half of the crack length. The index I represents mode I i.e. a normal separation of the crack subjected to a uniformly distributed tension stress.

$$K_I = Y\sigma_t\sqrt{\pi a} \qquad\qquad \text{[Equation 2.4]}$$

The geometry factor depends on the geometry of the crack, crack depth, the specimen geometry, the stress distribution and the proximity of the crack to the specimen boundaries (figure 2.3, left). If the stress intensity factor for mode I (K_I) reaches or exceeds the critical stress intensity factor (K_{IC}) the glass element fails instantaneously. The critical stress intensity factor can be considered as a material constant and is determined experimentally. The value for the critical stress intensity factor varies between 0.72 MPa·m$^{1/2}$ to 0.82 MPa·m$^{1/2}$ [Menčik 1992] and 0.75 MPa·m$^{1/2}$ is usually applied.
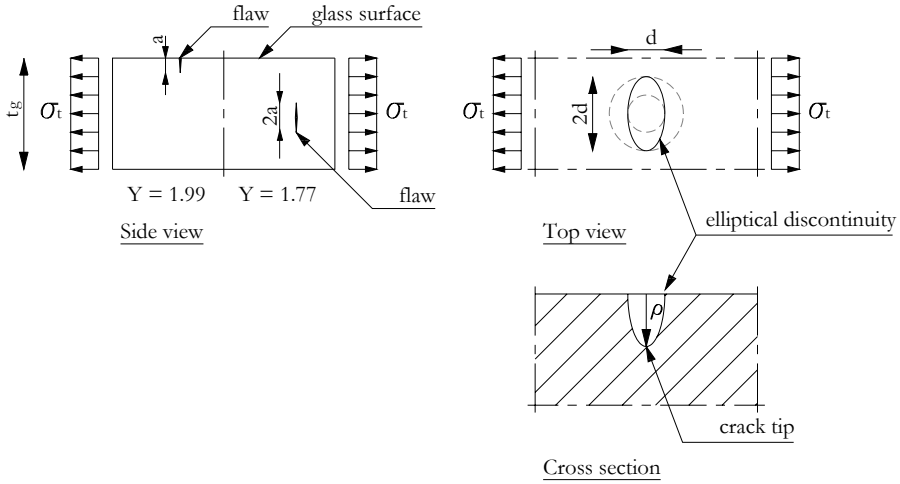
Figure 2.3:   *Relation between position of the crack and the geometry factor (Y) (left) and schematic representation of elliptical discontinuity (right)*

Glass has good durability properties, because glass is chemically an inert material (section 2.2.1). Nevertheless, glass is extremely susceptible to stress corrosion caused by water in the ambient environment [Wiederhorn et al. 1970]. This is called static fatigue and glass subjected to a long-term tension stress is able to fail in time. The water degrades the strained silicon oxygen bonds at the crack tip resulting in increasing of the stress intensity factor (figure 2.4, right).
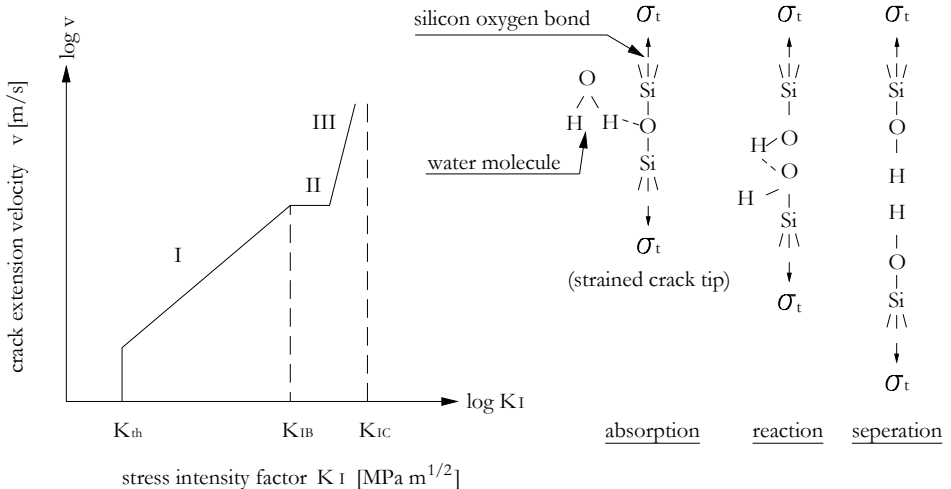
Figure 2.4:   *Schematic relation between the stress intensity factor (K_I) and the crack extension velocity (v) (left) and the interaction between a water molecule (H_2O) and a silicone oxygen bond at strained crack tip (right)*

Figure 2.4 at the left shows a schematic relation between the stress intensity factor (K_I) and the crack extension velocity (v). The parameters which influence the relation are humidity, temperature, loading rate, pH-value and chemical composition of glass [Haldimann et al. 2008]. No crack growth occurs below the threshold stress intensity factor (K_{th}). In region I the crack extension velocity increases with increasing stress intensity factor (sub-critical crack growth) and strongly depends on the environmental conditions which influences the chemical reaction at the crack tip and is described by equation 2.5 in which v_0 is the crack extension velocity constant and N is a dimensionless parameter. The crack extension velocity constant depends on relative humidity and temperature of the ambient environment and has to be determined experimentally. The extremely slow sub-critical crack growth (region I) has practical relevance for life-time prediction models of glass structures. For structural glass applications, the usual value of the crack velocity constant (v_0) is 6.0 mm/s and the usual value of the dimensionless parameter (N) is 16 [Haldimann et al. 2008].

$$v = v_o \left(\frac{K_I}{K_{IC}} \right)^N \qquad \text{[Equation 2.5]}$$

In region II the crack extension velocity is independent (constant) of the stress intensity factor and depends on the amount of humidity in the ambient environment which influences the kinetics of the chemical reaction at the crack tip. If the stress intensity factor is close to the critical stress intensity factor, the crack velocity is independent on the ambient environment and results in crack propagation with a velocity of 1500 m/s (supercritical crack growth). The principle of glass failure is described before and is the basis for lifetime prediction models. Equation 2.6 gives a lifetime prediction model of a single flaw in region I adopted from [Haldimann et al. 2008]. In which τ is the time, t_f is the time to failure (lifetime crack), a_i is the initial crack depth.

$$\int_0^{t_f} \sigma_t^N(\tau)d\tau = \frac{2}{(N-2) \cdot v_0 \cdot K_{IC}^{-N} \cdot (Y\sqrt{\pi})^N \cdot a_i^{(\frac{1}{2}(N-2))}} \qquad \text{[Equation 2.6]}$$

The compression strength of glass is not the failure criterion. The value for the compression strength ranges from 700 to 900 N/mm² according to [DIN 1249-10:1990]. This is also a significantly lower value than the intrinsic compression strength. Less scientific research projects have been done on the compression strength of glass yet [Luible 2004]. The decisive compression strength is found possibly by exceeding the tension strength perpendicular to the direction of the compression stress [Menčik 1992].

In literature the value for the Young's modulus (E_g) of soda lime silicate glass ranges between 70000 N/mm² to 74000 N/mm². This variation depends on glass compounding and temperature [Luible 2004]. The Young's modulus prescribed by many standards e.g. [EN 572-1 2004] is 70000 N/mm². In literature, the value of the Poisson's ratio (v_g) ranges from 0.20 to 0.24. The standard [EN 572-1 2004] gives a value for the Poisson's ratio of 0.20. In many researches the value for the Poisson's ratio is 0.23. Table 2.2 gives an overview of the usual values for soda lime silica glass.

Table 2.2:   *Properties of soda lime silica glass, relevant for mechanical behaviour*

Properties	Symbol	Unity	Value
Density	ϱ_g	kg/m³	2500
Young's modulus	E_g	N/mm²	70000
Shear modulus	G_g	N/mm²	28455
Poisson's ratio	ν_g	[--]	0.23
Thermal expansion coefficient	α_g	K⁻¹	$9 \cdot 10^{-6}$
Hardness according to Mohs scale	n_g	Mohs	6

2.3   Glass types and glass units

2.3.1   Glass types

A glass type is defined as a single glass pane with or without a follow-up treatment to increase the glass strength (read the load bearing capacity of a glass pane by prestress). Glass types are annealed, thermally toughened, heat strengthened and chemically toughened float glass.

Annealed float glass has no follow-up treatment to increase the glass strength. Annealed float glass has negligible residual stresses. This is realized by a controlled cooling down process in the annealing lehr (section 2.1). The material imperfections of annealed float glass are the unavoidable flaws in the glass pane faces during the float process, the edge damages by cutting and the increase in number of surface damages during service life (section 2.2.2). An annealed float glass pane subjected to mechanical loading in combination with a humid environment leads to crack growth and reduces the 'strength' of the glass (section 2.2.2). These material imperfections also have negative influences in case of change of temperature. The stress distribution is non uniform by e.g. shadow on the glass pane and the thermal flow between the glass pane and the bearing structure. Thermal fracture occurs at a change of temperature between 30 ℃ and 40 ℃ (table 2.3) [Luible 2004]. The geometric imperfections of annealed float glass are the irregular thickness of the glass pane by the float process and a very small initial out-of-plane imperfection [Luible 2004]. The crack pattern of annealed float glass is built up of large, sharp and irregular shards [Sedlacek et al. 1999].

Thermally toughened glass (or tempered glass), heat-strengthened glass and chemically toughened glass are follow-up treatments. The purpose of a follow-up treatment is to introduce compression stresses in the glass faces to suppress the surface flaws. So, the strength of glass increases against mechanical loadings and change of temperature. Thermal fracture occurs at a change of temperature about 100 ℃ for heat-strengthened glass and of about 200 ℃ (table 2.3) for thermally toughened glass [Luible 2004]. The core of the glass pane (perfect glass) has large tension stresses which are in equilibrium with the compression stresses in the glass faces. Thermally toughened glass and heat-strengthened glass are uniformly heated above the glass transition temperature ($T_g = 650$ ℃) in a furnace followed by a controlled cooling down process with a specific speed. The faster the cooling down process, the larger are the

internal residual stresses. Thermally toughened glass has a larger rate of cooling down (figure 2.5, left); heat-strengthened glass has a smaller rate of cooling down (figure 2.5, left). The ratio between tension stress and compression stress is 1:2 based on a parabolic stress distribution over the glass thickness. Thermally toughened glass and heat-strengthened glass can not be cut, ground or drilled after tempering. These treatments have to be done before tempering. If the equilibrium states of these glass types are disturbed, the glass panes immediately crack. Thermally toughened float glass fractures in small pieces of glass (± 100 mm²) and heat-strengthened glass in large glass shards [Sedlacek et al. 1999]. The geometric imperfections of thermally toughened and heat-strengthened glass panes have considerably larger initial out-of-plane imperfections than the initial out-of-plane imperfections of annealed glass panes [Luible 2004]. Tempered glass panes are subjected to an optical quality check whether or not the out-of-plane imperfections are within the limits (overall bow max 3 mm/m) [EN 12150-2 2004]. Thermally toughened glass can break spontaneously during service life caused by the nickel sulphide inclusions [Sedlacek et al. 1999, Wagner 2002]. Nickel sulphide inclusions can not be avoided completely during the production of float glass. Under influence of high temperature as in the tempering process, the nickel sulphide inclusions can increase in volume by 4 % by which the core of the thermally toughened glass is weakened. Nickel sulphide inclusions can be detected by a heat-soak test. During the heat-soak test the thermally toughened glass pane is slowly heating up to about 290 °C, after which the temperature remains constant for several hours. Most of the thermally toughened glass panes with nickel sulphide inclusions fail the heat-soak test.
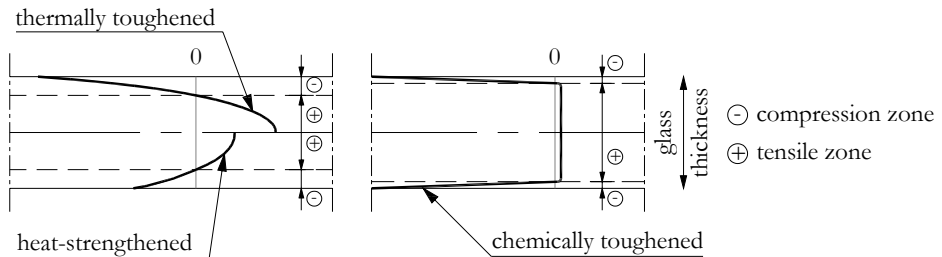
Figure 2.5: Distribution of the residual stresses for thermally toughened (left), heat strengthened glass pane (left) and chemically toughened glass pane (right)

Chemically toughened glass panes are rarely applied in buildings. It is used for special geometries e.g. strongly bent glass panes. Chemically toughened glass is based on exchanging of ions in the glass surfaces. In a chemical bath the small sodium ions are replaced by 30% larger potassium ions. The large potassium ions need more space than the sodium ions which results in a very thin compression zone at the glass face and a tension zone in the core of the glass pane (figure 2.5, left). The depth of the compression zone is time-dependent with a penetration velocity of about 20 µm in 24 hours. If a crack tip is deeper than the depth of the compression zone (section 2.2.2) a subcritical crack growth can occur resulting in spontaneous glass failure even if the glass pane is unloaded. This phenomenon is called self-fatigue. Cutting and drilling remains possible after tempering [Haldimann et al. 2008].

The glass strength is not a material property and has no unequivocal value, but strongly depends on the condition of the glass surface and the load duration (section 2.2.2). Moreover,

the strength of glass also depends on the glass type. Actually, the strength of glass, given in design standards (section 2.4), is the representative flexural tension strength of glass ($f_{mt;u;rep}$); not the tension strength of glass, because in common applications the glass pane is loaded out-of-plane resulting in bending of the glass pane. Four point bending tests and the coaxial double ring test (concentric ring-on-ring test) are commonly used to determine the flexural tension strength of glass [Haldimann 2006]. The statistical analysis of the experimental data is generally done by fitting a two-parameter Weibull distribution [Haldimann 2008]. The bending tension strength in standards (section 2.4) is valid to check the largest maximum principle stress on the glass pane surface and not along the edges of the glass pane. Table 2.3 gives the representative flexural tension strength of glass subjected to short term loading e.g. wind load for the usual glass types in buildings.

Table 2.3: Overview of the representative flexural tension strength for short term loading (NEN 2608-2 2007), maximum change of temperature and crack patterns of annealed, heat-strengthened and thermally toughened float glass

Glass type	$f_{mt;u;rep}$ [N/mm²]	ΔT [°C]	Description of the crack pattern
Annealed	45	30-40	Large and sharp shards
Heat-strengthened	70	100	Large and less sharp shards
Thermally toughened	120	200	Not sharp crumbly shards

2.3.2   Glass units

A glass unit is a composition of at least two glass panes such as laminated glass and insulated double glass units. A glass unit can be built up of different glass thicknesses of one glass type or different glass types depending on the application of the glass unit.

Insulated double glass units (figure 2.6, left) consist of two glass panes enclosing a hermetically sealed air cavity with the function to reduce thermal losses. The air cavity is filled with dehydrated air or gas e.g. argon to increase the thermal resistance. A circumferential spacer (aluminium or plastic tube) between the glass panes guarantees the air cavity. The spacer is also provided with desiccant which absorbs the enclosed humidity in the air cavity at manufacturing. The sealant (polyisobutene) between the spacer and the glass pane is an air barrier (primary sealant). The edge sealant (polysulfide or silicone) gives the structural robustness to the insulated double glass unit and is the secondary sealant. The loadings on the glass panes of insulated double glass units such as mechanical loads, temperature loads and the loads of the ambient atmospheric result in load sharing by the hermetically sealed air cavity (Boyle's Law/General Gas Law) [Vallabhan et al. 1990, Wörner et al. 1993, Huveners et al. 2003]. A new development in standardization is the insulated triple glass units (three glass panes and two hermetically sealed air cavities). They reduce more thermal losses than insulated double glass units.

Laminated glass consists of single glass panes bonded together with a transparent plastic interlayer. In an autoclave with a temperature of ±140 ºC and a pressure of ±14 bar the glass panes are adhered together without air inclusions between the glass panes and the interlayer [Hess 2004]. The advantage of laminated glass panes in relation to single glass panes is that the shards of the broken glass pane(s) remain sticking to the interlayer(s) for a while which is indicated as residual capacity (section 2.3.3). A common application of laminated glass is for overhead glazing to protect people against injury for falling glass [Haldimann et al. 2008].

A common plastic interlayer is polyvinyl butyral foil (PVB). The nominal thickness of the foil is 0.38 mm. Laminated glass has two, four or six foils between each glass pane depending on the tolerance of the glass type [Haldimann et al. 2008]. Polyvinyl butyral belongs to the group of amorphous thermoplastic polymers and exhibits viscoelastic behaviour below a temperature of about 140 °C to 200 °C [Schuler et al. 2004]. The viscoelastic behaviour strongly depends on the thermodynamic state of the material i.e. a heat can transform the chains of the polymer from a rigid state (glassy state) to a flexible state or even to liquid state (figure 2.6, right). The transition from a rigid state to a flexible state is also called the glass transition temperature (T_g) (section 2.2.1). Moreover, the load duration also has great influence on the behaviour of the polyvinyl butyral (creep) [Norville 1998]. At low temperatures (T = 0ºC) or at short load duration the interlayer is able to transfer full shear. At high temperatures or long load durations the shear capacity of the interlayer decreases significantly. Another type of interlayer is Sentry Glass Plus (SGP) of DuPont (Bennison et al. 2002). This interlayer has higher stiffness, better temperature resistance and larger strength than polyvinyl butyral and has better residual capacity after glass breakage [Decliné et al. 2008, Feirabend et al. 2008]. Other methods to laminate glass are resins or meltable plastics.
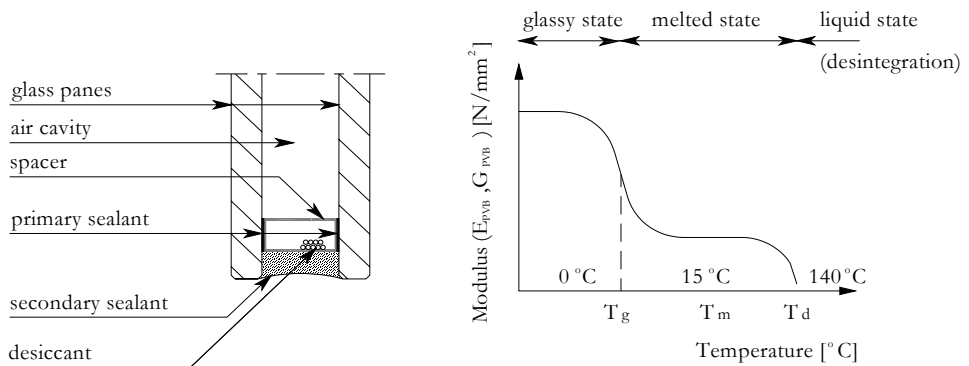
Figure 2.6:   Insulated double glass unit (left) and a schematic relation between the moduli and the temperature of polyvinyl butaryl (right)

2.3.3   Residual capacity

Laminated glass deals with the coherence of the broken glass panes (section 2.3.2) i.e. the adhered shards on the foil interlock [Sedlacek et al. 1999] and also has a structural relevance to improve the residual capacity of the broken glass pane. The residual capacity of a broken glass

pane is the duration between the glass breakage and the failure of the glass pane under dead weight and additional loading. The duration depends on the application of glass pane e.g. overhead glazing and accessible glazing. The interlocking depends on the fragmentation of the glass pane i.e. the larger the shards the better the residual capacity. Furthermore, the common boundary condition also plays an important role in the residual capacity [Ofner 2007]. Table 2.4 gives an overview of the residual capacity of two identical glass types in a laminated composition with regard to its boundary condition. The four-sided simply supported laminated annealed float glass and heat-strengthened float glass have good residual capacities by the large shards adhering on the foil. On the other hand, the residual capacity of laminated thermally toughened float glass is poor by the very small shards adhering on the foil (rolling up like carpet). The two-sided simply supported laminated glass of all glass types is poor, because the broken glass pane has a failure mechanism. Point fixed laminated heat-strengthened float glass have (slightly) better residual capacity than point fixed laminated thermally toughened float glass, because the laminated thermally toughened float glass tears off from the point fixed.

Table 2.4:   Residual capacity of two identical glass types in a laminated composition depending on the common boundary conditions

Glass type	Four-sided simply supported	Two-sided simply supported	Point fixed
Annealed	Very good	Poor	--
Heat-strengthened	Good	Poor	Moderate-good
Thermally toughened	Moderate-poor	Poor	Moderate-good

2.4   Current requirements

2.4.1   Requirements for glass applications

Table 2.5 gives an overview of the standards for glazing in the building envelope in Europe, the Netherlands, Germany, United Kingdom and the United States of America and their status. This section mainly deals with glazing in the building envelope at tertiary structural level (section 1.2). Accessible glazing, railings, balustrades and the like are beyond the scope. The purpose of standards is to guarantee the safety and the serviceability of building components and buildings by means of design rules. The standards for glass roofs and glass façades deal with the resistance against several out-of-plane loads (safety), the limitation of the out-of-plane displacements (serviceability) and often additional performance requirements (safety). However, the additional performance requirements are not fully covered by the standards [Haldimann et al. 2008] and therefore, full-scale tests have to be carried out to prove the safety of glass elements e.g. the residual capacity after glass breakage (section 2.3.3).

The standards distinguish between vertical glazing and overhead glazing at tertiary level. Vertical glazing has an inclination of less than 10° or 15° to the vertical. Overhead glazing has

an inclination of larger than 10° or 15° to the vertical, because people can be present under the glazing.

Table 2.5: *Overview of standards in Europe, the Netherlands, Germany, United Kingdom and the United States of America and their status*

Countries	Standard (series)	Status
Europe	prEN 13474-1 and 2	Withdrawn early 2007
The Netherlands	NEN 2608 1 to 4	Final/in preparation
Germany	DIN 18008 1 to 7	Draft/in preparation
UK	BS 6262	Final
USA	ASTM E 1300-04e1	Final

The withdrawn European standard prEN 13474-1:1999 [prEN 13474-1 1999] deals with the general basis for the design with glass panes subjected to out-of-plane loads. These standard series do not cover loads such as thermal loads, seismic loads, impact loads, in-plane loads and explosion loads. The structural design deals with ultimate limit state (strength) and serviceability limit state (out-of-plane displacements) based on partial safety factors. The structural safety verification given in equation 2.7 checks if the effective design stress ($\sigma_{eff;d}$) is not larger than the inherent flexural tension strength ($f_{g;d}$).

$$\sigma_{eff;d} \leq f_{g;d}$$ (Equation 2.7)

The maximum principle (tension) stresses at the glass surface determine the probability of fracture. Fracture of glass rather initiates in a tension area with comparatively large surface defects than at the position of the calculated largest maximum principle stress. Therefore, the probability of failure is determined by a weighted average value of the distribution of the max principle stresses at the surface calculated by equation 2.8 and is called the effective design stress ($\sigma_{eff;d}$).

$$\sigma_{eff;d} = \left[\frac{1}{A} \int_A \left(\sigma_{1(x,y)} \right)^\beta dxdy \right]^{\frac{1}{\beta}}$$ (Equation 2.8)

Parameter A is the entire surface of the glass pane. The maximum principle stress (σ_1) is located at point (x,y) on the surface. The effective design stress does not take into account the residual stresses. The parameter β is the shape parameter of the two parameter Weibull function representing the lower end of the glass strength distribution, i.e. $\beta = 25$. The design method for the inherent flexural tension strength in prEN 13474-1:1999 and prEN 13474-2:2000 [prEN 13474-2 2000] is based on the so-called DELR (Damage Equivalent Load and Resistance) design method [Sedlacek et al. 1999] and adapted by the design method of Shen

and Siebert [Haldimann 2006]. The inherent flexural tension strength for annealed float glass is given in equation 2.9a and for prestressed float glass is given in equation 2.9b.

$$f_{g;d} = k_{mod} \frac{f_{g;k}}{\gamma_m k_A} \gamma_n$$ (Equation 2.9a)

$$f_{g;d} = \frac{f_{b;k} - f_{g;k}}{\gamma_v} + k_{mod} \frac{f_{g;k}}{\gamma_m k_A} \gamma_n$$ (Equation 2.9b)

With $k_A = A^{0.04}$

The characteristic value for the inherent flexural tension strength ($f_{b;k}$) of annealed float glass is 45 N/mm². The characteristic value for the fracture strength of thermally toughened float glass and heat strengthened float glass ($f_{g;k}$) is 120 N/mm² and 70 N/mm² respectively. The contribution of the residual stress to the failure strength is included by subtracting the characteristic value for the fracture strength from the characteristic value for the inherent strength ($f_{b;k}-f_{g;k}$). The coefficient for the size factor (k_A) takes into account the size of the surface area and is independent of the residual stresses. The modification factor (k_{mod}) captures the load duration, load combination and environmental conditions (table 2.6). The partial factor (γ_m) takes into account the inherent strength in ultimate limit state e.g. float glass (γ_m =1.8). The partial factor (γ_n) takes into account the residual stresses in ultimate limit state e.g. float glass (γ_v =2.3). The national partial factor (γ_n) is mostly 1.0.

Table 2.6: Modification factor (k_{kmod}) adopted from prEN 13474-1:1999

Load duration	Load type	k_{mod}
Short	Wind	0.72
Medium	Snow	0.36
Long	Dead weight	0.27

The design procedure in prEN 13474-2:2000 (based on prEN 13474-1:1999) can be used for flat single glass panes, laminated and insulated double glass units of all glass types subjected to uniformly distributed out-of-plane loads such as dead weight, snow load, wind load and cavity pressure in insulated double glass units. The standard excludes in-plane loaded glass panes. The standard is applicable for rectangular, circular, right angled triangular and isosceles shapes of simply supported glass panes. Other shapes such as trapezoidal and rectangular glass panes with one raked edge or arched edge can also be calculated. A rectangular glass pane can be supported two-, three- and four-sided. The calculated maximum principle tension stresses (σ_{max}) and out-of-plane displacements (w) are calculated with the linear plate theory. The rectangular glass panes are only provided with effective design stresses ($\sigma_{eff;d}$). The four-sided simply supported rectangular glass panes can also be calculated with the theory of large out-of-plane

displacements. Finally, the standard mentions that if the glazing is part of the supporting structure the design has to be included that glass breakage shall not result in structural damage.

The structural regulations for common applications for buildings in the Netherlands are established by law in the NEN standards. Two structural standards are available for the calculation of glass panes at tertiary level. NEN 2608-1 [NEN 2608-1 2007] is a standard for the calculation of four-sided simply supported rectangular glazing in vertically installed glazing which is only subjected to the out-of-plane load case wind. The glass products are single glass panes, laminated and insulated double glass units. The verification is a load check given in equation 2.10. The design value of the local wind load (p_d) is equal or smaller than the design value of the ultimate limit state resistance against wind load (R_u) given in equation 2.11.

$$p_d \leq R_u \qquad \text{(Equation 2.10)}$$

$$R_u = \gamma_r \frac{f_{mt;u;rep}}{\gamma_m} \frac{t_{(e;)d}^2}{A} \qquad \text{(Equation 2.11)}$$

Equation 2.11 contains the ratio factor (γ_r) for the length and width of the glazing given in a table, the representative value for the ultimate flexural tension strength ($f_{mt;u;rep}$) is 50 N/mm², the material factor (γ_m), the thickness (t_d) of the monolithic glass pane or equivalent thickness ($t_{e;d}$) of the laminated or insulated double glazing and the size of the glazing (A).

NEN 2608-2 [NEN 2608-2 2007] deals with uniformly distributed out-of-plane loads such as dead weight, wind load, snow load and isochoric pressure in the cavity of non-vertically installed glazing. Non-vertically installed glazing has an angle between 0º to 80º with the horizontal. It is applicable for all rectangular glass types in monolithic glass panes, laminated and insulated double units. These NEN-series will be extended in the future by part 3 and 4 concerning specific loads e.g. concentrated load on non-vertical glazing accessible for maintenance and glass balustrades respectively. The scope of NEN 2608-2 clearly excludes the application of glass as secondary bearing structure such as beams and as primary bearing structure such as a stability system of a building. A stress check is used whether the glass pane meets the structural requirements (strength). Thereby is checked if the occurring bending tension stress/maximum principle stress ($\sigma_{i;d}$) which has to be equal or smaller than the ultimate flexural tension strength ($f_{mt;u;d}$) (equations 2.13a and 2.13b) according to equation 2.12. Furthermore, these standard series do not prescribe any requirements with respect to the consequence of failure. NEN 3569 [NEN 3569 2001] regulates the proper choice of glass panes in the considered application to prevent against injury of people after glass failure.

$$\sigma_{i;d} \leq f_{mt;u;d} \qquad \text{[Equation 2.12]}$$

$$f_{mt;u;d} = \frac{f_{g;k} k_b k_e k_{\text{mod}}}{\gamma_m} \qquad \text{[Equation 2.13a]}$$

$$f_{mt;u;d} = \frac{f_{g;k} k_b k_e k_{\mathrm{mod}}}{\gamma_m} + \frac{f_{b;k} - f_{g;k}}{\gamma_v}$$

[Equation 2.13b]

The characteristic values for the inherent flexural tension strength ($f_{b;k}$) of annealed float glass, the fracture strength ($f_{g;k}$) of thermally toughened float glass and heat strengthened float glass and the fracture strength from the characteristic value for the inherent strength ($f_{b;k}$-$f_{g;k}$) are the same as prescribed in the European standards. The crack behaviour of the glass pane, the quality of the edge finishing and the load duration are captured in factors k_b, k_e and k_{mod}, respectively. The partial factor (γ_m) takes into account the inherent strength in ultimate limit state e.g. float glass (γ_m =1.8). The partial factor (γ_v) takes into account the residual stresses in ultimate limit state e.g. float glass (γ_v =1.4).

In Germany, the draft versions of DIN 18008 series are very similar to the draft versions of the European standards. The draft versions of DIN 18008 series will consist of seven parts enclosing a broad application of glazing and are based on the partial safety factors which are in conformity with other structural standards such as steel and timber [Siebert et al. 2008]. The present design of glazing in Germany is regulated by easy design rules in e.g. TRLV [TRLV 2006] and TRAV [TRAV 2003] and are based on global safety concepts and experience [Siebert et al. 2008]. The TRLV deals with regulations and statements for vertical and overhead glazing supported by linear bearings subjected to uniformly distributed out-of-plane loads including climatic loads for insulated double glazing. Glazing which is adhesively bonded to the façade (structural sealant glazing), acting as bracing element (primary structural level) and bent glazing are beyond the scope of the regulation. The stress check is based on allowable stress (equation 2.14). In which σ_E is the maximum principle stress, calculated using the characteristic values of the loads in N/mm² and σ_{adm} is the allowable principle stress in N/mm² based on experimentally found fracture strength divided by a global safety factor which includes all uncertainties and variances associated with loads, resistance and modelling.

$$\sigma_E \leq \sigma_{adm}$$

[Equation 2.14]

In the United States, the standard ASTM E 1300 [ASTM E 1300 2004] deals with vertically installed and sloped (overhead) glazing subjected to out-of-plane load cases dead weight, wind and snow with a total value less or equal than 10 kPa. The glazing is single, laminated and insulated double glass units. The boundary conditions are four-sided, three-sided and two-sided simply supported and one sided clamp supported of rectangular glass pane sizes. The standard consists of extensive charts to determine the thickness of the glazing. The charts are based on the glass failure prediction model by Beason & Morgan [Beason et al. 1984] and on finite difference stress and deflection analysis by Vallabhan [Vallabhan 1983]. The verification format is given in equation 2.15. In which q is the uniformly distributed out-of-plane load, LR is the load resistance, NFL is the non-factored load and GTF is the glass type factor. The standard is not applicable for other glass structures such as balustrades, floors and point supported glazing.

$$q \leq LR = NFL \cdot GTF$$

[Equation 2.15]

In the United Kingdom, the standard for vertical glazing is BS 6262 Part 3 [BS 6262-3 2005]. This standard provides glass thickness selection charts for annealed, thermally toughened, heat-strengthened and insulated double glass units subjected to out-of-plane load case wind. The boundary conditions are limited to four-sided simply supported rectangular glass pane sizes. The standard BS 6262 Part 6 [BS 6262-6 2005] deals with practically detailing and dimensioning for special applications of glass such as glass fins, simply bolted glass barriers and glass partitions. For overhead glazing no mandatory requirements are available except for accessible glazing. Laminated glass is usually applied for overhead glazing [CWCT 2004] and if the overhead glazing is subjected to falling objects, the hard body impact test has to be carried out in conformity to the European Standard EN 356:1999 [EN 356 1999].

2.4.2 Requirements for adhesive bonded joints

Nowadays, the adhesive bonded joint for glass panes is restricted to silicone adhesives [Weller et al. 2006b] for structural sealant glazing (abbr. SSG) at tertiary structural level. Structural sealant glazing entered in the sixties of the 20th century [Schober et al. 2004]. The glass pane is two-, three- or four-sided bonded with a silicone joint to the façade frame. The conditions for the silicone adhesives and the adhesive bonded joint are prescribed in a European guide line [ETAG 002 2003]. Silicone adhesives are durable inorganic elastomers [Habenicht 2006] which have good resistance against chemicals, ultra violet radiation and temperature loads. Silicone adhesives preserve sufficient elasticity at low temperatures and withstand elevated temperature [Carbary 2007]. Adhesives in general including silicone adhesives are sensitive for moisture. The mechanical properties are low tension strength, low shear strength, low Young's modulus and creep sensitiveness. This results in a design with low stresses and large bonding surfaces. This adhesive fills up the gap and its tolerance between the adhesively bonded parts and leads to a large joint thickness. Through this, the adhesive bonded joint is able to reduce peak stresses at change of temperature, but it is also a less stiff connection to transfer out-of-plane loads as well as in-plane loads.

1   mechanical self-weight support
2   retaining device to reduce danger in case of adhesive bond failure
3   structural sealant
4   structural sealant support frame
5   glas pane/unit
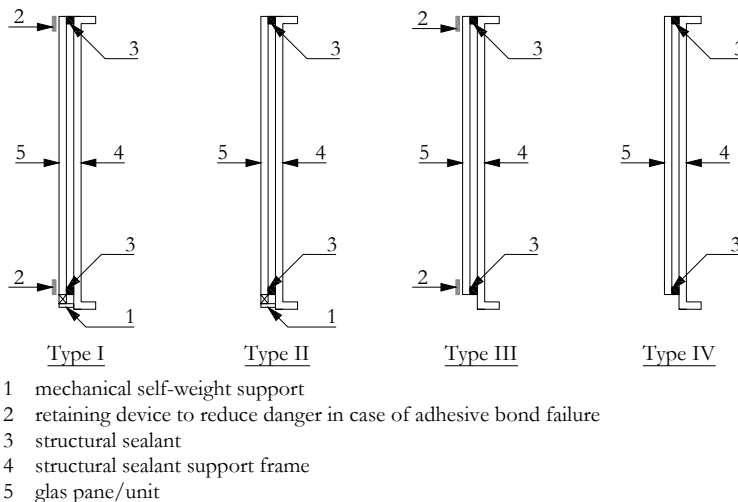
Figure 2.7:   *Types of structural sealant glazing in conformity to ETAG 002*

The ETAG 002 part 1 completed with European or national standards and national legislation deals with SSG in facades and roofs (tertiary structural level) which are supported (type I and II) or unsupported (type III and IV) (figure 2.7). The glass pane of type I has a mechanical self-weight support and a retaining device to reduce danger in case of adhesive bond failure. The structural sealant only resists out-of plane loads. Type II is comparable to type I, but has no retaining device. Type III has a retaining device only and the structural sealant resists out-of-plane loads and in-plane loads (dead weight). Type IV is comparable to type III, but has no retaining device. The restrictions are a linear silicone bead, factory applied and no edge may be entirely free. Type I and II are applicable for all types of glazing. Type III and IV are only applicable for single glass panes. The adhesion surfaces are uncoated or inorganic coated glass and anodised aluminium or stainless steel. The other parts of the European guideline deal with other adhesion surfaces such as organic coated glass and thermal breaks.

2.5 Research projects of in-plane loaded glass structures

The motivation to use in-plane loaded glass structures origins from the wish to create large transparent surfaces in the building envelope. The structural point of view is that a glass pane has the capacity to resist in-plane loads, but the absent of standards dealing with in-plane loads and the small amount of (scientific) research projects still make glass a uncommon structural material today. Table 2.7 gives an overview of research projects in which the glass pane is loaded in-plane. Some research projects of in-plane loaded glass structures are highlighted in sections 2.5.1 to 2.5.3.

Table 2.7:   Overview of research projects of in-plane loaded glass structures

Linear glass structures: columns
Güsgen 1998; Ludwig et al. 1998; Weiler 2000; Liess 2001b; Luible 2004; Kutterer 2005; Overend 2005 et al.

Linear glass structures: beams and fins
Carré 1997; Güsgen 1998; Hamm 2000; Hess 2000; Holberndt 2003; Wellershoff 2003; Freytag 2004; Kreher 2004; Luible 2004; Kasper 2005; Palumbo 2005; Belis 2006; Cruz et al. 2008b; Louter et al. 2008; Ølgaard et al. 2008; Antonelli et al. 2008, Hildebrand et al. 2008.

Glass plate structures
Rusch 2000; Laufs et al. 2001; Niedermaier 2003; Luible 2004; Schober et al. 2006; Wellershoff 2006; Englhardt 2008; Močibob 2008; Weller et al. 2008.

Linear adhesive bonded joints
Stutzki et al. 2004; Bucak et al. 2006; Hagl 2006; Weller et al. 2006b; Blandini 2007; Feldmann et al. 2008; Hagl 2008; Cruz et al. 2008a.

2.5.1   Linear glass structures

[Ludwig et al. 1998, Güsgen 1998] firstly investigated column buckling of glass elements for approvals followed by a systematic approach of single glass panes by [Weiler 2000, Liesss 2001b]. [Luible 2004] investigated the buckling behaviour of single and laminated glass. The glass types were heat-strengthened and thermally toughened glass panes. The boundary conditions were pinned connections. The glass columns had a constant width and variable column height. The main influences on the buckling strength were the initial out-of-plane imperfections, glass thickness, strength of the glass type and visco-elastic behaviour of the PVB-foil. The initial out-of-plane imperfections of annealed float glass were equal or smaller than L/2500 and of heat-strengthened, thermally toughened and laminated float glass were equal or smaller than L/300. Moreover, the measured glass thickness was always smaller than the nominal glass thickness. The strength of the glass panes depends on the glass type and the manufacturer of the heat-strengthened and tempered float glass. Exceeding the flexural tension strength on the glass surfaces leads to failure of the glass columns. [Overend et al. 2005] investigated cruciform glass columns and circular hollow glass columns subjected to a compression load. The boundary conditions were pinned connections. The cruciform glass columns were made with a continuous glass pane and two small glass panes which were perpendicular connected with an adhesive bonded joint to the middle of the continuous glass pane. The applied adhesive was epoxy. The applied glass types for the cruciform glass columns were annealed float glass and thermally toughened float glass. The applied glass type for the circular hollow glass column was borosilicate glass which was prestressed by an internal steel rod anchored at the end caps. The circular hollow glass columns showed significantly smaller values for failure load than predicted failure load (based on flexural buckling of the column), because glass breakage initiated at the end connection of the column. The cruciform glass columns also showed significantly smaller values for the failure load than predicted (based on the critical torsional buckling stress), because the end caps rotated.

[Carré 1997, Hess 2000] investigated glass beams to fracture and also observed the laterally out-of-plane displacement of the glass beam. [Güsgen 1998] investigated the lateral torsional buckling of single glass and laminated glass analytically. [Luible 2004, Kasper 2005] investigated the lateral torsional buckling of glass beams by means of experiments and finite element simulations. The out-of-plane displacements of the glass beam result in bending stresses in the weakest direction of the glass beam. The maximum bending tension stress in the glass beam was related to the reduced ultimate flexural tension strength of the applied glass pane. The reduction factor is a non dimensional decreasing factor presented in a diagram. [Belis 2006] investigated the lateral torsional buckling of single and laminated glass beams with experiments and finite element simulations. In the finite element analyses the laminated glass pane is transformed into a virtual single glass pane with the same out-of-plane stiffness. The equation for lateral torsional buckling was used for single as well as laminated glass.

Research projects of composed glass beams focus on obtaining ductile failure behaviour e.g. the glass pane acts as web and a ductile material such as steel acts as flange. The glass web is structurally bonded to the flange. So, the glass pane is loaded in-plane to transfer shear load and normal load. The flanges transfer normal loads and keep the composite glass beam together after glass failure, the desired ductility. [Hamm 2000, Kreher 2004] investigated the glass-timber beam. The web was single glass which was adhesively bonded to two timber flanges. The applied glass type was annealed float glass, because of the highest residual capacity

after the first cracks in the glass web ($F_{ultimate}/F_{crack} \approx 3$). The larger the residual stresses in the glass pane, the smaller the residual capacity of the glass-timber beam (thermally toughened glass $F_{ultimate}/F_{crack} = 1$). This glass-timber beam was realized as bearing element in a roof structure [Kreher et al. 2004]. [Palumbo 2005] investigated small span glass beams with adhesively bonded carbon fibre (external reinforcement) at the tension side of the glass beam. The applied glass type was annealed float glass, because of the favourable behaviour after cracking (residual capacity). This glass-carbon fibre beam was realized as a 6 meter span in a saddle roof. The glass beam was laminated in which the inner glass pane had structural performances and the two outer glass panes were the protective layers against accidental damages. [Cruz et al. 2008a, Cruz et al. 2008b] are investigating a suitable adhesive bonded joint (strength and stiffness) between the glass web and the timber flanges of a beam. The glass-timber beam is two sided simply supported with several spans and is subjected to a four point bending test. The timber flanges gives the ductility (residual capacity) and the glass pane the resistance and the stiffness. The motivations for the adhesive bonded joint are spreading in-plane loads between the timber flanges and the glass web, no weakening of the glass web by e.g. drilling holes and ductility of the composite beam. The applied adhesives were silicone, methacrylate, polyurethane, epoxy, acrylics superflex polymer and MS polymer. Shear test were carried out in which the test specimens were subjected to temperature and water saturation. More research has to be carried out such as UV radiation and aging. [Ølgaard et al. 2008] are investigating two-sided simply supported reinforced glass beams in which the adhesive bonded joint is a vital part. The bottom edge of the glass beam is provided with an adhesively bonded slack band. The purpose of the research is to realize a safe design with a ductile bending behaviour which is similar to an externally reinforced concrete beam. The applied adhesive is epoxy.

Some research projects deal with increasing the span larger than the maximum standard size of 6 meter (section 2.1) with respect to residual capacity. [Wellershoff 2003] investigated an adhesively bonded laminated glass pane web to two steel flanges with a span of 12 meter. [Freytag 2004] investigated a laminated glass web which was circumferentially enclosed by ultra high performance concrete (UHPC) with a span of 7.8 meter. The glass web was built up of single or laminated glass units. The glass type was thermally toughened glass. The glass-concrete beam has residual capacity after glass breakage. [Louter et al. 2008] are investigating two concepts, namely the reinforced single glass beam with stainless steel and the adhesively bonded multi-layered glass segments for large spans with regard to ductility and redundancy (safe failure behaviour). The applied glass type is annealed float glass. The reinforced glass beam is two-sided simply supported and is subjected to a four point bending test. The conditions of reinforced glass beams are: elevated temperature, salty moisture exposure and load duration which affects the strength of the adhesive. The applied adhesives are epoxy, polyurethane, acrylate and silicone. The reinforced glass beam is a redundant system which has a residual capacity even at elevated temperature, salty moisture conditions and long term load duration.

2.5.2   Glass plate structures

[Rusch et al. 2001] firstly investigated by means of experiments the behaviour of plate buckling of four-sided simply supported glass panes subjected to a uniformly distributed in-plane compression load in one direction. Non-metallic interlayers were placed between steel and glass pane. The applied glass panes were square (500 mm) with a nominal glass thickness of 6

mm. The glass types were annealed and thermally toughened float glass. The experiments clearly showed a post-buckling behaviour.

[Laufs et al. 2001] investigated the use of glass panes as bracing members in a flat lattice girder in combination with out-of-plane loads. The research was a theoretical approach with the support of finite element simulations. The investigation concentrated on the influence of the stability of the glass pane on varying boundary conditions and load introductions (figure 2.8). The in-plane compression loads were introduced at two opposite corners or at four corners of the glass pane. The boundary conditions for the out-of-plane loads were clamps at the corners or four-sided simply supported. Stability problems occurred for glass panes which were only supported by clamps at the corners. The strength of the glass edge reduced the in-plane capacity for the four-sided simply supported glass panes. The bending tension stress in the glass pane by the out-of-plane load was not critical.
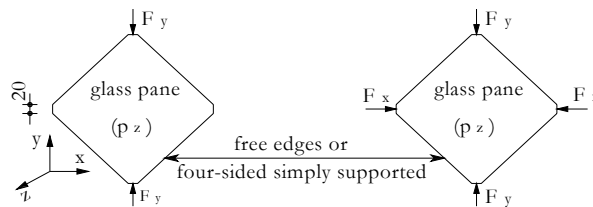
Figure 2.8: Research project Laufs et al.

[Luible 2004] investigated plate buckling of four-sided simply supported glass panes subjected to a uniformly distributed in-plane compression load in one direction (figure 2.9, left) by means of experiments, finite element simulations and analytical models. The applied glass panes consisted of square (laminated) heat-strengthened float glass with several glass thicknesses. The failure load was much larger than the ideal buckling load and showed post buckling behaviour. The glass panes failed by exceeding the ultimate flexural tension strength on the glass surface and restricted the buckling capacity of the glazing. The ultimate flexural tension strength of glass was dependent on the load duration, the amount of damages on both glass faces and the degree of residual stresses during tempering. Furthermore, other main parameters on the buckling capacity were the glass thickness and initial out-of-plane imperfections. The shear stiffness of the polyvinyl butyral foil is a main parameter for laminated glass.
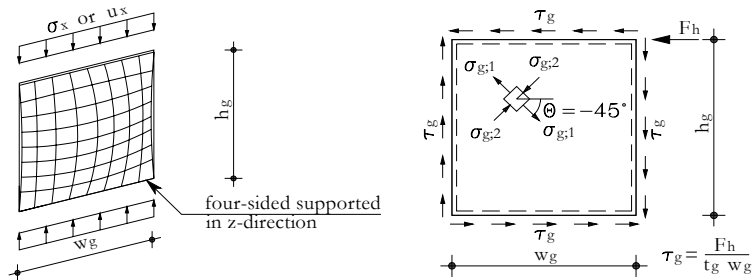
Figure 2.9: Research project Luible (left) and a glass pane subjected to purely in-plane shear load (right)

[Wellerhoff 2006] investigated the replacement of the compression members by plane glass panes in modern grid shells as stabilizing structural element by means of experiments, finite element simulations and analytical models. He defined two systems (figure 2.10). System A was a discrete connection provided with mortar or with a symmetrical countersink at each corner of the glass pane which acted as bracing element. The discrete connection was connected to the node of the spatial grid structure. System B was a circumferentially two-sided adhesively bonded glass pane to the spatial grid structure which acted as a pure shear wall (figure 2.9, right). The applied adhesives were polyurethane and acrylate. The applied glass panes were (laminated) heat-strengthened glass and were subjected to in-plane load only or were combined with out-of-plane load. The results of system B are given here. The linear buckling theory was applicable for circumferentially adhesively bonded single glass panes and laminated glass panes. The latter needed a correction factor to involve the effect of the shear stiffness of the PVB foil. The circumferentially adhesively bonded glass pane activated tension diagonals. Three positions with large surface tension stress concentrations were identified (figure 2.10), namely in the vicinity at the centre of the glass pane at the front side along the tension diagonal by the out-of-plane displacements (I), in the vicinity of the corners of the glass pane at the rear side along the compression diagonal by the out-of-plane displacements (II) and in the anchorage of the tension diagonal in the adhesive bonded joint (III). The size of the fragmentation of the broken glass pane depended on the magnitude of the stress concentration.

Positions with large surface tension stress concentrations
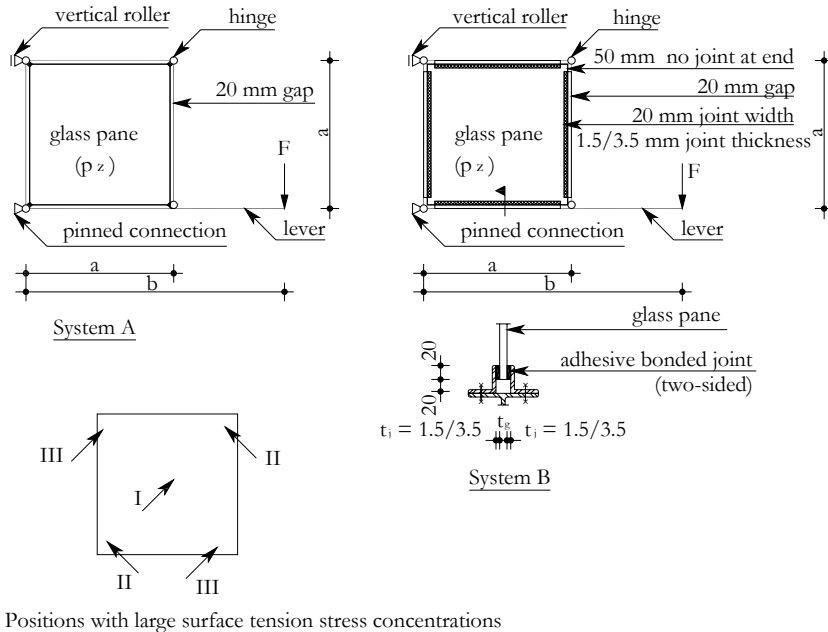
Figure 2.10:   *Research project Wellershoff*

[Močibob 2008] investigated two connection concepts to transfer a horizontal in-plane load at the top, a vertical in-plane load from the roof and a uniformly distributed out-of-plane load through a rectangular glass pane (figure 2.11). The two connection concepts were the point supported and the two-sided flexible linear supported glass panes. The point supported glass

panes were provided with four drilling holes. Each drilling hole was provided with a bolt and injection mortar to fill up the gap between the glass and the bolt. The injection mortar eliminated the play and forms a non metallic interlayer. Three different point supported connections were investigated in small tests, namely the axial rigid connection (figure 2.11), the eccentric rigid connection and the eccentric pinned connection. The point supported connection transferred in-plane loads as well as out-of-plane loads. The two-sided flexible linear supported glass panes had an adhesive bonded joint at the top and the bottom of the glass pane. The applied adhesive was structural silicone. Two setting blocks at the top as well as the bottom were placed between the glass pane and the transom. The adhesive bonded joint transferred the horizontal in-plane load, the vertical in-plane load as the result of in-plane rotation of the glass pane and the out-of-plane load. The setting block transferred the vertical in-plane load of the roof and the vertical in-plane load as the result of the in-plane rotation of the glass pane. All glazing was laminated and the applied glass type was heat-strengthened. His research consisted of experiments, finite element simulations and analytical models.

The axial rigid connection yielded the best results for the in-plane load transfer in the small scale tests and it was used in the full scale tests. The axial rigid connection is centric resulting in a larger resistance and smaller in-plane displacements than the eccentric rigid connection and the eccentric pinned connection. The full scale test of the point supported concept showed small horizontal in-plane displacements at the top and small out-of-plane displacements of the glass pane, because the tension diagonal supported the compression diagonal. The glass pane failed along the compression diagonal, initiated at the drilling hole. The horizontal in-plane stiffness increased at increasing glass pane thickness. The full scale tests of the linear supported concept showed large horizontal in-plane displacement at the top and large out-of-plane displacement of the glass pane, because the tension diagonal is not able to support the compression diagonal (no anchoring of the tension diagonal). The glass pane failed along the compression diagonal, initiated at the setting block. The horizontal in-plane stiffness also increased at increasing thickness of the glass pane. Yielding of the adhesive strongly influenced the buckling resistance of the glass pane and enlarged the ductility. Because of the large horizontal in-plane displacements and the small in-plane stiffnesses has the linear supported concept has a limited potential as a load bearing structure for transferring horizontal in-plane loads than the point supported concept.
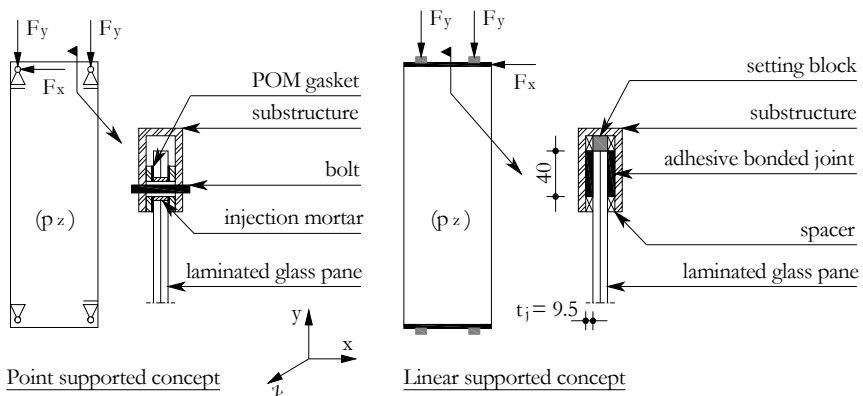
Figure 2.11:   Research project Močibob

[Niedermaier 2003] investigated the use of glass panes as stiffening element within light-weight timber structures. The glass pane was connected to the timber frame with a circumferentially adhesive bonded joint (figure 2.12). The load bearing capacity and the in-plane displacement at the top were investigated for normal use and in case of failure. The glass pane (0.8m x 1.6m) was bonded with silicone or polyurethane adhesive to the timber framework. The concentrated load acted at a top corner of the timber frame with a magnitude of 1 kN and represented wind load. The magnitude of the in-plane displacement at the top and the stress distribution in the glass pane was dependent on the geometry of the adhesive bonded joint and the adhesive type. The adhesive bonded joint was intact after testing. The bearing capacity of a broken glass pane was also investigated. A pendulum broke the glass pane before the glass pane was loaded in-plane. The displacement at the top was roughly two times larger than the tests of the unbroken glass panes. It showed good remaining bearing capacity.
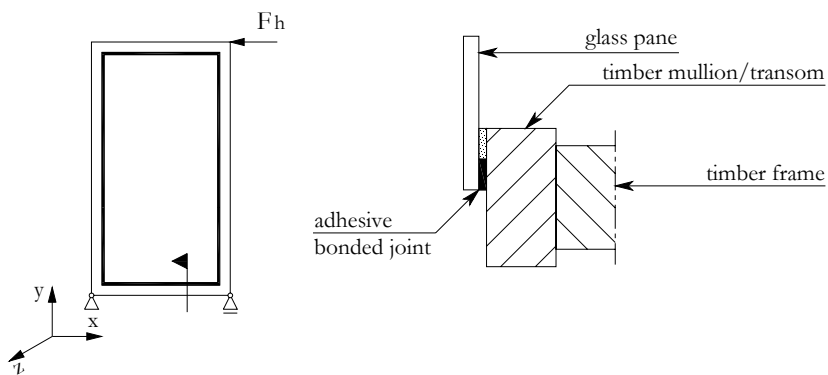
Figure 2.12:   Research project Niedermaier and Schober et al.

[Schober et al. 2006] investigated the circumferentially adhesive bonded insulated double glass unit (1.250m x 2.5m) to stiffen a timber structure of e.g. conservatories, facades and houses (figure 2.12). The research contained the structural, the physical and the realization aspects with the objective to achieve a general permission for applying in buildings in Germany. The applied adhesives were silicones and acrylates. The system was still intact at a horizontal in-plane load of 2 kN and 5 kN for the silicone and acrylate joint respectively at a horizontal in-plane displacement of 5 mm (height/500).

2.5.3   Linear adhesive bonded joints

The research projects in the field of adhesively bonded glass panes have been increasing over the last few years. This section gives a brief overview of the main motives for research projects on adhesives and adhesive bonded joints for glass applications.

The ETAG 002 guide line regulates the linear silicone joint, structural sealant glazing (section 2.4.2). Nevertheless, the knowledge of the real mechanical properties of silicone adhesives is limited and therefore, the silicone joint has to be tested destructively instead of the usual calculations by standards [Hagl 2006]. The structural sealant glazing and the ETAG 002 are not applicable for intentionally in-plane loaded glass panes. The working group FKG

(Fachverband Konstruktiver Glasbau) focuses on the development of theoretical models for silicone adhesives based on experiments and finite element analyses. The objectives are to design arbitrary bonding geometries, to optimize them with respect to the most apparent failure mechanism, to set up simple design rules and criteria and to limit the tests for each application. The research project is not limited to silicones. In the near future, adhesives such as acrylics, polyurethanes and epoxies will be investigated as adhesive bonded joint for glass structures. These adhesives could offer many advantages e.g. a transparently adhesive bonded joint and higher strength. The latter will lead to smaller bonding surfaces and thinner adhesive bonded joints. The advantages of other adhesive types than silicone are emphasized by many researchers [Blandini 2007, Feldmann et al. 2006, Nijsse 2004, Weller et al. 2006b]. The most of these adhesive types are organic adhesives i.e. the polymer has a carbon basis structure [Habenicht, 2006] and makes an adhesive more susceptible for aging, moisture, temperature and load duration. These conditions also have to be investigated [Louter et al. 2008, Blandini 2008].

[Weller 2007a] is investigating three types of adhesive bonded joints for the application in glass structures, namely the point, the linear and the surface adhesive bonded joint. The research is carried out by means of experiments and theory. The structural adhesives are silicones, polyurethanes, epoxies and acrylics. The research demonstrates that on adhesive bonded joints for glass application are possible. The building practice needs technical approval for adhesive bonded glass structures, because the expertise of adhesive bonded joints is restricted to a small group of people.

[Wellershoff et al. 2005] investigated the behaviour of two types of adhesive bonded joints for glass and steel, namely the point and linear adhesive bonded joints by means of experiments. The experiments for the linear adhesive bonded joints were carried out on an overlap at different load durations and different environments (UV-radiation, humidity and temperature). The structural adhesives were silicones, polyurethanes, epoxies and acrylics. The shear stiffnesses of the polyurethanes and the acrylics were larger than the shear stiffness of the usual silicones. On the other hand, the shear stiffnesses of the polyurethanes and the acrylics decreased at increasing temperature while the silicones remained unchanged.

[Overend 2002] investigated adhesive bonded double overlap and compared it with bolted double overlap tests. The failure load (glass failure) of the adhesive bonded double overlap was approximately three times larger than the bolted double overlap. Furthermore, initial stiffness of the adhesive bonded double overlap specimens was larger than the bolted double overlap, because the adhesive bonded double overlap had a very small play in relation to the bolted double overlap. The deformation at failure of the adhesive bonded double overlap was approximately three times smaller than the deformation at failure of the bolted double overlap.

[Blandini 2007, Blandini 2008] is investigating the adhesive bonded joint along the edges of the glass pane to design self-bearing structural glass shells without any metal frame or metal connection. The advantages of the adhesive bonded joint are to mobilize the in-plane capacity of the glass pane more efficiently and to increase the transparency by a small linear connection. Tension, shear and bending tests were designed and carried out under several temperatures and load durations on glass butt joints. The applied adhesives were acrylics, epoxies and polyurethanes. The adhesives were selected on a butt joint width of at least 1 mm, an acceptable viscosity for applying and curing the adhesive (not flow), a curing at room

temperature, a minimum bulk tension strength of 4 N/mm² and a Young's modulus of at least 200 N/mm². Further investigations are needed for suitable pre-treatments of the substrates and the long term behaviour. The adhesion problems at high temperatures require further product development.

2.6 Conclusions

A resume of the literature review has been given in this chapter and the following conclusions can be drawn.

The current requirements for glass applications are restricted to linearly supported glazing at tertiary structural level in the building envelope subjected to uniformly distributed out-of-plane loads. Therefore, the strength of glass is restricted to the ultimate bending tension strength only. Requirements for other types of out-of-plane load, other types of supporting structure and other glass applications at tertiary structural level have been developed. The requirements explicitly exclude intentionally in-plane loaded glass panes and glass structures at primary structural level.

The requirements for glass applications at tertiary structural level also prescribe that overhead glazing, with an angle larger than 10° to 15° with the vertical has to be laminated to protect people against injury against falling glass. Moreover, the laminated glazing has to withstand for a while in the substructure, the so-called residual capacity.

The current requirements for adhesive bonded joints are restricted to structural sealant glazing. The adhesive bonded joint is loaded by the out-of-plane load case wind and/or the dead weight of the glazing. The requirements also prescribe the type of adhesive, namely silicones. The requirements explicitly exclude intentionally in-plane loaded glazing.

Many research projects on glass beams/fins (secondary structural level) deal with the stability of the slender laminated glass structures. However, research projects on glass columns (primary structural level) are rare.

Residual capacity of glass structures at secondary and primary structural level is a main design parameter to handle with the brittleness of glass. These glass structures have to be laminated at least. Many research projects have investigated the improvements of the residual capacity after glass breakage of glass structures. Recent research projects on especially glass beams have been focussing on composite glass structures with the purpose to have residual capacity after glass breakage in which the adhesive bonded joint plays a vital role.

The structural advantages of the adhesive bonded joint for glazing are recognized by many designers of glass structures and researchers. The adhesive bonded joint loads the brittle glass structure more effectively than the usual mechanical connections. Moreover, for architectural reasons, the adhesive bonded joint is more aesthetic than mechanical connection.

Many research projects have investigated several adhesive types which have larger stiffness than the usual silicones used in structural sealant glazing. However, the behaviour of the adhesive under load duration and several ambient environments are still research topics.

A new field of research are in-plane loaded glass plate structures, because glass panes have the potential to stiffen frameworks (primary structural level). Most of these research projects focus on stability of the glass pane.

From the literature review in this chapter, it can be concluded that only a few research projects have been carried out to use the in-plane stiffness of glass panes for building stabilization (primary structural level). The circumferentially adhesively bonded glass panes were subjected to pure in-plane shear load. No research projects have been carried out to brace a steel façade frame with circumferentially adhesive bonded joint subjected to a horizontal in-plane load at which the circumferentially adhesive bonded joints are small or are carried out with epoxies.

3   Experiments

This chapter deals with experiments of the systems. Section 3.1 concerns the motivation and objective for carrying out these experiments. Section 3.2 discusses the test rig in which the system was placed. The system which is built up of a steel frame, glass pane and one of the three defined adhesive bonded joints including the applied adhesives are discussed in section 3.3. Section 3.4 discusses the measurements and the test programme. Section 3.5 discusses the response of the steel frame and section 3.6 discusses the measurement basics. Section 3.7 discusses the results and the evaluation of the experiments for system with joint types 1 to 3. Finally, this chapter ends with conclusions in section 3.8.

3.1   Motivation and objective

Several approaches can be used to understand and to solve a problem, such as analytical, numerical or experimental research. The latter is a time-consuming and expensive approach. However, experimental research reveals much more valuable information than other approaches can yield. Moreover, glass panes and adhesives are hardly used as structural building materials especially the circumferentially adhesive bonded glass panes for the stabilization of a one-storey building (primary structural level) (section 2.5.2). Therefore, the behaviour of in-plane loaded glass panes and the properties of adhesives (appendix C) have to be explored experimentally. After that, the next step is to simulate the experiments with finite element models (chapter 4). The results and the accompanying observations are necessary to calibrate the finite element model and, to define its restrictions. The calibrated finite element models are used for parametric studies in chapter 5.

The objective of the experiments is to gather information by observing and measuring the response of the adhesively bonded glass pane to a steel frame, called 'the system' in this thesis, subjected to a horizontally concentrated in-plane load at the right top corner (RTC) of the frame. The glass pane is the bracing element and is circumferentially adhesive bonded to the steel frame with one of the three defined adhesive bonded joints (section 3.3.3). The basic assumption is that the transoms and mullions are infinite stiff (section 1.5) to investigate the glass pane and the adhesive bonded joint. The response consists of the in-plane stiffness of the system, the maximum horizontal in-plane load (failure), the stress distribution in the glass pane and the crack initiation and propagation in the glass pane. Furthermore, the possible residual capacity of the system after failure (sections 2.3.3 and 2.5) will be observed.

3.2   Test rig

The test rig (figure 3.1) enclosed the system and was needed to introduce the horizontal in-plane load at the RTC of the system and to support the system at the left bottom corner (LBC) and at the right bottom corner (RBC). The test rig was built up of four wide flange steel beams (European HEB300) provided with a regular pattern of holes (Ø26) in the flange as well as in the web. The vertical beams were placed between the horizontal beams and were connected

stiffly by bolts. The bottom beam was connected on two cross beams of type HEB300 for lateral stability of the test rig.
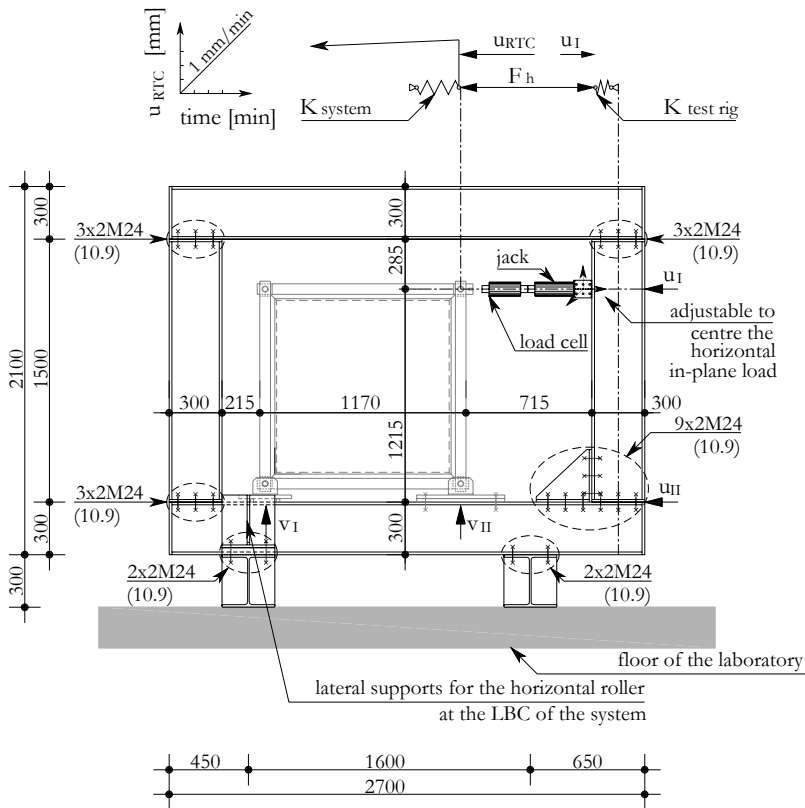
Figure 3.1:   Test rig including system

Three pilot tests (including a system) were carried out to check four in-plane displacements of the test rig till a horizontal in-plane load of 200 kN (range of the load cell). The four measured in-plane displacements were two vertical in-plane displacements of the bottom beam at the horizontal roller (v_I) and at the pinned connection (v_{II}) and two horizontal in-plane displacements at the bottom beam (u_{II}) and the right beam at the load introduction (u_I) (figure 3.1). The vertical in-plane displacements at the supporting structure and the horizontal in-plane displacement of the bottom beam were negligible small. On the other hand, the horizontal in-plane displacement of the test rig at the load introduction was large and not acceptable, because the displacement velocity of 1 mm/min at the RTC of the system (u_{RTC}) could not be guaranteed (figure 3.1). For improvement, a control loop was developed to guarantee the prescribed displacement velocity. Finally, the clearances in the test rig were also reduced after the pilot tests.

3.3   System

The test set-up of the system is given in figure 3.2. The system was built up of a steel frame, a supporting structure at the LBC and the RBC of the system, the introduction of the horizontal in-plane load at the RTC of the system and a square glass pane with one of the three defined joint types (section 3.3.3) adhesively bonded to the steel frame.

3.3.1   Steel frame

The steel frame is needed to gradually introduce the in-plane load into the brittle glass pane. Steel is a ductile material which redistributes stress concentrations at the load introduction, at the supporting structures and at the bolted connection between the outside beam and the beadwork. The steel frame had two steel transoms (bottom and top) and two steel mullions (right and left). Each transom and mullion was built up of two components, namely an outside beam and a replaceable beadwork. The beadwork supported the glass pane four-sided in z-direction. The outside beam had a rectangular cross section with width w_{ob} = 120 mm and height h_{ob} = 60 mm. The outside beam was provided with 14 smooth holes (diameter 10 mm) for connecting the beadwork. The outside beam of the transoms had a pen provided with a round hole and a sleeve-bearing bush at both ends. The sleeve-bearing bush was applied to reduce the friction under contact pressure. The outside beam of the mullions had a groove provided with a round hole at both ends. A round pin with diameter 30 mm connected the outside beam of the transom and the mullion to make a hinge connection. The pinned connection at the RBC of the system and the horizontal roller at the LBC of the system enclosed the outside bottom beam and were connected to the same pins. The pinned connection was bolted with 4 M24 -10.9 to the test rig. The horizontal roller was composed of two bars round 20 mm. The load introduction took place by a jack at the RTC of the system on an extended pen of the outside beam of the top transom. A socket and sphere were placed on the extended pen for a centric in-plane load introduction. The beadwork was made replaceable for two reasons. The first reason was that the groove was joint type dependent (figure 3.3). The second reason was that after each test the beadwork was removed to burn the adhesive from the beadwork safely in connection with noxious fumes. The beadwork was equipped with 14 holes with screw threat and was bolted with M10-10.9 to the outside beam. The beadworks and the steel strips were provided with a mitre at the ends. A small seam was made between the ends of the beadwork to avoid premature glass-steel contact. Appendix A.1 gives the specification of the applied components of the steel frame.

3.3.2   Glass pane

The glass panes were square with width w_g = 1.0 m and height h_g = 1.0 m. The nominal glass thickness $(t_{g,n})$ was 12 mm and the permitted tolerance varies between ±0.3 mm [EN 572-8 2004]. The nominal glass thickness of 12 mm with respect to its size of 1.0 m x 1.0 m is less susceptible for out-of-plane displacements. The mid-plane of the glass pane lined up with the centre of the outside beams and also coincided with the load introduction at the RTC of the system. The applied glass type was annealed float glass without additional surface finishing or follow-up treatment. Annealed float glass has the lowest strength of the available glass types (section 2.3.1), but on the other hand laminated annealed float glass has a favourable crack

pattern for residual capacity (table 2.4). In this research project was chosen for the investigation of single annealed float glass in stead of laminated glass to map a clear stress distribution in the glass pane induced by the adhesive bonded joint.
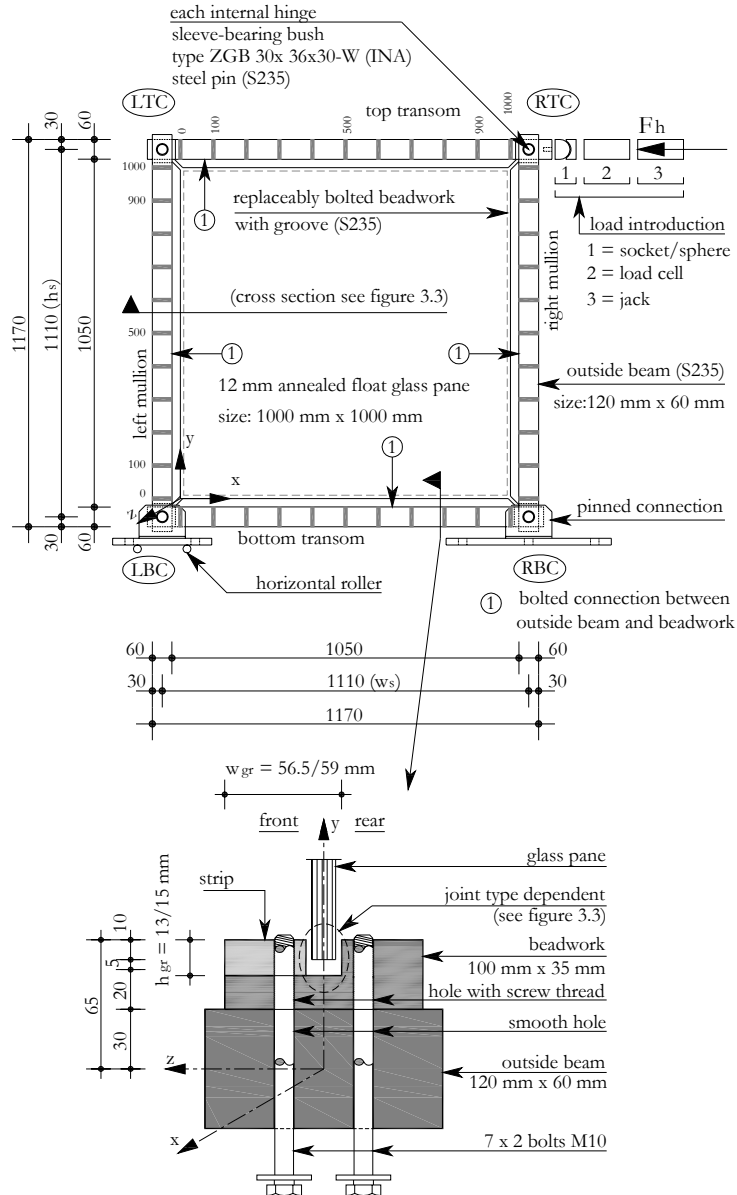
Figure 3.2:   *Specification of the system*

All edges of the glass pane were provided with two facets with an angle of roughly 45°. These facets were made in the plant of the glass supplier. The glass panes, used for joint type 1, had flat polished edges to increase the adhesion between the glass pane and the adhesive bonded joint. The glass panes, used for joint type 2 and 3, had flat ground edges. The flaws in the faces of new glass increase in amount and depth during service life (section 2.2.2). This aging process can be approached by pre-damages of the glass faces (section 2.2.2). Pre-damages also make the tin side and atmospheric side equally (sections 2.2.2). This is omitted, because the load duration was short to cause additional face damages. Moreover, the adhesive bonded joint was tested within few days and therefore the adhesive bonded joint was not subjected to considerable aging. The experiments can be considered as short duration tests (e.g. load case wind) at room temperature for new glass panes.

3.3.3 Adhesive bonded joints and adhesives applied

Three circumferentially adhesive bonded joints have been defined in this thesis to mobilize the in-plane stiffness of a glass pane. In spite of the well-known disadvantages of adhesive bonded joints e.g. aging, an adhesive bonded joint is a proper joining technique for glass structures (section 2.5.3). The main benefits of adhesive bonded joints for in-plane loaded glass panes are to spread the in-plane load between glass pane and steel and to avoid direct glass-steel contact (section 2.2.2). A main basic assumption was that the geometry of the adhesive bonded joint was kept as small as possible for the benefit of maximum transparency. The geometry of the adhesive bonded joint was determined by the type of adhesive.

Joint type 1 (figure 3.3, left top) was a circumferentially flexible adhesive bonded joint across the full thickness of the glass pane and was based on an integral profile. An integral profile is a rubber band between the glass pane and frame. The in-plane load transfer between glass pane and steel frame was centric. The gap between glass pane and steel frame depended on tolerances and therefore a gap-filling adhesive was the most suitable one e.g. silicone adhesives or polyurethane adhesives. The minimum joint thickness is 6 mm prescribed by [ETAG 002 2003]. Setting blocks were placed between the glass pane and the bottom transom to transfer the dead weight of the glass pane and to support the glass pane during curing. Joint type 2 (figure 3.3, right top) was a two-sided stiff adhesive bonded joint along the edges of the glass pane. The in-plane load transfer between glass pane and steel frame was also centric. The thickness of the joint depended on the tolerances of the glass pane and the steel frame. The adjustable strip accommodated these tolerances. To guarantee the joint thickness spacers were placed between the glass pane and the steel frame. The joint thickness can be kept small. Setting blocks were placed between the glass pane and the bottom transom to transfer the dead weight of the glass pane and to support the glass pane during curing. An appropriate adhesive was e.g. epoxy. Joint type 3 (figure 3.3, bottom) was a one-sided stiff adhesive bonded joint along the edges of the glass pane. This joint type had to carry out easier than joint type 2, but the in-plane load transfer between glass pane and steel frame was eccentric. The geometry, tolerances and type of adhesive of this one-sided adhesive bonded joint were comparable to joint type 2.

Two types of adhesive were applied, namely polyurethane adhesive for joint type 1 and epoxy adhesive for joint type 2 and 3. The polyurethane adhesive was Sikaflex-252 [Sika 2004] and behaves flexibly at room temperature. Appendix C gives mechanical properties (tension, compression and shear) of the polyurethane adhesive obtained by experiments. The

polyurethane adhesive is a one component adhesive and cures with moisture in the ambient air. The mechanical performances of polyurethane adhesives such as shear strength and shear modulus are better than silicone adhesives (section 2.5.3). Before applying the polyurethane adhesive a primer (Sika Activator) was used. This was recommended by the supplier. The epoxy adhesive was Scotch Weld 9323 B/A [3M 1995]. The epoxy adhesive is a two component adhesive with stiff and toughened properties at room temperature. Shear strength and shear modulus of the epoxy adhesive are larger than the polyurethane adhesive applied for joint type 1. Therefore, a small geometry of the adhesive bonded joint can be realized. Appendix C gives mechanical properties (shear) of the epoxy adhesive obtained by experiments. The application of the adhesive for each joint type is described in appendix A.2.
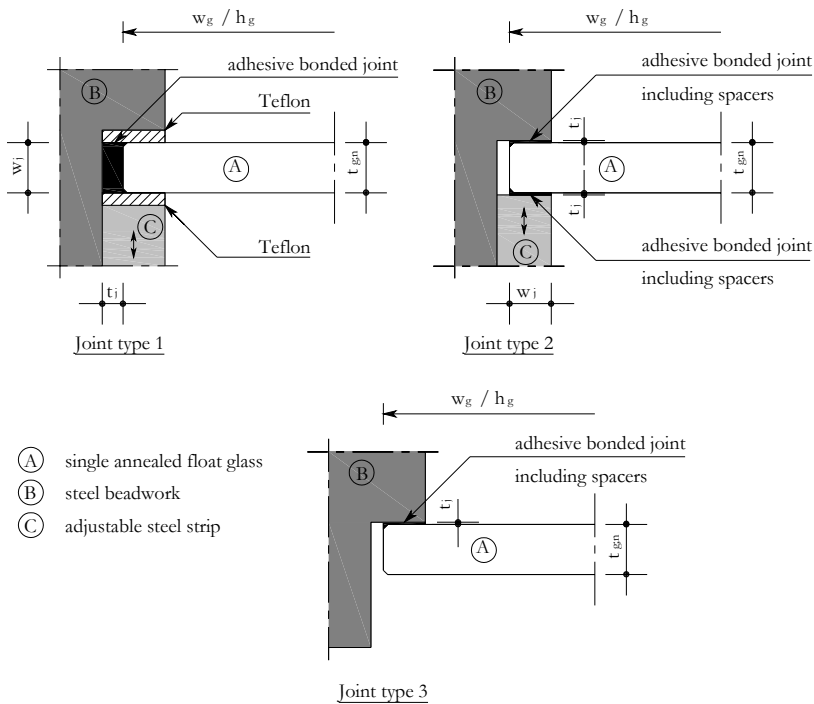
Figure 3.3:   Joint types 1 to 3

3.4   Measurement technique

3.4.1   Geometry of the glass pane

Figure 3.4 shows eight points for measuring the actual glass thickness (t_{g1} to t_{g8}) of each tested glass pane, namely at each corner and in the middle of the edge. The heights and the widths of the glass pane were also measured to determine the actual shape of the glass pane. The measurements are tabulated in appendix A.6. It has to be noticed that the out-of-plane imperfections of the entire glass pane in the system were not measured before testing.
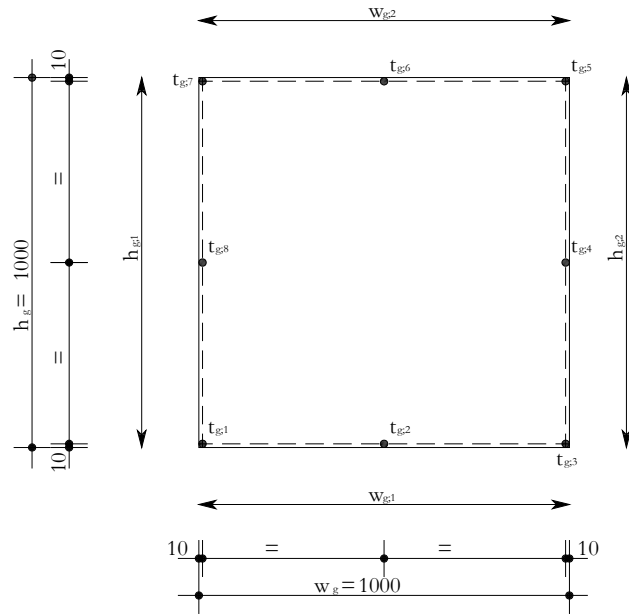
Figure 3.4:   *Measurement of actual glass thickness at points 1 to 8 ($t_{g;1}$ to $t_{g;8}$) and actual glass pane size*

3.4.2   Measuring the response of the system

The horizontal in-plane load (F_h) at the RTC of the system was displacement controlled with a velocity of 1 mm/min. A control loop guaranteed the velocity till the end of the test (section 3.2). The measuring programme is given in figure 3.5. The in-plane load was measured by a load cell. The horizontal in-plane displacements were measured with displacement gauges (LVDT = linear variable displacement transducer) at the LTC (u_{LTC}), RTC (u_{RTC}) and the LBC (u_{LBC}) of the steel frame (figure 3.5) with respect to the floor of the laboratory. A relative horizontal in-plane displacement ($u_{MT;rel}$) was measured between the glass pane and the top transom at the middle. A relative vertical in-plane displacement ($v_{MR;rel}$) was measured between the glass pane and the right mullion at the middle. The out-of-plane displacements were measured with displacement gauges (LVDT) at the centre of the glass pane (w_{centre}), at the LTC (w_{LTC}) and the RTC (w_{RTC}) at the rear side of the steel frame with respect to the floor of the laboratory. The strains were measured at five points on the front of the glass pane. Points 1, 2, 4 and 5 were located 100 mm from the edge of the glass pane in both directions and point 3 was located at the centre of the glass pane. At each point three strains (rosette) were measured in three different directions, namely horizontal (0°), vertical (90°) and at an angle of 45°. The additional measurement of the strain at an angle of 45° was needed for calculating the principle stress (section 3.6.2). All values were measured each 5 seconds. The measuring equipment is given in appendix A.4. Finally, during each test a high speed camera constantly recorded the glass pane for the crack initiation and propagation. The white lines on the steel frame with a regular distance of 100 mm (figures 3.5 and 3.6) are an aid to locate the crack initiation and propagation. The device specification of the high-speed camera and the measurements with the

high-speed camera are given in appendix A.5. Figure 3.6 gives an impression of the test set-up and table 3.1 gives an overview of the test programme. The ambient conditions in the laboratory are given in appendix A.3. The number of valid tests for each system with joint types 1 to 3 is at least 3.
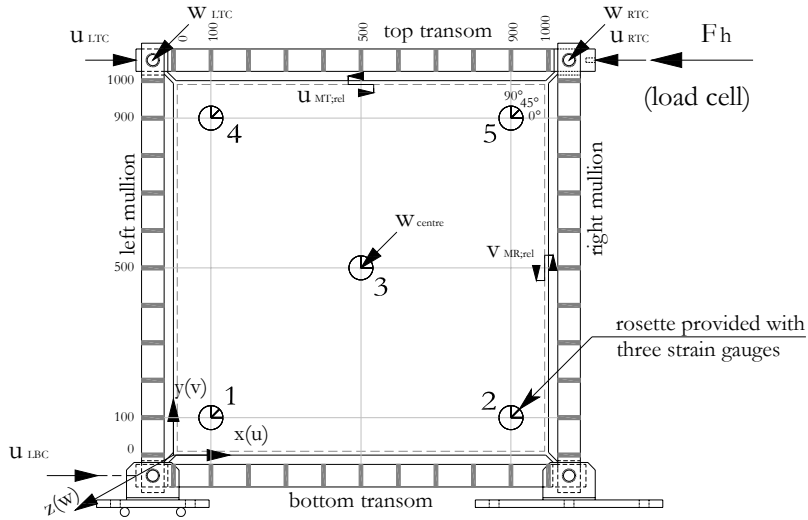
Figure 3.5:   Measuring programme
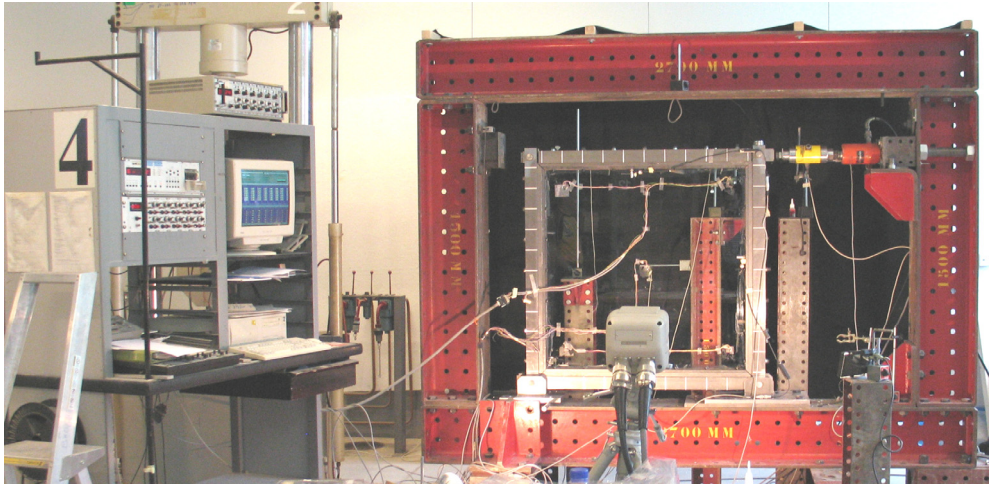
Figure 3.6:   Impression of the test set-up in Pieter van Musschenbroeck laboratory at Eindhoven University of Technology

Table 3.1:   *Overview of test programme*

Joint type			1	2	3
Test number			18, 19 and 20	2, 3 and 17	5, 6, 7 and 8
Type of adhesive			Polyurethane	Epoxy	Epoxy
Glass pane size	$w_g = h_g$	[mm]	1000	1000	1000
Nominal pane thickness	$t_{g;n}$	[mm]	12	12	12
Joint thickness	t_j	[mm]	6.0	0.5	0.5
Joint width	w_j	[mm]	12	10	10
Curing time before testing	t_c	[days]	7	3	3

3.5   Response of the steel frame

After the experiments of the systems with joint types 1 to 3 the response of the steel frame was further investigated. Two components of the system had influence on the system behaviour, namely the supporting structures and the bolted connection between the outside beam and the beadwork.

3.5.1   Boundary conditions of the supporting structures

The measured horizontal in-plane displacement at the RTC of the system was actually built up of two separate horizontal in-plane displacements, namely the horizontal in-plane displacement of the system and the horizontal in-plane displacement from the rotation of the entire system. The rotation of the entire system was the consequence of the vertical in-plane displacement of the pinned connection at the RBC of the system. This effect includes for all systems with joint types 1 to 3 and has to be eliminated. In an auxiliary test the response of the horizontal roller and the pinned connection was checked and described in appendix B.1. The in-plane displacements were acceptable for the assumed supporting structures except for the vertical in-plane displacement of the pinned connection. Therefore, the response of the pinned connection had to be adapted to a vertical spring with a stiffness of $K_{y;RBC}$ = 103.16 kN/mm[1] till a horizontal in-plane load of F_h = 100 kN. Equation 3.1 gives a correction on the horizontal in-plane displacement at the RTC of the system and is used in this thesis. So, $u_{RTC;s}$ is the in-plane stiffness of the system and u_{RTC} is the induced horizontal in-plane displacement at the RTC of the system including the effect of the vertical in-plane displacement at the RBC of the system. The system width (w_s) and the system height (h_s) are the distance between the hinge connections of the steel frame (figure 3.2).

$$u_{RTC;s} = u_{RTC} - \frac{F_h}{K_{y;RBC}} \left(\frac{h_s}{w_s} \right)^2 \qquad\qquad \text{(Equation 3.1)}$$

3.5.2 Behaviour of the bolted connection between the outside beam and the beadwork

The transoms and mullions of the steel frame were built up of an outside beam and a beadwork connected with bolts (section 3.3.1). The response of the bolted connection was checked by a four-point bending test. The results are given in appendix B.2. The bolted connection between the outside beam and the beadwork showed 'shear flexibility'. The shear flexibility is the result of the clearance of the hole in the outside beams. Moreover, the shear flexibility between the outside beam and the beadwork reduced the flexural stiffness of the transoms and the mullions. This shear flexibility is used in the finite element model for the simulations of systems with joint types 1 to 3 (chapter 4).

3.6 Measurement basics

3.6.1 In-plane stiffness of the system

An important value for the calculation of the stability of a building is the in-plane stiffness of the stabilizing elements. The in-plane stiffness of the system (K_s) is determined by equation 3.2 in which the horizontal in-plane displacement at the RTC of the system is the corrected horizontal in-plane displacement ($u_{RTC;s}$) adopted from equation 3.1.

$$K_s = \frac{F_h}{u_{RTC;s}}$$ (Equation 3.2)

3.6.2 Principle stresses

To find the in-plane load transfer through the glass pane, the measured strains had to be converted into principle stresses. The principle stresses are needed, because the failure criterion for glass is the maximum principle tension stress (sections 2.2.2 and 2.4.1). Furthermore, the distribution of the principle stresses more visualises the load transfer than the distribution of strains. The rosettes at points 1 to 5 measured the horizontal strain ($\varepsilon_{0°}$), the vertical strain ($\varepsilon_{90°}$) and the strain at an angle of 45° ($\varepsilon_{45°}$) (figure 3.7). The strain rosettes were placed on a sufficient distance from the edges of the glass pane and therefore it can be considered a two-dimensional strain/stress state. Equations 3.3a and 3.3b calculates the maximum principle stress ($\sigma_{g;1}$) and the minimum principle stress ($\sigma_{g;2}$) respectively from the measured strains of a rosette [Timoshenko et al. 1970]. Equation 3.4 gives the accompanying angle (θ) of the maximum principle stress with the horizontal. The actual Young's modulus (E_g) and the actual Poisson's ratio (v_g) of the glass panes were not measured. The values for the Young's modulus and the Poisson's ratio have been given in table 2.2.

$$\sigma_{g;1} = \frac{E_g}{2(1-v_g)}\left[(\varepsilon_{0°} + \varepsilon_{90°}) + \sqrt{2(\varepsilon_{90°} - \varepsilon_{45°})^2 + 2(\varepsilon_{0°} - \varepsilon_{45°})^2}\right]$$ (Equation 3.3a)

$$\sigma_{g;2} = \frac{E_g}{2(1-v_g)} \left[(\varepsilon_{0°} + \varepsilon_{90°}) - \sqrt{2(\varepsilon_{90°} - \varepsilon_{45°})^2 + 2(\varepsilon_{0°} - \varepsilon_{45°})^2} \right] \quad \text{(Equation 3.3b)}$$

$$\tan 2\theta = \frac{2\varepsilon_{45°} - \varepsilon_{90°} - \varepsilon_{0°}}{(\varepsilon_{0°} - \varepsilon_{90°})} \quad \text{(Equation 3.4)}$$
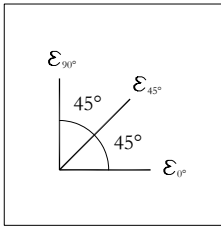
Figure 3.7:   Rosette with strain gauges

3.7 Results and evaluation of the experiments

3.7.1 Systems with joint type 1

<u>Test results</u>

Table 3.2 gives the horizontal in-plane displacement at the RTC of the system (u_{RTC}), the horizontal in-plane load (F_h), the corrected horizontal in-plane displacement at the RTC of the system ($u_{RTC;s}$), the in-plane stiffness of the system (K_s), the out of-plane displacement at the centre of the glass pane (w_{centre}), the relative horizontal in-plane displacement between the glass pane and the top transom ($u_{MT;rel}$), the relative vertical in-plane displacement between the glass pane and the right mullion ($v_{MR;rel}$) and the horizontal in-plane displacement at the LBC of the system (u_{LBC}) at limited horizontal in-plane displacement at the RTC of the system, at the glass-steel contact and at the maximum in-plane load. In advance of parametric studies (chapter 5) and mechanical models (chapter 6) the horizontal in-plane displacement has to be limited, in connection with the service life (section 2.5.2). The limitation of the horizontal in-plane displacement at the RTC of the system is $^1/_{300}$ of the height of the system ($u_{RTC;lim} = 3.70$ mm) [NEN 6702 2001].

Figure 3.8 shows the relation between the horizontal in-plane load and the horizontal in-plane displacement at the RTC of the system. The relation is bi-linear with a gradual transition between two stages. The first stage is less steep and more regular than the second stage. In the first stage the horizontal in-plane load gradually increases till the transition of two stages after which the in-plane load more increases in the second stage. For all stages, the horizontal in-plane displacements at the LTC of the system correspond with the horizontal in-plane displacements at the RTC of the system. The horizontal in-plane displacements at the LBC of the system were around 0.04 mm at the limited horizontal in-plane displacement at the RTC of

the system and around 0.16 mm and 0.60 mm at the glass-steel contact and at the maximum horizontal in-plane load respectively. All tests were stopped at a horizontal in-plane displacement at the RTC of the system of 40 mm, because the maximum displacement range of the jack was reached.
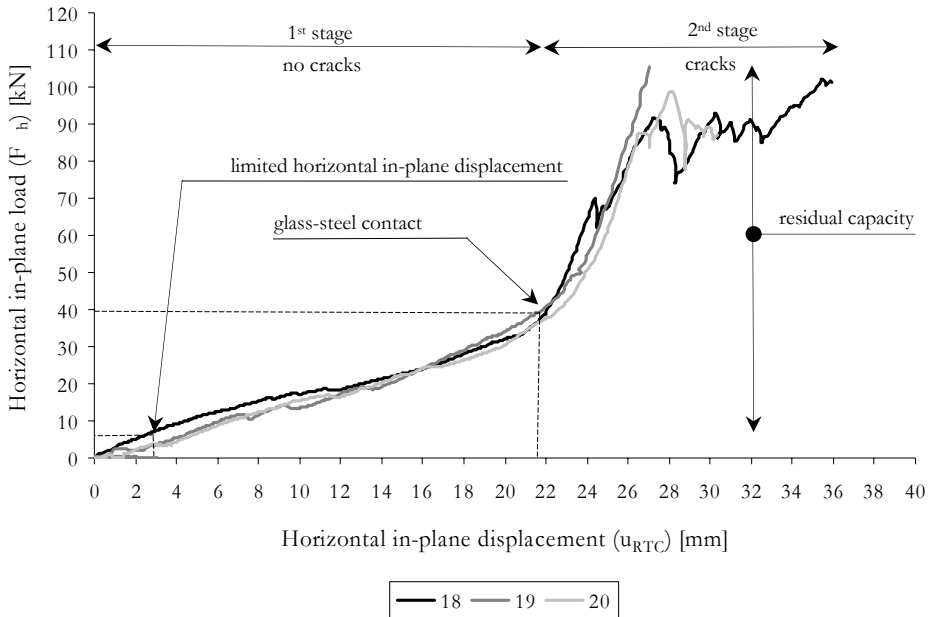
Figure 3.8:   Relation between the horizontal in-plane load and the horizontal in-plane displacement at the RTC of the system

In the first stage, the glass pane was gradually shifting horizontally in-plane and rotating in-plane which was observed visually (figure 3.11, left top). The horizontal in-plane displacements of the top transom were larger than the horizontal in-plane displacements of the top of the glass pane (relative horizontal in-plane displacements) and the vertical in-plane displacements of the right mullion were smaller than the vertical in-plane displacements of the right side of the glass pane (relative vertical in-plane displacements). Furthermore, the glass pane was still four-sided supported and had no cracks. The adhesive bonded joint was intact till halfway the first stage (figure 3.11, left top). Then the adhesive bonded joint was gradually pushing away at the LBC and the RTC and was gradually tearing and pulling off from the steel at the RBC and the LTC. At the end of the first stage, the adhesive bonded joint was completely pushed away at the LBC and RTC (figure 3.11, right top) and glass-steel contact occurred. At the beginning of the second stage the glass pane instantaneously started cracking and flaking off at the LBC and the RTC of the glass pane resulting in an in-plane shift of the glass-steel contact from the LBC and the RTC to the field of the transoms and the mullions (figure 3.11, bottom). Figure 3.9 visualizes the cracking of the glass pane at the moment of the maximum in-plane load (high-speed records). Moreover, the glass pane was only laterally supported at the LBC and the RTC of the glass pane. Cracking of the glass pane was audible and visible. The steel transoms

and mullions were slightly curved at the end of the first stage and were curving more and more in the second stage (figure 3.11 bottom) what could be observed visually.
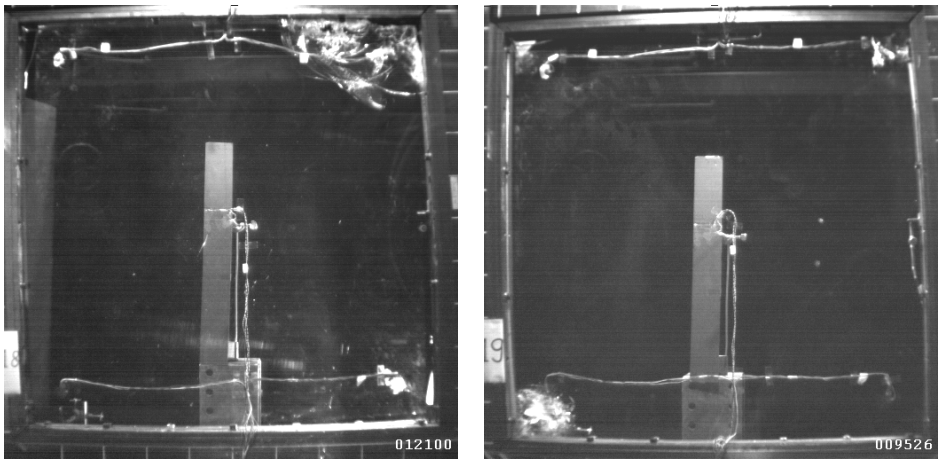
Figure 3.9:   High speed records at the moment of the maximum in-plane load for test 18 (left) and test 19 (right)
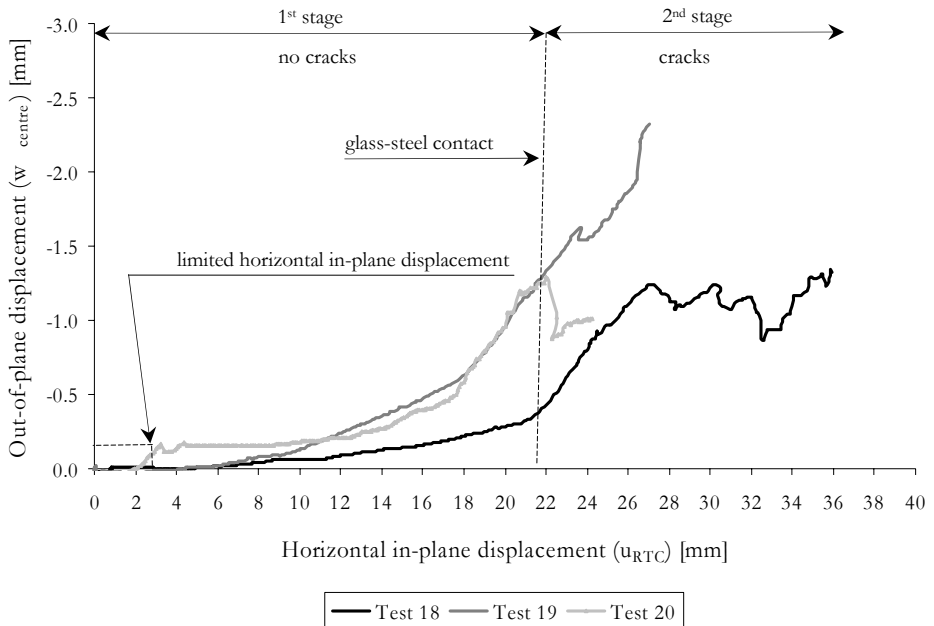
Figure 3.10:   Relation between the out-of-plane displacement at the centre of the glass pane and the horizontal in-plane displacement at the RTC of the system

Figure 3.10 shows the relation between the out-of-plane displacement at the centre of the glass pane and the horizontal in-plane displacement at the RTC of the system. The out-of-plane displacements gradually increase at increasing horizontal in-plane displacements at the RTC of the system in the first stage. In the second stage, the out-of-plane displacements increase more than in the first stage. However, the out-of-plane displacements of the LTC and the RTC of the steel frame remain close to zero during all tests.

adhesive bonded joint is torn and pulled off from the steel frame

F h

in-plane rotation

horizontal in-plane shift

adhesive bonded joint is pushed away

in-plane rotation

horizontal in-plane shift

F h

circumferentially adhesive bonded joint intact

all transoms and mullions are slightly curved

Stage 1 at small horizontal in-plane displacements

At glass-steel contact

in-plane shifting of the glass-steel contact by cracking and further pushing away of the adhesive bonded joint

F h

in-plane rotation

horizontal in-plane shift

adhesive bonded joint is further tearing and pulling off from the steel frame

curving of all transoms and mullions

Stage 2 from glass-steel contact

Figure 3.11:   States of the system at small horizontal in-plane displacement at the RTC of the system (left top), at glass-steel contact (right top) and in the second stage (bottom) (exaggerated drawn and the groove is skipped for clarity)

Table 3.2: *Overview of measuring results at limited horizontal in-plane displacement ($u_{RTC;lim}$ = 3.70 mm), at glass-steel contact and at maximum horizontal in-plane load*

	Test		18	19	20	Average	Standard deviation
Limited u_{RTC}	u_{RTC}	[mm]	3.65	3.71	3.70	3.69	0.03
	F_h	[kN]	5.05	4.67	3.55	4.42	0.78
	$u_{RTC;s}$	[mm]	3.60	3.67	3.66	3.64	0.04
	K_s	[kN/mm]	1.40	1.27	0.97	1.21	0.22
	w_{centre}	[mm]	0.00	0.01	0.01	0.01	0.00
	$u_{MT;rel}$	[mm]	1.19	0.88	1.15	1.07	0.17
	V_{MRrel}	[mm]	0.82	1.28	1.09	1.06	0.23
	u_{LBC}	[mm]	0.03	0.05	0.03	0.04	0.01
Glass-steel contact	u_{RTC}	[mm]	21.58	21.43	22.52	21.84	0.59
	F_h	[kN]	36.87	38.99	39.40	38.42	1.36
	$u_{RTC;s}$	[mm]	21.21	21.04	22.13	21.13	0.12
	$K_{s;sec}$	[kN/mm]	1.74	1.85	1.78	1.79	0.06
	w_{centre}	[mm]	-0.38	-0.25	-0.42	-0.35	0.09
	$u_{MT;rel}$	[mm]	6.12	6.57	6.01	6.23	0.30
	V_{MRrel}	[mm]	5.54	7.18	5.76	6.16	0.89
	u_{LBC}	[mm]	0.11	0.19	0.18	0.16	0.04
Maximum F_h	u_{RTC}	[mm]	27.30	27.01	28.18	27.50	0.61
	F_h	[kN]	91.54	105.50	98.75	98.60	6.98
	$u_{RTC;s}$	[mm]	26.38	25.96	27.19	26.51	0.63
	w_{centre}	[mm]	-1.24	-1.32	-1.28	-1.28	0.04
	u_{LBC}	[mm]	0.57	0.63	0.61	0.60	0.03

Figure 3.12 gives an overview of the maximum principle stresses ($\sigma_{g;1}$), the minimum principle stresses ($\sigma_{g;2}$) and their directions (θ) at limited horizontal in-plane displacement at the RTC of the system (figure 3.12, top), at glass-steel contact (figure 3.12, middle) and at maximum horizontal in-plane load (figure 3.12, bottom). The principle stresses at limited horizontal in-plane displacement at the RTC of the system are biaxial compression stresses at points 1 and 5 except for point 1 of test 18 and biaxial tension stresses at points 2 and 4 except for point 4 of tests 18 and 19. The principle stresses at point 3 have a tension stress directed to the RBC and a compression stress directed to the RTC. Moreover, the compression stresses were larger than the tension stresses in all points except for test 18. The principle stresses at glass-steel contact clearly show larger compression stresses at points 1, 3 and 5 compared to the tension stresses at all points. The principle stresses at points 1 and 5 are biaxial compression stresses in which the minimum principle stresses are the largest compression stresses. The principle stresses at point 3 have a tension stress directed to the RBC and a compression stress directed to RTC.

The sign of principle stresses at points 2 and 4 varies. The principle stresses at maximum horizontal in-plane load are comparable to the principle stresses at glass-steel contact, but the compression stresses at points 1, 3 and 5 are much larger.

Test 18 at Fh= 6.55 kN
Point 4: $\sigma_{g;1}$= 1.09, $\sigma_{g;2}$= -0.45, Θ = 1.06
Point 5: $\sigma_{g;1}$= -0.85, $\sigma_{g;2}$= -1.85, Θ = 35.78
Point 3: $\sigma_{g;1}$= 2.96, $\sigma_{g;2}$= -0.60, Θ = 36.52
Point 1: $\sigma_{g;1}$= 0.84, $\sigma_{g;2}$= -1.48, Θ = 29.52
Point 2: $\sigma_{g;1}$= 2.20, $\sigma_{g;2}$= 1.62, Θ = 39.93

Test 19 at Fh= 4.67 kN
Point 4: $\sigma_{g;1}$= 0.71, σ = -0.16, Θ = -33.70
Point 5: $\sigma_{g;1}$= -0.51, $\sigma_{g;2}$= -2.85, Θ = 35.78
Point 3: $\sigma_{g;1}$= 0.60, $\sigma_{g;2}$= -1.33, Θ = 45.00
Point 1: $\sigma_{g;1}$= -0.51, $\sigma_{g;2}$= -3.49, Θ = -21.73
Point 2: $\sigma_{g;1}$= 1.40, $\sigma_{g;2}$= 0.60, Θ = 40.93

Test 20 at Fh= 3.55 kN
Point 4: $\sigma_{g;1}$= 0.61, σ = 0.12, Θ = -22.50
Point 5: $\sigma_{g;1}$= -0.03, $\sigma_{g;2}$= -1.69, Θ = -15.48
Point 3: $\sigma_{g;1}$= 0.17, $\sigma_{g;2}$= -1.44, Θ = 40.93
Point 1: $\sigma_{g;1}$= -0.25, $\sigma_{g;2}$= -1.97, Θ = -0.73
Point 2: $\sigma_{g;1}$= 0.04, $\sigma_{g;2}$= 0.22, Θ = 13.28

Test 18 at Fh= 36.87 kN
Point 4: $\sigma_{g;1}$ -0.46, $\sigma_{g;2}$= -1.09, Θ = 2.60
Point 5: $\sigma_{g;1}$= -2.91, $\sigma_{g;2}$= -14.18, Θ = -0.58
Point 3: $\sigma_{g;1}$= 4.82, $\sigma_{g;2}$= -7.91, Θ = 41.41
Point 1: $\sigma_{g;1}$= -2.38, $\sigma_{g;2}$= -13.43, Θ = 17.25
Point 2: $\sigma_{g;1}$= 2.55, $\sigma_{g;2}$= 0.08, Θ = -32.01

Test 19 at Fh= 38.99 kN
Point 4: $\sigma_{g;1}$= 1.34, $\sigma_{g;2}$= 1.16, Θ = 45.00
Point 5: $\sigma_{g;1}$= -9.38, $\sigma_{g;2}$= -14.98, Θ = -14.58
Point 3: $\sigma_{g;1}$= 1.89, $\sigma_{g;2}$= -10.98, Θ = 43.73
Point 1: $\sigma_{g;1}$= -5.53, $\sigma_{g;2}$= -19.29, Θ = 21.83
Point 2: $\sigma_{g;1}$= 2.52, $\sigma_{g;2}$= -0.34, Θ = -42.71

Test 20 at Fh= 39.40 kN
Point 4: $\sigma_{g;1}$= 1.35, $\sigma_{g;2}$= -0.26, Θ = -40.93
Point 5: $\sigma_{g;1}$= -5.90, $\sigma_{g;2}$= -12.75, Θ = 0.94
Point 3: $\sigma_{g;1}$= 1.90, $\sigma_{g;2}$= -10.81, Θ = 41.91
Point 1: $\sigma_{g;1}$= -1.76, $\sigma_{g;2}$= -16.15, Θ = -12.02
Point 2: $\sigma_{g;1}$= 0.07, $\sigma_{g;2}$= -0.62, Θ = 40.27

Test 18 at Fh= 91.54 kN
Point 4: $\sigma_{g;1}$= -0.02, $\sigma_{g;2}$= -2.52, Θ = -21.58
Point 5: $\sigma_{g;1}$= -10.56, $\sigma_{g;2}$= -55.44, Θ = 30.52
Point 3: $\sigma_{g;1}$= 7.04, $\sigma_{g;2}$= -17.41, Θ = 41.26
Point 1: $\sigma_{g;1}$= -1.22, $\sigma_{g;2}$= -49.60, Θ = 39.27
Point 2: $\sigma_{g;1}$= 1.88, $\sigma_{g;2}$= 0.03, Θ = -13.67

Test 19 at Fh= 105.50 kN
Point 4: $\sigma_{g;1}$= 2.34, $\sigma_{g;2}$= -4.43, Θ = 44.28
Point 5: $\sigma_{g;1}$= -21.29, $\sigma_{g;2}$= -87.62, Θ = 39.76
Point 3: $\sigma_{g;1}$= 2.45, $\sigma_{g;2}$= -30.73, Θ = 44.66
Point 1: $\sigma_{g;1}$= -5.21, $\sigma_{g;2}$= -85.42, Θ = 44.29
Point 2: $\sigma_{g;1}$= 4.88, $\sigma_{g;2}$= -4.16, Θ = -42.11

Test 20 at Fh= 98.75 kN
Point 4: $\sigma_{g;1}$= 1.99, $\sigma_{g;2}$= -1.72, Θ = -42.80
Point 5: $\sigma_{g;1}$= -12.24, $\sigma_{g;2}$= -46.04, Θ = -43.41
Point 3: $\sigma_{g;1}$= 3.30, $\sigma_{g;2}$= -21.75, Θ = 42.98
Point 1: $\sigma_{g;1}$= -7.37, $\sigma_{g;2}$= -51.08, Θ = -37.10
Point 2: $\sigma_{g;1}$= 0.71, $\sigma_{g;2}$= -2.08, Θ = 44.42

Figure 3.12:   Overview of the principle stresses and their directions on the front of the glass pane at limited horizontal in-plane displacement (top), at glass-steel contact (centre) and at maximum horizontal in-plane load (bottom) at points 1 to 5

Discussion of the results

In the first stage, the flexibly enclosed glass pane has a gradually horizontal in-plane shift and an in-plane rotation within the steel frame that can be explained as follows. The top of the mullions has to follow the horizontal in-plane displacements of the top transom, because the mullions are hinged connected to the top transom. The top transom has larger horizontal in-plane displacements than the top of the glass pane which activates the adhesive bonded joint at the top in longitudinal direction ($u_{MT;rel}$ in table 3.2) resulting in horizontal shear stresses in longitudinal direction. The top side of the left mullion has more horizontal in-plane displacements than the top side of the glass pane which stretch out the adhesive bonded joint in normal direction resulting in normal tension stresses. The top side of the right mullion has more horizontal in-plane displacements than the top side of the glass pane which push in the adhesive bonded joint in normal direction resulting in normal compression stresses. The bottom of the mullions has smaller horizontal in-plane displacements than the top of the mullions. The horizontal in-plane displacements of the glass pane, activated by the top of the system, are pulled back by the bottom transom and the bottom side of the mullions. So, horizontal shear stresses in longitudinal direction occur in the bottom adhesive bonded joint, normal compression stresses (pushing in) in the underside of the left adhesive bonded joint between the left bottom side of the glass pane and the left bottom side of the mullion and normal tension stresses (stretching out) in the underside of the right adhesive bonded joint between the right bottom side of the glass pane and the bottom side of the right mullion.

The opposite horizontal in-plane displacements between the top side and the bottom side of the mullions result in in-plane rotation of the glass pane. So, the glass pane also undergoes vertical in-plane displacements directed to the transoms. The vertical in-plane displacements of the mullions are negligible small in relation to the vertical in-plane displacements of the glass pane (table 3.2). The right top side and the left bottom side of the glass pane have vertical in-plane displacements directed to the top transom and to the bottom transom respectively resulting in pushing in of the adhesive bonded joint (normal compression stresses). The left top side and the right bottom side of the glass pane have vertical in-plane displacements directed from the top transom and from the bottom transom respectively resulting in stretching out of the adhesive bonded joint (normal tension stresses).

At the beginning of the first stage, the circumferential adhesive bonded joint is intact and activates the glass pane in-plane (figure 3.11, left top). However, more in-plane load is transferred via the pushed in adhesive bonded joint (figure 3.12), because the lateral supports prevent bulging (out-of-plane displacements) which results in stiffer normal behaviour of the adhesive bonded joint. The stretched out adhesive bonded joint behaves less stiff, because the entangled chains of the polymers are restructured in load direction. This restructuring also concerns for the in-plane displacement in longitudinal direction of the adhesive bonded joint. Towards the end of the first stage, the in-plane load is more and more transferred by the pushed in adhesive bonded joint especially when the stretched out adhesive bonded tears (cohesion failure) or pulls off from the steel frame (adhesion failure). Moreover, the concentrated in-plane load transfer between the glass pane and the steel frame at the LBC and the RTC results in bending of the transoms and mullions (figure 3.11, right top).

In the first stage, the principle stresses in the glass pane are small and the glass pane is not susceptible for plate buckling. The influence of the initial out-of-plane imperfections such as

varying glass pane thickness and curvature of the glass pane on the out-of-plane displacement of the glass pane is small. Furthermore, the flexible adhesive bonded joint spreads the stresses in the glass pane resulting in no cracks in the glass pane.

At the end of the first stage, the adhesive bonded joint at the LBC and the RTC is pushed away between the glass pane and the steel frame and glass-steel contact occurs. From this point the second stage starts and the in-plane loads are only transferred by glass-steel contact (the stiffest way). The glass pane acts as a compression strut from the LBC to the RTC of the glass pane. The glass-steel contact leads to cracking of the glass pane in these corners. Furthermore, the in-plane load transfer between the steel frame and the corners of the glass pane leads to large local compression stresses accompanying with large tension stresses perpendicular to the compression stress (section 2.2.2) without any redistribution of stresses and cracks brittle. The flaking off of the LBC and the RTC leads to the rearrange of the glass-steel contact and thus the in-plane load transfer. The in-plane load transfer gradually goes away from the corner and loaded the transoms and mullions on bending which explains the clear curvature of the beams (figure 3.11, bottom).

The vertical in-plane displacements of the pinned connection at the RBC of the system (section 3.5.1) play more and more a role at increasing horizontal in-plane displacements at the RTC of the system. The vertical in-plane displacements of the RBC of the system lead to an in-plane rotation of the entire system. However, the contribution in the horizontal in-plane displacements of the RTC of the system is small (table 3.2) by the small in-plane stiffness of the system.

The in-plane stiffness of the system in the first stage is small, because the small normal stiffness of the adhesive bonded joint determines the in-plane stiffness of the system. The in-plane stiffness of the system at the beginning of the second stage increases by glass-steel contact. However, the in-plane stiffness of the system in the second stage strongly depends on the cracks.

Finally, the residual capacity is good after limited horizontal in-plane displacement of 3.70 mm, because a largely visual horizontal in-plane displacement without cracking in the first stage followed by visually and audibly cracking of the glass pane in second stage at increasing horizontal in-plane load.

3.7.2   Systems with joint type 2

Test results

Figure 3.13:   Relation between the horizontal in-plane load and the horizontal in-plane displacement at the RTC of the system

Table 3.3 gives the values for the horizontal in-plane displacement at the RTC of the system (u_{RTC}), the horizontal in-plane load (F_h), the out-of-plane displacement at the centre of the glass pane (w_{centre}), the relative horizontal in-plane displacement between the top transom and the glass pane ($u_{MT;rel}$), the relative vertical in-plane displacement between the right mullion and the glass pane (v_{MRrel}) and the horizontal in-plane displacement at the LBC of the system (u_{LBC}) at the first and final crack. Table 3.4 gives the values as mentioned in table 3.3, but at a horizontal in-plane load of about 46 kN, in which the glass pane of all tests were non-cracked to compare the measured results better. Table 3.4 is completed with the corrected horizontal in-plane displacement at the RTC of the system ($u_{RTC;s}$) and the in-plane stiffness of the system (K_s).

Figure 3.13 shows the relation between the horizontal in-plane load and the horizontal in-plane displacement at the RTC of the system. The relation gradually declines at increasing horizontal in-plane displacement at the RTC of the system. The discontinuities in the relation are the cracks in the glass pane. Figure 3.15 left shows a schematic overview of the crack sequence. The first crack of all tests (number 1 in figure 3.15 left) occurred at the RBC of the glass pane at different horizontal in-plane loads (table 3.3). The crack was small and had a fancy-like pattern. The following crack (number 2 in figure 3.15 left) was a diagonal at the RBC or the LTC corner of the glass pane. The crack at the RBC of the glass pane initiated from the bottom transom to the right mullion and was observed at test 2 and 3. The crack at the LTC of

61

the glass pane initiated from the left mullion to the top transom and was observed at test 17. The final crack of all tests (number 3 in figure 3.15 left) was a diagonal initiating from the LBC to the RTC of the glass pane at different horizontal in-plane load (table 3.3). Figure 3.16 shows high-speed shots at the moment of the final crack for test 3 (left) and test 17 (right). The glass pane was disintegrated at a different way. Test 2 had many glass shards which were fractured regularly at an angle of 45° and the broken glass pane remained in the system after the test (figure 3.15, right). At test 3 the glass pane enclosed by the LBC, RBC and the RTC was bounced out and at test 17 the entire glass pane bounced out. Moreover, the fragmentation of the glass pane of tests 3 and 17 were smaller than the fragmentation of the glass pane of test 2. All cracks were audible and visible, but the first crack was hardly to see in some cases. Moreover, the adhesive bonded joint remained intact and pieces of glass stuck on the adhesive bonded joint. The horizontal in-plane displacement of the top transom was slightly more than the horizontal in-plane displacement of the top of the glass pane (relative horizontal in-plane displacement). The vertical in-plane displacement of the right side of the glass pane was slightly more than the vertical in-plane displacement of the right mullion (relative vertical in-plane displacement).
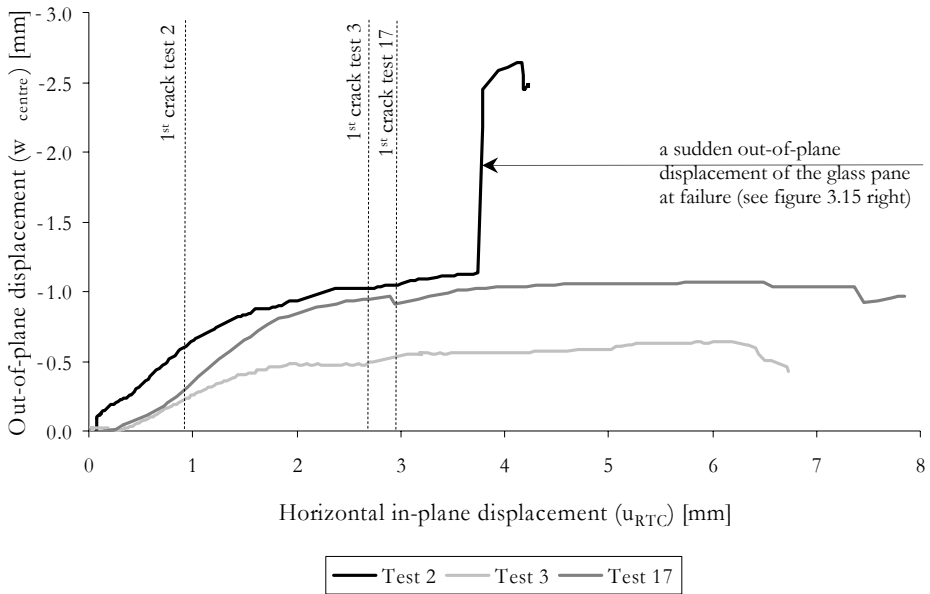
Figure 3.14:   Relation between the out-of-plane displacement at the centre of the glass pane and the horizontal in-plane displacement at the RTC of the system

Figure 3.14 shows the relation between the out-of-plane displacement at the centre of the glass pane and the horizontal in-plane displacement at the RTC of the system. The out-of-plane displacement at the centre of the glass pane was small and directed to the negative z-axis (rear) for all tests. The out-of-plane displacement of the LTC and the RTC of the system was negligible small and slightly increased to a maximum of two-tenth millimetre at the LTC at the failure load for all tests.

Table 3.3:   *Overview of measuring results at first crack and final crack*

	Test		2	3	17
First crack	u_{RTC}	[mm]	0.95	2.73	2.90
	F_h	[kN]	45.92	102.44	110.44
	w_{centre}	[mm]	-0.54	-0.49	-0.96
	$u_{MT;rel}$	[mm]	0.002	0.010	0.011
	$v_{MR;rel}$	[mm]	0.004	0.010	0.010
	u_{LBC}	[mm]	0.25	0.39	0.02
Final crack	u_{RTC}	[mm]	3.74	6.56	7.85
	F_h	[kN]	120.47	164.32	218.02
	w_{centre}	[mm]	-1.13	-0.51	-0.96
	$u_{MT;rel}$	[mm]	0.012	0.040	0.072
	$v_{MR;rel}$	[mm]	0.015	0.011	0.013
	u_{LBC}	[mm]	1.13	0.98	0.92
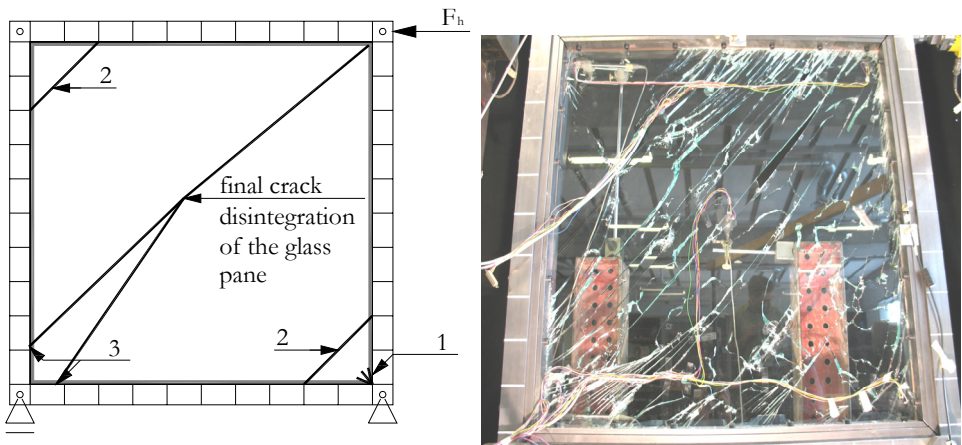
Figure 3.15:   *Schematic overview of the crack sequence for all tests (left): the first crack (1), second crack (2) and the final crack (3) and the cracked glass pane after test 2 (right)*
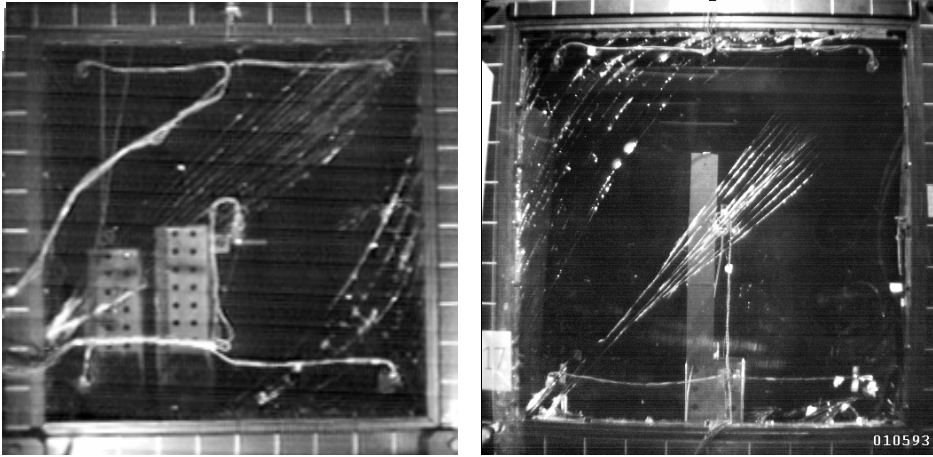
Figure 3.16:   High-speed shots at the moment of the final crack for test 3 (left) and test 17 (right)

Table 3.4:   Overview of non-cracked glass pane at a horizontal in-plane load of about 46 kN

Test		2	3	17	Average	Standard deviation
u_{RTC}	[mm]	0.95	1.01	1.14	1.03	0.10
F_h	[kN]	45.92	45.84	46.86	46.21	0.83
$u_{RTC;s}$	[mm]	0.49	0.53	0.67	0.56	0.09
K_s	[kN/mm]	93.56	83.10	69.79	82.15	11.91
w_{centre}	[mm]	-0.54	-0.26	-0.45	-0.42	0.14
$u_{MT;rel}$	[mm]	0.002	0.003	0.005	0.003	0.0015
$v_{MR;rel}$	[mm]	0.004	0.004	0.004	0.004	0.00
u_{LBC}	[mm]	0.25	0.12	0.02	--	--

Figure 3.17 gives an overview of the maximum principle stress ($\sigma_{g;1}$), the minimum principle stress ($\sigma_{g;2}$) and their directions (θ) at a horizontal in-plane load of about 46 kN (top) and at the moment of the final crack (bottom). At a horizontal in-plane load of about 46 kN, the maximum principle stresses are tension stresses and the minimum principle stresses are compression stresses for all tests except for the maximum principle stress in points 5 and 1 of test 2 and 3 respectively. The values for the principle stresses are almost equal in size and small. However, the maximum principle stress in point 2 shows larger maximum principle stresses for all tests. The direction of the principle stresses has an angle of about ±45° for all points and for all tests except in point 1 of test 2 and in point 2 of all tests. At the final crack, the maximum principle stresses are also tension stresses and the minimum principle stresses are also compression stresses for all tests except for the minimum principle stress in point 2 of

test 2 and the maximum tension stress in points 5 and 4 of tests 2 and 3 respectively. The values for the minimum principle stresses in points 1, 3 and 5 clearly show large compression stresses. The value for the maximum principle stress in point 4 of test 17 is larger than in tests 2 and 3. The value of the maximum principle stress in point 2 of tests 2 and 3 decreases compared to the maximum principle stress before the first crack. The direction of the principle stress of point 3 is nearby +/-45° and varies in the other points.

Test 2 at Fh= 45.92 kN

Point 4: $\sigma_{g;1}= 2.39$, $\sigma_{g;2}= -2.11$, $\Theta = -43.91$
Point 5: $\sigma_{g;1}= -0.80$, $\sigma_{g;2}= -3.89$, $\Theta = 30.47$
Point 3: $\sigma_{g;1}= 2.59$, $\sigma_{g;2}= -2.77$, $\Theta = 43.78$
Point 1: $\sigma_{g;1}= 3.06$, $\sigma_{g;2}= -3.15$, $\Theta = 44.74$
Point 2: $\sigma_{g;1}= 7.71$, $\sigma_{g;2}= -0.16$, $\Theta = -18.97$

Test 3 at Fh= 44.90 kN

Point 4: $\sigma_{g;1}= 1.80$, $\sigma_{g;2}= -2.18$, $\Theta = -44.18$
Point 5: $\sigma_{g;1}= 2.53$, $\sigma_{g;2}= -2.80$, $\Theta = 41.63$
Point 3: $\sigma_{g;1}= 2.68$, $\sigma_{g;2}= -2.95$, $\Theta = -44.71$
Point 1: $\sigma_{g;1}= -1.96$, $\sigma_{g;2}= -3.59$, $\Theta = -37.27$
Point 2: $\sigma_{g;1}= 6.29$, $\sigma_{g;2}= -2.47$, $\Theta = -34.72$

Test 17 at Fh= 46.86 kN

Point 4: $\sigma_{g;1}= 2.98$, $\sigma_{g;2}= -3.80$, $\Theta = 44.76$
Point 5: $\sigma_{g;1}= 3.17$, $\sigma_{g;2}= -2.72$, $\Theta = 41.95$
Point 3: $\sigma_{g;1}= 2.97$, $\sigma_{g;2}= -3.24$, $\Theta = -44.74$
Point 1: $\sigma_{g;1}= 3.08$, $\sigma_{g;2}= 2.44$, $\Theta = -44.11$
Point 2: $\sigma_{g;1}= 5.82$, $\sigma_{g;2}= -3.37$, $\Theta = -31.96$

Test 2 at Fh= 120.47 kN

Point 4: $\sigma_{g;1}= 1.46$, $\sigma_{g;2}= -3.55$, $\Theta = -7.57$
Point 5: $\sigma_{g;1}= -27.23$, $\sigma_{g;2}= -30.95$, $\Theta = 11.71$
Point 3: $\sigma_{g;1}= 7.09$, $\sigma_{g;2}= -9.64$, $\Theta = -45.00$
Point 1: $\sigma_{g;1}= 0.44$, $\sigma_{g;2}= -34.65$, $\Theta = 7.23$
Point 2: $\sigma_{g;1}= 1.51$, $\sigma_{g;2}= 0.49$, $\Theta = 45.00$

Test 3 at Fh= 165.05 kN

Point 4: $\sigma_{g;1}= -5.63$, $\sigma_{g;2}= -0.99$, $\Theta = -29.18$
Point 5: $\sigma_{g;1}= 17.79$, $\sigma_{g;2}= -51.79$, $\Theta = -35.35$
Point 3: $\sigma_{g;1}= 5.71$, $\sigma_{g;2}= -17.26$, $\Theta = 43.51$
Point 1: $\sigma_{g;1}= 9.11$, $\sigma_{g;2}= -27.84$, $\Theta = 28.79$
Point 2: $\sigma_{g;1}= 5.46$, $\sigma_{g;2}= -0.37$, $\Theta = 25.67$

Test 17 at Fh= 218.02 kN

Point 4: $\sigma_{g;1}= 20.44$, $\sigma_{g;2}= -6.98$, $\Theta = -38.65$
Point 5: $\sigma_{g;1}= 7.20$, $\sigma_{g;2}= -44.41$, $\Theta = 40.76$
Point 3: $\sigma_{g;1}= 11.99$, $\sigma_{g;2}= -19.99$, $\Theta = -44.49$
Point 1: $\sigma_{g;1}= 6.26$, $\sigma_{g;2}= -35.99$, $\Theta = 40.00$
Point 2: $\sigma_{g;1}= 5.18$, $\sigma_{g;2}= -3.73$, $\Theta = 31.72$

Figure 3.17:   Overview of the principle stresses and their directions at a horizontal in-plane load about 46 kN (top) and just at the moment of the final crack (bottom) for all tests

Discussion of the results

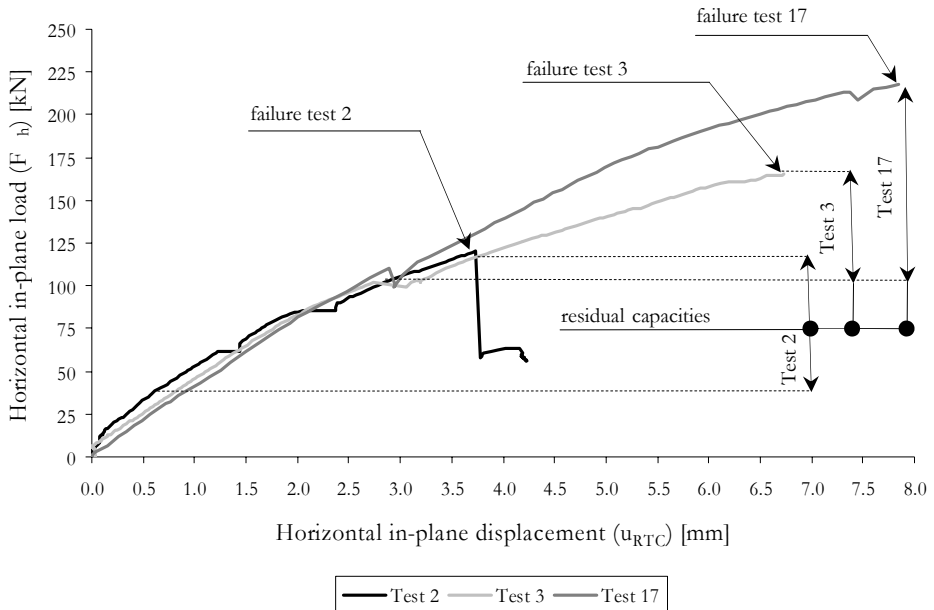The relation between the horizontal in-plane load and the horizontal in-plane displacement at the RTC of the system has a declining curve (figure 3.13) and is predominately ascribed to the toughened adhesive behaviour at larger relative in-plane displacement of the adhesive bonded joint (appendix C.1.3). The relation is irregular by cracking of the glass pane by which the relation more declines. Nevertheless, the in-plane load keeps increasing, because the adhesively bonded glass pane is able to redistribute the in-plane load such as the redistribution of the in-plane load at the anchorage of the tension diagonal (figure 3.15). Other plausible non-linear behaviours of the system are the vertical spring at the RBC of the system (section 3.5.1 and appendix B.1) and the in-plane displacements (sliding) of the bolted connection between the

outside beam and the beadwork accompanying with contact friction in the compressed zone (section 3.5.2 and appendix B.2).

The in-plane rotation of the entire system caused by the vertical in-plane displacement of the pinned connection at the RBC of the system significantly influences the horizontal in-plane displacement at the top of the system (table 3.4). Thus, the actual horizontal in-plane displacement of the system itself is much smaller than measured. The actual horizontal in-plane displacement at the RTC of the system is ascribed to the in-plane deformation of the glass pane (figure 3.17), the relative in-plane displacements of the circumferentially adhesive bonded joint (table 3.4) and the in-plane displacements of the bolted connection between the outside beam and the beadwork (section 3.5.2). The contribution of the in-plane deformation of the non-cracked glass pane in the horizontal in-plane displacement at the RTC of the system is the result of predominately in-plane shear load, because the distribution of the principle stresses and their directions (figure 3.17 top) correspond with a purely uniformly in-plane shear load acting along the edges of the glass pane (figure 2.9 right). The deviation in the distribution of the principle stresses can be ascribed to bending of the glass pane by initial imperfections such as varying glass pane thickness and the curving of the glass pane and the prevented free in-plane displacements and in-plane rotations of the glass pane along the edges by the stiff adhesive bonded joint. The contribution of the adhesive bonded joint in the horizontal in-plane displacement at the RTC of the system is small, because the relative horizontal and vertical in-plane displacement of the adhesive bonded joint are small (table 3.4). The contribution of the horizontal and vertical in-plane displacement of the bolted connection between the outside beam and the beadwork (clearance of the hole) is expected to have more influence on the horizontal in-plane displacement at the RTC of the system. Furthermore, the flexural stiffness of the transoms and mullions are also reduced.

At larger horizontal in-plane load the in-plane load transfer in the glass pane more and more concentrated in the compression diagonal (figure 3.17 bottom), because the glass pane is cracked at the vicinity of the RBC and the LTC by which the anchorages of the tension diagonal are cut off. Moreover, the compression diagonal remains the stiffest and the directed way to transfer the horizontal in-plane load.

The out-of-plane displacements at the centre of the glass pane are small and therefore, the system has a robust behaviour even at large horizontal in-plane loads. The circumferentially adhesive bonded joint has a stiffened effect on the out-of-plane displacements of the glass pane and therefore, the boundary condition of the glass pane can be considered as four-sided clamped supported. Equation 3.5 [Wellershoff 2006] gives the critical shear stress ($\tau_{g;crit}$) for plate buckling under uniformly distributed shear load on the edges of a non-cracked glass pane in which k_τ is the buckling value depending on the boundary conditions given in equations 3.6a and 3.6b [Wellershoff 2006]. Equation 3.5a gives the critical maximum ($\sigma_{g;crit;1}$) and the minimum ($\sigma_{g;crit;2}$) principle stresses. They are equal in size, but the critical maximum principle stress is a tension stress and the critical minimum principle stress is a compression stress. The direction has an angle of 45° with the horizontal (figure 2.9 right). Equation 3.6a and 3.6b give the buckling value for four-sided simply supported and the four-sided clamped supported rectangular glass panes respectively in which α is the ratio between the largest size and the smallest size of the glass pane. The critical maximum principle stress for four-sided simply supported glass pane is 81.75 N/mm² and for four-sided clamped supported glass pane is 127.63 N/mm². These values are larger than given in figure 3.17 for the non-cracked and the

cracked glass pane. Actually, the local exceeding of the strength of glass is the criterion and therefore, plate buckling is not under discussion.

$$\tau_{g;crit} = \frac{\pi^2 E_g}{12(1-v_g)}\left(\frac{t_g}{w_g}\right)k_\tau \qquad \text{(Equation 3.5)}$$

$$\sigma_{g;crit;1} = \tau_{g;crit} \quad \wedge \quad \sigma_{g;crit;2} = -\tau_{g;crit} \qquad \text{(Equation 3.5a)}$$

$$\begin{aligned} k_\tau &= 4.00 + 5.34\alpha^{-2} \quad \alpha < 1 \\ k_\tau &= 5.34 + 4.00\alpha^{-2} \quad \alpha \geq 1 \end{aligned} \qquad \text{(Equation 3.6a)}$$

$$\begin{aligned} k_\tau &= 5.60 + 8.98\alpha^{-2} \quad \alpha < 1 \\ k_\tau &= 8.98 + 5.60\alpha^{-2} \quad \alpha \geq 1 \end{aligned} \qquad \text{(Equation 3.6b)}$$

The adhesive bonded joint was intact after the final crack. This indicates that the applied epoxy well adheres on the tin side as well as on the atmospheric side of the glass pane. Moreover, the adhesive bonded joint was able to resist shocks of the cracking glass pane, because of the toughened behaviour of the adhesive.

The first fancy-like crack at the RBC of the glass pane is the result of tension stresses in three different directions. The glass pane along the adhesive bonded joint of the right mullion displaces upwards, the glass pane along the adhesive bonded joint of the bottom transom displaces to the negative x-axis (u_{LBC}) and the tension diagonal from the RBC to LTC. The maximum principle stress in point 2 of all tests points to it (figure 3.17 top). The second cracks occurs almost perpendicular to the tension diagonal close to the corners in which it is anchored to the adhesive bonded joint. This region has larger tension stresses. The final crack occurred at the LBC of the glass pane and this is possibly caused by the tension stresses perpendicular to the large compression stresses (section 2.2.2). At the final crack, the size of the fragmentation of the glass pane at test 3 and 17 was smaller than at test 2. This is caused by the stress concentration in the glass pane (section 2.5.2).

The residual capacity based on the first crack at the smallest horizontal in-plane load is very good (figure 3.13). After the first crack the glass pane frequently cracks at increasing horizontal in-plane load. The audible and visible cracks were a warning for overloading. This is the result of the choice of the glass type, namely annealed float glass which has a favourable crack pattern for residual capacity (table 2.4) and the favourable effect of the circumferential adhesive bonded joint (section 3.5) which makes redistributions of the in-plane load possible.

3.7.3   Systems with joint type 3

Test results

Figure 3.18:   Relation between the horizontal in-plane load and the horizontal in-plane displacement at the RTC of the system

Table 3.5 gives the values for the horizontal in-plane displacement at the RTC of the system (u_{RTC}), the horizontal in-plane load (F_h), the out-of-plane displacement at the centre of the glass pane (w_{centre}), the relative horizontal in-plane displacement between the top transom and the glass pane ($u_{MT;rel}$), the relative vertical in-plane displacement between the right mullion and the glass pane (v_{MRrel}) and the horizontal in-plane displacement at the LBC of the system (u_{LBC}) at the first and final crack. Table 3.6 gives the values as mentioned in table 3.5, but at a horizontal in-plane load of about 31 kN, in which the glass pane of all tests were non-cracked to compare the measured results better. Table 3.6 is completed with the corrected horizontal in-plane displacement at the RTC of the system ($u_{RTC;s}$) and the in-plane stiffness of the system (K_s).

Figure 3.18 shows the relation between the horizontal in-plane load and the horizontal in-plane displacement at the RTC of the system. The relation gradually declines at increasing horizontal in-plane displacement at the RTC of the system. The discontinuities in the relation are the cracks in the glass pane. Figure 3.20 left shows a schematic overview of the crack sequence. The first crack of tests 6 to 8 (number 1 in figure 3.20 left) initiated at the RBC of the glass pane after which the crack gradually propagated along the right bottom of the adhesive bonded joint of the right mullion at different horizontal in-plane loads (table 3.5). The final crack (number 2 in figure 3.20 left) was a diagonal and initiated at approximately 100 mm above the LBC of the left mullion after which the crack propagated to the RTC of the glass pane. Figure

3.21 shows the high-speed shots at the moment of the final crack for test 7 (left) and test 8 (right). This crack initiation and propagation were observed for all tests and occurred quickly after the first crack. The final crack disintegrated the glass pane. The entire glass pane fell out and some small pieces of glass were pulled off from the adhesive bonded joint. Moreover, the one-sided adhesive bonded joint was intact and was not pulled off from the steel frame. However, test 5 deviated from tests 6 and 7 and therefore an additional test 8 was carried out. The first crack of test 5 was the final crack. Then the horizontal in-plane load dropped to about 18 kN and restarted to increase till about 38 kN after which the glass pane gave away (figure 3.18). All cracks were audible and visible, but the first crack was hardly to see.
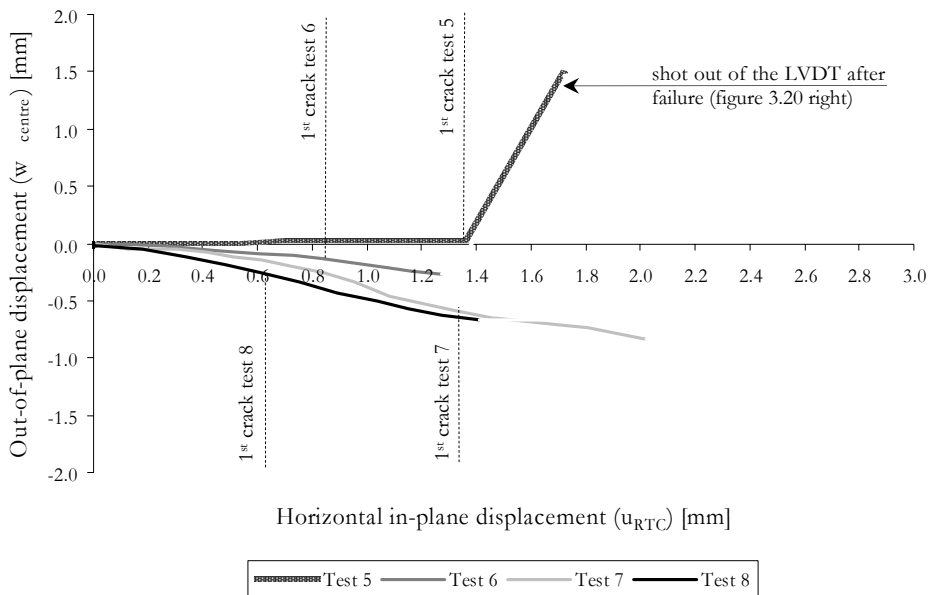
Figure 3.19: *Relation between the out-of-plane displacement at the centre of the glass pane and the horizontal in-plane displacement at the RTC of the system*

The horizontal in-plane displacement of the top transom slightly displaced more than the top of the glass pane (relative horizontal in-plane displacement). The vertical in-plane displacement of the right side of the glass pane slightly displaced more than the right mullion (relative vertical in-plane displacement).

Figure 3.19 shows the relation between the out-of-plane displacement at the centre of the glass pane and the horizontal in-plane displacement at the RTC of the system. The out-of-plane displacement at the centre of the glass pane was small and directed to the negative z-axis (rear) except for test 5. The out-of-plane displacement of the LTC and the RTC of the system was negligible small.

Table 3.5:   *Overview of measured results at first and final crack*

	Test		5	6	7	8
First crack	u_{RTC}	[mm]	1.36	0.84	1.32	0.61
	F_h	[kN]	40.07	31.99	53.98	37.25
	w_{centre}	[mm]	0.04	-0.13	-0.59	-0.34
	$u_{MT;rel}$	[mm]	0.0045	0.0040	0.0065	0.0010
	$v_{MR;rel}$	[mm]	0.0063	0.0051	0.0071	0.0046
	u_{LBC}	[mm]	0.12	0.09	0.13	0.13
Final crack	u_{RTC}	[mm]	--	1.27	2.02	1.41
	F_h	[kN]	--	40.87	69.94	62.53
	w_{centre}	[mm]	--	-0.27	-0.83	-0.71
	$u_{MT;rel}$	[mm]	--	0.0030	0.0119	0.0021
	$v_{MR;rel}$	[mm]	--	--	0.0145	0.0088
	u_{LBC}	[mm]	--	0.18	0.27	0.29
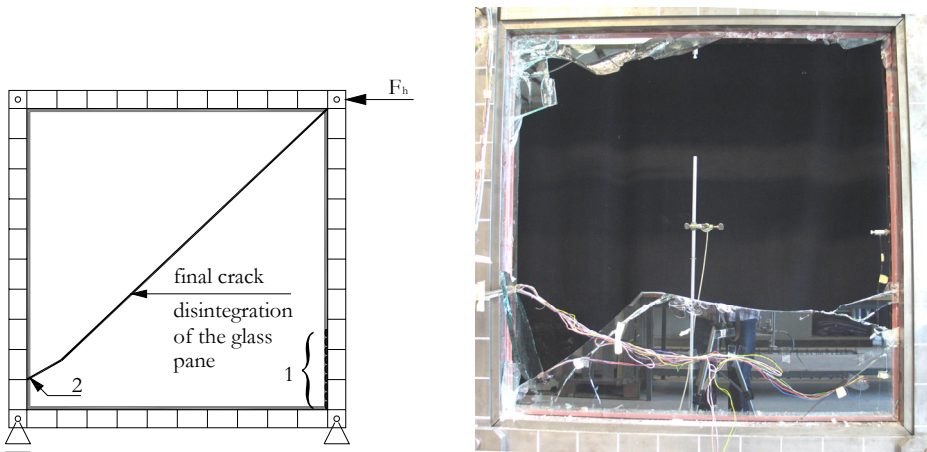
Figure 3.20:   *Schematic overview of the crack sequence for all tests (left): the first crack (1) and the final crack (2) and the cracked glass pane after test 5 (right)*
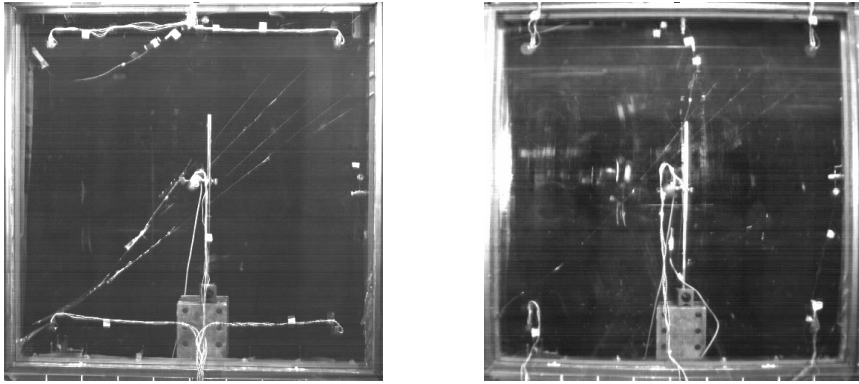
Figure 3.21:   High-speed shots at the moment of the final crack for test 7 (left) and test 8 (right)

Table 3.6:   Overview of non-cracked glass pane at a horizontal in-plane load of about 31 kN

Test		5	6	7	8	Average	Standard deviation
u_{RTC}	[mm]	0.93	0.84	0.72	0.75	0.81	0.09
F_h	[kN]	30.38	31.99	31.19	32.17	31.43	0.82
$u_{RTC;s}$	[mm]	0.63	0.52	0.41	0.43	0.50	0.10
K_s	[kN/mm]	48.51	61.51	76.43	75.11	65.39	13.11
w_{centre}	[mm]	0.04	-0.13	-0.20	-0.25	--	--
$u_{MT;rel}$	[mm]	0.0034	0.0040	0.0034	0.0028	0.0034	0.0005
$v_{MR;rel}$	[mm]	0.0055	0.0051	0.0040	0.0037	0.0046	0.0009
u_{LBC}	[mm]	0.10	0.09	0.01	0.13	--	--

At a horizontal in-plane load of about 31 kN (figure 3.22), the maximum principle stresses were tension stresses and the minimum principle stresses were compression stresses for all tests except for the minimum principle stress in point 4 of test 8. The values for the principle stresses were equal in size and small for tests 5 and 6 except the maximum principle stress in point 1. The maximum principle stress was considerably larger. The values for the maximum principle stress were predominately larger than the minimum principle stress for tests 7 and 8. The direction of the principle stress varied for all points.
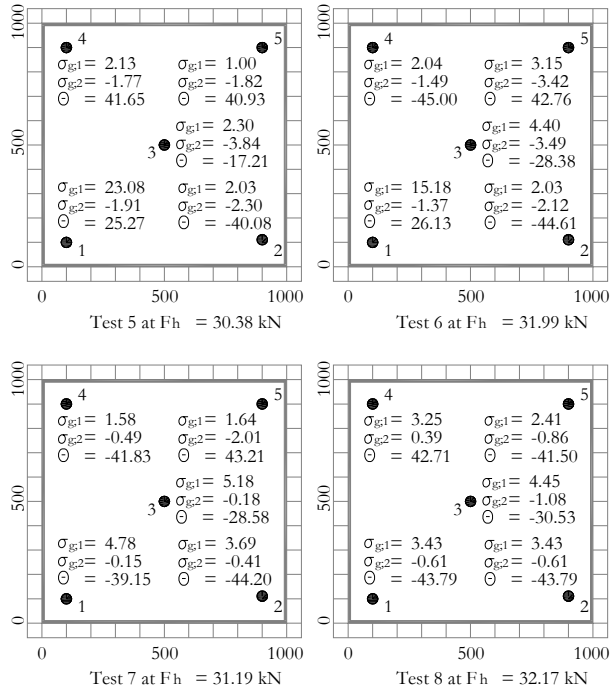
Figure 3.22: *Overview of the principle stresses and their directions at a horizontal in-plane load of about 31 kN*

Discussion of the results

The results of the systems with joint type 3 show similarities with the results of the systems with joint type 2. The similarities are enumerated below and discussed in section 3.7.2.
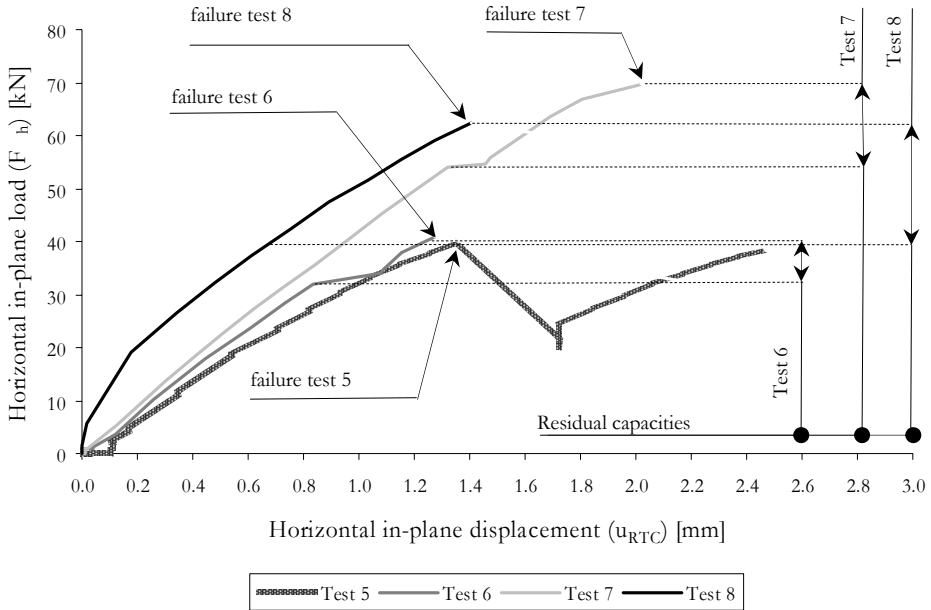- The declining relation between the horizontal in-plane load and the horizontal in-plane displacement at the RTC of the system.
- The influence of the vertical in-plane displacement of the pinned connection at the RBC of the system.
- The contribution of the glass pane, adhesive bonded joint and the bolted connection between the outside beam and the beadwork in the horizontal in-plane displacement at the RTC of the system.
- The boundary condition of the system.

Besides the similarities with systems of joint type 2, systems with joint type 3 also shows main differences by the one-sided adhesive bonded joint. The relative in-plane displacements of the adhesive bonded joint are larger than the relative in-plane displacements of the adhesive bonded joint for systems with joint type 2, because the in-plane load has to be transferred through one adhesive bonded joint between glass pane and steel frame.

The first crack occurred at the RBC of the glass pane and has a small influence on the relation between the horizontal in-plane load and horizontal in-plane displacement at the RTC of the

system, because the in-plane loads redistributed quickly around the crack region. The first crack at the RBC of the glass pane gradually propagates along the right bottom of the adhesive bonded joint of the right mullion. This corner of the glass pane is subjected to three tension loads, namely the vertical in-plane displacement of the glass pane along the right mullion in positive y-direction, the horizontal in-plane displacement of the glass pane along the bottom transom in negative direction and the tension diagonal from the RBC to the LTC of the glass pane. These three tension loads are directed from the RBC of the glass pane. Moreover, the eccentric connection between glass pane and adhesive bonded joint results in bending stresses in the glass pane.

The final crack (number 2 in figure 3.20) initiates at the LBC of the glass pane. This can be explained by the tension stress perpendicular to the large compression stress in the compression diagonal from the LBC to the RTC. Moreover, the eccentric in-plane load transfer between the glass pane and the steel frame results in bending stresses in the glass pane. The final crack completely disintegrated the glass pane. The combination of small out-of-plane displacements at the centre of the glass pane, bending of the glass pane by the eccentric connection and compression stresses in the compression diagonal easier pushes the glass pane out-of-plane. The adhesive bonded joint was intact on the steel frame. This also indicates that the adhesive bonded joint resists shocks by the toughened behaviour of the adhesive at room temperature.

The residual capacity based on the first crack at the smallest horizontal in-plane load is very poor. After the first crack the glass pane frequently cracks, but the final crack suddenly occurred after the first crack or the first crack is even the final crack as observed at test 5. The cracks were audible and visible, but these warnings for overloading the glass pane and the perception by humans are too short. The one-sided stiff and toughened adhesive bonded joint is not able to keep the shard on the adhesive bonded joint.

3.8   Conclusions

Systems built up of a steel frame, a square glass pane and one of the three defined circumferential adhesive bonded joints were subjected to a horizontal in-plane load at the RTC of the system. The glass pane was annealed float glass and it had one size (1.0 m x 1.0 m) and one nominal thickness (12 mm). The adhesive bonded joints were a flexible joint over the fully thickness of the glass pane between the glass pane and the steel frame (joint type 1), a two-sided stiff and toughened joint along the edges of the glass pane (joint type 2) and a one-sided stiff and toughened joint along the edges of the glass pane (joint type 3). The experiments focussed on the in-plane stiffness of the system, the distribution of the in-plane load in the glass pane, the crack initiation and propagation in the glass pane and the residual capacity of the systems. The following conclusions can be drawn regarding systems with joint types 1 to 3.

Systems with joint type 1

The relation between the horizontal in-plane loads and the horizontal in-plane displacements at the RTC of the system is bilinear. The first stage has small in-plane stiffness of the system caused by the flexible adhesive bonded joint while the glass pane is non-cracked. The principle stresses are much smaller than the bending tension strength of annealed float glass. So, plate buckling of the four-sided supported glass pane does not occur. The second stage has larger in-plane stiffness of the system caused by the direct in-plane load transfer between the glass pane and the steel frame at the LBC and the RTC accompanying with cracking of the glass pane at glass-steel contact. Cracking of the glass pane results in larger horizontal in-plane displacements at the RTC of the system with nearly constant horizontal in-plane loads. The cracking of the glass pane is arbitrary. At large horizontal in-plane displacements at the RTC of the system, the glass pane is only supported laterally at the LBC and the RTC. The large compression load in the compression diagonal and the new boundary conditions make the glass pane susceptible for plate buckling which more corresponds with column buckling.

At the beginning of the first stage, the adhesive bonded joint is intact and mobilizes the glass pane along the four edges of the glass pane. The in-plane load more and more transfers via the compression zones of the adhesive bonded joint, because the adhesive bonded joint behaves stiffer under compression than under shear and tension. Halfway the first stage, the tension regions of the adhesive bonded joint show large relative in-plane displacements resulting in adhesive as well as cohesive failure. So, the horizontal in-plane loads are more and more transferred in the glass pane via the compression region of the adhesive bonded joint. At the end of the first stage, the compression regions of the adhesive bonded joint are gradually pushed away between the glass pane and the steel frame resulting in glass-steel contact: the transition of bi-linear relation.

The residual capacity of the system is good by applying of annealed float glass. In the first stage, the system visibly warns by large horizontal in-plane displacements at the RTC of the system accompanying with an increase of horizontal in-plane load. In the second stage, the system visibly and audibly warns by cracking of the glass pane accompanying with an increase of horizontal in-plane load. In practice, the criteria will be the limitation of the horizontal in-plane displacement at the RTC of the system, because of the small in-plane stiffness of the system and the limitation of the relative in-plane displacement of the adhesive bonded joint.

Systems with joint type 2

The relation between the horizontal in-plane loads and the horizontal in-plane displacements at the RTC of the system gradually declines with a few discontinuities. The gradual decline is caused by the toughened behaviour of the applied epoxy adhesive and the discontinuities are caused by several cracks of the glass pane. The in-plane stiffness of the system is much larger compared to the in-plane stiffness of systems with joint type 1.

The horizontal in-plane displacement at the RTC of the system is built up of the in-plane deformation of the glass pane, the relative in-plane displacements of the adhesive bonded joint and the in-plane displacements of the bolted connection between the outside beam and the beadwork. The contribution of the bolted connection in the horizontal in-plane displacement at the RTC of the system is the result of the in-plane displacements (sliding) between the

beadwork and the outside beam caused by the clearance of the holes. The flexural stiffness of the transoms and the mullions is also reduced. Furthermore, the vertical in-plane displacement of the pinned connection at the RBC of the system results in an in-plane rotation of the system which enlarges the horizontal in-plane displacement at the RTC of the system.

The adhesive bonded joint continuously mobilizes the non-cracked and the cracked glass pane in-plane till the moment of failure of the system. The adhesively bonded glass pane constantly redistributes the in-plane load after each crack. The adhesive bonded joint remains intact and resists shocks of the cracking glass pane.

At small horizontal in-plane loads, the distribution of the principle stresses in the glass pane corresponds with the distribution of the principle stresses of a shear wall loaded by a uniformly distributed in-plane shear load along the edges of the glass pane. However, the stiff adhesive bonded joint influences the distribution of the principle stresses along the edges of the glass pane. Moreover, the adhesive bonded joint can be considered as a four-sided clamped supported glass pane and introduces bending stresses along the edge of the glass. At larger horizontal in-plane loads, the in-plane loads are more and more transferred via the compression diagonal. The glass pane locally cracks by exceeding the strength of glass. Plate buckling does not occur.

The first crack occurs at the RBC of the glass pane in which the tension diagonal is anchored and it has a fancy-like pattern. The RBC of the glass pane is subjected to tension load along the right mullion, along the bottom transom and the tension diagonal. The final crack occurs at the LBC of the glass pane by exceeding the strength of glass perpendicular to the local large compression load in the compression diagonal.

The residual capacity of the system is very good because of the circumferentially stiff adhesive bonded joint and applying of annealed float glass. The system audibly and visibly warns for overloading at which the horizontal in-plane load still increases. In practice, the criteria will be the strength of glass and the limitation of the relative in-plane displacement of the adhesive bonded joint.

Systems with joint type 3

The relation between the horizontal in-plane loads and the horizontal in-plane displacements at the RTC of the system gradually declines with a few discontinuities. The gradual decline is caused by the toughened behaviour of the applied epoxy adhesive and the discontinuities are caused by several cracks of the glass pane. The in-plane stiffness of the system is comparable to the in-plane stiffness of systems with joint type 2.

The horizontal in-plane displacement at the RTC of the system is built up of the in-plane deformation of the glass pane, the relative in-plane displacements of the adhesive bonded joint and the in-plane displacements of the bolted connection between the outside beam and the beadwork. The contribution of the bolted connection in the horizontal in-plane displacement at the RTC of the system is the result of the in-plane displacements (sliding) between the beadwork and the outside beam caused by the clearance of the holes. The flexural stiffness of the transoms and the mullions is also reduced. Furthermore, the vertical in-plane displacement

of the pinned connection at the RBC of the system results in an in-plane rotation of the system which enlarges the horizontal in-plane displacement at the RTC of the system.

The adhesive bonded joint mobilizes the non-cracked and the cracked glass pane in-plane till the moment of failure of the system. The adhesive bonded joint remains intact and resists shocks of the cracking glass pane.

The distribution of the principle stresses in the glass pane corresponds with the distribution of the principle stresses of a shear wall loaded by a uniformly distributed in-plane shear load along the edges of the glass pane. However, the stiff adhesive bonded joint influences the distribution of the principle stresses along the edges of the glass pane. Moreover, the adhesive bonded joint can be considered as a four-sided clamped supported glass pane and introduces bending stresses along the edge of the glass which are enlarged by the eccentric in-plane load transfer. The glass pane locally cracks by exceeding the strength of glass. Plate buckling does not occur.

The first crack occurs at the RBC of the glass pane in which the tension diagonal is anchored which gradually cracks along the adhesive bonded joint of the right mullion. The RBC of the glass pane is subjected to tension load along the right mullion, along the bottom transom, the tension diagonal and bending of the glass pane by the eccentric in-plane load transfer. The final crack occurs at the LBC of the glass pane by exceeding the strength of glass perpendicular to the local large compression load in the compression diagonal and bending of the glass pane by the eccentric in-plane load transfer.

The residual capacity of the system is very poor caused by the eccentric in-plane load transfer between the steel frame and the glass pane. The system audibly and visibly warns for overloading, but too short. In practice, the criteria will be the strength of glass and the limitation of the relative in-plane displacement of the adhesive bonded joint.

Due to the limited number of tests for each system with one of the three adhesive bonded joints, finite element simulations have to be carried out to verify these conclusions. In chapter 4 a finite element model for each joint type is developed and calibrated with the experiments. The finite element model is used for parametric studies which are described in chapter 5.

4   Finite element simulations

This chapter discusses the development and the calibration of the finite element models for the simulation of the experiments described in chapter 3. The motivation and the objective are described in section 4.1. Section 4.2 describes the geometry of the finite element model. Section 4.3 describes the element types, section 4.4 the mesh density and section 4.5 the material input. Section 4.6 deals with geometrical imperfections. Section 4.7 discusses the solution strategy. Section 4.8 discusses the global and local behaviour of all systems and the calibration of the finite element model with the experiments of the systems with joint types 1 to 3. Section 4.9 ends this chapter with the conclusions. The calibrated finite element model is used for the parametric studies which are discussed in chapter 5.

4.1   Motivation and objective

The previous chapter discussed the experiments of systems with joint types 1 to 3 and yielded valuable information about the behaviour of the systems. However, the discussions as well as the conclusions were based on a limited number of tests for each system. To corroborate the conclusions and to get more insight in the behaviour of the system, the next step is to simulate the experiments by means of finite element method. Finite element simulations have to be a fair representation of the real structure, but for simulations of highly complex structural compositions such as systems with joint types 1 to 3, it is inevitable to make simplifications. A calibrated finite element model is a convenient tool to produce additional information about the experiments and to use in parametric studies which will be discussed in chapter 5.

For systems with joint type 1, the flexibly enclosed glass pane had a horizontal shift and an in-plane rotation within the steel frame in the first stage till glass-steel contact. However, the RBC and the LTC of the adhesive bonded joint was gradually torn off halfway the first stage. After the glass-steel contact, the LBC and the RTC of the compression diagonal was subjected to large in-plane compression loads resulting in cracking and flaking of these corners. Systems with joint type 2 and 3 firstly cracked at the RBC of the glass pane at small horizontal in-plane displacements at the RTC of the system. Then the glass regularly cracked till failure of the system. For all systems, a random redistribution of the in-plane load took place after each crack in the glass pane. The in-plane stiffness of the system was influenced by the in-plane sliding of the bolted connection between the outside beam and the beadwork and the vertical in-plane displacement of the pinned connection at the RBC of the system.

The phenomena that have to be capture in the finite element model are the boundary conditions of the system, the behaviour of the steel frame, the in-plane as well as the out-of-plane behaviour of the glass pane, the behaviour of the polyurethane joint including glass-steel contact for systems with joint type 1 and the behaviour of the epoxy joint for systems with joint type 2 and 3. The objective of the finite element model is to simulate the experiments till glass-steel contact for systems with joint type 1 or up to the onset of the first crack in the glass pane for systems with joint type 2 and 3. Probably, the finite element model is sufficient for the purpose of non-cracking design of the systems.

4.2   Geometry

Figure 3.2 shows the geometry of the system that is built up of a steel frame, a supporting structure at the LBC and the RBC of the system, the introduction of the horizontal in-plane load at the RTC of the system and a square glass pane with one of the three defined joint types. For simulating the geometry of the system, the finite element model has to fulfil the following eight requirements:

- the mid-plane of the glass pane lines up with the centre line of the outside beam;
- the outside beam of the transom and the mullion is coupled and released for rotation around the z-axis (internal hinge);
- the centre line of the outside beam of the transom and the mullion coincides with the centre of the internal hinge;
- the line of action of the horizontal in-plane load coincides with the centre line of the top outside beam;
- the centre of the roller at the LBC and centre of the pinned connection at the RBC coincide with the centre of the internal hinge;
- the centre line of the outside beam of the transom and the mullion has a distance to the edge of the glass pane (eccentricity);
- the pinned connection at the RBC behaves elastic in vertical direction (section 3.5.1);
- the shear flexibility of the bolted connection between the outside beam and the beadwork behaves elastic (section 3.5.2).

Figure 4.1 shows the outline of the entire model and figure 4.2 shows the cross section of the bottom transom which also represents the top transom and the mullions. The steel frame is divided into three parts, namely the outside beam, the beadwork and the bolted connection between the outside beam and the beadwork. The real rectangular cross section of the outside beam is modelled for only the half height (h_2) with shell elements and completed with beam elements (w_1 x h_1) in the centre line of the outside beam. The real beadwork is modelled to a forked cross section to enclose the glass pane and the interfaces A to C. The height of the 'handle' of the forked cross section (h_4) is the distance between the bolted connection and the bottom of interface B. The width of the forked cross section (w_5) corresponds to the thickness of the glass pane (t_{10}) and the thicknesses of interface A (t_8) and interface C (t_9). The prong of the forked cross section (h_7) corresponds to the thickness of interface B (t_6) and the width of interfaces A and C (w_8, w_9). The geometrical properties of the modelled cross section with shell elements meet the geometrical properties of the real outside beam and the real beadwork (appendix D). The bolted connection between the outside beam and the beadwork is modelled with two-dimensional interface elements. At each corner, the transom and the mullion have an overlap with uncoupled nodes except the common node of the beam element (figure 4.3). Figure 4.5 shows the in-plane displacements of the steel frame only (tilting mechanism) which correspond with the non-braced steel frame of the system. This node is coupled and released for rotation around z-axis to simulate the internal hinge. The ends of all beadworks are straight in stead of a mitre (figure 3.2) and it is a local simplification in the finite element model.
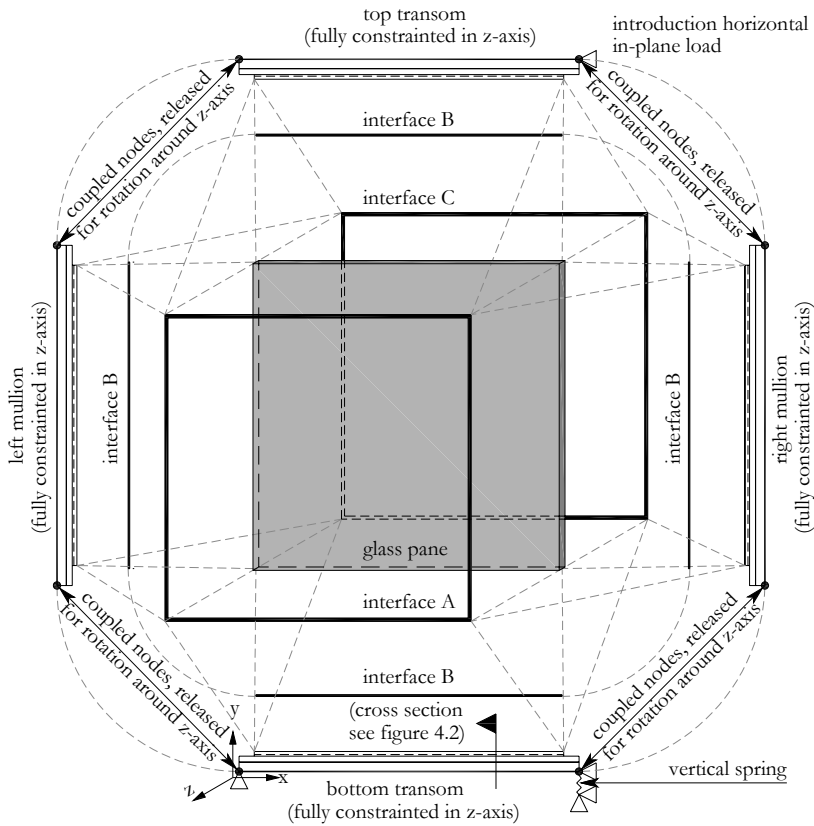
Figure 4.1:   Pulled out finite element model

The steel frame is supported at the LBC with a horizontal in-plane roller at the intersection of the centre line of the outside beam of the bottom transom and the left mullion. The RBC of the steel frame is supported by a vertical in-plane roller at the intersection of the centre line of the outside beam of the bottom transom and the right mullion. A vertically spring (section 3.5.1) is placed between the vertical in-plane roller and the in-plane pin. The steel frame is fully supported in z-direction, because in the experiments the out-of-plane displacements of the LTC and the RTC of the system were negligible small.

Interface A is placed along the four edges of the glass pane between the prong of the forked cross section and the front of the glass pane and interface C is also placed along the four edges of the glass pane, but between the prong of the forked cross section and on the rear of the glass pane. The length of interfaces A and C corresponds with the width (w_g) and the height of the glass pane (h_g). At the corners interfaces A as well as C have an overlap to avoid unreal stresses in the glass pane at a premature end of the interface elements on the glass pane. Interface B is placed between the glass pane and the bottom of the forked cross section. The geometry of systems with joint types 1 to 3 is implemented in one finite element model. The use of interfaces A to C depends on the system with one of the defined joint types (figure 4.4).

Systems with joint type 1 have polyurethane properties for interface B and have Teflon properties for interfaces A and C. Systems with joint type 2 have epoxy properties for interfaces A and C and an inactivated interface B. Systems with joint type 3 have epoxy properties for interface C and inactivated interfaces A and B. The glass pane is modelled with solid elements to describe better the three-dimensional stress distribution along the edges of the glass pane. Furthermore, the edges of the glass pane are modelled without facets.
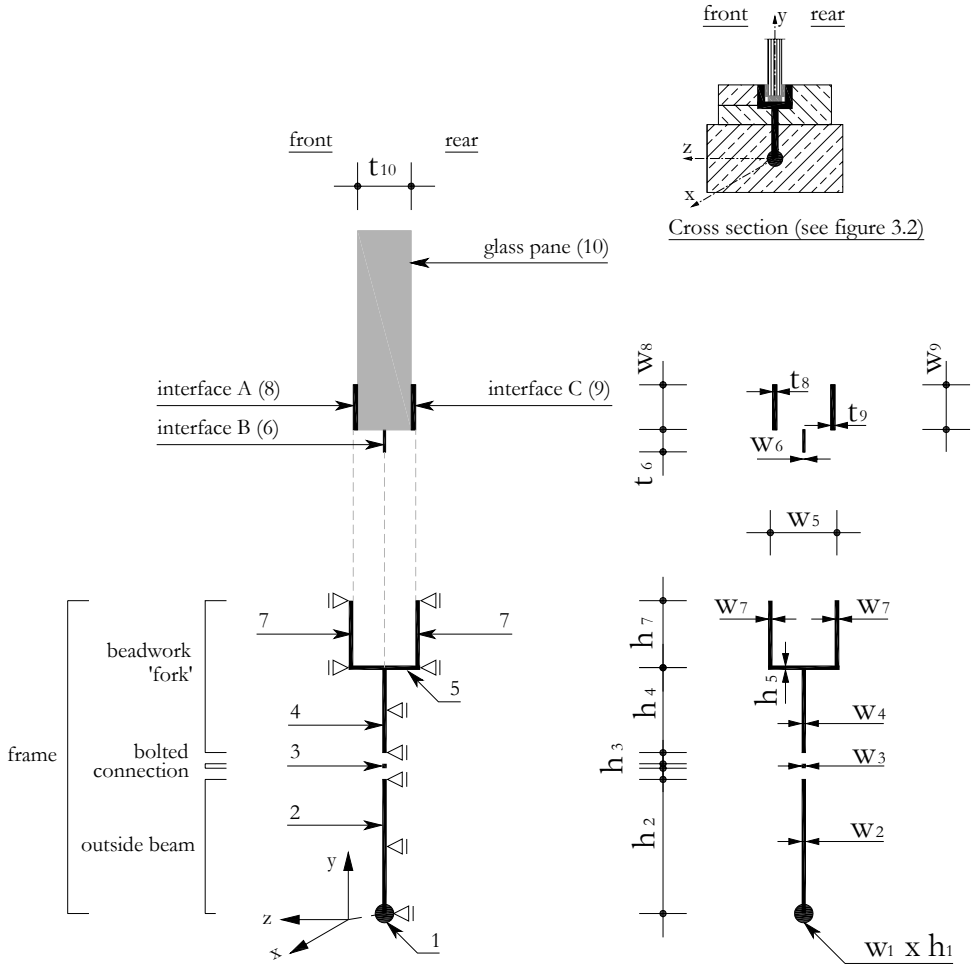
Figure 4.2:   Modelled cross section of the steel frame, the interfaces and the glass pane (drawn: bottom transom)
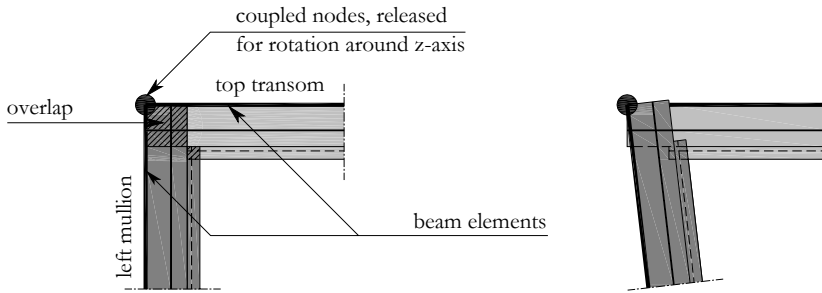
Figure 4.3: Simulation of the internal hinge and the tilting mechanism of the non-braced steel frame (left) (drawn: LTC of the system)
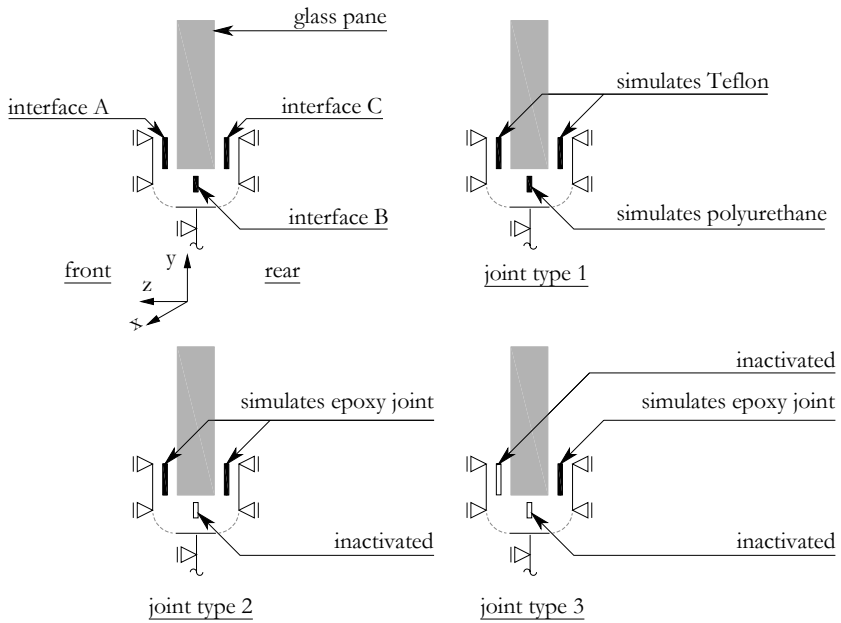
Figure 4.4: The use of interfaces A to C for systems with joint types 1 to 3
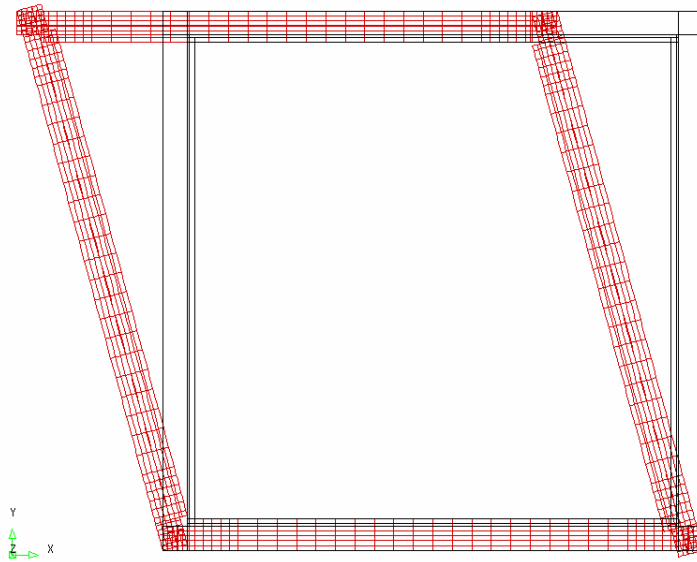
Figure 4.5:   *In-plane displacements of the unbraced steel frame (scale factor 10)*

4.3   Elements

The geometry of the system is now modelled and elements have to be chosen for the finite element model. Table 4.1 gives an overview of the applied elements [DIANA 2005] and the geometrical data. The bolted connection between the outside beam and the beadwork is simulated as a continuous interlayer with structural interface elements of type CL12I. Interface B has the same structural interface elements for simulating the adhesive bonded joint for systems with joint type 1. Element type CL12I is an interface element between two lines with two times three nodes in a two-dimensional configuration. This element is based on quadric interpolation. The relative in-plane displacements in normal direction and the relative in-plane displacements in longitudinal direction of the interface are independent of each other. Interfaces A and C also have structural interface elements for simulating the adhesive bonded joints for systems with joint type 2 and 3 or Teflon for systems with joint type 1. The applied element type is CQ48I. This element is an interface element between two planes with two times eight nodes in a three-dimensional configuration. The element is based on quadric interpolation. The relative out-of-plane displacements in normal direction, the relative in-plane displacements in longitudinal direction and the relative in-plane displacements in transversal direction are independent of each other.

A part of the outside beam and the entire forked cross section of the beadwork consist of element type CQ40F, a regular eight-nodes isoparametric quadrilateral flat shell element. This element type describes plate bending and plane stressses in a flat plane without a coupling between membrane and bending behaviour. The other part of the outside beam is provided of beam elements of type L12BE. This is a straight two nodes and three dimensional beam element. The vertical spring at the RBC of the steel frame is element type SP2TR, a two-node

translation spring/dashpot element. Finally, the glass pane consists of element type CHX60, a twenty-node isoparametric solid element. The element is based on quadric interpolation.

Table 4.1:   Elements applied and geometrical data input

	Number (i) (fig. 4.2)	Element type	Thickness (t_i) [mm]	Width (w_i) [mm]	Height (h_i) [mm]
Outside beam	1	L12BE	--	118	60
	2	CQ40F	--	3	30
Bolted connection	3	CL12I	--	15	1
Beadwork	4	CQ40F	--	98	19
	5	CQ40F	--	13	15
	7	CQ40F	--	19	15
Vertical spring at the RBC of the steel frame	-	SP2TR	--	--	--
Glass pane	10	CHX60	12	--	--
Interfaces A and C	8/9	CQ48I	0.5	--	--
Interface B	6	CL12I	12	--	--

4.4   Mesh density

The mesh density depends on the expected strain gradient in the steel frame, the adhesive bonded joint and especially the glass pane. The strain gradient is larger along the edges of the glass pane, especially at the corners. These strain gradients were not measured in the experiments. In the experiments of systems with joint types 1 to 3, the crack initiated at the vicinity of the corners of the glass pane (figures 3.11, 3.15 and 3.20). Therefore, the mesh of the glass pane is refined along the edges (zone of 100 mm from the edge of the glass pane) and is more refined at the corners (zone of 100 mm x 100 mm). The mesh density along the edges of the glass pane is continued to the interfaces and the fork cross section. The mesh in the centre of the glass pane is coarse (figure 4.6). However, the mesh refinement at the vicinity of the utmost corners of the glass pane is still not sufficient (discretisation fault) to describe the strain gradient well in the finite element model [Smulders 2009] especially for the glass-steel contact for systems with joint type 1 and the stiff adhesive bonded joint for systems with joint type 2 and 3 (figure 4.7).

In advance of the parameter studies the width, the height and the thickness of the glass pane (section 5.2) vary and can give problems with the mesh quality. One of the tests for the mesh quality is the aspect ratio.

incorrectly described strain gradient
discretisation fault

finest mesh

X_1 = Y_1 =	10 mm		
X_2 = Y_2 =	90 mm		
X_3 = X_4 =	200 mm for	w_g =	1000 mm
X_3 = X_4 =	325 mm for	w_g =	1500 mm
X_3 = X_4 =	700 mm for	w_g =	3000 mm
Y_3 = Y_4 =	200 mm for	h_g =	1000 mm
Y_3 = Y_4 =	325 mm for	h_g =	1500 mm
Y_3 = Y_4 =	700 mm for	h_g =	3000 mm

coarse mesh
aspect ratio problems
for smaller glass pane
thicknesses
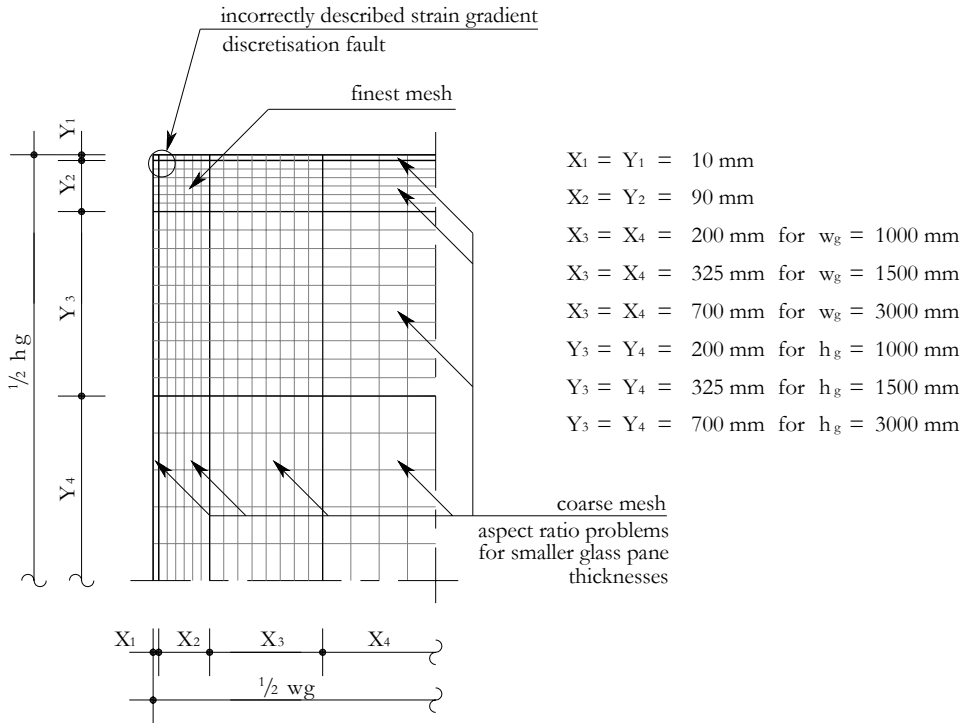
Figure 4.6:   Mesh of one fourth of the glass pane (drawn glass pane size 1.0 m x 1.5 m with t_g = 3.8 mm)
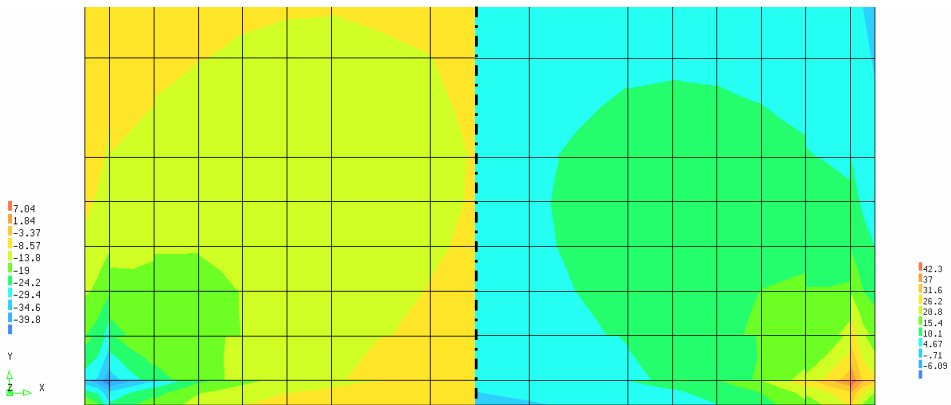
Figure 4.7:   Distribution of the minimum principle stresses at the LBC of the glass pane (left) and the distribution of the maximum principle stresses at the RBC of the glass pane (right) of systems with joint type 2 with u_{RTC} = 1.03 mm (element output)

The aspect ratio evaluates whether an element deviates significantly from the theoretical ideal by means of the ratio between the largest size and the smallest size of the element. The default value for the aspect ratio of CHX60 element is minimum 0.12 [DIANA 2005]. Table 4.2 gives the number and size of the elements for modelling the glass pane. Furthermore, two elements are always applied over the thickness of the glass pane. Nevertheless, a great number of elements does not meet the criterion aspect ratio in the centre and along the edges of the glass pane especially for glass pane thicknesses of 3.8 mm and 7.7 mm, but produces good results for the strains/stresses.

Table 4.2:   *Element sizes of the glass pane (see figure 4.6)*
         (1)   aspect ratio warning

w_g x h_g [m]	t_g [mm]	X_1 [mm]	X_2 [mm]	X_3 [mm]	X_4 [mm]	Y_1 [mm]	Y_2 [mm]	Y_3 [mm]	Y_4 [mm]
1.0x1.0	3.8	10	15	25[1]	50[1]	10	15	25[1]	50[1]
	7.7	10	18	25	50[1]	10	18	25	50[1]
	11.7	10	18	40	40	10	18	40	40
1.5x1.5	3.8	10	15	32.5[1]	32.5[1]	10	15	32.5[1]	32.5[1]
	7.7	10	18	32.5[1]	32.5[1]	10	18	32.5[1]	32.5[1]
	11.7	10	18	32.5	32.5	10	18	32.5	32.5
1.0x1.5	3.8	10	15	25[1]	50[1]	10	15	32.5[1]	32.5[1]
	7.7	10	18	25	50[1]	10	18	32.5[1]	32.5[1]
	11.7	10	18	40	40	10	18	32.5	32.5
1.0x3.0	3.8	10	15	25[1]	50[1]	10	15	≈31.8[1]	≈63.3[1]
	7.7	10	18	25	50[1]	10	18	≈31.8[1]	≈63.3[1]
	11.7	10	18	40	40	10	18	35	35
1.5x1.0	3.8	10	15	32.5[1]	32.5[1]	10	15	25[1]	50[1]
	7.7	10	18	32.5[1]	32.5[1]	10	18	25	50[1]
	11.7	10	18	32.5	32.5	10	18	40	40
3.0x1.0	3.8	10	15	≈31.8[1]	≈63.3[1]	10	15	25[1]	50[1]
	7.7	10	18	≈31.8[1]	≈63.3[1]	10	18	25	50[1]
	11.7	10	18	35	35	10	18	40	40

4.5 Material input

4.5.1 Material input for interfaces

Figure 4.8 defines the directions for the interfaces A to C and the bolted connection between the outside beam and the beadwork used as indices in the notations. For linear material behaviour, the normal stiffness and the shear stiffness are the material inputs for interface elements. For non-linear material behaviour, the material input is by means of multiple-linear relation between the normal stresses and the relative in-plane displacements in normal direction and multiple-linear relation between the shear stresses in longitudinal/transversal direction and the relative in-plane displacements in longitudinal/transversal direction.
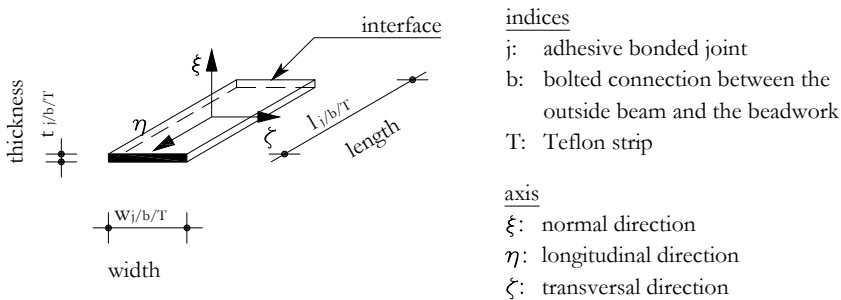
Figure 4.8:   Definition of the directions for interfaces A to C and the bolted connection between the outside beam and the beadwork

The feature of interface elements are that the normal direction and the longitudinal direction of the two-dimensional interface elements are independent of each other (section 4.3) i.e. that the normal stresses have no influence on the shear stresses and vice versa. This element formulation also concerns for the three-dimensional interface elements. The material properties for the shear stiffness in longitudinal direction and the shear stiffness in transversal direction have a common material input. Section 4.5.3 discusses how to simulate the independent non linear material input for interface elements.

4.5.2 Linear material behaviour

This section describes the attribution of the materials to the used elements in the model. Table 4.3 gives an overview of the materials and components which are assumed to have a linear material behaviour. The material properties of glass and steel are adopted from the Dutch standards [NEN 2608-2 2007, NEN 6770 1997]. Furthermore, it is assumed that annealed float glass has no material imperfections and it behaves isotropic and linear elastic (section 2.2.2) till the ultimate flexural tension strength (section 2.4.1). The steel also behaves isotropic and linear elastic and it is assumed that steel also has no material imperfections. Moreover, local yielding of the steel frame, e.g. around the bolted connection between the outside beam and the beadwork, is assumed to have no influence on the global behaviour of the system (Saint-Venant's principle).

The vertical spring stiffness ($K_{y;RBC}$) was determined experimentally (section 3.5.1 and appendix B.1). The vertical spring stiffness is assumed to be constant and applicable until a horizontal in-plane load about 100 kN. Section 3.5.2 discusses the shear flexibility of the bolted connection between the outside beam and the beadwork. The shear flexibility results in an in-plane sliding of the beadwork over the outside beam caused by the clearance of the holes in the outside beam (figure 3.2). The relative in-plane displacements between the outside beam and the beadwork and the in-plane displacements of the entire beam were measured in four point bending tests. The tests were simulated in finite element models (appendix B.2) and yielded a value for the shear flexibility of the bolted connection ($k_{b;\eta}$). The shear flexibility of the bolted connection simulates the in-plane sliding and the contact friction and is assumed to be linear. Furthermore, it is assumed that the shear flexibility concerns for all lengths of transom and mullion used in parametric studies. The normal stiffness of the bolted connection between the outside beam and the beadwork ($k_{b;\xi}$) is assumed to be large.

Table 4.3:   *Material properties with physically linear behaviour*

Material/component	Properties			Remarks
Glass	E_g ν_g	[N/mm²] [-]	70000 0.23	Source: NEN 2608-2:2007 nl
Steel	E_s ν_s	[N/mm²] [-]	210000 0.30	Source: NEN 6770:1997 nl – TGB 1990
Vertical spring stiffness at the RBC of the system	$K_{y;RBC}$	[N/mm]	10^5	Determined experimentally (Appendix B.1)
Bolted connection between the outside beam and the beadwork	$k_{b;\xi}$ $k_{b;\eta}$	[N/mm³] [N/mm³]	10^6 10	Large normal stiffness (assumed) Determined experimentally (Appendix B.2)
Initial normal stiffness of the epoxy joint (interfaces A and C for systems with joint type 2 and 3)	$k_{j;\xi;ini}$	[N/mm³]	1260	Derived from the linear stage of the shear stress-strain relation (Appendix C.1.3)
Inactivated interfaces A and B (figure 4.4)	$k_{j;\xi}$ $k_{j;\eta/\zeta}$	[N/mm³] [N/mm³]	10^{-9} 10^{-9}	Very small normal stiffness Very small shear stiffness
Teflon (interfaces A and C for systems with joint type 1)	$k_{T;\,\eta/\zeta}$	[N/mm³]	10^{-9}	Assumed to be very small shear stiffness

The initial normal stiffness of the epoxy joint ($k_{j;\zeta;ini}$) is derived from the linear stage of the experimentally found shear stress-strain relation (appendix C.1.3). The shear stiffness of the epoxy joint shows a bi-linear relation (section 4.5.2), but for the normal stiffness of the epoxy joint is assumed to remain constant over the two stages. Moreover, the normal stiffness of the epoxy joint is assumed to be constant over the joint length. So, it has no material imperfections e.g. varying Young's modulus and geometric imperfections e.g. varying joint thickness and joint width. The inactivated interface B for systems with joint type 2 and the inactivated interfaces A and B for systems with joint type 3 (figure 4.4) are assigned with a very small normal stiffness and shear stiffness. So, these interfaces are eliminated in the in-plane load transfer between the glass pane and the steel frame. The Teflon strips (interfaces A and C), used as lateral support of the glass pane for systems with joint type 1, can move freely in the longitudinal as well as in the transversal direction. The contact friction between Teflon and the glass pane is assumed to be very small and has a very small value for the shear stiffness ($k_{T;\eta/\zeta}$).

4.5.3 Non linear material behaviour

Figure 4.9 gives an overview of the non linear material behaviour for interfaces A to C. Teflon properties are attributed to the interfaces A and C for systems with joint type 1. The applied Teflon has a Young's modulus of 500 N/mm² and the thickness of the Teflon strip is 3 mm (figure 3.3). Figure 4.9 at the left top shows the relation between the normal stresses ($\sigma_{T;\xi}$) and the relative out-of-plane displacements ($w_{T;\xi;rel}$) for the Teflon strip. The out-of-plane loads only transfer between the glass pane and the Teflon strips by contact pressure. This is simulated by a large linear normal stiffness in the compression zone and a very small linear normal stiffness in the tension zone.

Epoxy properties are attributed to the interfaces A and C for systems with joint type 2 and to interface C only for systems with joint type 3. Figure 4.9 at the right top shows the relation between the average shear stresses ($\tau_{j;\eta/\zeta;ave}$) and the average relative in-plane displacements ($u_{j;\eta/\zeta;rel;ave}/v_{j;\eta/\zeta;rel;ave}$) in longitudinal direction as well as in transversal direction. This relation is derived from the experimentally found average shear stress-strain relation and converted into a average shear stress-relative in-plane displacement relation (section C.1.3). The normal stresses perpendicular to the shear stresses in longitudinal direction and in transversal direction are assumed to be small, because systems with joint type 2 and 3 predominately transfer the in-plane load via shear stresses in the adhesive bonded joint. The independent material inputs in normal direction and in longitudinal/transversal direction are justified (section 4.5.1). Furthermore, it is plausible that positive as well as negative relative in-plane displacements in longitudinal direction as well as in transversal direction result in the same value for the shear stresses. Therefore, the relation between the shear stresses and the relative in-plane displacements is symmetrical.

Polyurethane properties are attributed to interface B for systems with joint type 1. Figure 4.9 at the left bottom shows the relation between the average shear stresses ($\tau_{j;\eta;ave}$) and the average relative in-plane displacements in longitudinal direction ($u_{j;\eta;rel;ave}$). The relation is derived from the experimentally found average shear stress-strain relation and converted into a relation between average shear stresses and average relative in-plane displacements in longitudinal direction (appendix C.1.2). At large relative in-plane displacements in longitudinal direction the adhesive bonded joint is gradually pushed away in the compression zone at the LBC and the RTC and is gradually stretched out in the tension zone at the RBC and the LTC (section 3.8.1).
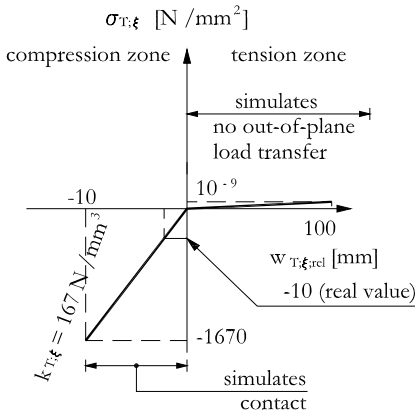
Teflon
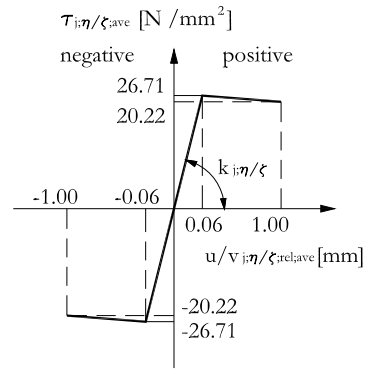
Epoxy

Polyurethane
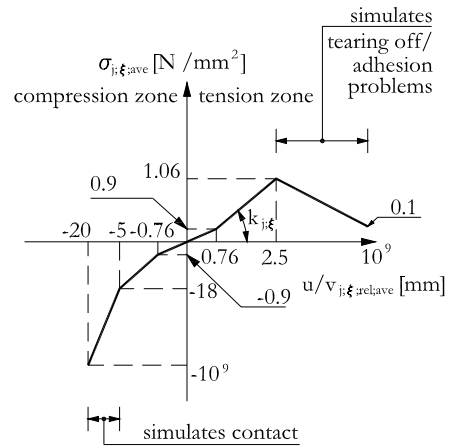
Polyurethane

Figure 4.9: *Input of non linear material behaviour for interfaces A to C: relation between the normal stresses and the relative out-of-plane displacements for Teflon (left top), relation between the average shear stresses and average relative in-plane displacements for epoxy (right top), relation between the average shear stresses and average relative in-plane displacements for polyurethane (left bottom) and relation between the average normal stresses and average relative in-plane displacements for polyurethane (right bottom)*

The absence of the adhesive bonded joint in the compression zone and the tearing off/adhesion problems in the tension zone results in no in-plane shear load transfer. Therefore, the relation between the shear stresses and the relative in-plane displacements in longitudinal direction is adjusted to a very small shear stiffness after passing the negative as

well as the positive relative in-plane displacement of 5 mm and simulates the absent of in-plane shear load. However, the adjustment is arbitrary. Furthermore, it is plausible that a positive as well as a negative relative displacement results in the same value for the shear stresses. Therefore, the relation between the shear stresses and the relative in-plane displacements is symmetrical.

Figure 4.9 at the right bottom shows the relation between the average normal stresses ($\sigma_{j;\xi;ave}$) and average relative in-plane displacements in normal direction ($u_{j;\xi;rel;ave}/v_{j;\xi;rel;ave}$). Tests were carried out for the determination of the relation between the average compression stresses and the average relative in-plane displacements in normal directio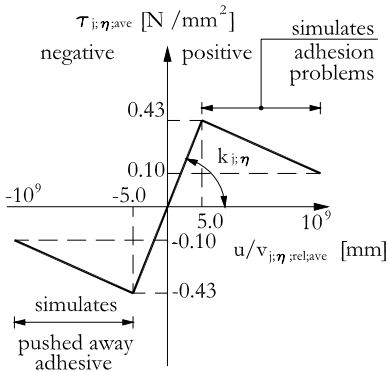n (section C.2.3) and the relation between the average tension stresses and the average relative in-plane displacements in normal direction (section C.2.2). The tests represented a part of the adhesive bonded joint including the boundary conditions, namely four-sided enclosed (figure 3.3). In the compression zone, the glass-steel contact (section 3.7.1) is simulated by a very large normal stiffness of the adhesive bonded joint after passing the relative in-plane displacement in normal direction of 5.0 mm as based on visual observations. In the tension zone, tearing off and adhesion problems (section 3.7.1) are simulated by a very small normal stiffness of the adhesive bonded joint after passing the relative in-plane displacement in normal direction of 2.5 mm as based on visual observations (section 3.7.1).

The tests for the average compression stress-strain relation, the average tension stress-strain relation and the average shear stress-strain relation were determined separately. The influence of the normal stresses (compression and tension stresses) on the shear stresses were not taken into account. The relation between the average shear stresses and the average relative in-plane displacements in longitudinal direction ends at a relative in-plane displacement of 5 mm then no in-plane load transfer takes place by shear stresses in longitudinal direction. However, the adhesive bonded joint in the tension zone was torn off and had adhesion problems halfway the first stage. Exactly, no in-plane load transfer by shear stresses in longitudinal direction took place. On the other hand, the adhesive bonded joint in the compression zone remained transferring the in-plane load by shear stresses in longitudinal direction and even more [Habenicht 2006] than found in the shear tests, because the compression stresses perpendicular to the shear direction results in an increase of capacity to transfer shear stresses in longitudinal direction. It is assumed that the adhesive bonded joint remains transferring the shear stresses in longitudinal direction in the compression zone as well as in the tension zone till a relative in-plane displacement of 5 mm.

4.6 Geometrical imperfections

Geometrical imperfections are substantial parameters for slender in-plane loaded plate structures such as glass panes. The geometrical imperfections for glass panes are varying glass pane thickness and out-of-plane imperfection [Haldimann 2008]. The varying glass pane thickness is the result of the float process. These production tolerances have a lower limit and an upper limit prescribed in [EN 572-8 2004]. In general, the real glass pane thickness is smaller than the nominal glass pane thickness and this also concerns for the measured glass pane thickness (appendix A.6). The applied glass pane thickness in the finite element models is the lower limit and is 11.7 mm for nominal glass pane thickness of 12 mm. The out-of-plane imperfection is mainly caused by follow-up treatment for increasing the glass strength (section

2.3.1). The applied glass type is annealed float glass and has a very small out-of-plane imperfection. An out-of-plane imperfection of the glass pane is more realistic especially for smaller glass pane thicknesses and larger glass pane sizes. The maximum out-of-plane imperfection at the centre of the glass panes is the largest size of the glass pane divided by 2000 [Luible 2004] and this value is used in the finite element models.

4.7 Solution strategy

The solution strategy consisted of two analyses. The purpose of the first analysis was applying the initial out-of-plane deformation on the glass pane. The glass pane was four sided supported in the steel frame realized by the material input for interfaces A and C and subjected to a uniformly distributed out-of-plane load. The maximum out-of-plane displacements at the centre of the glass pane corresponded with the largest size of the glass pane divided by 2000. The out-of-plane deformations of the glass pane were read in a new finite element model. So, the initial out-of-plane deformation of the glass pane was incorporated without any pre-stress. The type of analysis was geometrical and physical linear.

The second analysis was the simulations of the experiments of the systems with joint types 1 to 3. The type of analysis was geometrical and physical non linear. The geometrical non linear calculation was needed for the out-of-plane displacements of the glass pane with an initial out-of-plane deformation subjected to in-plane loads. A regular Newton-Raphson iteration scheme was applied i.e. the tangential stiffness matrix is set up before each iteration. The deformations were described with a Lagrange description i.e. the strain is defined with reference to the undeformed geometry. For the physical non linear calculation the option interface non linear behaviour was activated only. The sizes of the load steps depended on the system with joint types 1 to 3 e.g. smaller load steps at the moment of glass steel contact for systems with joint type 1. The horizontal in-plane load (F_h) is displacement controlled and is centrically introduced in the negative x-direction at the right side of the outside beam of the top transom.

4.8 Calibration

In the previous sections, the geometry of the finite element model, the applied elements and the material input have been discussed to simulate systems with joint types 1 to 3. This section deals with the calibration of the finite element model with the experiments (section 3.7). The calibration starts with the global and local behaviour of all systems to investigate the influence of the vertical spring at the RBC of the system (section 3.5.1) and the shear flexibility of the bolted connection between the outside beam and the beadwork (3.5.2). Sensitivity studies are carried out to investigate the influence of the shear flexibility of the bolted connection between the outside beam and the beadwork on the global behaviour of the system. Sensitivity studies are also carried out to investigate the influence of the variation of the shear stiffness of the adhesive bonded joint of systems with joint type 2 and 3 on the global behaviour of the system. Then the simulations of systems with joint types 1 to 3 are calibrated separately. The calibrations are the relation between the horizontal in-plane displacements at the RTC of the system and the horizontal in-plane load, the relation between the horizontal in-plane displacements at the RTC of the system and the out-of-plane displacements at the centre of the glass pane and the relation between the horizontal in-plane displacements at the RTC of

the system and the principle stresses on the front of the glass pane at interesting points. The calibrations of the principle stresses on the front of the glass pane in other points were published in [Huveners 2008a].

4.8.1   Global behaviour of all systems

The vertical in-plane displacements at the RBC of the system (section 3.5.1) and the shear flexibility of the bolted connection between the outside beam and the beadwork (section 3.5.2) were mentioned as main causes for the reduction of the in-plane stiffness of the system. These two main causes were determined experimentally (appendix B) and were simulated in the finite element model. These influences on the global behaviour of the systems with joint types 1 to 3 were investigated by means of varying the spring stiffnesses at the RBC of the system and varying the shear flexibility of the bolted connection between the outside beam and the beadwork and are given in columns I to IV of table 4.4. Column I gives a very large spring stiffness ($K_{y;RBC} = 10^{20}$ N/mm) and a very large shear stiffness ($k_{b;\eta} = 10^6$ N/mm^3) which have to correspond with the basic assumptions of the system (section 3.1). Column II gives a very large spring stiffness ($K_{y;RBC} = 10^{20}$ N/mm) and the experimentally found shear stiffness ($k_{b;\eta} = 10$ N/mm^3) which investigates the shear flexibility on the global behaviour of the systems only. Column III gives the experimentally found spring stiffness ($K_{y;RBC} = 1.03 \cdot 10^5$ N/mm) and a very large shear stiffness ($k_{b;\eta} = 10^6$ N/mm^3) which investigates the vertical in-plane displacements of the RBC on the global behaviour of the systems only. Column IV gives the experimentally found spring stiffness ($K_{y;RBC} = 1.03 \cdot 10^5$ N/mm) and the experimentally found shear stiffness ($k_{b;\eta} = 10$ N/mm^3) which have to simulate the experiments. Column V gives the values from the experiments (section 3.7) and column VI gives the deviation between the simulation (column IV) and the experiments (column V). Table 4.4 gives an overview of the horizontal in-plane load (F_h), the actually horizontal in-plane displacement at the RTC of the system ($u_{RTC;s}$) (section 3.5.1) and the in-plane stiffness of the system (K_s) (section 3.6.1) at limited horizontal in-plane displacement at the RTC of the system and at glass-steel contact for systems with joint type 1 (table 3.2) and at a horizontal in-plane load about 46 kN for systems with joint type 2 (table 3.4) and at a horizontal in-plane load about 31 kN for systems with joint type 3 (table 3.6). Furthermore, the out-of-plane imperfection at the centre of the glass pane was -0.5 mm.

For systems with joint type 1, varying the spring stiffnesses at the RBC of the system and the shear flexibility of the bolted connection between the outside beam and the beadwork had slightly influence on the global behaviour of the system at limited horizontal in-plane displacement at the RTC of the system as well as at glass-steel contact. For systems with joint type 2 and 3, varying the spring stiffnesses at the RBC of the system and the shear flexibility of the bolted connection between the outside beam and the beadwork had large influence on the global behaviour of the system with non-cracked glass panes. A very large spring stiffness at the RBC of the system and a very large shear flexibility of the bolted connection (column I) resulted in a horizontal in-plane load which is 5.43 times larger than the experiments of systems with joint type 2 and 3. A very large spring stiffness and a shear flexibility of $k_{b;\eta} = 10$ N/mm^3 (column II) resulted in a horizontal in-plane load which is 1.80 times larger than the experiments of systems with joint type 2 and 3. A spring stiffness of $K_{y;RBC} = 1.03 \cdot 10^5$ N/mm and a very large shear flexibility (column III) resulted in a horizontal in-plane load which is 1.58 and 1.85 times larger than the experiments of systems with joint type 2 and 3 respectively. A spring stiffness of $K_{y;RBC} = 1.03 \cdot 10^5$ N/mm and a shear flexibility of $k_{b;\eta} = 10$ N/mm^3

(column IV) resulted in a horizontal in-plane load which almost corresponds with the experiments of systems with joint type 2 and 3, but systems with joint type 3 differs more.

Table 4.4:   Overview of the global behaviour of systems with joint types 1 to 3 at four different combinations of the spring stiffness at the RBC of the system and the shear flexibility of the bolted connection between the outside beam and the beadwork compared with the behaviour found in experiments

			I	II	III	IV	V	VI
	$K_{y;RBC}$	[N/mm]	10^{20}	10^{20}	$1.03 \cdot 10^5$	$1.03 \cdot 10^5$	Exp.	Dev.
	$k_{s;\eta}$	[N/mm³]	10^6	10	10^6	10		[%]
System 1	u_{RTC}	[mm]	3.69	3.69	3.69	3.69	3.69	0.00
	F_h	[kN]	4.37	4.33	4.30	4.27	4.42	-3.40
	$u_{RTC;s}$	[mm]	3.69	3.69	3.65	3.65	3.65	0.00
	K_s	[kN/mm]	1.18	1.17	1.18	1.17	1.21	-3.30
	u_{RTC}	[mm]	23.40	23.40	23.40	23.40	21.84	7.14
	F_h	[kN]	39.10	37.20	36.70	37.70	36.87	2.25
	$u_{RTC;s}$	[mm]	23.01	23.03	23.03	23.02	21.13	8.96
System 2	u_{RTC}	[mm]	1.02	1.02	1.02	1.02	1.02	0.00
	F_h	[kN]	249.33	82.62	72.31	45.56	45.89	-0.72
	$u_{RTC;s}$	[mm]	1.02	1.02	0.30	0.56	0.56	0.00
	K_s	[kN/mm]	239.65	79.41	243.56	80.72	81.79	-1.30
System 3	u_{RTC}	[mm]	0.81	0.81	0.81	0.81	0.81	0.00
	F_h	[kN]	182.52	55.80	58.21	33.80	31.43	7.54
	$u_{RTC;s}$	[mm]	0.81	0.81	0.23	0.47	0.50	-6.00
	K_s	[kN/mm]	225.33	68.89	253.09	71.91	65.39	9.97

The shear flexibility of the bolted connection between the outside beam and the beadwork results in relative horizontal and vertical in-plane displacements between the outside beam and the beadwork (figure 4.10). Moreover, the flexural stiffness of the mullions and transoms are also reduced. These relative in-plane displacements between the outside beam and the beadwork and the reduction of the flexural stiffness of the transoms and the mullions reduce the in-plane stiffness of the system resulting in smaller horizontal in-plane loads (column II). The vertically in-plane loaded spring at the RBC of the system has vertical in-plane displacements resulting in an in-plane rotation of the entire system. The in-plane rotation of the entire system reduces the in-plane stiffness of the system resulting in smaller horizontal in-plane loads (column III). The in-plane stiffness of the systems is more reduced by the interaction between the shear flexibility of the bolted connection between the outside beam

and the beadwork and the spring stiffness at the RBC of the system (column IV). This interaction more simulates the experiments (columns V and VI).
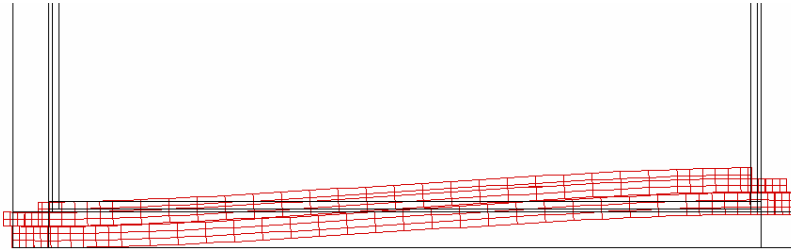
Figure 4.10:   Horizontal and vertical in-plane displacements of the bottom transom 'Shear flexibility' of the bolted connection between the outside beam and the beadwork, the discrete vertical spring at the RBC and bending of the bottom transom of systems with joint type 2 with $u_{RTC} = 1.02$ mm (scale 1:100)

The shear flexibility of the bolted connection between the outside beam and the beadwork was determined by means of a four-point bending test and finite element simulations (appendix B.2). The shear flexibility was $k_{b;\eta} = 10$ N/mm^3 and matched well with the experiments (table 4.4). Nevertheless, the influence of the shear flexibility on the global behaviour of the system for systems with joint type 2 and 3 was further investigated in the finite element model by means of a sensibility study. Figure 4.11 shows the relation between the horizontal in-plane load and the shear flexibility of the bolted connection between the outside beam and the beadwork. The experimentally found shear flexibility is located in the slope between a small and a large shear flexibility (figure 4.11). For systems with joint type 2, halving ($k_{b;\eta} = 5$ N/mm^3) or doubling ($k_{b;\eta} = 20$ N/mm^3) the shear flexibility with regard to a shear flexibility of $k_{b;\eta} = 10$ N/mm^3 results in a horizontal in-plane load of 42.6 kN (-9.17%) and 52.8 kN (12.48%) respectively. For systems with joint type 3, halving or doubling the shear flexibility with regard to a shear flexibility of $k_{b;\eta} = 10$ N/mm^3 results in a horizontal in-plane load of 27.6 kN (-11.82%) and 36.1 kN (15.33%) respectively. Varying the shear flexibility of the bolted connection between the outside beam and the beadwork around 10 N/mm^3 has clearly influence on the global behaviour of the systems with joint type 2 and 3, because the shear flexibility is located in the steepest slope of the relation in which a decrease or an increase of the shear stiffness influence the global behaviour of the system.

For systems with joint type 2 and 3, the influence of the shear stiffness of the adhesive bonded joint on the global behaviour of the system was also subjected to a sensibility study. Figure 4.12 shows the relation between the horizontal in-plane load and the shear stiffness of the adhesive bonded joint for systems with joint type 2 and 3. The relation between the average shear stress and the average relative in-plane displacement of epoxy (figure 4.9 right top) was used with the assumption that the average shear stresses varied and the accompanying relative in-plane displacements remained the same. The normal stiffness of the epoxy adapted to the shear stiffness.

The graph shows "Horizontal in-plane load (F_h) [kN]" on the y-axis (0 to 80) versus "Shear flexibility ($k_{b;\eta}$) of the bolted connection between the outside beam and the beadwork (logarithm) [N/mm^3]" on the x-axis (1 to 10000, logarithmic).

Labels on graph:
- System with joint type 2 at u_{RTC} = 1.03 mm
- F_h = 46.90 kN
- System with joint type 3 at u_{RTC} = 0.81 mm
- F_h = 31.30 kN
- 5 N/mm^3
- 10 N/mm^3
- 20 N/mm^3
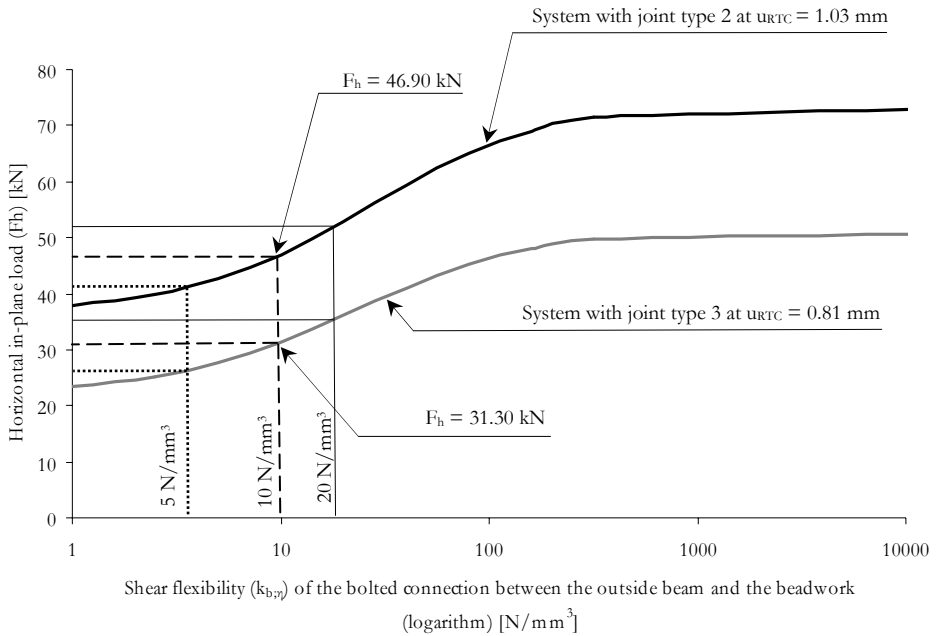
Figure 4.11:   Variation of the shear flexibility of the bolted connection between the outside beam and the beadwork on the horizontal in-plane load for systems with joint type 2 and 3

The initial linear shear stiffness of the applied adhesive bonded joint is 432 N/mm^3 and is located in a less steep slope of the relation. For systems with joint type 2, halving ($k_{j;\eta}$ = 216 N/mm^3) or doubling ($k_{j;\eta}$ = 864 N/mm^3) the shear stiffness of the adhesive bonded joint with regard to the initial linear shear stiffness of $k_{j;\eta}$ = 432 N/mm^3 results in a horizontal in-plane load of 44.5 kN (-5.12%) and 48.9 kN (4.26%) respectively. For systems with joint type 3, halving or doubling the shear stiffness of the adhesive bonded joint with regard to the initial linear shear stiffness of $k_{j;\eta}$ = 432 N/mm^3 results in a horizontal in-plane load of 29.4 kN (-6.07%) and 32.8 kN (4.79%) respectively. Varying the shear stiffness of the adhesive bonded joint around 432 N/mm^3 has small influence on the global behaviour of systems with joint type 2 and 3, because the shear stiffness is located in a lesser steep slope of the relation in which a decrease or an increase of the shear stiffness hardly influence the global behaviour of the system.

The experimentally found spring stiffness at the RBC of the system (appendix B.1), shear stiffness of the bolted connection between the outside beam and the beadwork (appendix B.2) and the shear stiffness of the adhesive bonded joint (appendix C.1.3) for systems with joint type 2 and 3 match well with the experiments and are used for the parametric studies (chapter 5).

The y-axis is labelled "Horizontal in-plane load (F_h)[N/mm^2]" and the x-axis is labelled "Shear stiffness ($k_{j;\eta}$) of the adhesive bonded joint (logarithm)[N/mm^3]".

Labels within the figure:
- System with joint type 2 at u_{RTC} = 1.03 mm
- F_h = 46.90 kN
- F_h = 31.30 kN
- System with joint type 3 at u_{RTC} = 0.81 mm
- 216 N/mm^3
- 432 N/mm^3
- 864 N/mm^3
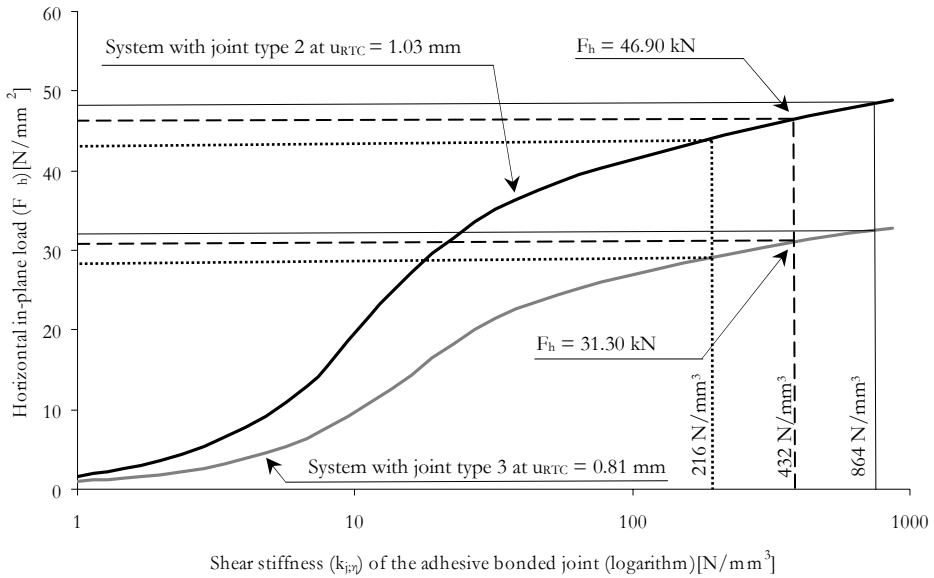
Figure 4.12: Variation of the shear stiffness of the adhesive bonded joint on the horizontal in-plane load for systems with joint type 2 and 3

4.8.2 Local behaviour of all systems

Table 4.5 gives an overview of the principle stresses and their directions at points 1 to 5 located on the front of the glass pane (figure 3.5) for systems with joint types 1 to 3. The material input is given in section 4.5. Furthermore, the glass pane has an out-of-plane imperfection at the centre of the glass pane of -0.50 mm (double curved glass pane). The principle stresses and their directions belong to the limited horizontal in-plane displacement at the RTC of the system for systems with joint type 1, at a horizontal in-plane load around 46 kN for systems with joint type 2 and at a horizontal in-plane load around 31 kN for systems with joint type 3. The experimentally found principle stresses and their directions are given in figure 3.12 top, figure 3.17 top and figure 3.22 for systems with joint types 1 to 3 respectively.

The simulation of systems with joint type 1 have bilateral compression stresses at points 1 and 5, bilateral tension stresses at points 2 and 4 and tension stresses and compression stresses at point 3 at limited horizontal in-plane displacement at the RTC of the system. The directions of the maximum principle stresses are around -45° with the horizontal at points 1 to 5. The stress state is two-dimensional. The experiments show larger minimum principle stresses at points 1, 3 and 5 and larger maximum principle stresses at points 2 and 4 than the simulation. The simulation of systems with joint type 2 and 3, the maximum principle stresses are tension stresses and the minimum principle stresses are compression stresses at points 1 to 5 at a horizontal in-plane load around 46 kN and 31 kN respectively. The directions of the maximum principle stresses are around -45° with the horizontal at points 1 to 5. The stress state is two-

dimensional. For systems with joint type 2, the simulation shows larger minimum principle stresses at points 1, 3 and 5 and larger maximum principle stresses at points 2, 3 and 4 than the experiments. For systems with joint type 3, the simulation shows larger minimum principle stresses at points 1 and 5 and larger maximum principle stresses at points 2, 3 and 4 than the experiments.

Table 4.5: Overview of the principle stresses and their directions at points 1 to 5 (front of the glass pane) for systems with joint types 1 to 3 with an out-of-plane imperfection of -0.5 mm

	u_{RTC} [mm]	F_h [kN]			Point 1	Point 2	Point 3	Point 4	Point 5
System 1	3.70	4.42	$\sigma_{g;1}$	[N/mm²]	-0.55	0.87	0.79	0.87	-0.55
			$\sigma_{g;2}$	[N/mm²]	-0.91	0.55	-0.80	0.55	-0.91
			θ	[°]	-44.38	-44.91	-44.89	-44.91	-44.73
System 2	1.02	45.89	$\sigma_{g;1}$	[N/mm²]	1.57	9.48	4.15	8.57	1.56
			$\sigma_{g;2}$	[N/mm²]	-9.04	-1.42	-4.16	-1.69	-9.03
			θ	[°]	-43.38	-44.91	-44.96	-44.93	-43.40
System 3	0.81	31.43	$\sigma_{g;1}$	[N/mm²]	2.93	7.18	4.06	6.64	2.93
			$\sigma_{g;2}$	[N/mm²]	-6.90	-2.90	-4.07	-2.92	-6.90
			θ	[°]	-43.31	-44.97	-44.97	-44.97	-43.41

The simulation of systems with joint type 1, the glass pane has a horizontal in-plane shift and an in-plane rotation within the steel frame (section 3.7.1) resulting in pushing in of the adhesive bonded joint at the LBC and RTC and stretching out of the adhesive bonded joint at the RBC and the LTC. The pushed in adhesive bonded joint transfers compression load resulting in bilateral compression stresses at points 1 and 5 and the stretched out adhesive bonded joint transfers tension load resulting in bilateral tension stresses at points 2 and 4. The simulation of systems with joint type 2 and 3, the glass pane acts like a shear wall i.e. tension stresses at an angle of -45° with the horizontal and compression stresses at an angle of 45° at a horizontal in-plane load around 46 kN and 31 kN respectively. Moreover, the tension stresses and compression stresses are equal in size. However, the principle stresses at points 1, 2, 4 and 5 deviate from the distribution of the principle stresses of a shear wall, because the adhesive bonded joint has influence on the distribution of the principle stresses in the glass pane. The simulation of systems with joint type 3, the eccentric in-plane load transfer also influences the distribution of the principle stresses in the glass pane. The influence of the steel frame and the adhesive bonded joint on the distribution of the principle stresses in the glass pane will be explained extensively in chapter 5. The simulations of systems with joint types 1 to 3 show a more double symmetrical (idealized) distribution of the principle stresses and their directions than the experiments. The experiments showed much dispersal, because the measurements of

small strains are susceptible for variation e.g. by a locally irregular in-plane load transfer of the adhesive bonded joint.

4.8.3   Systems with joint type 1

Figure 4.13 shows the comparison between simulation and experiments of the relation between the horizontal in-plane loads and the horizontal in-plane displacements at the RTC of the system for glass pane size of 1.0 m x 1.0 m. The out-of-plane imperfection at the centre of the glass pane is -0.5 mm. The simulation coincides with the experiments in the first stage. On the other hand, the simulation deviates from the experiments at the vicinity of the transition of two stages (glass-steel contact) and the second stage. The simulation gives a sharper transition of two stages than the experiments which was more gradual. The simulation gives a straight relation for the second stage than the experiments which had an irregular pattern. Moreover, the glass pane is still supported laterally at glass-steel contact. Figure 4.14 shows the comparison between simulation and experiments of the relation between the out-of-plane displacements at the centre of the glass pane and the horizontal in-plane displacements at the RTC of the system. The simulation coincides with the experiments at the beginning of the first stage. Then the simulation more and more deviates from the experiments, namely the simulation gives smaller out-of-plane displacements than found in the experiments. The simulated out-of-plane displacements more and more displace out-of-plane after passing the glass-steel contact. Figure 4.15 shows the comparison between simulation and experiments of the relation between the principle stresses and the horizontal in-plane displacements at the RTC of the system at point 5. The simulation coincides with the experiments except for the transition of two stages (glass-steel contact) and the second stage. The simulation gives a sharper transition of two stages than the experiments which was more gradual. The simulation gives a straight relation for the second stage than the experiments. Figure 4.16 shows the distribution of the minimum principle stresses of the entire system (figure 4.16 left) and the glass pane only (figure 4.16 right) at the moment of the glass-steel contact from the finite element model.

The simulation gives a sharper transition of two stages than the experiments for the relation between the horizontal in-plane load and the horizontal in-plane displacement at the RTC of the system as well as the distribution of the principle stresses. The sharper transition is the result of the simplified multiple linear relation between the normal compression stresses and the relative in-plane displacements of the adhesive bonded joint (figure 4.9 right bottom). Glass-steel occurs at impressing of the entire joint thickness. The simulation gives a smooth straight line in the second stage deviating from the results of the experiments, because in the finite element model the cracking of the glass pane is not implemented. Furthermore, cracking and flaking off of the corners of the glass pane lead to change of the in-plane load transfer between the steel frame and the glass pane and this is also not implemented in the finite element model.

Figure 4.13:   Comparison between simulation (bolt dots) and experiments (continuous lines) of the relation between the horizontal in-plane loads and the horizontal in-plane displacement at the RTC
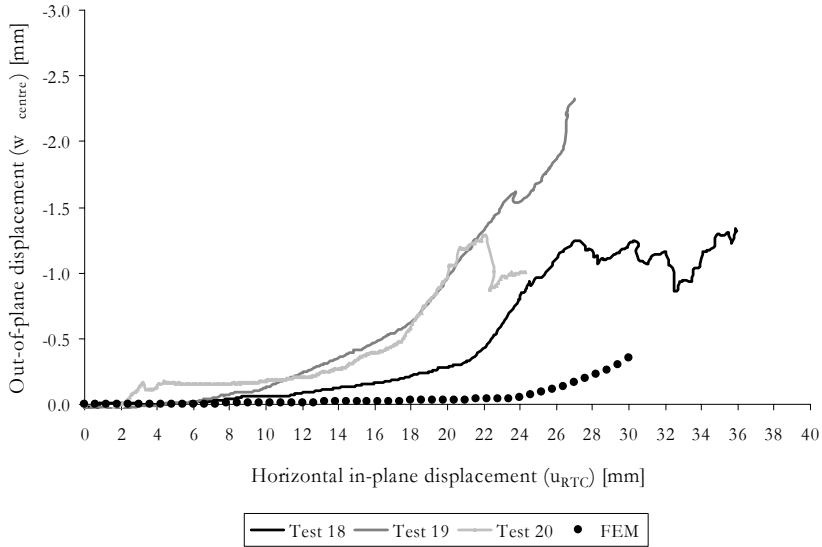
Figure 4.14:   Comparison between simulation (bolt dots) and experiments (continuous lines) of the relation between the out-of-plane displacements at the centre of the glass pane and the horizontal in-plane displacements at the RTC of the system

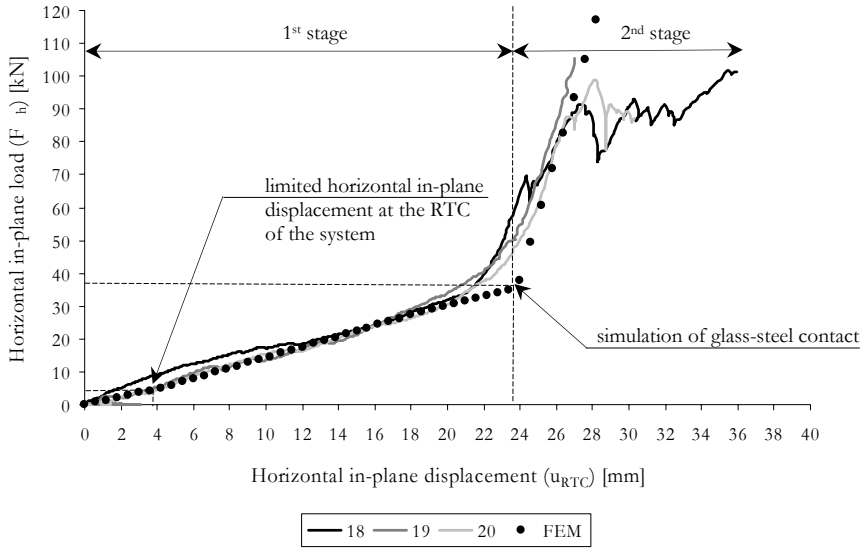*Figure 4.15:   Comparison between simulation (bolt dots) and experiments (continuous lines) of the relation between the principle stresses and horizontal in-plane displacements at the RTC of the system at point 5*

Figure 4.16:   Distribution of the minimum principle stresses at the moment of glass-steel contact at u_{RTC} = 23.4 mm of the entire system (left) and the glass pane only (right)

4.8.4 Systems with joint type 2

Figure 4.17 shows the comparison between simulation and experiments of the relation between the horizontal in-plane load and the horizontal in-plane displacement at the RTC of the system for glass pane size of 1.0 m x 1.0 m. The out-of-plane imperfection at the centre of the glass pane is -0.5 mm. The simulation coincides with the experiments at small horizontal in-plane displacements at the RTC of the system. Then the simulation more and more deviates from the experiments, namely the simulation gives larger in-plane loads than found in the experiments. Furthermore, the simulation is slightly curved. Figure 4.18 shows the comparison between simulation and experiments of the relation between the out-of-plane displacements at the centre of the glass pane and the horizontal in-plane dis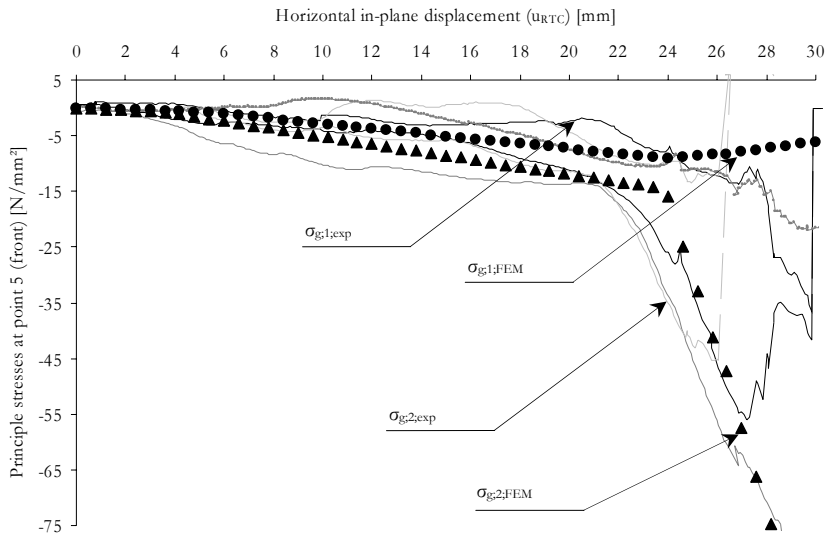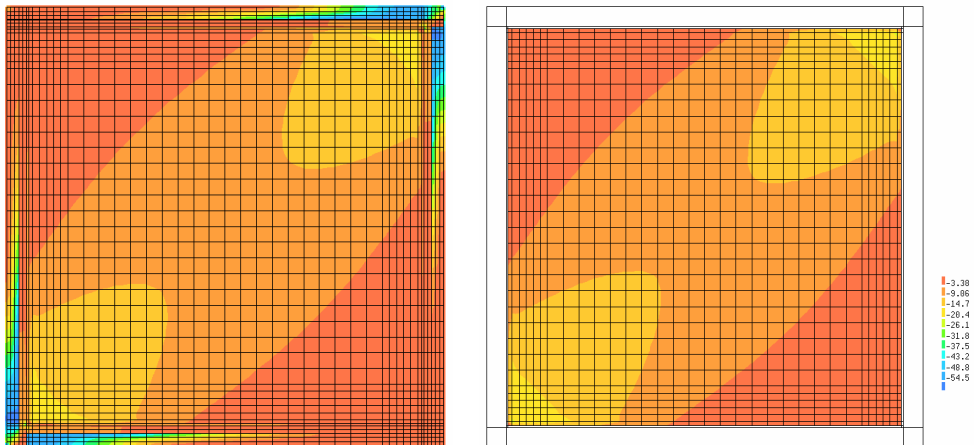placements at the RTC of the system. The simulation coincides with the experiments at the very beginning of the relation except for test 2. Then the simulation more and more deviates from the experiments, namely the simulation gives smaller out-of-plane displacements than found in the experiments. Moreover, the simulation shows a gradual smooth increase of the out-of-plane displacements than found in the experiments. Figure 4.19 shows the comparison between simulation and experiments of the relation between the principle stresses and the horizontal in-plane displacements at the RTC of the system at point 1. The simulation coincides with the experiments at small horizontal in-plane displacements at the RTC of the system. Then the simulation more and more deviates from the experiments, namely the simulation gives larger minimum principle stresses than found in the experiments. The minimum principle stresses are compression stresses and the maximum principle stresses are tension stresses which become compression stresses at larger horizontal in-plane displacements at the RTC of the system. Figure 4.20 shows the comparison between simulation and experiments of the relation between the principle stresses and the horizontal in-plane displacements at the RTC of the system at point 2. The simulation coincides with the experiments at small horizontal in-plane displacements at the RTC of the system. Then the simulation more and more deviates from the experiments, namely the simulation gives larger maximum principle stresses than found in the experiments. The maximum principle stresses are tension stresses and the minimum principle stresses are compression stresses which become tension stresses at larger horizontal in-plane displacements at the RTC of the system.

The deviation between the simulation and the experiments for the horizontal in-plane loads, out-of-plane displacements at the centre of the glass pane and the principle stresses at larger horizontal in-plane displacements at the RTC of the system is the result of constantly cracking of the glass pane (figure 3.15) till failure. Cracking of the glass pane is not implemented in the finite element model. The relation between the horizontal in-plane load and the horizontal in-plane displacement at the RTC of the system is slightly curved for the simulation as well as the experiments because of the plastic-like behaviour (figure 4.9 right top) of the adhesive. At the end of the adhesive bonded joint the plastic-like behaviour of the adhesive occurs at the shear stresses in transversal direction. The zone of the plastic-like behaviour of the shear stresses in transversal direction at the end of the adhesive bonded joint increase in longitudinal direction of the adhesive bonded joint at increasing horizontal in-plane displacements at the RTC of the system. This influence the distribution of the principle stresses at the corners of the glass pane. So, the LBC of the glass pane is more and more subjected to compression stresses resulting in a change of sign of the maximum principle stresses (figure 4.19) and the RBC of the glass is more and more subjected to tension stresses resulting in a change of sign of the minimum principle stresses (figure 4.20). The plastic like behaviour of the adhesive is demonstrated in

the global and local behaviour of the simulation as well as the experiments. The influences of the shear flexibility of the bolted connection between the outside beam and the beadwork and the spring stiffness at the RBC of the system (sections 3.7.2 and 3.7.3) hardly contribute in the non linear behaviour of the system. The extrapolation of the relation between the shear stress and the relative in-plane displacement (appendix C.1.3) can be justified, because the minimum principle stresses of the simulation and the experiments show the same image (figure 4.19). The simulation of the out-of-plane displacements at the centre of the glass pane are incorrectly described by the finite element model. Probably, the systems set during the run-up of the tests. Furthermore, the principle stresses are small for seriously out-of-plane displacements at the centre of the glass regarding plate buckling (section 3.7.2). Exactly, an unequivocal explanation can not be given.

Figure 4.17:   Comparison between simulation (bolt dots) and experiments (continuous lines) of the relation between the horizontal in-plane load and the horizontal in-plane displacement at the RTC

Figure 4.18:   Comparison between simulation (bolt dots) and experiments (continuous lines) of the relation between the out-of-plane displacements at the centre of the glass pane and the horizontal in-plane displacements at the RTC of the system

Figure 4.19:   Comparison between simulation (bolt dots and bolt triangles) and experiments (continuous lines) of the relation between the principle stresses and horizontal in-plane displacements at the RTC of the system at point 1

103
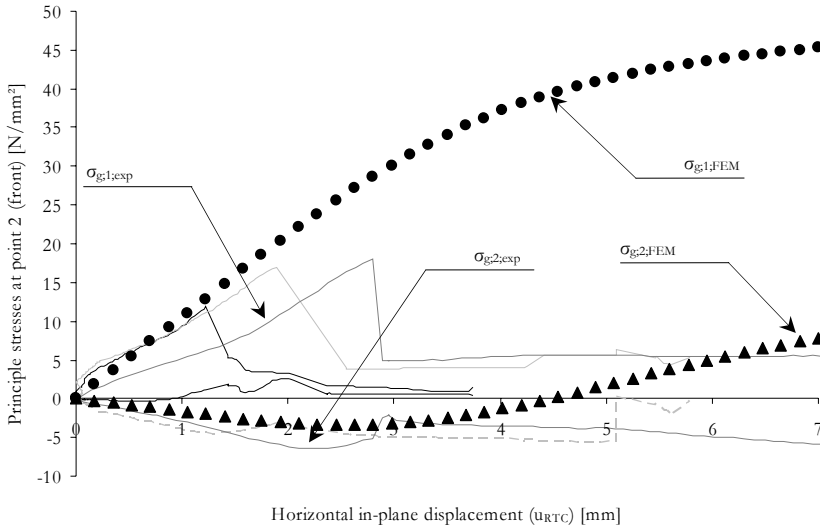
Figure 4.20: Comparison between simulation (bolt dots and bolt triangles) and experiments (continuous lines) of the relation between the principle stresses and horizontal in-plane displacements at the RTC of the system at point 2

4.8.5   Systems with joint type 3

Figure 4.21 shows the comparison between simulation and experiments of the relation between the horizontal in-plane load and the horizontal in-plane displacement at the RTC of the system for glass pane size of 1.0 m x 1.0 m. The out-of-plane imperfection at the centre of the glass pane is -0.5 mm. The simulation coincides with the experiments at small horizontal in-plane displacements at the RTC of the system. Then the simulation more and more deviates from the experiments, namely the simulation gives larger in-plane loads than found in the experiments. Furthermore, the relation is slightly curved. Figure 4.22 shows the comparison between simulation and experiments of the relation between the out-of-plane displacements at the centre of the glass pane and the horizontal in-plane displacements at the RTC of the system. The simulation coincides with the experiments at the very beginning of the relation. Then the simulation more and more deviates from the experiments, namely the simulation gives smaller out-of-plane displacements than found in the experiments. Figure 4.23 shows the comparison between simulation and experiments of the relation between the principle stresses and the horizontal in-plane displacements at the RTC of the system at point 2. The simulation coincides with the experiments at small horizontal in-plane displacements at the RTC of the system. Then the simulation more and more deviates from the experiments, namely the simulation gives larger maximum and minimum principle stresses than found in the experiments. The maximum principle stresses are tension stresses and the minimum principle stresses are compression stresses.
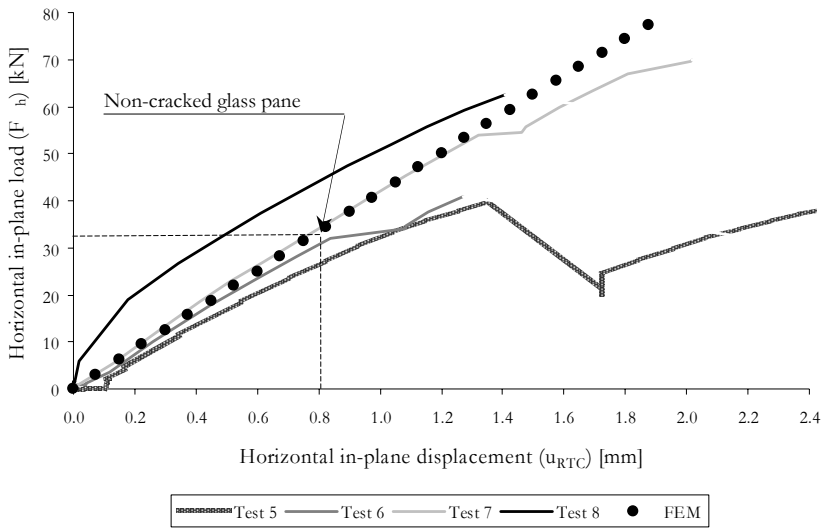
Figure 4.21: *Comparison between simulation (bolt dots) and experiments (continuous lines) of the relation between the horizontal in-plane load and the horizontal in-plane displacement at the RTC*
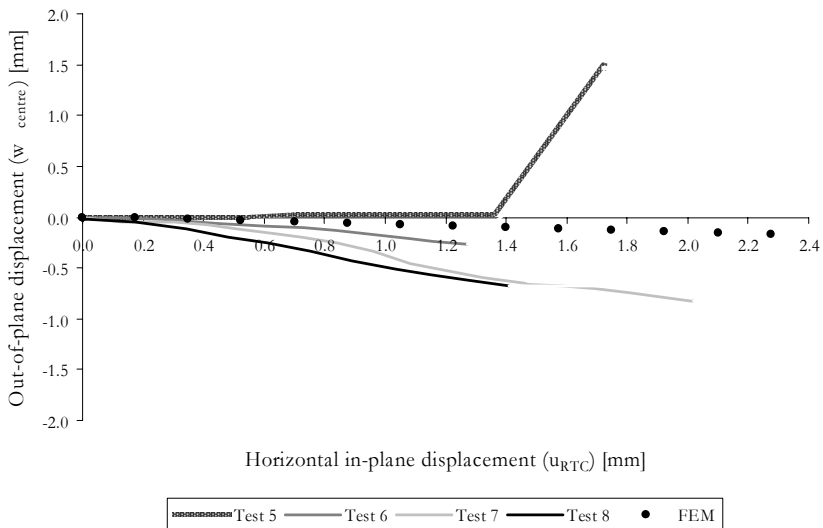
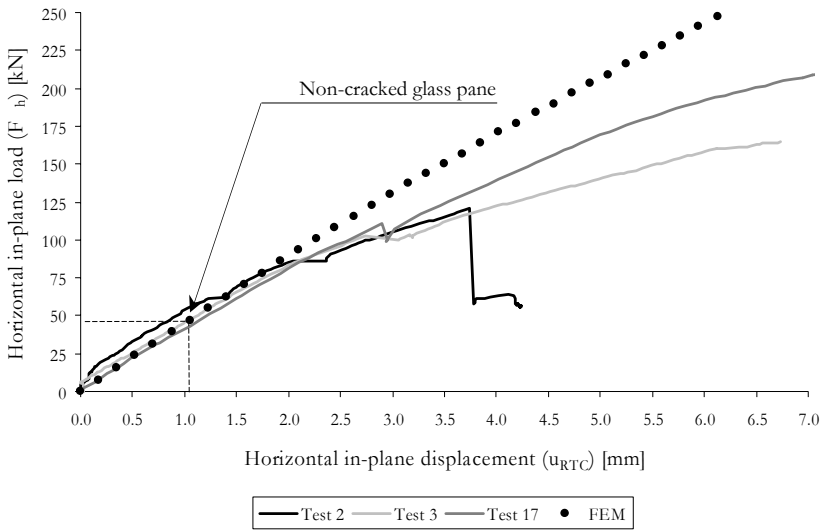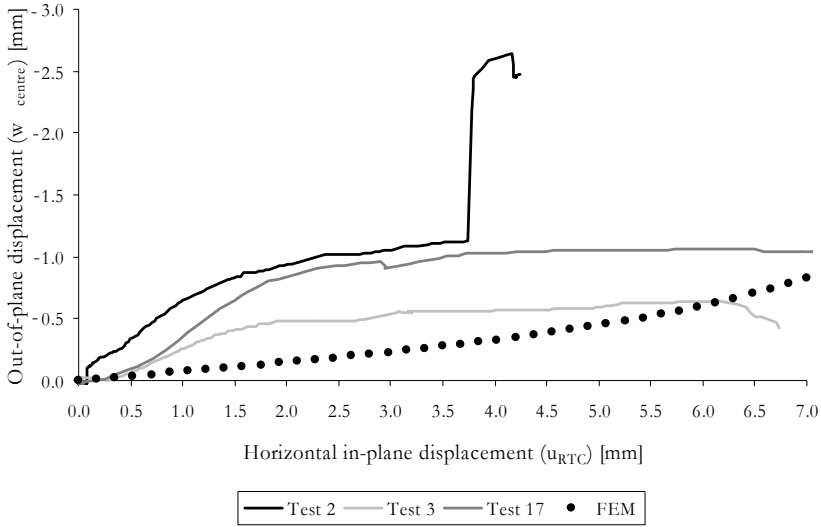*Figure 4.22:* *Comparison between simulation (bolt dots) and experiments (continuous lines) of the relation between the out-of-plane displacements at the centre of the glass pane and the horizontal in-plane displacements at the RTC of the system*
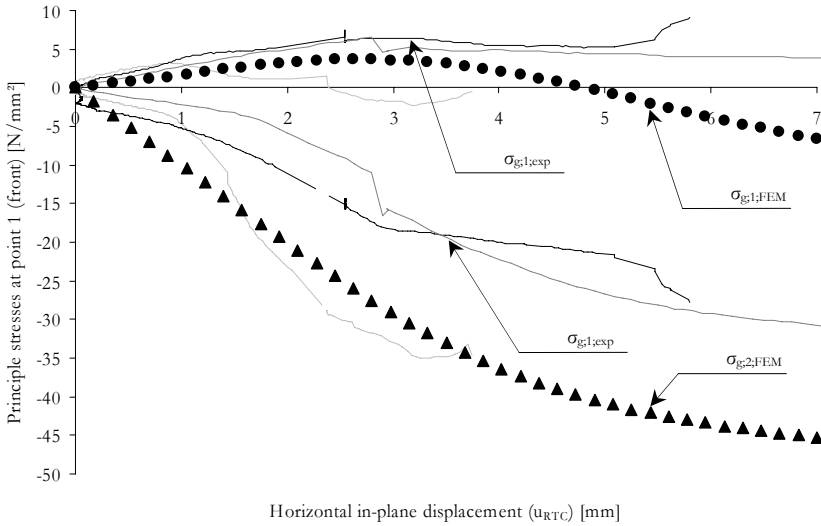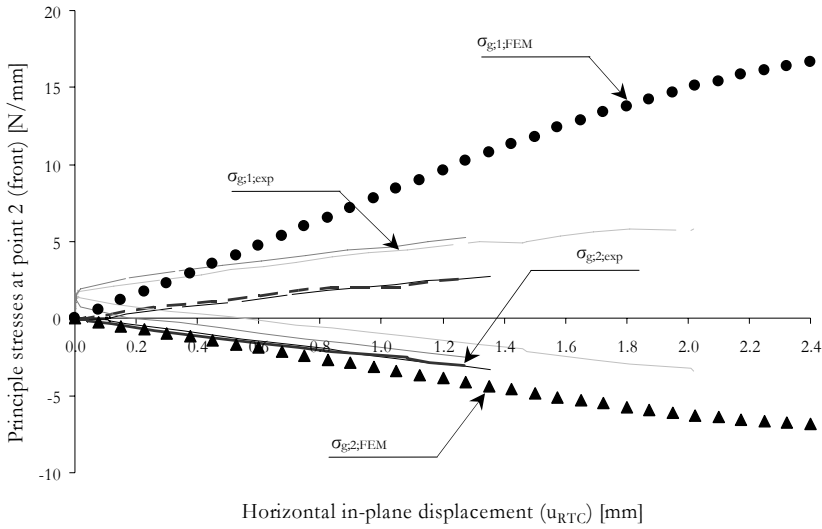
Figure 4.23: Comparison between simulation (bolt dots and triangles) and experiments (continuous lines) of the relation between the principle stresses and horizontal in-plane displacements at the RTC of the system at point 2

The relation between the horizontal in-plane loads and the horizontal in-plane displacements at the RTC of the system deviates between the simulation and the experiments, because the glass pane constantly cracks and cracking is not implemented in the simulations. The relation is slightly curved, because the shear stresses in transversal direction at the ends of the adhesive bonded joints show plastic-like behaviour (section 4.8.4). The simulation of the out-of-plane displacements at the centre of the glass pane are also incorrectly described by the finite element model. A possible explanation is given in section 4.8.4, but an unequivocal explanation can not be given.

4.9   Conclusions

One universal finite element model has been developed that simulates systems with joint types 1 to 3 by means of material input for interfaces A to C. The finite element model consists of solid elements for the glass pane, interface elements for the adhesive bonded joints and the bolted connection between the outside beam and the beadwork, shell elements and beam elements for the steel frame, releasing for rotation around the z-axis of the beam elements for the internal hinges and a spring element in vertical direction to adapt the pinned connection at the RBC of the system. To capture the geometrical imperfections of the glass pane in the finite element model the glass pane has an out-of-plane imperfection and the lower limit is used for the glass pane thickness. The material properties for glass and steel and the normal stiffness of the epoxy adhesive bonded joint are linear. The shear flexibility of the bolted connection between the outside beam and the beadwork and the spring stiffness at the RBC of the system are determined by tests and are implemented in the finite element model with linear material

behaviour. The non linear material input is only for interfaces A to C and are determined by tests.

The finite element model well describes the strain gradient in the glass pane except the strain gradient at the vicinity of all utmost corners of the glass pane. These strain gradients are described incorrectly especially at glass-steel contact for systems with joint type 1 and the stiff adhesive bonded joint for systems with joint type 2 and 3. However, the accuracy of the principle stresses at the vicinity of these utmost corners of the glass pane is not substantial, but shows the location where the first crack occurs.

For systems with joint type 1, the finite element model well simulates the in-plane stiffness of the system, the principle stresses at points 1 to 5 on the front of the glass pane and the glass-steel contact which has a sharper transition between two stages than found in the experiments. On the other hand, the finite element model incorrectly simulates the out-of-plane displacements of the glass pane. The finite element model is applicable till the glass-steel contact, because cracking of the glass pane is not implemented. For systems with joint type 2 and 3, the finite element model well simulates the in-plane stiffness of the system. On the other hand, the finite element model less simulates the principle stresses at points 1 to 5 on the front of the glass pane and the out-of-plane displacements of the glass pane. However, the relation between the principle stresses and the horizontal in-plane displacement of the simulation matches well with the experiments. The shear flexibility of the bolted connection between the outside beam and the beadwork and the spring stiffness at the RBC of the system significantly reduce the in-plane stiffness of the system. Furthermore, the in-plane stiffness of the system decreases with decent decrease of the shear stiffness of the adhesive bonded joint. The finite element model is applicable up to the onset of the first crack, because cracking of the glass pane is not implemented.

In chapter 5 the finite element model will be used to investigate the behaviour of systems with joint types 1 to 3 by means of varying the geometry of the glass pane and for systems with joint type 2 and 3, a virtual material input for interfaces A and C which represent the adhesive bonded joint.

5 Parameter studies

This chapter discusses the results of parameter studies for systems with joint types 1 to 3 by varying the nominal glass thickness and the glass pane size using the finite element model that was described in chapter 4. Section 5.1 deals with the motivation and the objective of parameter studies. Section 5.2 deals with the geometric parameters of the glass pane. Sections 5.3 to 5.5 discuss parameter studies for systems with joint types 1 to 3 respectively. The chapter ends with conclusions in section 5.6.

5.1 Motivation and objective

Chapter 4 describes the finite element model and produces results for non-cracked glass panes and non-failed adhesive bonded joints in addition to the limited data of the experiments (chapter 3). Moreover, the finite element model gave more insight into the behaviour of systems with joint types 1 to 3 such as the influence of the bolted connection between the outside beam and the beadwork (section 4.8.1). The next step is to perform parameter studies to gain more information on the behaviour of systems with joint types 1 to 3 by varying several parameters using the finite element model. In this research, the parameter studies are restricted to the geometry of the glass pane, a main parameter in a design process, by varying the nominal glass thickness, the width and the height of the glass pane. The objective is to get more insight into the influence of the geometry on the behaviour of the system and to capture the main parameters needed for the design by means of mechanical models which will be discussed in chapter 6.

5.2 Geometric parameters

As stated above the parameter studies are restricted to the geometry of the glass pane by varying the nominal glass thickness, the width and the height of the glass pane. Three nominal glass thicknesses are chosen, namely 4 (3.8) mm, 8 (7.7) mm and 12 (11.7) mm. The values between the brackets are the lower limit values for the nominal glass thickness (section 4.6) as they are used in the finite element model. Six glass pane sizes are chosen, namely two square glass panes (1.0 m x 1.0 m and 1.5 m x 1.5 m), two rectangular glass panes with smaller width than height (1.0 m x 1.5 m and 1.0 m x 3.0 m) and two rectangular glass panes with larger width than height (1.5 m x 1.0 m and 3.0 m x 1.0 m). For the out-of-plane imperfection at the centre of the glass pane 1/2000 times the largest size of the glass pane is assumed (section 4.6), directed to the negative z-axis. Varying the geometry of the glass pane leads to an adjustment of the width, the height and the 'fork' (figure 4.2) of the steel frame, the lengths of the adhesive bonded joints and the width of the adhesive bonded joints for joint type 1 only (figure 3.3). The remaining parameters of the geometry are unchanged such as the cross sectional data of the steel frame and the dimensions of the adhesive bonded joints for systems with joint type 2 and 3. Also the material properties remain unchanged (section 4.5). Note: all nominal glass thicknesses and glass pane sizes mean the chosen three nominal glass thicknesses and six glass pane sizes in this chapter.

5.3 Systems with joint type 1

5.3.1 Relation between horizontal in-plane load and horizontal in-plane displacement at the RTC of the system

Figures 5.1 at the left (square glass panes) and 5.2 at the top (rectangular glass panes) show the relation between the horizontal in-plane load and the horizontal in-plane displacement at the RTC of the system and the glass-steel contacts for all nominal glass thicknesses. Table 5.1 gives an overview of the in-plane stiffness of the system ($K_{s;lim}$), the horizontal in-plane load ($F_{h;lim}$) at limited horizontal in-plane displacement at the RTC of the system ($u_{RTC;lim}$) and the horizontal in-plane loads ($F_{h;1}$ and $F_{h;2}$) and the horizontal in-plane displacements ($u_{RTC;1}$ and $u_{RTC;2}$) at the RTC of the system at first and second glass-steel contact respectively. For systems with square glass panes, the relation between the horizontal in-plane load and the horizontal in-plane displacement at the RTC of the system is bi-linear for all nominal glass thicknesses and glass pane sizes except the second stage for a nominal glass thickness of 8 mm with glass pane 1.5 m x 1.5 m and a nominal glass thickness of 4 mm with glass pane sizes 1.0 m x 1.0 m and 1.5 m x 1.5 m (slightly curved). The second stage is steeper than the first stage (figure 5.1). Furthermore, the thicker the nominal glass thickness the steeper both stages and the larger the glass pane the steeper both stages (figure 5.1 and table 5.1). Systems with square glass pane sizes have one glass-steel contact. The LBC of the glass pane makes contact with the bottom transom and the left mullion and the RTC of the glass pane simultaneously makes contact with the top transom and the right mullion (Figure 5.1 right). The glass panes are still four-sided supported at glass-steel contact.

Figure 5.1: *Relation between horizontal in-plane load and horizontal in-plane displacement at the RTC of the system (left) and first glass-steel contact for three nominal glass thicknesses and two square glass pane sizes (right)*

For systems with rectangular glass panes, the relation between the horizontal in-plane load and the horizontal in-plane displacement at the RTC of the system is tri-linear for all rectangular

glass panes with nominal glass thickness of 12 mm. For all rectangular glass panes with nominal glass thicknesses of 4 and 8 mm, the first stage is linear and the second and third stage are curved in which the third stage is more curved than the second stage (figure 5.2). The second stage is steeper than the first stage and the third stage is steeper than the second stage (figure 5.2). Furthermore, the greater the nominal glass thickness the steeper the stages, the larger the width of the glass pane the steeper the stages and the larger the height of the glass pane the less steeper the stages (figure 5.2, top and table 5.1). Systems with rectangular glass panes have two glass-steel contacts (transition between two stages). Glass panes with a smaller width than height (figure 5.2, bottom left) make first glass-steel contact with the bottom transom at the LBC and the top transom at the RTC. After a while, the glass panes make second glass-steel contact with the left mullion at the LBC and the right mullion at the RTC. Glass panes with a larger width than height (figure 5.2, bottom right) make first glass-steel contact with the left mullion at the LBC and the right mullion at the RTC. After a while, the glass panes make second glass-steel contact with the bottom transom at the LBC and the top transom at the RTC. Furthermore, the glass panes of all systems are four-sided supported at first and second glass-steel contact except for systems with a larger width than height at second glass-steel contact.
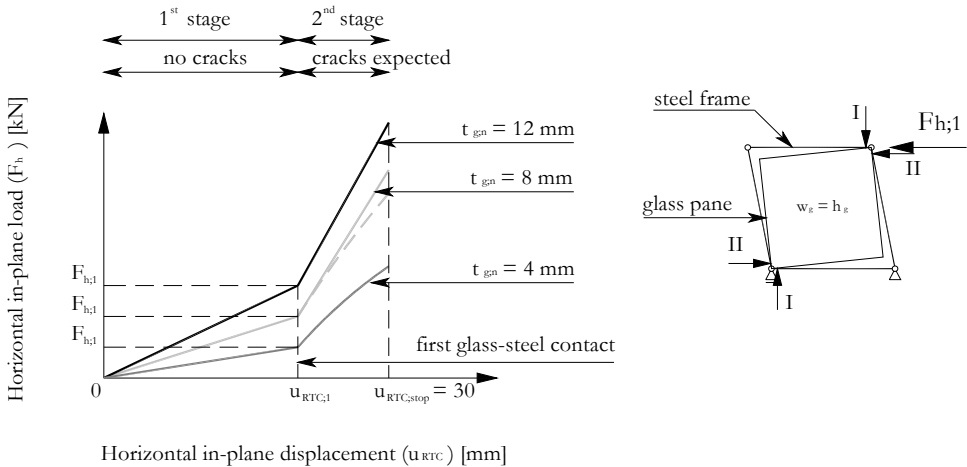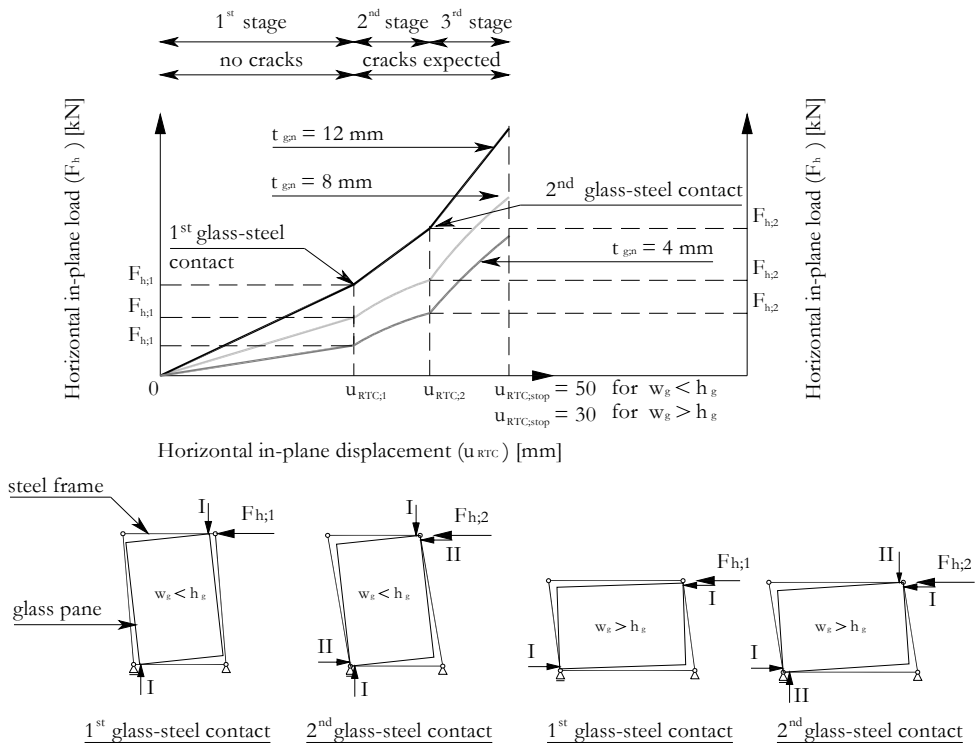

Figure 5.2: Relation between horizontal in-plane load and horizontal in-plane displacement at the RTC of the system (top) and the first and second glass-steel contact for three nominal glass thicknesses and four rectangular glass pane sizes (bottom)

Table 5.1:   Overview of the horizontal in-plane load ($F_{h;lim}$) and the in-plane stiffness of the system ($K_{s;lim}$) at limited horizontal in-plane displacement at the RTC of the system ($u_{RTC;lim}$) and the horizontal in-plane load ($F_{h;1}$ and $F_{h;2}$) and horizontal in-plane displacement at the RTC of the system ($u_{RTC;1}$ and $u_{RTC;2}$) at first and second glass-steel contact for three nominal glass thicknesses and six glass pane sizes (X = not reached)

Size [m]	$t_{g;n}$ [mm]	$u_{RTC;lim}$ [mm]	$F_{h;lim}$ [kN]	$K_{s;lim}$ [kN/mm]	$u_{RTC;1}$ [mm]	$F_{h;1}$ [kN]	$u_{RTC;2}$ [mm]	$F_{h;2}$ [kN]
1.0 x 1.0	4		1.45	0.39	23.25	14.80	--	--
	8	3.70	2.92	0.80	23.15	25.70	--	--
	12		4.41	1.20	23.63	37.70	--	--
1.5 x 1.5	4		3.51	0.66	23.20	20.30	--	--
	8	5.40	6.86	1.30	23.58	41.70	--	--
	12		10.03	1.90	23.98	61.50	--	--
1.0 x 1.5	4		1.69	0.32	23.21	9.11	29.61	18.50
	8	5.40	3.37	0.63	23.61	18.40	29.35	31.10
	12		4.88	0.92	24.39	29.20	29.05	45.80
1.0 x 3.0	4		1.41	0.14	35.57	5.94	X	X
	8	10.40	2.83	0.28	35.00	11.30	X	X
	12		4.17	0.42	34.58	16.10	X	X
1.5 x 1.0	4		2.46	0.67	17.29	16.70	19.90	22.50
	8	3.70	4.92	1.34	17.19	30.70	20.62	55.70
	12		7.35	2.01	16.51	41.60	20.50	71.45
3.0 x 1.0	4		4.10	1.11	12.80	15.50	19.50	X
	8	3.70	8.12	2.20	13.16	30.90	19.65	114.00
	12		12.42	3.36	13.20	44.30	20.00	154.00

The in-plane load ($F_{h;lim}$) increases with increasing thickness of the glass pane at limited horizontal in-plane displacement at the RTC of the system in a certain glass pane size and at first and second glass-steel contact (table 5.1). The in-plane stiffness of the system ($K_{s;lim}$) with nominal glass thicknesses of 8 mm and 12 mm doubles and triples respectively compared to systems with a nominal glass pane thickness of 4 mm in a certain glass pane size. The horizontal in-plane displacement at the RTC of the system at glass-steel contacts is the same within a certain glass pane size. Glass-steel contact is not desirable (section 2.2.2) and will certainly lead to splintering and flaking off at the LBC and the RTC of the glass pane after first glass-steel contact (section 3.7.1) and strongly influences the second and third stage (figure 4.13). In the next sections parameter studies for systems with joint type 1 focus on a limited horizontal in-plane displacement at the RTC of the system and the moment of first glass-steel contact.

5.3.2 In-plane deformations of the steel frame

Figure 5.3 (left) shows the in-plane deformations of the steel frame at limited horizontal in-plane displacement at the RTC of the system for all nominal glass thicknesses and glass pane sizes. The in-plane deformations of the transoms and mullions have an undulated curvature and are negligible small for all nominal glass pane thicknesses and glass pane sizes except for glass pane width and height of 3.0 m. Figure 5.3 (right) shows the in-plane deformation character of the steel frame at the moment of the first glass-steel contact for all nominal glass thicknesses and glass pane sizes. The in-plane deformations of the transoms and mullions are one-sided curved with the largest in-plane deformations at the vicinity of the LBC and RTC of the steel frame as was also observed in experiments (figure 3.11). The larger the transoms and mullions, the more they are curved. The thicker the glass pane, the more the transoms and mullions are curved. Finally, the relative in-plane displacements of the bolted connection between the outside beam and the beadwork are negligible small in all stages.
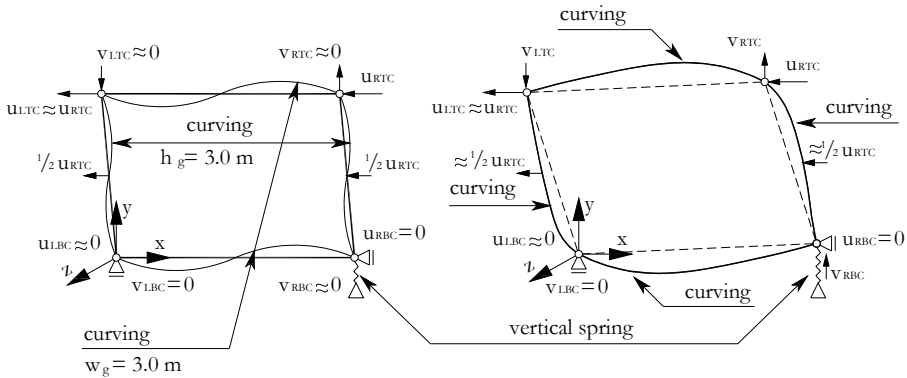
Figure 5.3:   Overview of in-plane deformations of the steel frame at limited horizontal in-plane displacement at the RTC of the system (left) and at the moment of first glass-steel contact (right) for three nominal glass thicknesses and six glass pane sizes

5.3.3 Out-of-plane displacements of the glass pane

Figure 5.4 shows the relations between the horizontal in-plane load and the out-of-plane displacement at the centre of the glass pane for all nominal glass thicknesses and glass pane sizes till the imposed horizontal in-plane displacement at the RTC of the system ($u_{RTC;stop}$). All glass pane sizes have an out-of-plane imperfection of 1/2000 times the largest glass pane. In a certain glass pane, the out-of-plane displacements at the centre of the glass pane are the largest for systems with nominal glass thickness of 4 mm and the smallest for systems with nominal glass pane thickness of 12 mm. Systems with a larger width than height have larger out-of-plane displacements at the centre of the glass pane than systems with square glass panes. Systems with square glass panes have larger out-of-plane displacements at the centre of the glass pane than systems with a smaller width than height. The horizontal in-plane load at first glass-steel contact for systems with nominal glass thickness of 4 mm and all glass pane sizes (table 5.1) is in the vicinity of the horizontal part of the relation between the horizontal in-plane load and the out-of-plane displacement of the centre of the glass pane (figure 5.4).
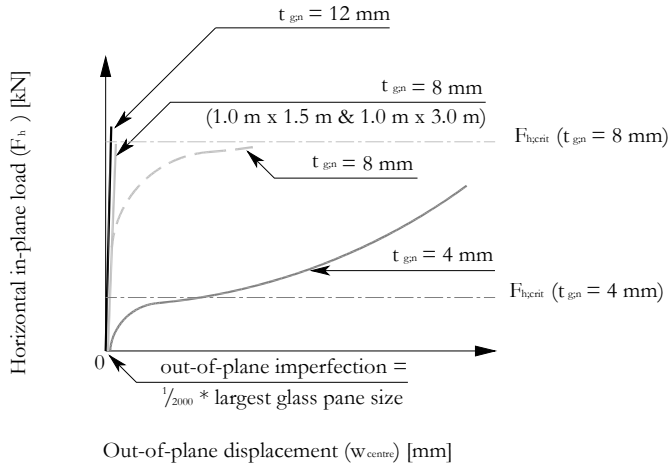
Figure 5.4:   *Relations between the horizontal in-plane load and the out-of-plane displacement at the centre of the glass pane till u$_{RTC;stop}$ (figures 5.1 and 5.2) for three nominal glass thicknesses and six glass pane sizes*
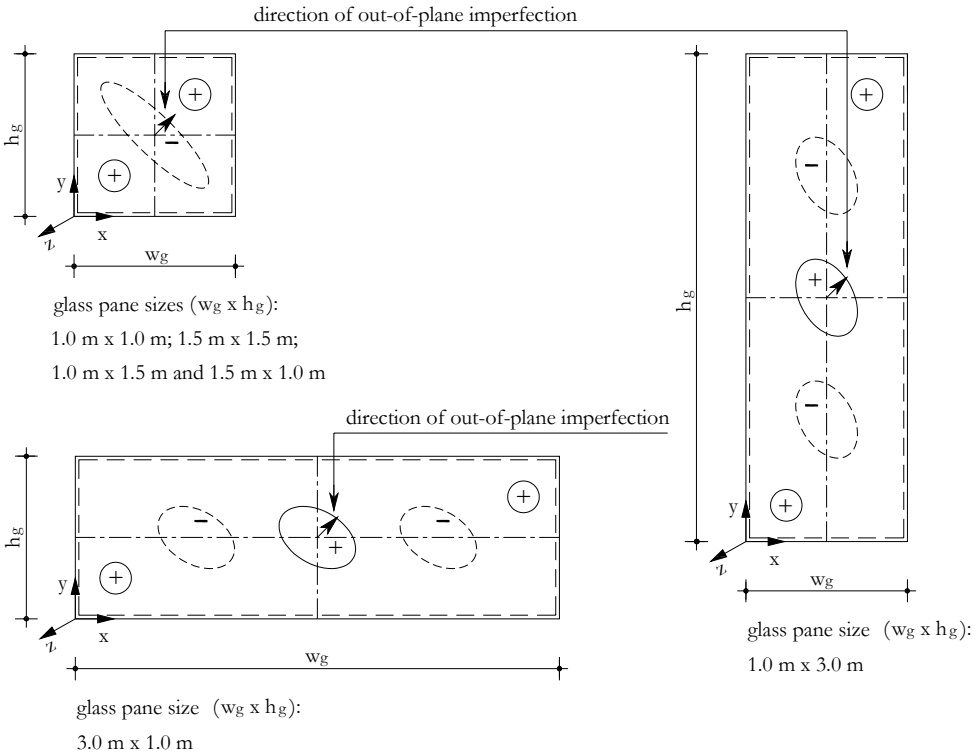
Figure 5.5:   *Overview of the out-of-plane displacements of the glass pane till first glass-steel contact for three nominal glass thicknesses and six glass pane sizes*

Figure 5.5 gives an overview of the out-of-plane displacements of the glass pane till first glass-steel contact. The out of-plane displacements for all nominal glass thicknesses and glass pane sizes 1.0 m x 1.0 m, 1.5 m x 1.5 m, 1.0 m x 1.5 m and 1.5 m x 1.0 m undulate along the diagonal from the LBC to the RTC of the glass pane and follows a half sine along the diagonal from the RBC to the LTC of the glass pane (figure 5.5, left top). The out of-plane displacements remain small till first glass-steel contact (figures 3.10 and 4.14) except for glass pane 1.5 m x 1.5 m with a nominal glass pane thickness of 4 mm. The out-of-plane displacements for glass pane sizes 1.0 m x 3.0 m (figure 5.5, right) and 3.0 m x 1.0 m (figure 5.5, left bottom) and all nominal glass thicknesses are different. The glass pane displaces out-of-plane in the negative z-axis at two places. At the vicinity of the LBC and the RTC and the centre of the glass pane, the glass pane slightly displaces out-of-plane in positive z-axis. At the moment of the first glass-steel contact, the out-of-plane displacements for all glass pane sizes with nominal glass pane thickness of 4 mm and 8 mm increase more than for all glass pane sizes with nominal thicknesses of 12 mm.

5.3.4   In-plane displacements of the glass pane

Figure 5.6 (left) shows the relation between the horizontal in-plane displacement of the bottom glass pane edge (directed to the negative x-axis) and the horizontal in-plane displacement at the RTC of the system for all nominal glass thicknesses and glass pane sizes. Figure 5.6 (right) shows the relation between the vertical in-plane displacement of the left glass pane edge (directed to the negative y-axis) and the horizontal in-plane displacement at the RTC of the system for all nominal glass thicknesses and glass pane sizes. For systems with non-cracked square glass panes and all nominal glass thicknesses, the horizontal in-plane displacement of the bottom glass pane edge is slightly larger than the vertical in-plane displacement of the left glass pane edge in the first stage. For systems with non-cracked rectangular glass panes with a smaller width than height and all nominal glass thicknesses, the horizontal in-plane displacement of the bottom glass pane edge is smaller than the vertical in-plane displacement of the left glass pane edge in the first stage. In the second stage the horizontal in-plane displacement of the bottom glass pane edge increases more than the vertical in-plane displacement of the left glass pane edge. For systems with non-cracked rectangular glass panes with a larger width than height and all nominal glass thicknesses, the horizontal in-plane displacement of the bottom glass pane edge is larger than the vertical in-plane displacement of the left glass pane edge in the first stage. In the second stage the horizontal in-plane displacement of the bottom glass pane edge less increases than the vertical in-plane displacement of the left glass pane edge. In the second stage of non-cracked square glass panes and the third stage of non-cracked rectangular glass panes and all nominal glass pane thicknesses, the horizontal in-plane displacement of the bottom glass pane edge slightly more increases than the vertical in-plane displacement of the left glass pane edge. Furthermore, the horizontal in-plane displacement at the centre of the glass pane corresponds with the half of the horizontal in-plane displacement at the RTC of the system and the vertical in-plane displacements at the centre of the glass pane remain unchanged for all nominal glass thicknesses and glass pane sizes.
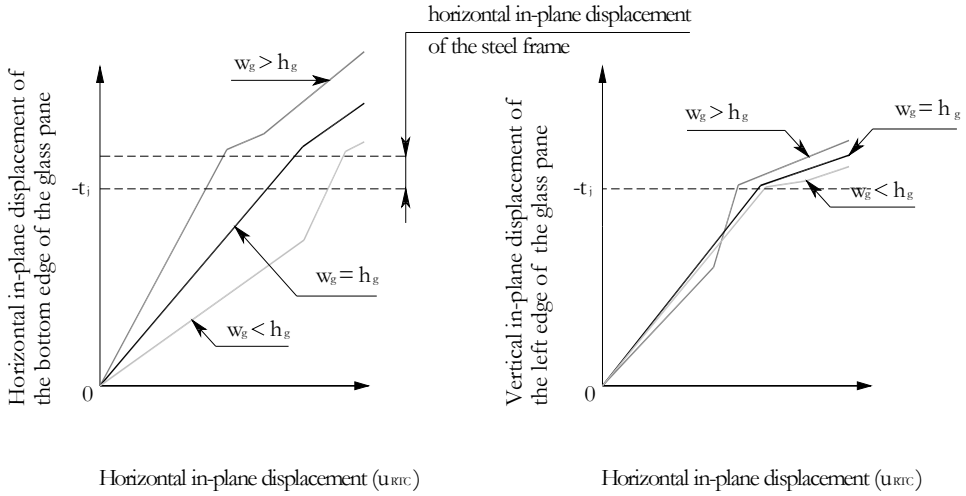
Figure 5.6: *Relations between the horizontal in-plane displacement of the bottom glass pane edge (left) and the vertical in-plane displacement of the left glass pane edge (right) and the horizontal in-plane displacement at the RTC of the system (u_{RTC}) for three nominal glass thicknesses and six glass pane sizes*

5.3.5 Principle stresses in the glass pane
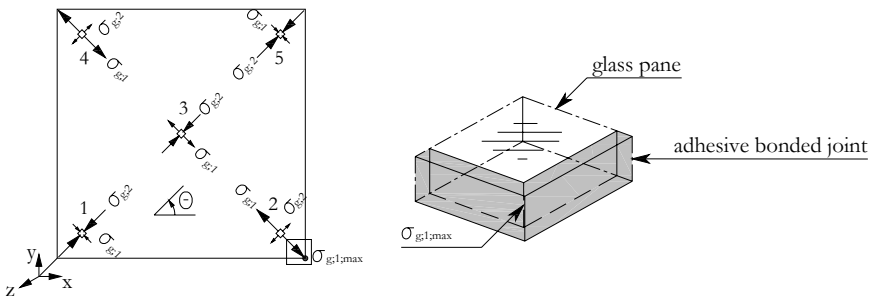
Figure 5.7: *Overview of the principle stresses and their directions at points 1 to 5 (left) and the position of the largest maximum principle stress (right) at limited horizontal in-plane displacement at the RTC of the system for three nominal glass thicknesses and six glass pane sizes*

The size and direction of the principle stresses at points 1 to 5 for all nominal glass thicknesses and glass pane sizes are given with vectors in figure 5.7. The principle stresses at points 1 and 5 are bilateral compression stresses at which the size of the minimum principle stress is larger than the maximum principle stress. The minimum principle stress at points 1 and 5 increases for all glass panes sizes except glass pane 3.0 m x 1.0 m with regard to glass pane size 1.0 m x 1.0 m. The principle stresses at points 2 and 4 are bilateral tension stresses at which the size of the maximum principle stress is larger than the minimum principle stress. The maximum principle stress at points 2 and 4 increases for all glass pane sizes except glass pane size 3.0 m x 1.0 m with regard to glass pane size 1.0 m x 1.0 m. The angle of the principle stresses at points

1, 2, 4 and 5 vary. At point 3, the maximum principle stress is a tension stress with an angle of about -45° and the minimum principle stress is a compression stress with an angle of about 45°. The maximum and minimum principle stresses at point 3 increase for all glass pane sizes except for glass pane sizes 1.0 m x 3.0 m and 3.0 m x 1.0 m. The position of the largest maximum principle stress is located at the RBC of the glass pane. Furthermore, the value, the sign and the direction of the principle stresses at points 1 to 5 and the largest maximum principle stress at RBC of the glass pane (table 5.2) are constant through the thickness of the glass pane irrespective of the nominal glass thickness in a certain glass pane size. The stress-state is two-dimensional.

5.3.6 Distribution of normal and shear stresses in the adhesive bonded joint
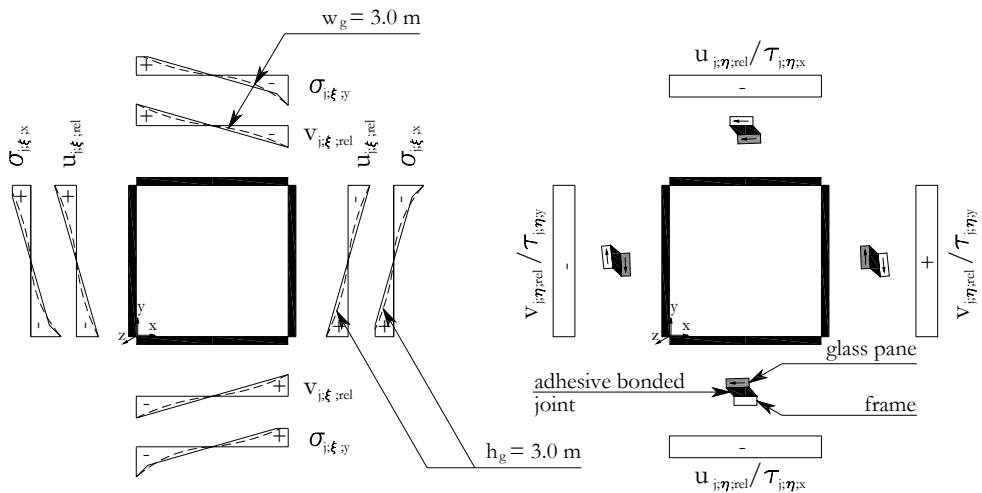
Figure 5.8: *Distributions of the relative in-plane displacements in normal direction ($u_{j;\xi;rel}$/$v_{j;\xi;rel}$), the normal stresses ($\sigma_{j;\xi;x}$/$\sigma_{j;\xi;y}$), the relative in-plane displacements in longitudinal directions ($u_{j;\eta;rel}$/$v_{j;\eta;rel}$) and the shear stresses ($\tau_{j;\tau;x}$/$\tau_{j;\tau;y}$) of the adhesive bonded joint at limited horizontal in-plane displacement at the RTC of the system for three nominal glass thicknesses and six glass pane sizes*

Figure 5.8 (left) shows the distribution of the relative horizontal and vertical in-plane displacements in normal direction ($u_{j;\xi;rel}$ and $v_{j;\xi;rel}$ respectively) and the distribution of the normal stresses in x- and y-direction ($\sigma_{j;\xi;x}$ and $\sigma_{j;\xi;y}$ respectively) of the adhesive bonded joint at limited horizontal in-plane displacement at the RTC of the system for all nominal glass thicknesses and glass pane sizes. Table 5.2 gives the accompanying maximum values. The distribution of the relative horizontal and vertical in-plane displacements in normal direction of the adhesive bonded joint is linear with its maximum at the ends of the adhesive bonded joint for all nominal glass thicknesses and glass pane sizes except for glass pane sizes with a width or height of 3.0 m which shows a curvature. For systems with square glass panes, the relative horizontal and vertical in-plane displacements in normal direction are equal. For systems with rectangular glass panes with a smaller width than height, the relative vertical in-plane

displacements in normal direction are larger than the relative horizontal in-plane displacements in normal direction. For systems with rectangular glass panes with a larger width than height, the relative horizontal in-plane displacements in normal direction are larger than the relative vertical in-plane displacements in normal direction. Furthermore, the relative horizontal and vertical in-plane displacements in normal direction are constant through the thickness of the glass pane irrespective of the thickness of the glass pane in a certain glass pane size. The distribution of the normal stresses in x- and y-direction is linear or a curvature (glass pane width/height of 3.0 m) till a relative in-plane displacement of 0.76 mm (figure 4.9 right). At larger relative in-plane displacements of the adhesive bonded joint the compression stresses increase more at the LBC and the RTC of the adhesive bonded joint and the tension stresses smooth at the RBC and the LTC of the adhesive bonded joint.

Table 5.2: *Overview of relative in-plane displacements, normal stresses and shear stresses of the adhesive bonded joint (figure 5.8) and maximum principle stress in the glass pane (figure 5.7) for three nominal glass thicknesses and six glass pane sizes*

		1.0x1.0	1.5x1.5	1.0x1.5	1.0x3.0	1.5x1.0	3.0x1.0
$u_{j;\xi;rel;max}$	[mm]	0.81	1.18	0.67	0.42	1.16	1.46
$v_{j;\xi;rel:max}$	[mm]	0.81	1.19	1.16	1.41	0.69	0.42
$u_{j;\eta;rel:max}$	[mm]	0.99	1.37	0.86	0.63	1.36	1.70
$v_{j;\eta;max}$	[mm]	0.98	1.37	1.33	1.61	0.85	0.60
$\sigma_{j;\xi;x;LBC/RTC}$	[N/mm²]	-1.04	-2.61	-0.80	-0.50	-2.49	-3.68
$\sigma_{j;\xi;y;LBC/RTC}$	[N/mm²]	-1.07	-2.65	-2.50	-3.58	-0.81	-0.50
$\sigma_{j;\xi;x;RBC/LTC}$	[N/mm²]	0.93	0.94	0.80	0.49	0.96	0.99
$\sigma_{j;\xi;y;RBC/LTC}$	[N/mm²]	0.93	0.94	0.94	0.95	0.80	0.47
$\tau_{j;\eta;x;max}$	[N/mm²]	0.09	0.12	0.07	0.05	0.12	0.15
$\tau_{j;\eta;y;max}$	[N/mm²]	0.09	0.12	0.11	0.14	0.07	0.05
$\sigma_{g;1;max;RBC}$	[N/mm²]	1.27	1.34	1.09	1.21	1.27	1.31

Figure 5.8 (right) shows the distribution of the relative horizontal and vertical in-plane displacements in longitudinal direction ($u_{j;\eta;rel}$ and $v_{j;\eta;rel}$ respectively) and the distribution of the shear stresses in x- and y-direction ($\tau_{j;\eta;x}$ and $\tau_{j;\eta;y}$ respectively) of the adhesive bonded joint at limited horizontal in-plane displacement at the RTC of the system for all nominal glass thicknesses and glass pane sizes. Table 5.2 gives the accompanying maximum values. The distribution of the relative horizontal and vertical in-plane displacements in longitudinal direction of the adhesive bonded joint is uniform for all nominal glass thicknesses and glass pane sizes. For systems with square glass panes, the relative horizontal and vertical in-plane displacements in longitudinal direction are equal. For systems with rectangular glass panes with a smaller width than height, the relative vertical in-plane displacements in longitudinal direction are larger than the relative horizontal in-plane displacements in longitudinal direction. For systems with rectangular glass panes with a larger width than height, the relative horizontal in-plane displacements in longitudinal direction are larger than the relative vertical in-plane

displacements in longitudinal direction. Furthermore, the relative horizontal and vertical in-plane displacements in longitudinal direction are constant through the thickness of the glass pane irrespective of the thickness of the glass pane in a certain glass pane size. The distribution of the relative in-plane displacements in longitudinal direction reflects the distribution of the shear stresses.

5.3.7 Discussion

The mutual relations when varying the nominal glass thickness and glass pane of systems with joint type 1 are discussed in this section. The normal and shear stiffnesses of the adhesive bonded joint determine the in-plane stiffness of the system in the first stage (table 5.1). The in-plane stiffness of the system increases at increasing width and length of the adhesive bonded joint at which the width of the adhesive bonded joint corresponds with the nominal glass thickness. The nominal glass thickness plays a role in the in-plane stiffness of the system in the second and third stage. Slender transoms and mullions are subjected to bending (figure 5.3, left) resulting in a non-linear distribution of the relative in-plane displacements in normal direction (figure 5.8, left). The in-plane loads are more transferred through the normal stiffness of the adhesive bonded joint in the compression zone resulting in one-sided bending of the transoms and mullions especially at glass-steel contact (figure 5.3, right).

The large out-of-plane displacements at the centre of the glass pane (figure 5.4) result in a slightly curved relation between the horizontal in-plane load and the horizontal in-plane displacement at the RTC of the system in the second and third stage (figures 5.1 and 5.2). Moreover, the critical plate buckling load is reached at first glass-steel contact for systems with nominal glass thickness of 4 mm and all glass pane sizes.

If the width and height of square glass panes increase, the vertical in-plane load along the left and right glass pane edge and the horizontal in-plane load along the bottom and top glass pane edge increase by larger normal and shear stiffness caused by the larger length of the adhesive bonded joint. The normal stiffnesses of the adhesive bonded joint are equal because of equal length of the adhesive bonded joint. Therefore, one glass-steel contact occurs between glass pane and steel frame (figure 5.1). After glass-steel contact, the horizontal in-plane shift and the in-plane rotation of the glass pane are prevented (figure 5.6).

If the height of rectangular glass panes increases, the vertical in-plane load along the left and right glass pane edge is larger than the horizontal in-plane load along the bottom and top glass pane edge. The larger vertical in-plane load along the left and right glass pane edge perpendicularly loads the bottom and top adhesive bonded joint in-plane. These joints have the smallest normal stiffness because of the length of the adhesive bonded joint. Therefore, the first glass-steel contact occurs between glass pane and transoms at the LBC and the RTC (figure 5.2). Between first and second glass-steel contact the glass pane only has a horizontal in-plane displacement, because the in-plane rotation of the glass pane is prevented (figure 5.6). The relative vertical in-plane displacements in normal direction at the end of the bottom and top adhesive bonded joint (figure 5.8, right) causes the relative vertical in-plane displacements in longitudinal direction of the left and right adhesive bonded joint. This displacement is enlarged with an opposite relative in-plane displacement in longitudinal direction as the result of the thickness of the horizontally displaced steel mullion (figure 5.8, right).

If the width of rectangular glass panes increases, the horizontal in-plane load along the bottom and top glass pane edge is larger than the vertical in-plane load along the left and right glass pane edge. The larger horizontal in-plane load along the bottom and left glass pane edge perpendicularly loads the left and right adhesive bonded joint in-plane which has the smallest normal stiffness because of the length of the adhesive bonded joint. Therefore, first glass-steel contact occurs between glass pane and mullions at the LBC and the RTC (figure 5.2). Between first and second glass-steel contact the glass pane only has an in-plane rotation, because the horizontal in-plane displacement of the glass pane is prevented (figure 5.6). The relative horizontal in-plane displacement in normal direction at the end of the left and right adhesive bonded joint (figure 5.8, right) causes the relative horizontal in-plane displacement in longitudinal direction of the bottom and top adhesive bonded joint. This displacement is enlarged with the difference between the horizontal in-plane displacements of the steel mullion and the horizontal glass pane edge (figures figure 4.5 and 5.8, right).

5.4   Systems with joint type 2

5.4.1   Relation between horizontal in-plane load and horizontal in-plane displacement at the RTC of the system
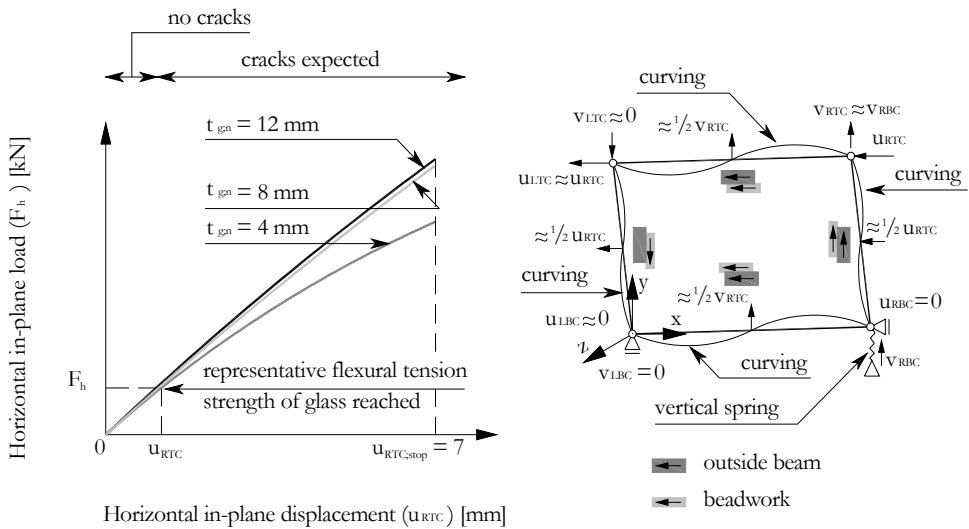
Figure 5.9:   Relation between horizontal in-plane load and horizontal in-plane displacement at the RTC of the system (left) and schematic overview of in-plane displacements of the steel frame (right) for three nominal glass thicknesses and six glass pane sizes

Figure 5.9 (left) shows the relation between the horizontal in-plane load and the horizontal in-plane displacement at the RTC of the system for all nominal glass thicknesses and glass pane sizes. Table 5.3 gives the horizontal in-plane displacement at the RTC of the system (u_{RTC}), the horizontal in-plane load (F_h), the actually horizontal in-plane displacement at the RTC of the system ($u_{RTC;y}$) and the in-plane stiffness of the system (K_s) at the moment that the largest

maximum principle stress is equal to the representative flexural tension strength of glass (section 2.4.1) (figure 5.12) for all nominal glass thicknesses and glass pane sizes.

Table 5.3: Overview of the horizontal in-plane displacement at the RTC of the system (u_{RTC}), the horizontal in-plane load (F_h), the actually horizontal in-plane displacement of the system ($u_{RTC;s}$), the in-plane stiffness of the system (K_s) and the relative horizontal and vertical in-plane displacements of the bolted connection between the outside beam and the beadwork ($u_{b;\eta;rel}$ and $v_{b;\eta;rel}$) at the moment that the largest maximum principle stress is equal to the representative flexural tension strength of glass for three nominal glass thicknesses and six glass pane sizes

$t_{g;n}$ [mm]	Size	[m]	1.0x1.0	1.5x1.5	1.0x1.5	1.0x3.0	1.5x1.0	3.0x1.0
4	u_{RTC}	[mm]	0.712	0.734	1.019	2.246	0.551	0.418
	F_h	[kN]	23.69	25.47	20.39	15.88	29.83	45.11
	$u_{RTC;s}$	[mm]	0.475	0.479	0.590	0.999	0.409	0.361
	K_s	[kN/mm]	49.87	52.76	34.56	15.89	72.93	124.96
	$u_{b;\eta;rel}$	[mm]	0.065	0.056	0.068	0.042	0.068	0.071
	$v_{b;\eta;rel}$	[mm]	0.063	0.057	0.083	0.069	0.055	0.042
8	u_{RTC}	[mm]	0.974	1.048	1.434	3.262	0.732	0.542
	F_h	[kN]	39.88	44.60	34.13	25.70	49.66	73.03
	$u_{RTC;s}$	[mm]	0.575	0.602	0.716	1.244	0.496	0.449
	K_s	[kN/mm]	69.36	74.09	47.67	20.66	100.12	162.65
	$u_{b;\eta;rel}$	[mm]	0.093	0.090	0.078	0.057	0.100	0.106
	$v_{b;\eta;rel}$	[mm]	0.092	0.090	0.100	0.104	0.078	0.056
12	u_{RTC}	[mm]	1.020	1.236	1.698	3.818	0.957	0.602
	F_h	[kN]	45.56	57.20	43.35	31.35	71.70	89.34
	$u_{RTC;s}$	[mm]	0.564	0.644	0.786	1.365	0.616	0.488
	K_s	[kN/mm]	80.72	88.82	55.15	22.97	116.40	183.07
	$u_{b;\eta;rel}$	[mm]	0.110	0.106	0.094	0.065	0.136	0.124
	$v_{b;\eta;rel}$	[mm]	0.110	0.106	0.119	0.122	0.103	0.064

If the glass pane is non-cracked, the relation is slightly curved for systems with nominal glass thicknesses of 8 mm and 12 mm and more curved for systems with nominal glass thickness of 4 mm. The horizontal in-plane load increases with increasing nominal glass thickness. The parameter studies for the behaviour of this system are restricted to the moment of the first crack (maximum principle stress is equal to the representative flexural tension strength of glass) (figure 3.15). For systems with increasing square glass panes, the horizontal in-plane load and the actually horizontal in-plane displacement at the RTC of the system increase for all nominal glass thicknesses. For systems with increasing rectangular glass panes with smaller width than height, the horizontal in-plane load decreases and the actually horizontal in-plane displacement at the RTC of the system increases for all nominal glass thicknesses. For systems with increasing rectangular glass panes with a larger width than height, the horizontal in-plane

load increases and the actually horizontal in-plane displacement at the RTC of the system decreases for all nominal glass thicknesses.

5.4.2   In-plane deformations of the steel frame

Figure 5.9 (right) shows the in-plane deformation character of the steel frame for all nominal glass thicknesses and glass pane sizes. Table 5.3 gives the relative horizontal and vertical in-plane displacement ($u_{b;\eta;rel}$ and $v_{b;\eta;rel}$ respectively) of the bolted connection between the outside beam and the beadwork. The larger the transoms and the mullions the larger the curvature and the thicker the nominal glass thickness the larger the curvature. For systems with square glass panes, the relative horizontal and vertical in-plane displacements of the bolted connection are equal for all nominal glass thicknesses and glass pane sizes. For systems with rectangular glass panes with smaller width than height, the relative horizontal in-plane displacement of the bolted connection is smaller than the relative vertical in-plane displacement of the bolted connection for all nominal glass thicknesses and glass pane sizes. For systems with rectangular glass panes with larger width than height, the relative horizontal in-plane displacement of the bolted connection is larger than the relative vertical in-plane displacement of the bolted connection for all nominal glass thicknesses and glass pane sizes. For all glass pane sizes at increasing nominal glass thickness, the relative horizontal and vertical in-plane displacement of the bolted connection increase in a certain glass pane size.

5.4.3   Out-of-plane displacements of the glass pane
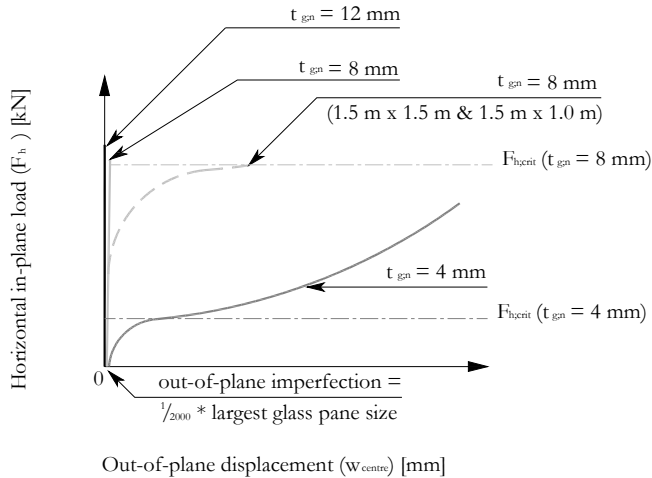
Figure 5.10:   Relations between the horizontal in-plane load and the out-of-plane displacement at the centre of the glass pane till $u_{RTC;stop}$ (figure 5.9) for three nominal glass thicknesses and six glass pane sizes

Figure 5.10 shows schematic relations between the out-of-plane displacement at the centre of the glass pane and the horizontal in-plane load for all nominal glass thicknesses and glass panes till the imposed horizontal in-plane displacement at the RTC of the system ($u_{RTC;stop}$). All glass

pane sizes have an out-of-plane imperfection of 1/2000 times the largest glass pane. Appendix E gives an overview of the critical plate buckling load subjected by pure in-plane shear load for four-sided simply supported glass panes, four-sided clamped supported glass panes and from finite element models. In a certain glass pane, the out-of-plane displacements at the centre of the glass pane are the largest for systems with nominal glass thickness of 4 mm and the smallest for systems with nominal glass pane thickness of 12 mm. Systems with a larger width than height in a certain glass pane size have larger out-of-plane displacements at the centre of the glass pane than systems with square glass panes. Systems with square glass panes have larger out-of-plane displacements at the centre of the glass pane than systems with a smaller width than height in a certain glass pane. Furthermore, the horizontal in-plane load at the moment that the largest maximum principle stress is equal to the representative flexural tension strength of glass is smaller than the horizontal part of the relation between the horizontal in-plane load and the out-of-plane displacement of the centre of the glass pane for all nominal glass thicknesses and glass pane sizes (table 5.3 and table E.1).
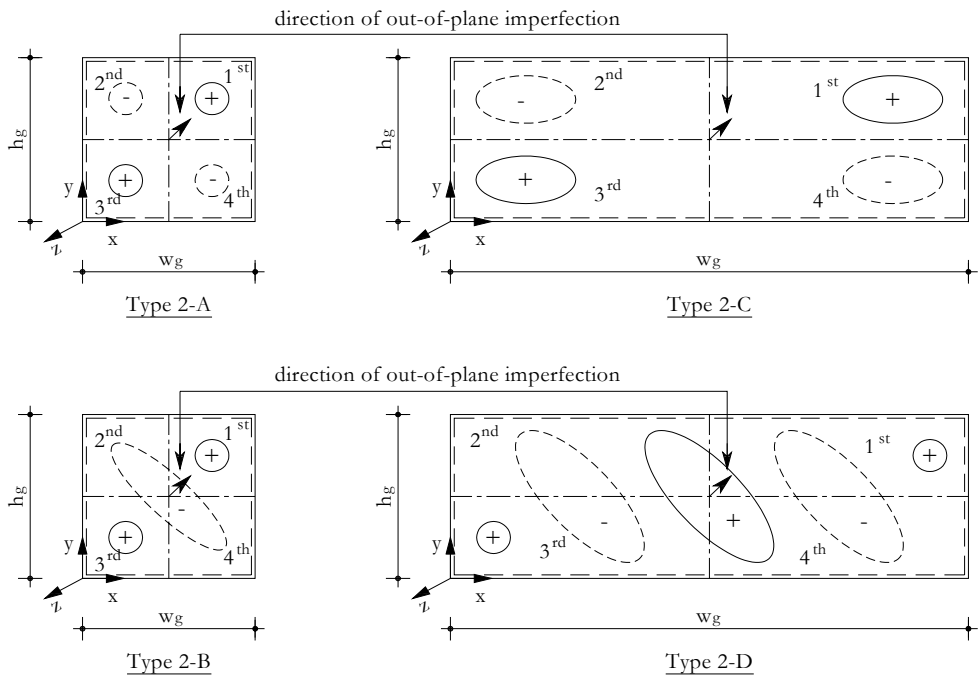
Figure 5.11: *Overview of out-of-plane displacements of the glass pane at the moment that the largest maximum principle stress is equal to the representative flexural tension strength of glass for three nominal glass thicknesses and six glass pane sizes*

Figure 5.11 shows an overview of out-of-plane displacement types (types A to D). In table 5.4, these types are tabulated for different combinations of nominal glass thickness and glass pane representing the moment that the largest maximum principle stress is equal to the representative flexural tension strength of glass. For systems with glass pane 1.0 m x 1.0 m and for all nominal glass thicknesses, the out-of-plane displacements of the glass pane are directed

to the positive z-axis at the centre of the first and third quadrant and directed to the negative z-axis at the centre of the second and fourth quadrant (type 2-A). For systems with glass pane sizes 1.5 m x 1.5 m, 1.0 m x 1.5 m and 1.5 m x 1.0 m and for all nominal glass thicknesses, the out-of-plane displacements of the glass pane undulate along the diagonal from the LBC to the RTC of the glass pane and the out-of-plane displacements along the diagonal from the RBC to the LTC of the glass pane are directed to the negative z-axis which corresponds with a half sine (type 2-B). For systems with glass panes sizes 1.0 m x 3.0 m and 3.0 m x 1.0 m and nominal glass thicknesses of 8 mm and 12 mm the out-of-plane displacements are comparable to type 2-A, but the centre of the out-of-plane displacements is closer to the corners (type 2-C). Systems with glass panes sizes 1.0 m x 3.0 m and 3.0 m x 1.0 m and a nominal glass thickness of 4 mm have positive out-of-plane displacements of the glass pane at the vicinity of the LBC and the RTC of the glass pane and at the centre of the glass pane and negative out-of-plane displacements between the positive out-of-plane displacements (type 2-D).

Table 5.4:   Overview of types for different combinations of nominal glass thickness and glass pane sizes representing the moment that the largest maximum principle stress is equal to the representative flexural tension strength of glass

$t_{g;n}$ [mm]	1.0x1.0	1.5x1.5	1.0x1.5	1.0x3.0	1.5x1.0	3.0x1.0
4	2-A	2-B	2-B	2-D	2-B	2-D
8	2-A	2-B	2-B	2-C	2-B	2-C
12	2-A	2-B	2-B	2-C	2-B	2-C

5.4.4   Principle stresses in the glass pane
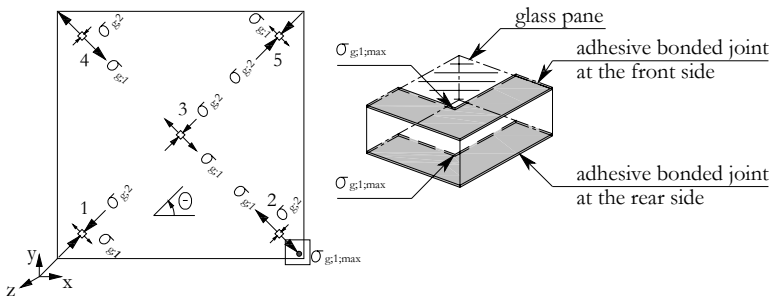
Figure 5.12:   Overview of the principle stresses and their directions at points 1 to 5 (left) and the position of the largest maximum principle stress (right) at the moment that the maximum principle stress is equal to the representative flexural tension strength of glass for three nominal glass thicknesses and six glass pane sizes

The size and direction of the principle stresses at points 1 to 5 for all nominal glass thicknesses and glass pane sizes are given with vectors in figure 5.12 (section 4.8.2). At all points, the

maximum principle stress is a tension stress and the minimum principle stress is a compression stress and have a two-dimensional stress state except in a small zone at the vicinity of the corners of the glass pane. These principle stresses are bi-lateral compression stresses at the LBC and the RTC of the glass pane and bi-lateral tension stresses at the RBC and LTC of the glass pane. The stress state is three-dimensional. The largest maximum principle stress is located at the front or rear at the vicinity of the RBC of the glass pane. At points 1 and 5, the minimum principle stresses are larger than the maximum principle stresses. At points 2 and 4, the maximum principle stresses are larger than the minimum principle stresses. The difference between the principle stresses at the front and the rear is small and getting smaller at increasing nominal glass thickness in a certain glass pane size. Furthermore, the minimum and maximum principle stresses at points 1, 2, 4 and 5 slightly decrease at increasing glass pane. At point 3, the maximum and minimum principle stresses at the front and the rear of the glass pane are almost equal for all nominal glass thicknesses and glass pane sizes except for glass pane sizes with a nominal glass thickness of 4 mm. The directions of the principle stresses at points 1 to 5 at the front and the rear are about 45° except for glass pane sizes 1.0 m x 3.0 m and 3.0 m x 1.0 m which have a direction of about 35°.

5.4.5 Distribution of normal and shear stresses in the adhesive bonded joint

Figure 5.13 shows the distributions of the relative out-of-plane displacements ($w_{j;\zeta;rel}$) and the normal stresses ($\sigma_{j;\zeta;z}$) (left top), the relative horizontal and vertical in-plane displacements in longitudinal direction ($u_{j;\eta;rel}$ and $v_{j;\eta;rel}$ respectively) and the shear stresses in longitudinal x- and y-direction ($\tau_{j;\eta;x}$ and $\tau_{j;\eta;y}$ respectively) (right top) and the relative horizontal and vertical in-plane displacements in transversal direction ($u_{j;\zeta;rel}$ and $v_{j;\zeta;rel}$ respectively) and the shear stresses in transversal x- and y-direction ($\tau_{j;\zeta;x}$ and $\tau_{j;\zeta;y}$ respectively) (bottom) of the adhesive bonded joint at the moment that the largest maximum principle stress is equal to the representative flexural tension strength of glass (figure 5.12) for all nominal glass thicknesses and glass pane sizes. The images of the relative out-of-plane displacements of the adhesive bonded joint concern for the rear and front adhesive bonded joint and for all nominal glass thicknesses and glass pane sizes. The distribution of the relative out-of-plane displacements has an undulated image along the length and varies over the width of the adhesive bonded joint with its maximum at the ends of the adhesive bonded joint. The adhesive bonded joint is pushed in at the LBC and the RTC and stretched out at the RBC and the LTC. The relative out-of-plane displacements increase with increasing nominal glass thickness. The distribution of the relative out-of-plane displacements reflects the distribution of the normal stresses.

The distribution of the relative in-plane displacements in longitudinal direction slightly varies over the length and width of the adhesive bonded joint except at the vicinity of the ends of the adhesive bonded joint for all nominal glass thicknesses and glass pane sizes. At the vicinity of the ends of the adhesive bonded joint the relative in-plane displacements in longitudinal direction gradually decrease to zero followed by a rapid increase accompanying with a change of sign. The largest relative in-plane displacements in longitudinal direction are located at the end of the adhesive bonded joint. The image of the in-plane displacements in longitudinal direction of the adhesive bonded joint concerns for the rear and front adhesive bonded joint and for all nominal glass thicknesses and sizes. The relative in-plane displacements in longitudinal direction of the largest length of the adhesive bonded joint are larger than those of the smallest length of the adhesive bonded joint. Moreover, the relative in-plane displacements

in longitudinal direction increase with increasing nominal glass thickness. The distribution of the relative in-plane displacements in longitudinal direction reflects the distribution of the shear stresses in longitudinal direction.
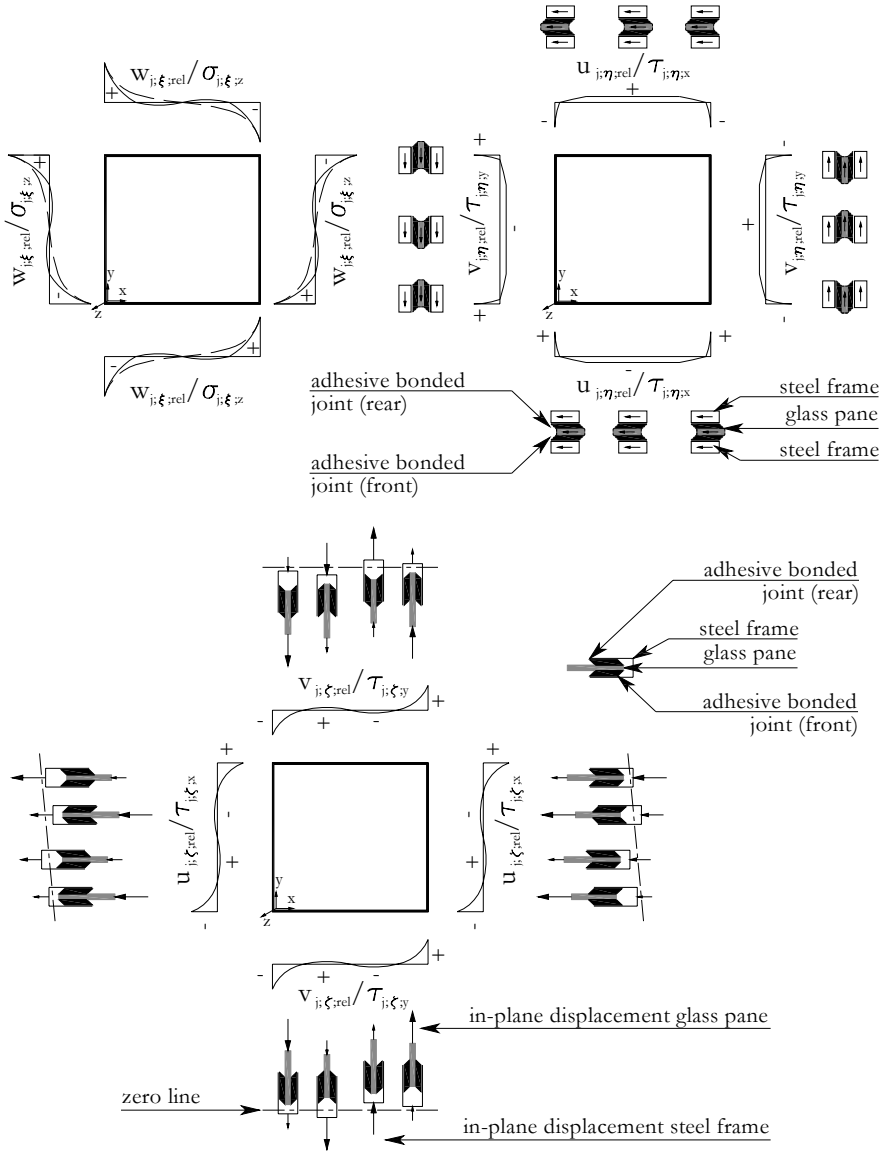
Figure 5.13:   Distribution of relative out-of-plane displacements and normal stresses (left top), the distribution of relative in-plane displacements and shear stresses in longitudinal direction (right top) and the distribution of relative in-plane displacements and shear stresses in transversal direction (bottom) of the adhesive bonded joint at the moment that the largest maximum principle stress is equal to the representative flexural tension strength of glass for three nominal glass thicknesses and six glass pane sizes

The distribution of the relative in-plane displacements in transversal direction of the adhesive bonded joint has an undulated image along the length and slightly varies over the width of the adhesive bonded joint. The largest relative in-plane displacements in transversal direction are located at the end of the adhesive bonded joint. The image of the in-plane displacements in transversal direction of the adhesive bonded joint concerns for the rear and front adhesive bonded joint and for all nominal glass thicknesses and sizes. The in-plane displacements in transversal direction of the smallest length of the adhesive bonded joint are larger than of the largest length of the adhesive bonded joint. The relative in-plane displacements in transversal direction increase with increasing nominal glass thickness. The distribution of the relative in-plane displacements in transversal direction reflects the distribution of the shear stresses in transversal direction.

5.4.6 Discussion

The mutual relations when varying the nominal glass thickness and glass pane of systems with joint type 2 are discussed in this section. The relation between the horizontal in-plane load and the horizontal in-plane displacement at the RTC of the system (figure 5.9 left) is slightly curved for nominal glass pane thicknesses of 8 mm and 12 mm and all glass pane sizes, caused by the non-linear material behaviour of the adhesive bonded joint (section 4.8.4) and is more curved for nominal glass pane thickness of 4 mm caused by out-of-plane displacements of the glass pane (section 5.4.3). The horizontal in-plane load increases at increasing glass pane thickness, because the in-plane stiffness of the glass pane increases (table 5.3). Increasing width of the glass pane makes the system squatter resulting in an increase of the maximum horizontal in-plane load and a decrease of the horizontal in-plane displacement at the RTC of the system (table 5.3). Increasing height of the glass pane makes the system slender resulting in a decrease of the maximum horizontal in-plane load and an increase of the horizontal in-plane displacement at the RTC of the system (table 5.3).

The horizontal in-plane load at the RTC of the system generates a horizontal and vertical in-plane load in the bolted connection between the outside beam and the beadwork which due to shear flexibility (section 4.8.1) results in relative horizontal and vertical in-plane displacements respectively. The influence of the shear flexibility of the bolted connection between the outside beam and the beadwork on the adhesive bonded joint and glass pane is explained using the right mullion. This explanation also concerns for the left, bottom and top adhesive bonded joint. The relative vertical in-plane displacements of the bolted connection between the outside beam and the beadwork of the right mullion are larger than the vertical in-plane deformation (bending) of the transoms at the vicinity of the internal hinge at the RBC and RTC of the steel frame (figure 5.9, right). So, the bottom of the right adhesive bonded joint displaces more in-plane from the bottom transom and the top of the right adhesive bonded joint displaces more in-plane to the top transom. In both cases the sign of the relative vertical in-plane displacements changes accompanied with a rapid increase of the relative vertical in-plane displacement in a small zone. This also effects the relative vertical in-plane displacement in transversal direction at the right bottom and top of the adhesive bonded joint. The larger the vertical in-plane load by increasing height of the glass pane, the larger the relative vertical in-plane displacement of the bolted connection between the outside beam and the beadwork of the right mullion, the larger the opposite relative vertical in-plane displacements in longitudinal direction at the ends of the adhesive bonded joints, the larger the relative vertical in-plane displacement in transversal direction at the ends of the adhesive bonded joints. The large

locally opposite shear stresses in longitudinal direction and the large locally shear stresses in transversal direction at the RBC and LTC (figure 5.13, right top and bottom respectively) results in local large tension stresses and in a rapid increase of the maximum principle stress (figure 5.12). This local influence results in the first crack in the glass pane (figure 3.15).

The relative out-of-plane displacement of the adhesive bonded joint increases at increasing nominal glass thickness caused by the larger eccentricity and larger in-plane load transfer between the glass pane and the steel frame at the front and rear. Furthermore, the out-of-plane displacement of the glass pane (figure 5.11) influences the distribution of the relative out-of-plane displacements of the adhesive bonded joint (figure 5.13, left top). The glass pane is four-sided clamped by the two-sided adhesive bonded joint (figure 5.13, left top) and therefore, the glass pane is also subjected to bending along the adhesive bonded joint resulting in a difference between the principle stresses at the front and rear of the glass pane (section 5.4.4) especially for smaller nominal glass thicknesses. Furthermore, the out-of-plane displacements of the glass pane with nominal glass thickness of 4 mm influence the principle stresses at the centre of the glass pane.

5.5 Systems with joint type 3

Systems with joint type 3 have many similarities with systems with joint type 2. The main similarities are the relation between the horizontal in-plane load and the horizontal in-plane displacement at the RTC of the system (section 5.4.1), the in-plane displacements of the steel frame (section 5.4.2), the relation between the horizontal in-plane load and the out-of-plane displacement at the centre of the glass pane (section 5.4.3) and the distribution of the normal and shear stresses of the rear adhesive bonded joint (section 5.4.5). The differences between systems with joint type 2 and 3 are given in the next sections.

5.5.1 Relation between horizontal in-plane load and horizontal in-plane displacement at the RTC of the system

Figure 5.14 (left) shows the relation between the horizontal in-plane load and the horizontal in-plane displacement at the RTC of the system at the moment the largest maximum principle stress is equal to the representative flexural tension strength of glass for all nominal glass thicknesses and glass pane sizes. Table 5.5 gives the horizontal in-plane displacement at the RTC of the system (u_{RTC}), the horizontal in-plane load (F_h), the actually horizontal in-plane displacement at the RTC of the system ($u_{RTC;a}$) and the in-plane stiffness of the system (K_s) at the moment the largest maximum principle stress is equal to the representative flexural tension strength of glass for all nominal glass thicknesses and glass pane sizes. The horizontal in-plane load and the horizontal in-plane displacement at the RTC of the system are smaller than for systems with joint type 2 for all nominal glass thicknesses and glass pane sizes. The parameter studies for the behaviour of this system are restricted to the moment of the first crack (at the moment the largest maximum principle stress is equal to the representative flexural tension strength of glass) (figure 3.20).
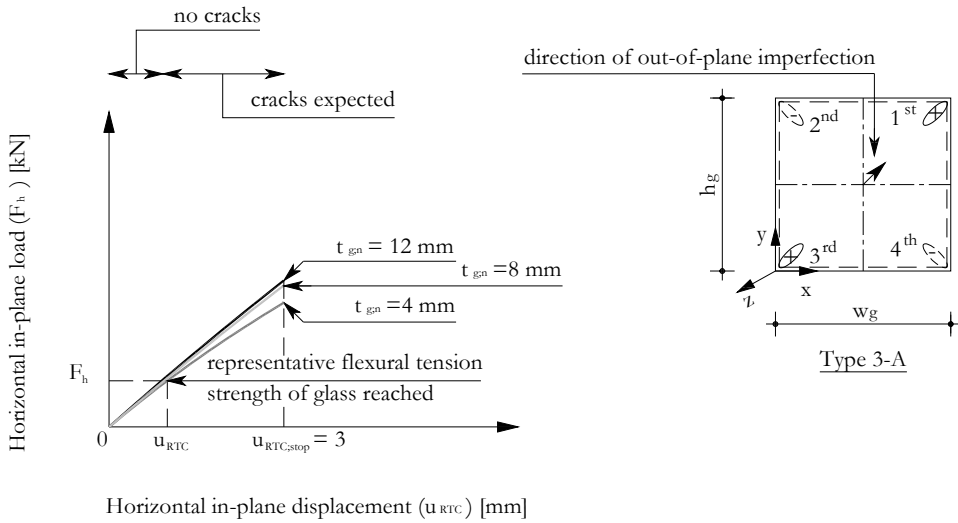
Figure 5.14: *Relation between horizontal in-plane load and horizontal in-plane displacement at the RTC of the system for three nominal glass thicknesses and six glass pane sizes (left) and type 3-A of out-of-plane displacements of the glass pane at the moment the largest maximum principle stress is equal to the representative flexural tension strength of glass (right)*

5.5.2   Out-of-plane displacements of the glass pane

Figure 5.14 (right) shows an overview of out-of-plane displacement type 3-A and figure 5.11 shows the out-of-plane displacement types 2-B and 2-C (section 5.4.3) which also occurs for systems with joint type 3. In table 5.6, these types are tabulated for different combinations of nominal glass thickness and glass pane representing the moment that the largest maximum principle stress is equal to the representative flexural tension strength of glass. Systems with glass pane sizes 1.0 m x 1.0 m, 1.5 m x 1.5 m, 1.0 m x 1.5 m and 1.5 m x 1.0 m and nominal glass thickness of 4 mm correspond with type 2-B (figure 5.11, left bottom). Systems with glass pane sizes 1.0 m x 3.0 m and 3.0 m x 1.0 m with nominal glass thickness of 4 mm correspond with type 2-C (figure 5.11, right top). For the other glass pane sizes and nominal glass thicknesses of 8 mm and 12 mm, small out-of-plane displacements occur in direction of positive z-axis at the LBC and the RTC of the glass pane and in negative z-axis at the RBC and the LTC of the glass pane (type 3-A). Furthermore, the schematic relations between the out-of-plane displacement at the centre of the glass pane and the horizontal in-plane load (figure 5.10) for all nominal glass thicknesses and glass pane sizes of systems with joint type 2 corresponds with systems with joint type 3. All glass panes have an out-of-plane imperfection of 1/2000 times the largest glass pane. Appendix E gives an overview of the critical plate buckling load subjected by pure in-plane shear load for four-sided simply supported glass panes, four-sided clamped supported glass panes and from finite element models. Furthermore, the horizontal in-plane load at the moment that the largest maximum principle stress is equal to the representative flexural tension strength of glass is smaller than the horizontal part of the relation between the horizontal in-plane load and the out-of-plane

displacement of the centre of the glass pane for all nominal glass thicknesses and glass pane sizes (table 5.5 and table E.1).

Table 5.5: *Overview of the horizontal in-plane displacement at the RTC of the system (u_{RTC}), the horizontal in-plane load (F_h), the actually horizontal in-plane displacement of the system ($u_{RTC;s}$), the in-plane stiffness of the system (K_s) and the relative horizontal and vertical in-plane displacements of the bolted connection between the outside beam and the beadwork ($u_{b;\eta;rel}$ and $v_{b;\eta;rel}$) at the moment that the largest maximum principle stress is equal to the representative flexural tension strength of glass for three nominal glass thicknesses and six glass pane sizes*

$t_{g;n}$ [mm]	Size	[m]	1.0x1.0	1.5x1.5	1.0x1.5	1.0x3.0	1.5x1.0	3.0x1.0
4	u_{RTC}	[mm]	0.753	0.825	1.090	2.410	0.590	0.452
	F_h	[kN]	24.11	27.80	21.15	16.77	30.76	47.30
	$u_{RTC;s}$	[mm]	0.512	0.547	0.643	1.094	0.444	0.392
	K_s	[kN/mm]	47.10	50.82	32.89	15.33	69.31	120.74
	$u_{b;\eta;rel}$	[mm]	0.071	0.066	0.059	0.047	0.076	0.077
	$v_{b;\eta;rel}$	[mm]	0.070	0.067	0.072	0.076	0.062	0.047
8	u_{RTC}	[mm]	0.714	0.838	1.060	2.464	0.548	0.417
	F_h	[kN]	27.61	34.12	24.11	19.01	35.15	53.59
	$u_{RTC;s}$	[mm]	0.438	0.497	0.552	0.972	0.381	0.349
	K_s	[kN/mm]	63.05	68.70	43.70	19.56	92.28	153.67
	$u_{b;\eta;rel}$	[mm]	0.072	0.074	0.062	0.047	0.086	0.088
	$v_{b;\eta;rel}$	[mm]	0.072	0.075	0.078	0.082	0.069	0.053
12	u_{RTC}	[mm]	0.699	0.755	1.048	2.464	0.530	0.399
	F_h	[kN]	29.28	32.74	25.44	19.71	36.93	55.70
	$u_{RTC;s}$	[mm]	0.406	0.428	0.513	0.917	0.354	0.328
	K_s	[kN/mm]	72.80	76.57	49.61	21.50	104.19	169.79
	$u_{b;\eta;rel}$	[mm]	0.072	0.069	0.062	0.047	0.089	0.093
	$v_{b;\eta;rel}$	[mm]	0.072	0.068	0.079	0.083	0.071	0.055

Table 5.6: *Overview of types for different combinations of nominal glass thickness and glass pane sizes representing the moment that the largest maximum principle stress is equal to the representative flexural tension strength of glass (for type 3A see figure 5.14, left; for types 2-B and 2-C see figure 5.11)*

$t_{g;n}$ [mm]	1.0x1.0	1.5x1.5	1.0x1.5	1.0x3.0	1.5x1.0	3.0x1.0
4	2-B	2-B	2-B	2-C	2-B	2-C
8	3-A	3-A	3-A	3-A	3-A	3-A
12	3-A	3-A	3-A	3-A	3-A	3-A

5.5.3 Principle stresses in the glass pane

The size and direction of the principle stresses at points 1 to 5 for all nominal glass thicknesses and glass pane sizes are given with vectors in figure 5.15. The size and direction corresponds with the size and direction of the principle stresses for systems with joint type 2. However, the size of the principle stresses over the glass thickness varies at points 1, 2, 4 and 5 and varies even more at the vicinity of the corners of the glass pane for all nominal glass thicknesses and glass pane sizes. The larger the nominal glass thickness the larger the difference between the principle stresses at the front and the rear of the glass pane. At point 3, the maximum and minimum principle stresses at the front and rear of the glass pane are almost equal for all nominal glass thicknesses and glass pane sizes except for glass pane sizes 1.0 m x 1.0 m, 1.5 m x 1.5 m, 1.0 m x 1.5 m and 1.5 m x 1.0 m with nominal glass thickness of 4 mm. The largest maximum principle stress is located at the front or rear at the vicinity of the RBC of the glass pane (figure 5.15, right).
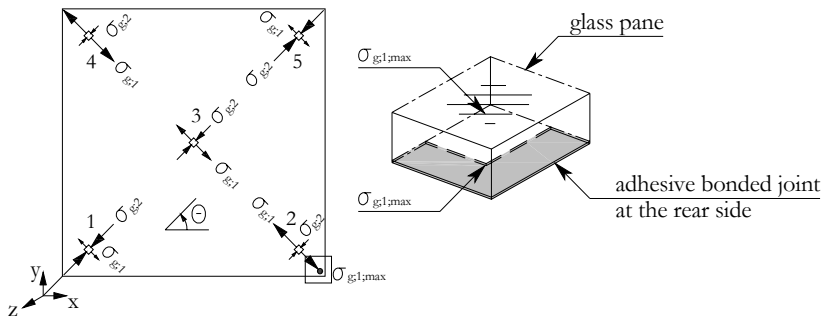
Figure 5.15:   Overview of the principle stresses and their direction at points 1 to 5 (left) and the position of the largest maximum principle stress (right) at the moment that the largest maximum principle stress is equal to the representative flexural tension strength of glass for three nominal glass thicknesses and six glass pane sizes

5.5.4 Distribution of normal and shear stresses in the adhesive bonded joint

Systems with joint type 3 have one circumferential adhesive bonded joint at the rear side. The findings of the distribution of the normal and shear stresses of the adhesive bonded joint only concern the rear adhesive bonded joint (figure 5.13). The distribution of the relative out-of-plane displacements ($w_{j;\varsigma;rel}$) and the normal stresses ($\sigma_{j;\varsigma}$) of the adhesive bonded joint are comparable to systems with joint type 2 (section 5.4.5), but the values are clearly larger for systems with joint type 3. The normal stresses at the end of the adhesive bonded joint increase at increasing nominal glass thickness. The distributions of the relative horizontal and vertical in-plane displacements in longitudinal direction ($u_{j;\eta;rel}$ and $v_{j;\eta;rel}$ respectively), the shear stresses in longitudinal x- and y-direction ($\tau_{j;\eta;x}$ and $\tau_{j;\eta;y}$ respectively), the relative horizontal and vertical in-plane displacements in transversal direction ($u_{j;\varsigma;rel}$ and $v_{j;\varsigma;rel}$ respectively) and the shear stresses in transversal x- and y-direction ($\tau_{j;\varsigma;x}$ and $\tau_{j;\varsigma;y}$ respectively) are comparable to systems with joint type 2 (section 5.4.5).

131

5.5.5   Discussion

Systems with joint type 3 have many similarities with systems with joint type 2 (section 5.4.6). The main differences between systems with joint type 3 and joint type 2 are the distribution of the principle stresses in the glass pane and the normal stresses in the adhesive bonded joints. The normal stresses in the adhesive bonded joints are larger than for systems with joint type 2, because the in-plane load transfer between the glass pane and steel frame is eccentric. The one-sided adhesive bonded joint clamps the glass pane and has to transfer the out-of-plane loads over the width of the adhesive bonded joint. Furthermore, the out-of-plane displacements of the glass pane influence the distribution of the normal stresses in the adhesive bonded joints. The clamp boundary condition at one side of the glass pane results in more bending of the glass pane and a larger stress gradient over the thickness of the glass pane besides the distribution of the principle stresses caused by the in-plane load.

5.6   Conclusions

Systems with joint type 1

Conclusions regarding the first stage of figure 5.1:

- The in-plane stiffness of the system is determined by the glass pane which determines the distribution of the normal and shear stresses of the adhesive bonded joint;
- The in-plane stiffness of the system linearly increases with the width of the adhesive bonded joint which is coupled to nominal glass thickness;
- The in-plane stiffness of the system more increases at larger relative in-plane displacement in normal direction of the adhesive bonded joint in the compression zone;
- The bolted connection between the outside beam and the beadwork has no influence on the distribution of the normal and shear stresses of the adhesive bonded joint and the distribution of the principle stresses;
- The glass pane is four-sided activated by the adhesive bonded joint by normal stresses and shear stresses;
- The normal stresses in the adhesive bonded joint are linearly or bi-linearly distributed and the distribution depends on maximum relative in-plane displacements in normal direction of the adhesive bonded joint (adhesive property);
- The distribution of the relative in-plane displacements in normal direction of the adhesive bonded joint is linear except at slender transoms and mullions;
- The shear stresses in the adhesive bonded joint are uniformly distributed;
- The largest maximum principle stress in the glass pane is not a design criterion;
- A design criterion is the relative in-plane displacement in normal direction and the relative in-plane displacement in longitudinal direction of the adhesive bonded joint;
- The horizontal in-plane displacement of the centre of the glass pane corresponds with the half of the horizontal in-plane displacement at the RTC of the system;
- The glass pane rotates in-plane around the horizontally displaced centre of the glass pane.
- Slender glass pane sizes are susceptible for out-of-plane displacements.

Conclusions regarding the moment of glass-steel contact(s):

- The critical plate buckling load can be reached for slender glass panes;
- For systems with square glass panes, the LBC and the RTC of the glass pane simultaneously make contact with the transoms and mullions (one glass-steel contact);
- For systems with rectangular glass panes with a smaller width than height, the LBC and the RTC of the glass pane make first glass-steel contact with the transoms followed by second glass-steel contact with the mullions;
- For systems with rectangular glass panes with a larger width than height, the LBC and the RTC of the glass pane make first glass-steel contact with the mullions followed by second glass-steel contact with the transoms;
- The glass pane can take off from the groove of the steel frame at large horizontal in-plane displacements at the RTC of the system;
- The steel frame is subjected to bending at the vicinity and after glass-steel contact.

Systems with joint type 2

The following conclusions can be drawn:

- Exceeding the representative flexural tension strength of glass firstly occurs than the critical plate buckling load;
- The in-plane stiffness of the system is determined by the glass pane, the nominal glass thickness, the shear stiffness of the bolted connection between the outside beam and the beadwork and the out-of-plane displacements of slender glass panes;
- A small shear flexibility of the bolted connection between the outside beam and the beadwork and a large shear stiffness of the adhesive bonded joint negatively influence the distribution of the shear stresses in longitudinal and transversal direction of the adhesive bonded joint and the distribution of the principle stresses in the glass pane;
- The design criteria are the largest maximum principle stress in the glass pane and the relative in-plane displacements in longitudinal and transversal direction of the adhesive bonded joint which are concentrated in a small zone at the RBC of the glass pane;
- The out-of-plane displacements of the glass pane influence the distribution of the normal stresses of the adhesive bonded joint;
- The two-sided adhesive bonded joint is a clamp condition for the glass pane.

Systems with joint type 3

The conclusions for systems with joint type 2 can be adopted for the one-sided adhesive bonded joint and completed with the following conclusions:

- Glass panes and especially slender glass panes are more susceptible for out-of-plane displacements;
- The glass pane is more subjected to bending along the edges and the corners;
- By the eccentric in-plane load transfer between the steel frame and the glass pane the normal stresses of the adhesive bonded joint are larger than for systems with joint type 2.

6 Mechanical models

This chapter describes the mechanical models derived for systems with circumferentially adhesive bonded glass panes to steel frames. Section 6.1 deals with the motivation and objective. Section 6.2 presents mechanical models for systems with joint type 1. Section 6.3 gives a proposal for possible mechanical models for systems with joint types 2 and 3. The chapter ends with section 6.4 that lists the conclusions.

6.1 Motivation and objective

Finite element simulations are convenient tools to get more insight into complex structural system behaviours such as systems with joint types 1 to 3. However, finite element simulations are not suitable tools at the beginning of a design process for buildings, because the development, the necessary calibration and the interpretation of information of finite element simulations are time-consuming activities. The building practice needs simple design tools to design a building structure at an early phase. The dimensions of the structure in mind have to be predicted such that they fulfil the building requirements. The development of mechanical models is a suitable tool to capture the main parameters of each system. The main parameters are the in-plane stiffness of the system, the critical plate buckling load, the maximum normal and shear stress of the adhesive bonded joint, the largest maximum principle stress in the glass pane and the residual capacity of the system. It is envisaged that mechanical models will be the basis of design rules and can be implemented in the partial factor approach for the ultimate and serviceability limit states, which is usual in European standards (section 2.4.1).

6.2 Systems with joint type 1

6.2.1 Outline

The relation between the horizontal in-plane load and the horizontal in-plane displacement at the RTC of the system has two stages for systems with square glass panes (figures 4.13 and 5.1) and three stages for systems with rectangular glass panes (figure 5.2) which is summarized in figure 6.1. The transition between two stages is glass-steel contact. The relation has two points of practical interest, namely at limited horizontal in-plane displacements at the RTC of the system and first glass-steel contact. The horizontal in-plane displacement at the RTC of the system is limited from the point of view of serviceability of a building regulated by building standards. The steel frame, the non-cracked glass pane and the non-failed adhesive bonded joint take part in the in-plane load transfer. At first glass-steel contact, the system has predictable residual capacity, because the glass pane is non-cracked. The steel frame, the non-cracked glass pane and the adhesive bonded joint under compression take part in the in-plane load transfer. After first glass-steel contact, it is very plausible that the glass pane cracks. So, the relation between the horizontal in-plane load and the horizontal in-plane displacement at

the RTC of the system is crack dependent and the additional residual capacity is not predictable anymore (figure 4.13).

The in-plane load transfer at first glass-steel contact depends on the glass pane size. For systems with square glass panes, the in-plane load is transferred by glass-steel contact only (figure 5.1, right). For systems with rectangular glass panes with a smaller width than height, the in-plane load is transferred at the LBC and RTC of the glass pane by glass-steel contact between glass pane and transoms and also by a partly pushed in adhesive bonded joint between glass pane and mullions (figure 5.2, left bottom). For systems with rectangular glass pane sizes with a larger width than height, the in-plane load is transferred at the LBC and RTC of the glass pane by glass-steel contact between glass pane and mullions and also by a partly pushed in adhesive bonded joint between glass pane and transoms (figure 5.2, right bottom).
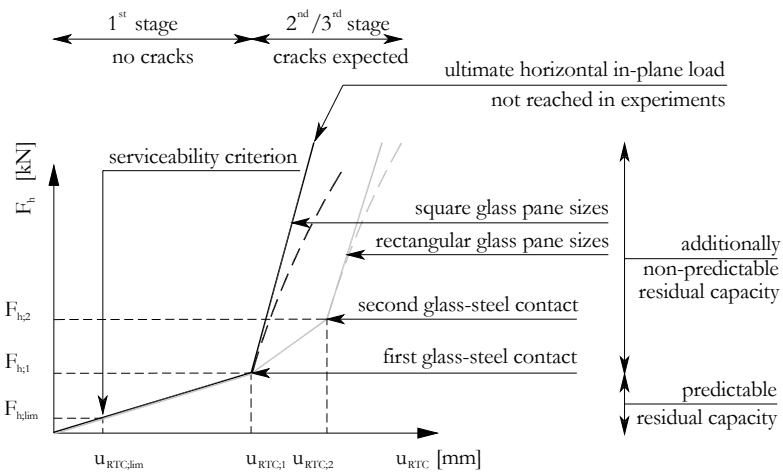
Figure 6.1: *Relation between the horizontal in-plane load and the horizontal in-plane displacement at the RTC of the system*

Figure 6.2 shows the distributions of the relative horizontal and vertical in-plane displacements in normal direction ($u_{j;\xi;rel}$ and $v_{j;\xi;rel}$ respectively) and the relative horizontal and vertical in-plane displacements in longitudinal direction ($u_{j;\eta;rel}$ and $v_{j;\eta;rel}$ respectively) of the adhesive bonded joint at limited horizontal in-plane displacement at the RTC of the system. The relative horizontal and vertical in-plane displacements in normal direction of the adhesive bonded joint are linearly distributed except for slender transoms and mullions (sections 5.3.6 and 5.3.7). The relative horizontal and vertical in-plane displacements in longitudinal direction of the adhesive bonded joint are uniformly distributed. Furthermore, the thickness of the steel frame enlarged the relative horizontal and vertical in-plane displacements in longitudinal direction of the adhesive bonded joint (sections 5.3.6 and 5.3.7). Figure 6.2 also shows the distributions of the normal stresses in x- and y-direction ($\sigma_{j;\xi;x}$ and $\sigma_{j;\xi;y}$ respectively) and the shear stresses in x- and y-direction ($\tau_{j;\eta;x}$ and $\tau_{j;\eta;y}$ respectively) of the adhesive bonded joint at limited horizontal in-plane displacement at the RTC of the system. The distribution of the normal stresses of the adhesive bonded joint is linear or bi-linear and it depends on the value of the relative in-plane displacement in normal direction (figure 4.9 right bottom). Bending of slender transoms and mullions reflects on the distribution of the normal stresses of the adhesive bonded joint. The

normal stiffness of the adhesive bonded joint under compression increases at increasing relative in-plane displacements in normal direction and the normal stiffness of the adhesive bonded joint under tension increases but to a lesser extent at increasing relative in-plane displacements in normal direction. The largest maximum principle stress ($\sigma_{g;1;max}$) is located at the RBC of the glass pane.
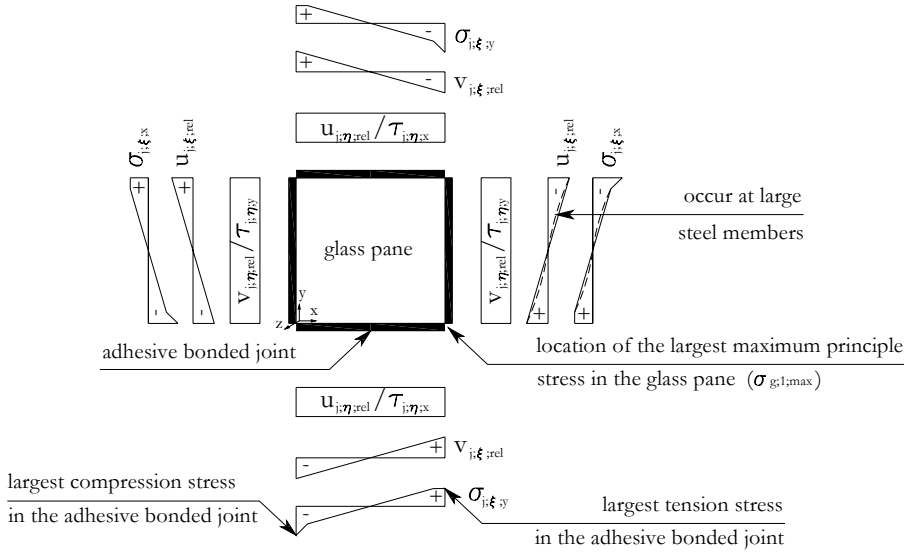
Figure 6.2: Distributions of the relative in-plane displacements in normal ($u_{j;\xi;rel}$ and $v_{j;\xi;rel}$) and longitudinal ($u_{j;\eta;rel}$ and $v_{j;\eta;rel}$) direction and the normal ($\sigma_{j;\xi;x}$ and $\sigma_{j;\xi;y}$) and shear stresses ($\tau_{j;\eta;x}$ and $\tau_{j;\eta;y}$) of the adhesive bonded joint and the location of the largest maximum principle stress in the glass pane ($\sigma_{g;1;max}$) at limited horizontal in-plane displacement at the RTC of the system

At limited horizontal in-plane displacement at the RTC of the system, the mechanical models have to predict:
- the in-plane stiffness of the system ($K_{s;lim}$);
- the maximum relative horizontal and vertical in-plane displacement in normal direction of the adhesive bonded joint ($u_{j;\xi;rel;max}$ and $v_{j;\xi;rel;max}$ respectively);
- the maximum normal stress in x- and y-direction ($\sigma_{j;\xi;x;max}$ and $\sigma_{j;\xi;y;max}$ respectively);
- the maximum relative horizontal and vertical in-plane displacement in longitudinal direction of the adhesive bonded joint ($u_{j;\eta;rel;max}$ and $v_{j;\eta;rel;max}$ respectively);
- the maximum shear stress in x- and y-direction ($\tau_{j;\eta;x;max}$ and $\tau_{j;\eta;y;max}$ respectively);
- the largest maximum principle stress at the RBC of the glass pane ($\sigma_{g;1;max}$).

At first glass-steel contact, the mechanical models have to predict:
- the horizontal in-plane load ($F_{h;1}$);
- the horizontal in-plane displacement at the RTC of the system ($u_{RTC;1}$).
- the horizontal in-plane load for critical plate buckling ($F_{h;crit}$).

6.2.2 Models at limited horizontal in-plane displacement at the RTC of the system

The mechanical models are based on the parameter studies (section 5.3). The partial factor approach for the ultimate and serviceability limit states is not taken into account (section 2.4.1). Figure 6.3 at the left top shows the geometrical parameters of the system. The geometrical parameters are the lower limit value for the nominal glass thickness (t_g), the glass pane width (w_g), the glass pane height (h_g), the system width (w_s), the system height (h_s), the thickness of the steel frame (t_f), the joint thickness (t_j), and the joint width (w_j). Furthermore, the centre of the glass pane is coupled to the middle of a construction line (d_s) from the hinge at the LBC to the hinge of the RTC of the system. Figure 6.3 at the right top shows the parameters at limited horizontal in-plane displacement at the RTC of the system. Figure 6.3 at the bottom shows an enlarged view of the RBC of the system. The parameters are the horizontal in-plane load (F_h), the horizontal in-plane displacement at the RTC of the system (u_{RTC}), the in-plane rotation of the right mullion around the internal hinge at the RBC (β), the in-plane rotation of the glass pane around its centre (φ), the maximum relative horizontal and vertical in-plane displacement in normal direction ($u_{j;\xi;rel;max}$ and $v_{j;\xi;rel;max}$ respectively), the maximum relative horizontal and vertical in-plane displacement in longitudinal direction ($u_{j;\eta;rel;max}$ and $v_{j;\eta;rel;max}$ respectively) and the additionally relative horizontal and vertical in-plane displacement in longitudinal direction ($\lrcorner u_{j;\eta;rel}$ and $\lrcorner v_{j;\eta;rel}$ respectively).

Basic assumptions for the mechanical models are:

- no initial out-of-plane displacements of the glass pane (section 5.3.3);
- the glass pane acts rigid in-plane;
- the centre of the horizontally in-plane displaced glass pane is thought to coincide with the middle of the construction line (section 5.3.4);
- the in-plane rotation of the glass pane is thought to occur around the middle of the construction line (section 5.3.4);
- no deformation in axial direction of the steel mullions and transoms;
- no vertical in-plane displacements of the transoms and mullions;
- no bending of the steel transoms and mullions (section 5.3.2);
- no shear deformation of the bolted connection between the beadwork and the outside beam (section 5.3.1);
- linear distribution of the relative in-plane displacements in normal direction (section 5.3.6);
- linear distribution of the normal stresses of the adhesive bonded joint;
- uniform distribution of the relative in-plane displacements in longitudinal direction (section 5.3.6);
- uniform distribution of the shear stresses of the adhesive bonded joint;
- equal diagonals of the horizontally in-plane displaced steel frame (parallelogram) at limited horizontal in-plane displacement at the RTC of the system.
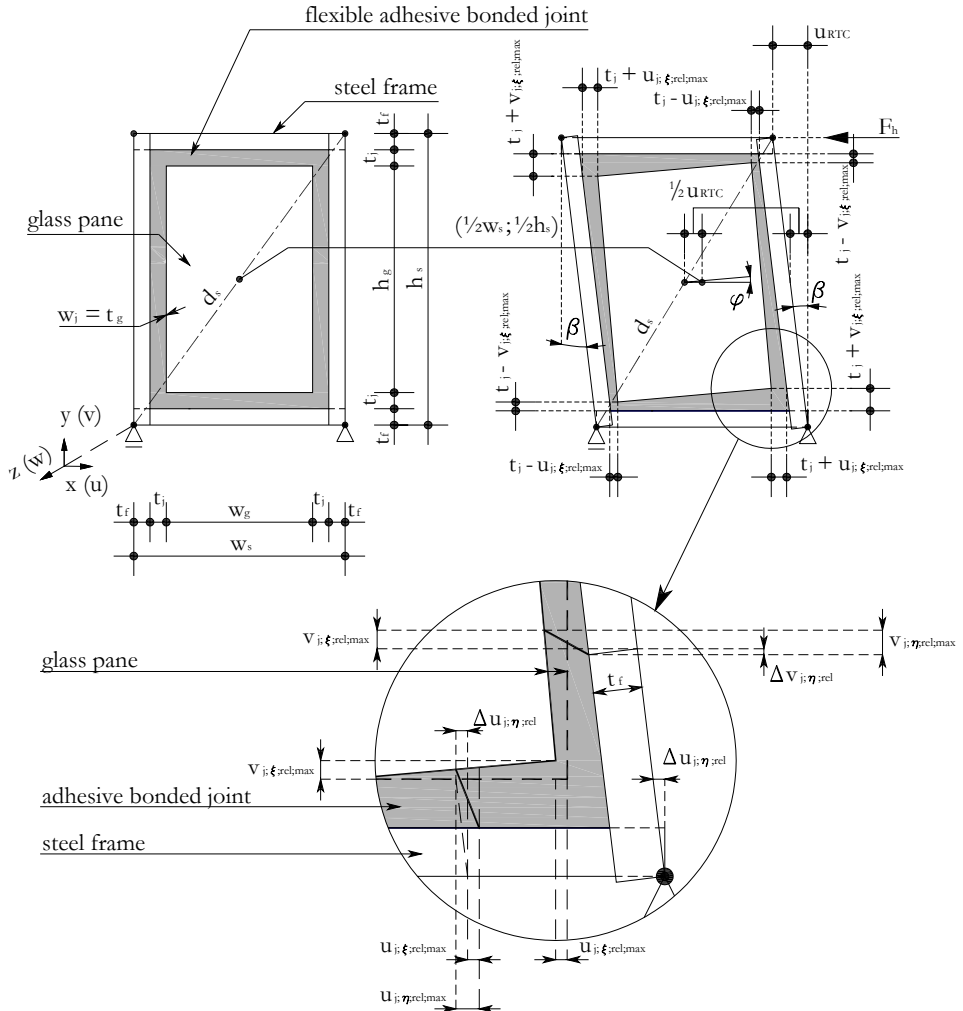
Figure 6.3:   Geometry of the system (left top), a displaced situation of the system at limited horizontal in-plane displacement at the RTC of the system (right top) and an enlarged view of the RBC of the system

The continuous normal stiffness of the adhesive bonded joint ($k_{j;\xi}$) is the quotient of the Young's modulus of the adhesive (E_a) and the joint thickness (t_j) represented in equation 6.1a. This equation is suitable for linear material behaviour of the adhesive bonded joint. For adhesive bonded joints with non-linear material behaviour (see figure 4.9 right bottom), equations 6.1b and 6.1c are more suitable in a point [Habenicht 2006]. These equations are the quotient of the normal stress and the relative in-plane displacement in normal direction.

$$k_{j;\xi} = \frac{E_a}{t_j} \qquad k_{j;\xi;x} = \frac{\sigma_{j;\xi;x}}{u_{j;\xi;rel}} \qquad k_{j;\xi;y} = \frac{\sigma_{j;\xi;y}}{v_{j;\xi;rel}} \qquad \text{(Equation 6.1a-c)}$$

139

The continuous shear stiffness of the adhesive bonded joint ($k_{j;\eta}$) is the quotient of the shear modulus of the adhesive (G_a) and the joint thickness represented in equation 6.2a and is also suitable for linear material behaviour of the adhesive bonded joint. For adhesive bonded joints with non-linear material behaviour, equations 6.2b and 6.2c are more suitable in a point [Habenicht 2006]. These equations are the quotient of the shear stress and the relative in-plane displacement in longitudinal direction.

$$k_{j;\eta} = \frac{G_a}{t_j} \qquad k_{j;\eta;x} = \frac{\tau_{j;\eta;x}}{u_{j;\eta;rel}} \qquad k_{j;\eta;y} = \frac{\tau_{j;\eta;y}}{v_{j;\eta;rel}} \qquad\qquad \text{(Equation 6.2a-c)}$$
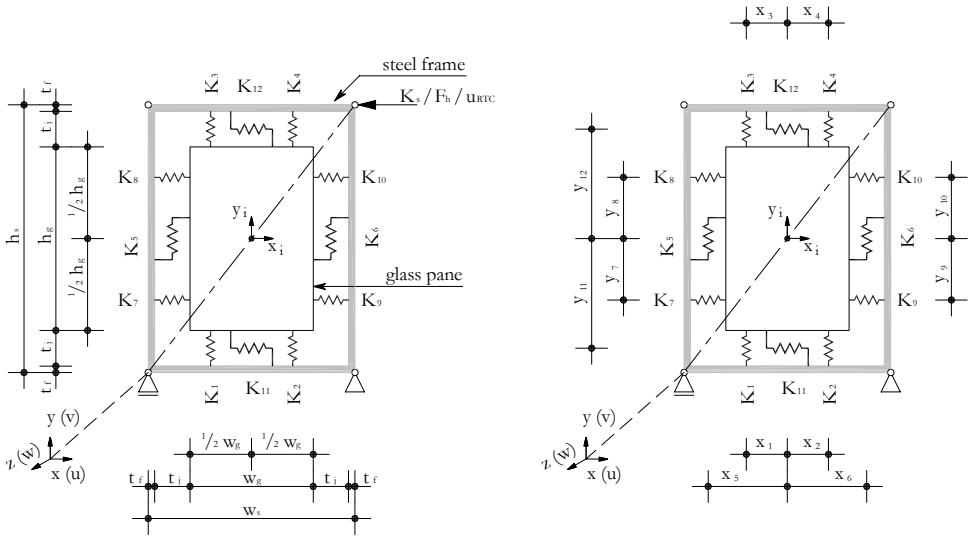
Figure 6.4:   *System with twelve discrete springs representing the circumferentially adhesive bonded joint (left) and their positions in relation to the centre of the glass pane (right)*

Figure 6.4 at the left shows the mechanical model in which the continuous normal and shear stiffness of the circumferentially adhesive bonded joint are transformed into twelve discrete springs (K_1 to K_{12}) and figure 6.4 at the right the position of the twelve discrete springs in relation to the centre of the glass pane. K_1 to K_4 are discrete normal springs in y-direction, K_7 to K_{10} are discrete normal springs in x-direction, K_5 and K_6 are discrete shear springs in y-direction and K_{11} and K_{12} are discrete shear springs in x-direction. The normal stiffness of the normal discrete springs is a conversion of the continuous normal stiffness of the adhesive bonded joint based on a linear distribution of the normal stresses and is represented in equations 6.3 and 6.4. In these equations are involved the width ($t_j = t_g$) and the length (w_g and h_g) of the adhesive bonded joint. The position of the horizontal discrete normal springs is two-third of the half of the height of the glass pane in relation to the centre of the glass pane (y_7 to y_{10}). The position of the vertical discrete normal springs is two-third of the half of the width of the glass pane in relation to the centre of the glass pane (x_1 to x_4).

$$K_1 = K_2 = K_3 = K_4 = \tfrac{3}{8} k_{j;\xi;y} t_g w_g \qquad \text{(Equation 6.3)}$$

$$K_7 = K_8 = K_9 = K_{10} = \tfrac{3}{8} k_{j;\xi;x} t_g h_g \qquad \text{(Equation 6.4)}$$

The shear stiffness of the discrete shear springs is also a conversion of the continuous shear stiffness of the adhesive bonded joint based on a uniform distribution of the shear stresses and is represented in equations 6.5 and 6.6. In these equations are involved the width ($t_j = t_g$) and the length (w_g and h_g) of the adhesive bonded joint. The position of the horizontal discrete shear springs (y_{11} and y_{12}) is the half of the height of the glass pane enlarged with the half of the joint thickness in relation to the centre of the glass pane. The position of the vertical discrete shear springs (x_5 and x_6) is the half of the width of the glass pane enlarged with the half of the joint thickness in relation to the centre of the glass pane.

$$K_5 = K_6 = k_{j;\eta;y} t_g h_g \qquad \text{(Equation 6.5)}$$

$$K_{11} = K_{12} = k_{j;\eta;x} t_g w_g \qquad \text{(Equation 6.6)}$$
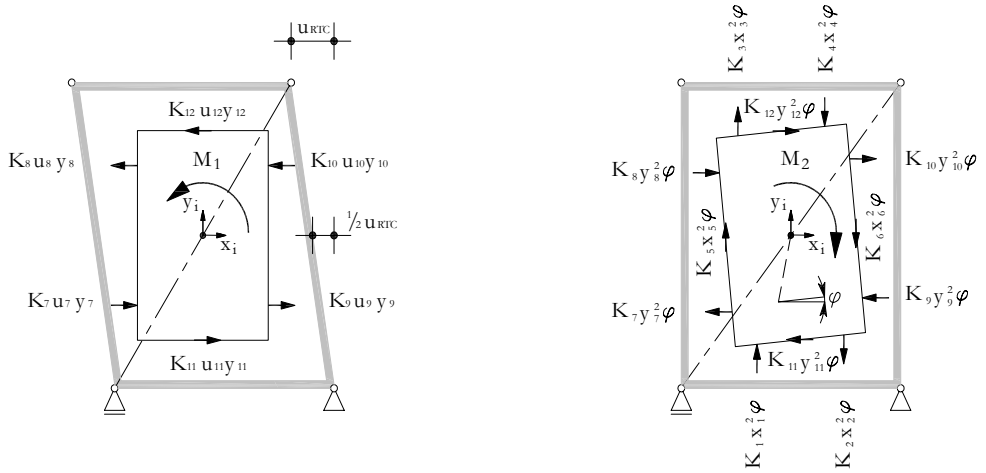
Figure 6.5:   Horizontal in-plane loads imposed by the horizontal in-plane displacement at the RTC of the system (left) and all in-plane loads imposed by the in-plane rotation of the glass pane (right)

The system has four generalized in-plane displacements. Figure 6.5 at the left shows the first two generalized in-plane displacements, namely the imposed horizontal in-plane displacement at the RTC of the steel frame and the horizontal in-plane displacement of the glass pane. Figure 6.5 at the right shows the other two generalized in-plane displacements, namely the horizontal and vertical in-plane displacements of the glass pane within the non-displaced steel frame. These horizontal and vertical in-plane displacements are the result of the in-plane rotation of the glass pane (φ).

141

The horizontal in-plane displacements (u_7 to u_{12}) are the difference between the horizontal in-plane displacements of the glass pane and the steel frame at the location of the discrete springs 7 to 12. The horizontal in-plane displacements of the glass pane correspond with the half of the horizontal in-plane displacement at the RTC of the system and the horizontal in-plane displacements of the steel frame are linearly distributed over the height represented in equation 6.7.

$$u_i = \frac{y_i u_{RTC}}{h_s}$$
(Equation 6.7)

The in-plane moment (M_1) is the sum of the product of the stiffness of the discrete springs (K_7 to K_{12}), the horizontal in-plane displacements (u_7 to u_{12}) and the vertical levers (y_7 to y_{12}). With the horizontal in-plane displacements (u_7 to u_{12}) represented in equation 6.7, results in equation 6.8.

$$M_1 = \sum_{i=7}^{12} K_{x;i} u_i y_i = \frac{u_{RTC}}{h_s} \sum_{i=7}^{12} K_{x;i} y_i^2$$
(Equation 6.8)

The in-plane moment (M_2) is the sum of the product of the stiffness of the discrete springs (K_1 to K_{12}), the accompanying in-plane displacements as a result of the in-plane rotation ($x_1\varphi$ to $x_6\varphi$ and $y_7\varphi$ to $y_{12}\varphi$) and their levers (x_1 to x_6 and y_7 to y_{12}). This is represented in equation 6.9.

$$M_2 = \varphi\left(\sum_{i=1}^{6} K_{y;i} x_i^2 + \sum_{i=7}^{12} K_{x;i} y_i^2 \right)$$
(Equation 6.9)

After equating the in-plane moments of equations 6.8 and 6.9, the in-plane rotation of the glass pane is a function of the horizontal in-plane displacement at the RTC of the system represented in equation 6.10.

$$\varphi = K_\varphi \frac{u_{RTC}}{h_s}$$
(Equation 6.10)

In equation 6.10 is introduced the in-plane rotation stiffness (K_φ) represented in equation 6.11. The in-plane rotation stiffness is a system constant which depends on the stiffnesses of the discrete springs and their positions.

$$K_\varphi = \frac{\displaystyle\sum_{i=7}^{12} K_{x;i} y_i^2}{\left(\displaystyle\sum_{i=1}^{6} K_{y;i} x_i^2 + \sum_{i=7}^{12} K_{x;i} y_i^2 \right)}$$
(Equation 6.11)
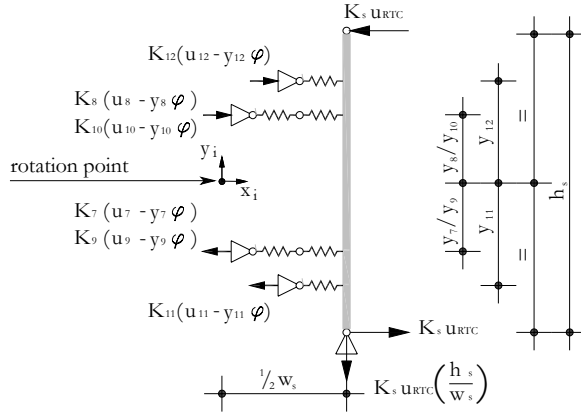
Figure 6.6: *Determination of the in-plane stiffness of the system represented by a vertical member supported by horizontal discrete springs K_7 to K_{12}*

Figure 6.6 shows a vertical member with horizontal discrete springs (K_7 to K_{12}) in equilibrium state which is equivalent to the system needed for the prediction of the in-plane stiffness of the system. The in-plane stiffness of the system is the result of the sum of the moment around the centre of the glass pane. This is represented in equation 6.12.

$$K_s = \frac{(1 - K_\varphi)}{h_s^2} \sum_{i=7}^{12} K_{x;i} y_i^2 \qquad \text{(Equation 6.12)}$$

The prediction of the horizontal in-plane load (F_h) is the product of the in-plane stiffness of the system (equation 6.12) and the horizontal in-plane displacement at the RTC of the system represented in equation 6.13.

$$F_h = K_s u_{RTC} \qquad \text{(Equation 6.13)}$$

The maximum relative horizontal in-plane displacements in normal direction of the left and right adhesive bonded joint are located at the corners of the glass pane (figure 6.3, right top and bottom). This displacement is the difference between the horizontal in-plane displacement of the steel frame at half height of the glass pane ($\frac{1}{2}\beta \cdot h_g$) and the horizontal in-plane displacement of the glass pane at the half of the height of the glass pane ($\frac{1}{2}\varphi \cdot h_g$). This is represented in equation 6.14 in which the angle (β) is the ratio between the horizontal in-plane displacement at the RTC of the system (u_{RTC}) and the height of the system (h_s) and the in-plane rotation of the glass pane (φ) is substituted by 6.10.

$$u_{j;\xi;rel;\max} = \tfrac{1}{2} \beta h_g - \tfrac{1}{2} \varphi h_g = \frac{(1 - K_\varphi) h_g u_{RTC}}{2 h_s} \qquad \text{(Equation 6.14)}$$

The maximum relative vertical in-plane displacements in normal direction of the bottom and top adhesive bonded joint are located at the corners of the glass pane (figure 6.3, right top and bottom). This displacement is the product of the in-plane rotation of the glass pane and the half of the glass pane width represented in equation 6.15 in which the in-plane rotation of the glass pane (φ) is substituted by 6.10.

$$v_{j;\xi;rel;\max} = \tfrac{1}{2} w_g \varphi = \frac{w_g K_\varphi u_{RTC}}{2h_s} \qquad \text{(Equation 6.15)}$$

The maximum relative horizontal in-plane displacements in longitudinal direction of the bottom and top adhesive bonded joint are built up of the maximum relative horizontal in-plane displacement in normal direction of the left and right adhesive bonded joint (equation 6.14) and an additionally horizontal in-plane displacement of the steel frame at the horizontal edge of the glass pane (figure 6.3). This is represented in equation 6.16.

$$u_{j;\eta;rel;\max} = u_{j;\xi;rel;\max} + (t_f + t_j)\beta = \frac{(h_s - h_g K_\varphi)u_{RTC}}{2h_s} \qquad \text{(Equation 6.16)}$$

The maximum relative vertical in-plane displacement in longitudinal direction of the left and right adhesive bonded joint is built up of the maximum relative vertical in-plane displacement in normal direction of the bottom and top adhesive bonded joint (equation 6.15) and an opposite vertical in-plane displacement of the steel frame (figure 6.3). This is represented in equation 6.17.

$$v_{j;\eta;rel;\max} = v_{j;\xi;rel;\max} + t_f \beta = \frac{(2t_f + w_g K_\varphi)u_{RTC}}{2h_s} \qquad \text{(Equation 6.17)}$$

The prediction of the maximum normal stresses is the product of the maximum relative in-plane displacement in normal direction of the adhesive bonded joint (equations 6.14 and 6.15) and the accompanying continuous normal stiffness (figure 4.9, bottom right) represented in equations 6.1b and 6.1c. Exactly, the normal stiffness of the adhesive bonded joint is non linear and leads to a fault. This is justified, because the adhesive bonded joint has a very small stiffness in relation to the stiff glass pane and steel frame. The prediction of the maximum shear stresses is the product of the maximum relative in-plane displacement in longitudinal direction of the adhesive bonded joint (equations 6.16 and 6.17) and the accompanying continuous shear stiffness (figure 4.9, left) represented in equations 6.2b and 6.2c. Finally, the prediction of the largest maximum principle stress at the RBC of the glass pane is an approximation and is based on the maximum tension and shear stresses at the RBC of the adhesive bonded joint represented in equations 6.1b and 6.1c and the maximum shear stress is the largest of equations 6.2b and 6.2c.

$$\sigma_{g;1;\max} = \frac{\sigma_{j;\xi;x;\max} + \sigma_{j;\xi;y;\max}}{2} + \sqrt{\left(\frac{\sigma_{j;\xi;x;\max} - \sigma_{j;\xi;y;\max}}{2}\right)^2 + \tau_{j;\eta;\max}^2} \quad \text{(Equation 6.18)}$$

6.2.3 Models at first glass-steel contact

The purpose of the mechanical models at first glass-steel contact is to predict the horizontal in-plane load and the horizontal in-plane displacement at the RTC of the system needed for the predictably residual capacity of the system. Figure 6.7 shows a system at the moment of first glass-steel contact. The parameters are the horizontal in-plane load ($F_{h;1}$), the horizontal in-plane displacement at the RTC of the system ($u_{RTC;1}$), the in-plane rotation of the glass pane around its centre (φ) and the maximum relative horizontal and vertical in-plane displacement in normal direction of the adhesive bonded joint ($u_{j;\xi;rel;max;1}$ and $v_{j;\xi;rel;max;1}$ respectively).
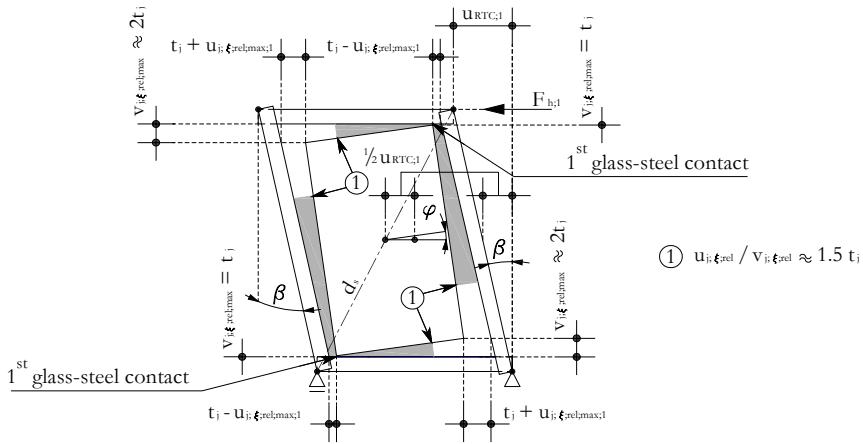
Figure 6.7:   First glass-steel contact (drawn: system with glass pane size $w_g \leq h_g$)

The prediction of the horizontal in-plane displacement at the RTC of the system at first glass-steel contact only depends on the geometry of the system (section 5.3.1). The in-plane rotation stiffness (equation 6.11) is used with the assumption that the glass pane behaves linearly till first glass-steel contact. Systems with square glass panes and rectangular glass panes with a smaller width than height firstly make contact with the transoms. The maximum relative vertical in-plane displacement of the bottom and top adhesive bonded joint in normal direction at the LBC and the RTC of the glass pane corresponds with the joint thickness. So, the maximum relative vertical in-plane displacement in normal direction ($v_{j;\xi;rel;max;1}$) is substituted by the joint thickness in equation 6.15. This is represented in equation 6.19.

$$u_{RTC;1} = \frac{2t_j h_s}{w_g K_\varphi} \qquad \text{for } w_g \leq h_g \qquad \text{(Equation 6.19)}$$

The accompanying maximum relative horizontal in-plane displacement in normal direction ($u_{j;\xi;rel;max;1}$) of the left and right adhesive bonded joint at the LBC and the RTC of the glass pane is the product of the joint thickness and the ratio between the maximum relative horizontal in-plane displacement in normal direction (equation 6.14) and the maximum relative vertical in-plane displacement in normal direction (equation 6.15) at limited horizontal in-plane displacement at the RTC of the system. This is represented in equation 6.20.

145

$$u_{j;\xi;rel;\max;1} = \frac{u_{j;\xi;rel;\max}\ t_j}{v_{j;\xi;rel;\max}}$$

(Equation 6.20)

Systems with rectangular glass panes with a larger width than height firstly make contact with the mullions. The maximum relative horizontal in-plane displacement in normal direction of the left and right adhesive bonded joint at the LBC and the RTC of the glass pane corresponds with the joint thickness. So, the maximum relative horizontal in-plane displacement in normal direction ($u_{j;\xi;rel;max;1}$) is substituted by the joint thickness in equation 6.14. This is represented in equation 6.21.

$$u_{RTC;1} = \frac{2t_j h_s}{(1 - K_\varphi)h_g} \qquad \text{for } w_g \geq h_g$$

(Equation 6.21)

The accompanying maximum relative vertical in-plane displacement in normal direction ($v_{j;\xi;rel;max;1}$) of the bottom and top adhesive bonded joint at the LBC and RTC of the glass is the product of the joint thickness and the ratio between the maximum relative vertical in-plane displacement in normal direction (equation 6.15) and the maximum relative horizontal in-plane displacement in normal direction (equation 6.14) at limited horizontal in-plane displacement at the RTC of the system. This is represented in equation 6.22.

$$v_{j;\xi;rel;\max;1} = \frac{v_{j;\xi;rel;\max}\ t_j}{u_{j;\xi;rel;\max}}$$

(Equation 6.22)

For the prediction of the horizontal in-plane load at first glass-steel contact, the actually continuous normal stiffness of the adhesive bonded joint has to be calculated. However, the continuous normal stiffness of the adhesive bonded joint is not constant. It increases under compression and it remains very small under tension. Moreover, the adhesive bonded joint under tension is even torn off by the large relative in-plane displacements in normal and longitudinal direction and it is eliminated in the in-plane load transfer (figure 3.11). To avoid non-linear calculations, the varying continuous normal stiffness of the adhesive bonded joint is converted into an equivalent continuous normal stiffness which is distributed linearly. This is justified, because the horizontal in-plane load at the first glass-steel contact is a global value. Appendix F gives derivations for the equivalent continuous normal stiffness of the adhesive bonded joint for the applied adhesive with a joint thickness of 5 mm. The continuous normal stiffness in equations 6.3 and 6.4 is substituted by the equivalent continuous normal stiffness in y-direction and in x-direction respectively based on the maximum relative horizontal and vertical in-plane displacements in normal direction of the adhesive bonded joint at first glass-steel contact. From this, a new in-plane rotation stiffness at first glass-steel contact ($K_{\varphi;1}$) is found. The horizontal in-plane load at first glass-steel contact is predicted by equation 6.23.

$$F_{h;1} = \frac{(1 - K_{\varphi;1})u_{RTC;1}}{h_s^2} \sum_{i=7}^{12} K_{x;i} y_i^2$$

(Equation 6.23)

6.2.4   Models versus parameter studies

Table 6.1 gives an overview of the predictions of the in-plane stiffness of the system ($K_{s;lim}$) and the horizontal in-plane load ($F_{h;lim}$) at limited horizontal in-plane displacement at the RTC of the system and the horizontal in-plane displacement at the RTC of the system ($u_{RTC;l}$) and the horizontal in-plane load ($F_{h;l}$) at first glass-steel contact for three nominal glass thicknesses and six glass pane sizes compared with parameter studies (table 5.1) including deviations.

Table 6.1:   Overview of the predictions of the in-plane stiffness of the system ($K_{s;lim}$) and the horizontal in-plane load ($F_{h;lim}$) at limited horizontal in-plane displacement at the RTC of the system ($u_{RTC;lim}$) and the predictions of the horizontal in-plane displacement at the RTC of the system ($u_{RTC;l}$) and the horizontal in-plane load ($F_{h;l}$) at first glass-steel contact for three nominal glass pane thicknesses and six glass pane sizes including deviations (Δ) (compared with table 5.1)

Size [m]	$t_{g;n}$ [mm]	$u_{RTC;lim}$ [mm]	$K_{s;lim}$ [kN/mm]	$\Delta K_{s;lim}$ [%]	$F_{h;lim}$ [kN]	$u_{RTC;l}$ [mm]	$\Delta u_{RTC;l}$ [%]	$F_{h;l}$ [kN]	$\Delta F_{h;l}$ [%]
1.0 x 1.0	4		0.37	-5.1	1.37			12.12	-18.1
	8	3.70	0.75	-6.3	2.78	22.20	-4.9	24.57	-4.4
	12		1.14	-5.0	4.22			37.33	-1.0
1.5 x 1.5	4		0.59	-10.6	3.17			18.80	-7.4
	8	5.37	1.20	-7.7	6.44	21.47	-9.0	38.09	-8.7
	12		1.83	-3.7	9.83			57.88	-5.9
1.0 x 1.5	4		0.29	-9.4	1.56			8.77	-3.7
	8	5.37	0.58	-7.9	3.11	21.64	-8.9	17.77	-3.4
	12		0.88	-4.4	4.73			27.00	-7.5
1.0 x 3.0	4		0.12	-14.3	1.24			5.29	-10.9
	8	10.37	0.25	-10.7	2.59	32.88	-6.2	10.73	-5.0
	12		0.37	-11.9	3.84			16.30	1.2
1.5 x 1.0	4		0.60	-10.5	2.22			12.72	-23.8
	8	3.70	1.22	-9.0	4.51	14.92	-12.3	25.78	-16.0
	12		1.85	-8.0	6.85			39.17	-5.8
3.0 x 1.0	4		0.95	-14.4	3.52			14.84	-4.3
	8	3.70	1.93	-12.3	7.14	11.74	-10.1	30.05	-2.8
	12		2.94	-12.5	10.88			45.67	3.1

The predictions of the in-plane stiffness of the system at limited horizontal in-plane displacement at the RTC yield smaller values than obtained from parameter studies which also reflect the horizontal in-plane load. At the first glass-steel contact, the predictions of the

horizontal in-plane displacement at the RTC of the system and the horizontal in-plane load yield smaller values than obtained from parameter studies.

Table 6.2: *Overview of the predictions of the maximum relative horizontal and vertical in-plane displacements in normal direction ($u_{j;\xi;rel;max}$ and $v_{j;\xi;rel;max}$ respectively), the maximum relative horizontal and vertical in-plane displacements in longitudinal direction ($u_{j;\eta;rel;max}$ and $v_{j;\eta;rel;max}$ respectively), the maximum normal stresses in x- and y-direction ($\sigma_{j;\xi;x;max}$ and $\sigma_{j;\xi;y;max}$ respectively) and the maximum shear stresses in x- and y-direction ($\tau_{j;\eta;x;max}$ and $\tau_{j;\eta;y;max}$ respectively) of the adhesive bonded joint and the largest maximum principle stress in the glass pane ($\sigma_{g;1;max}$) for three nominal glass thicknesses and six glass pane sizes including deviations (Δ) (compared with table 5.2)*

Size	[m]	1.0x1.0	1.5x1.5	1.0x1.5	1.0x3.0	1.5x1.0	3.0x1.0
$u_{j;\xi;rel;max}$	[mm]	0.83	1.25	0.64	0.27	1.24	1.58
$\Delta u_{j;\xi;rel;max}$	[%]	2.45	5.93	-4.48	-35.71	6.90	8.22
$v_{j;\xi;rel;max}$	[mm]	0.83	1.25	1.24	1.58	0.64	0.27
$\Delta v_{j;\xi;rel;max}$	[%]	2.45	5.93	6.90	8.22	-4.48	-35.71
$u_{j;\eta;rel;max}$	[mm]	1.02	1.43	0.82	0.45	1.42	1.76
$\Delta u_{j;\eta;rel;max}$	[%]	3.03	4.38	-4.65	-28.57	4.41	3.53
$v_{j;\eta;rel;max}$	[mm]	1.00	1.42	1.41	1.74	0.81	0.44
$\Delta v_{j;\eta;rel;max}$	[%]	2.04	3.65	6.02	8.07	-4.71	-26.67
$\sigma_{j;\xi;x;max;LBC/RTC}$	[N/mm²]	-1.20	-2.88	-0.74	-0.31	-2.84	-4.19
$\Delta\sigma_{j;\xi;x;max;LBC/RTC}$	[%]	15.38	10.34	-7.50	-38.00	14.06	13.86
$\sigma_{j;\xi;y;max;LBC/RTC}$	[N/mm²]	-1.20	-2.88	-2.84	-4.19	-0.76	-0.32
$\Delta\sigma_{j;\xi;y;max;LBC/RTC}$	[%]	12.15	8.68	13.60	17.04	-6.17	-36.00
$\sigma_{j;\xi;x;max;RBC/LTC}$	[N/mm²]	0.91	0.95	0.76	0.32	0.95	0.98
$\Delta\sigma_{j;\xi;x;max;RBC/LTC}$	[%]	-2.15	1.06	-5.00	-34.69	-1.04	-1.01
$\sigma_{j;\xi;y;max;RBC/LTC}$	[N/mm²]	0.91	0.95	0.95	0.98	0.76	0.32
$\Delta\sigma_{j;\xi;y;max;RBC/LTC}$	[%]	-2.15	1.06	1.06	3.15	-5.00	-31.91
$\tau_{j;\eta;x;max}$	[N/mm²]	0.09	0.12	0.07	0.04	0.12	0.15
$\Delta\tau_{j;\eta;x;max}$	[%]	0.00	0.00	0.00	-20.00	0.00	0.00
$\tau_{j;\eta;y;max}$	[N/mm²]	0.09	0.12	0.12	0.15	0.07	0.04
$\Delta\tau_{j;\eta;y;max}$	[%]	0.00	0.00	9.09	7.14	0.00	-20.00
$\sigma_{g;1;max;RBC}$	[N/mm²]	0.99	1.07	1.03	1.14	1.03	1.14
$\Delta\sigma_{g;1;max;RBC}$	[%]	-22.05	-20.15	-5.50	-5.79	-18.90	-12.98

Table 6.2 gives an overview of the predictions of the maximum relative horizontal and vertical in-plane displacements in normal direction of the adhesive bonded joint ($u_{j;\xi;rel;max}$ and $v_{j;\xi;rel;max}$ respectively), the maximum relative horizontal and vertical in-plane displacements in longitudinal direction of the adhesive bonded joint ($u_{j;\eta;rel;max}$ and $v_{j;\eta;rel;max}$ respectively), the maximum normal stresses in x- and y-direction of the adhesive bonded joint at the LBC and RTC ($\sigma_{j;\xi;x;max;LBC/RTC}$ and $\sigma_{j;\xi;y;max;LBC/RTC}$ respectively), the maximum normal stresses in x- and y-direction of the adhesive bonded joint at the RBC and LTC ($\sigma_{j;\xi;x;max;RBC/LTC}$ and $\sigma_{j;\xi;y;max;RBC/LTC}$ respectively), the maximum shear stresses in x- and y-direction of the adhesive bonded joint ($\tau_{j;\eta;x;max}$ and $\tau_{j;\eta;y;max}$ respectively) and the largest maximum principle stress in the glass pane at the RBC ($\sigma_{g;1;max;RBC}$) for three nominal glass thicknesses and six glass pane sizes at limited horizontal in-plane displacement at the RTC of the system. These results are compared with parametric studies (table 5.2) and deviations are also given in table 6.2. The predictions of the maximum relative horizontal in-plane displacements in normal direction of the adhesive bonded joint yield larger values than obtained from parameter studies except for systems with glass pane sizes 1.0 m x 1.5 m and 1.0 m x 3.0 m. The predictions of the maximum relative vertical in-plane displacements in normal direction of the adhesive bonded joint yield larger values than obtained from parameter studies except for systems with glass pane sizes 1.5 m x 1.0 m and 3.0 m x 1.0 m. The predictions of the maximum relative horizontal in-plane displacements in longitudinal direction of the adhesive bonded joint yield larger values than obtained from parameter studies except for systems with glass pane sizes 1.0 m x 1.5 m and 1.0 m x 3.0 m. The predictions of the maximum relative vertical in-plane displacements in longitudinal direction of the adhesive bonded joint yield larger values than obtained from parameter studies except for systems with glass pane sizes 1.5 m x 1.0 m and 3.0 m x 1.0 m. The relative horizontal and vertical in-plane displacements in normal and longitudinal direction also reflect the maximum normal stresses and maximum shear stresses respectively of the adhesive bonded joint. Systems with glass pane sizes of 1.0 m x 3.0 m and 3.0 m x 1.0 m have the largest deviations. The predictions of the largest maximum principle stress at the RBC of the glass pane yield smaller values than obtained from parameter studies.

Table 6.3:   Overview of the in-plane stiffness of the system with no shear stiffness of the adhesive bonded joint and the reduction for three nominal glass thicknesses and six glass pane sizes

$t_{g;n}$ [mm]		Size [m]	1.0x1.0	1.5x1.5	1.0x1.5	1.0x3.0	1.5x1.0	3.0x1.0
4			0.30	0.49	0.22	0.07	0.47	0.58
8	$K_{s;lim}$	[kN/mm]	0.61	0.99	0.45	0.15	0.95	1.19
12			0.93	1.50	0.68	0.23	1.44	1.80
	$\Delta K_{s;lim}$	[%]	-18.42	-18.03	-22.73	-37.84	-22.16	-38.78

Table 6.3 gives an overview of the in-plane stiffness of the system with no shear stiffness of the adhesive bonded joint and the reduction for three nominal glass thicknesses and six glass pane sizes. Systems with rectangular glass pane sizes with 1.0 m x 3.0 m and 3.0 m x 1.0 m have the largest reduction of the in-plane stiffness of the system.

6.2.5   Discussion

To avoid non-linear calculations at an early design phase, the distribution of the normal stresses of the adhesive bonded joint is assumed to be linear in the mechanical models. If the maximum relative horizontal and vertical in-plane displacements in normal direction of the adhesive bonded joint is larger than 0.76 mm (figure 4.9 right bottom) the continuous normal stiffness in the compression zone more increases than the continuous normal stiffness in the tension zone or even tears off. Through this, the predictions of the in-plane stiffness of the system at limited horizontal in-plane displacement at the RTC of the system and the horizontal in-plane load at first glass-steel contact are smaller than found in parameter studies. The predictions of the horizontal in-plane displacement at the RTC of the system at first glass-steel contact are smaller than found in parameter studies, because the steel frame is subjected to bending by the large in-plane load-transfer between the glass pane and steel frame (section 5.3.2) resulting in additional in-plane displacements.

For systems with square glass panes, the predictions of the maximum relative vertical and horizontal in-plane displacement in normal directions of the adhesive bonded joint are larger than found in parameter studies because of the non-linear behaviour of the adhesive bonded joint. An increase of the continuous normal stiffness results in smaller maximum relative vertical and horizontal in-plane displacement in normal direction of the adhesive bonded joint. For systems with rectangular glass panes with smaller width than height, the predictions of the maximum relative vertical in-plane displacement in normal direction of the adhesive bonded joint are larger than found in parameter studies because of the non-linear behaviour of the adhesive bonded joint. An increase of the continuous normal stiffness in vertical direction of the adhesive bonded joint results in smaller maximum relative vertical in-plane displacement in normal direction and larger maximum relative horizontal in-plane displacement in normal direction of the adhesive bonded joint. For systems with rectangular glass panes with larger width than height, the predictions of the maximum relative horizontal in-plane displacement in normal direction of the adhesive bonded joint are larger than found in parameter studies because of the non-linear behaviour of the adhesive bonded joint. An increase of the continuous normal stiffness in horizontal direction of the adhesive bonded joint results in smaller maximum relative horizontal in-plane displacement in normal direction and larger maximum relative vertical in-plane displacement in normal direction of the adhesive bonded joint. The deviation in the maximum relative horizontal and vertical in-plane displacement in normal direction reflects the maximum relative horizontal and vertical in-plane displacement in longitudinal direction. Nevertheless, the small continuous shear stiffness of the adhesive bonded joint contributes more to the in-plane stiffness of the system by increasing joint length. Furthermore, the maximum relative horizontal and vertical in-plane displacement in normal as well as longitudinal direction have to be checked whether they are smaller than the maximum allowable relative in-plane displacement in normal and longitudinal direction (appendix F.2). So, the predicted maximum relative horizontal and vertical in-plane displacement in normal direction of the six glass pane sizes, except glass pane size 1.0 m x 1.0 m, has to be limited (table 6.2 and appendix F.2).

A small fault in the predictions is acceptable to avoid non-linear calculations. However, the fault in the predictions for systems with glass pane sizes 1.0 m x 3.0 m and 3.0 m x 1.0 m (table 6.1 and 6.2) yields the largest deviations compared with parameter studies. The mechanical models underestimate the in-plane stiffness at limited horizontal in-plane displacements at the

RTC of the system and the horizontal in-plane load and the horizontal in-plane displacement at the RTC of the system at first glass-steel contact. On the other hand, the mechanical models overestimate the largest maximum relative horizontal and vertical in-plane displacements in normal direction and in longitudinal direction of the adhesive bonded joint. At limited horizontal in-plane displacement at the RTC of the system, the largest maximum principle stress, which is underestimated in the prediction, is not the criterion. Furthermore, it is recommended to use finite element simulations for plate buckling as proposed in figure E.1. So, the presented mechanical models can be considered as a safe approach in an early design phase.

6.3   Systems with joint types 2 and 3

The large shear stiffness of the adhesive bonded joint and the small shear flexibility of the bolted connection between the outside beam and the beadwork result in complex distributions of the shear stresses in longitudinal and transversal direction of the adhesive bonded joint (sections 5.4.5 and 5.5.4). Through this, the maximum principle stresses at the RBC of the glass pane rapidly increase locally (sections 5.4.4 and 5.5.3) resulting in inevitably cracking. This is at the expense of the in-plane load capacity of the glass pane. The mutual relation between the shear stiffness of the adhesive bonded joint and the shear flexibility of the bolted connection between the outside beam and the beadwork makes it impossible to develop mechanical models for systems with joint types 2 and 3. Therefore, it is wise to develop finite element models to map the behaviour of systems with joint types 2 and 3. Furthermore, with the view of thermal stresses in the glass pane [Koggel et al. 2006] is advisable to use less stiff adhesive bonded joints by a lower shear modulus of the adhesive and a larger joint thickness without loosing of the in-plane stiffness of the system as found in this research project (figure 4.12). This will be discussed further in section 7.1.2.

6.4   Conclusions

Systems with joint type 1

The mechanical models are based on the assumption that the distribution of the normal stresses is linear to avoid non-linear calculations at an early design phase. The following conclusions can be drawn:

- The predictions of the in-plane stiffness of the system at limited horizontal in-plane displacement at the RTC of the system slightly yield smaller values than found in parametric studies;
- The predictions of the horizontal in-plane load at first glass-steel contact yield smaller values than found in parameter studies;
- The predictions of the horizontal in-plane displacement at first glass-steel contact yield smaller values than found in parametric studies;
- For systems with square glass panes and with rectangular glass panes with a smaller width than height, the maximum relative vertical in-plane displacement in normal direction of the adhesive bonded joint (also the criterion) yields larger values than found in parametric studies;

- For systems with rectangular glass panes with a larger width than height, the maximum relative horizontal in-plane displacement in normal direction of the adhesive bonded joint (also the criterion) yields larger values than found in parametric studies;
- The predictions of the largest maximum principle stress at the RBC of the glass pane yield smaller values than found in parametric studies, but is not a criterion;
- Systems with glass pane sizes 1.0 m x 3.0 m and 3.0 m x 1.0 m and all three nominal glass thicknesses give the largest deviation between predictions and parametric studies on all points;
- The small shear stiffness of the adhesive bonded joint can not be neglected for larger glass pane sizes;
- Simplified finite element models (figure E.1) are needed for the prediction of the critical plate buckling load.

Systems with joint type 2 and 3

The mutual relation between the large shear stiffness of the adhesive bonded joint and the small shear flexibility of the bolted connection between the outside beam and the beadwork is difficult to capture in mechanical models. Therefore, finite element models are needed.

7 Discussion, conclusions and recommendations

This chapter deals with the main results of systems with joint types 1 to 3. Section 7.1 gives an overall discussion of each system. Section 7.2 summarizes the main conclusions. The chapter ends with recommendations for future work.

7.1 Overall discussion

To brace steel frames in a façade of a one-storey building, a system has been developed with glass panes acting as diaphragm, bonded to steel frames. A vertical stability system belongs to the primary structural level (section 1.2) and it has to fulfil two requirements prescribed by standards, namely strength (safety) and in-plane stiffness (serviceability). In this thesis, the research project focused on rectangular steel frame with infinite stiff transoms and mullions with a circumferentially adhesive bonded single annealed glass pane. Three joint types were defined which were kept as small as possible for architectural reasons. The research methodology was by means of experiments, finite element simulations and parameter studies to get more insight into the structural behaviour and to set-up mechanical models and possibly design rules. The overall discussion of each system is given in the next sections.

7.1.1 Systems with joint type 1

Joint type 1 is a flexible adhesive bonded joint across the full thickness of the glass pane (figure 3.3). The applied adhesive is polyurethane. The normal and shear stiffness of the adhesive bonded joint are small because of the very small Young's and shear modulus of the adhesive in combination with a large joint thickness. Through this, the in-plane stiffness of the system is small. Moreover, a flexible adhesive bonded joint is favourable at thermal loads, because the glass pane can deform almost unrestricted. At limited horizontal in-plane displacement at the RTC of the system, mechanical models were developed to predict the in-plane stiffness of the system, the maximum relative horizontal and vertical in-plane displacement in normal and longitudinal direction and the largest maximum principle stress of the non-cracked glass pane and non-failed adhesive bonded joint. The criteria are the limited horizontal in-plane displacement at the RTC of the system and the allowable maximum relative in-plane displacement in normal and longitudinal direction of the adhesive bonded joint. Systems with square glass panes have one glass-steel contact (figure 5.1, right). The LBC and the RTC of the glass pane simultaneously make contact with the transoms and mullions. Systems with rectangular glass panes have two glass-steel contacts. The first glass-steel contact depends on which size of the glass pane is larger (figure 5.2, bottom). Systems with rectangular glass panes with smaller width than height the LBC and the RTC of the glass pane firstly make contact with the transoms and after a while with the mullions. Systems with rectangular glass panes with larger width than height the LBC and the RTC of the glass pane firstly make contact with the mullions and after a while with the transoms. The steel frame is subjected to bending by the in-plane load transfer between glass pane and steel frame at the LBC and the RTC. The system yields good results for the residual capacity by large visual in-plane displacements at the RTC of the system accompanying with increasing horizontal in-plane load. At the moment of

first glass-steel contact, the glass pane is non-cracked and the adhesive bonded joint is gradually pushed away in the compression zone and gradually torn off in the tension zone. Till first glass-steel contact the horizontal in-plane load and the horizontal in-plane displacement at the RTC of the system are predictable and captured in mechanical models. The critical plate buckling load can be a criterion especially for slender glass panes. The glass pane starts cracking at first glass-steel contact after which the horizontal in-plane load still increases. This is an additional residual capacity which is not predictable. A substantial number of glass panes have to be structurally bonded to the steel frame of the façade to guarantee the stability of the building as well as the required redundancy (section 2.5.1).

7.1.2   Systems with joint type 2

Joint type 2 is a two-sided stiff adhesive bonded joint along the glass pane edges (figure 3.3). The applied adhesive is epoxy. The normal and shear stiffness of the adhesive bonded joint are large because of the large Young's and shear modulus of the adhesive in combination with a very small joint thickness. This system produced the best results for a vertical stability system of buildings, because it has a large in-plane stiffness of the system and a very good residual capacity at overloading. The system visually and audibly warns by constantly cracking accompanying with increasing horizontal in-plane load. So, glass panes in few bays in the façade are sufficient to guarantee the stability of the building and additional bays are needed for the required redundancy. The distribution of the principle stresses and their directions correspond with a pure shear wall. However, along the edges of the glass pane the distribution of the principle stresses deviates from a pure shear wall caused by the stiff adhesive bonded joint. Furthermore, large out-of-plane displacements of slender glass panes also influence the distribution of the principle stresses and their directions. The research shows that a very large shear stiffness of the adhesive bonded joint and a small shear flexibility (section 4.5.2) of the bolted connection between the outside beam and the beadwork as used in the test set-up (section 3.3.1) lead to unfavourable distribution of the shear stresses in longitudinal and transversal direction at the ends of the adhesive bonded joint. Through this, the principle stresses rapidly increase at the corners of the glass pane. Moreover, both in-plane principle stresses are compression stresses at the LBC and the RTC of the glass pane and are tension stresses at the RBC and LTC of the glass pane at which the glass pane locally cracks. The failure criterion is the representative flexural tension strength of glass and the allowable relative in-plane displacement in longitudinal and transversal direction of the adhesive bonded joint. The mutual relation between the very large shear stiffness of the adhesive bonded joint and a small shear flexibility of the bolted connection between the outside beam and the beadwork is difficult to capture in mechanical models. From a mechanical point of view, a stiff adhesive bonded joint has the preference. From a thermal point of view, a less stiff adhesive bonded joint is preferred. So, an optimal shear stiffness of the adhesive bonded joint has to be found which is discussed below.

The relation between the horizontal in-plane load and varying shear stiffness of the adhesive bonded joint were discussed in section 4.8.1 (figure 4.12). Figure 7.1 shows the relations between the horizontal in-plane load (F_h), the in-plane stiffness of the system (K_s), the largest maximum principle stress at the RBC of the glass pane ($\sigma_{g;1;max}$) and varying shear stiffness of the adhesive bonded joint for systems with nominal glass thickness of 12 mm and glass pane size of 1.0 m x 1.0 m at a horizontal in-plane displacement at the RTC of the system of 1.02 mm adopted from finite element simulations. The shear flexibility of the bolted connection

between the outside beam and the beadwork remains constant ($k_{b;\eta}$ = 10 N/mm³). The varying shear stiffness of the adhesive bonded joint is based on the relation between the shear stress and the relative in-plane displacements given in figure 4.9 at the right top in which the shear stresses only change at the same relative in-plane displacements. The normal stiffness of the adhesive bonded joint adapts to the initial shear stiffness. The relations can be divided into three zones (zones 1 to 3) based on the distribution of the shear stresses in longitudinal and transversal direction.
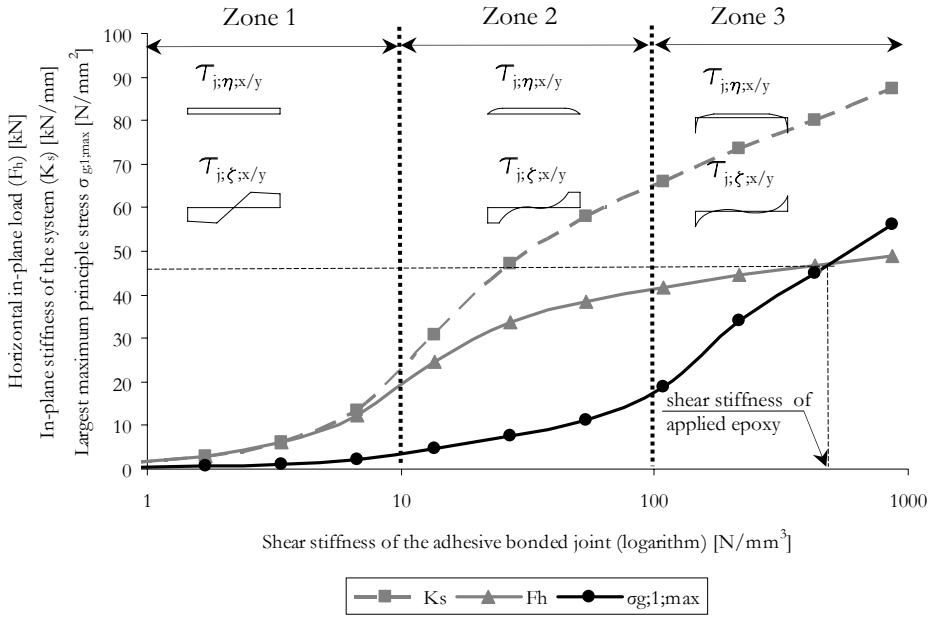
Figure 7.1: *Relations between the horizontal in-plane load (F_h), the in-plane stiffness of the system (K_s), the largest maximum principle stress in the RBC of the glass pane ($\sigma_{g;1;max}$) and varying shear stiffness of the adhesive bonded joint for systems with nominal glass thickness of 12 mm and glass pane size of 1.0 m x 1.0 m and constant shear flexibility of the bolted connection between the outside beam and the beadwork ($k_{b;\eta}$ = 10 N/mm³) at a horizontal in-plane displacement at the RTC of the system of 1.02 mm adopted from finite element simulations*

Zone 1, the shear stiffness is smaller than 10 N/mm³. The small shear stiffness of the adhesive bonded joint results in a small horizontal in-plane stiffness of the system and a small largest maximum principle stress at the RBC of the glass pane. The distribution of the shear stresses in longitudinal direction is uniform and the distribution of the shear stresses in transversal direction is multi-linear corresponding with the assumed relation between the shear stress and the relative in-plane displacement (figure 4.9 right top). Zone 2, the shear stiffness lies between 10 N/mm³ and 100 N/mm³. In this range, the horizontal in-plane stiffness of the system increases and the largest maximum principle stress at the RBC of the glass pane slightly increases. The distribution of the shear stresses in longitudinal direction is uniform which gradually decrease to zero at the ends of the adhesive bonded joint. The distribution of the shear stresses in transversal direction is uniform at the ends of the adhesive bonded joint and

fluctuates around zero at the middle of the adhesive bonded joint caused by the bending of the steel frame (figures 5.9, right and 5.13, bottom). Zone 3, the shear stiffness is larger than 100 N/mm³. The large shear stiffness of the adhesive bonded joint results in a large horizontal in-plane stiffness of the system and a rapid increase of the largest maximum principle stress at the RBC of the glass pane. The distributions of the shear stresses in longitudinal and transversal direction were described in section 5.4.5, because the applied epoxy adhesive is located in this zone. It can be concluded that a shear stiffness of the adhesive bonded joint in zone 2 is the best option from a mechanical and thermal point of view. The in-plane capacity of the system increases, because a less stiff adhesive bonded joint better smoothes peak stresses resulting in a favourable distribution of the principle stresses in the glass pane.

7.1.3 Systems with joint type 3

Joint type 3 is a one-sided stiff adhesive bonded joint along the glass pane edges (figure 3.3). A one-sided adhesive bonded joint is easier to make than a two-sided adhesive bonded joint. The applied adhesive is the same epoxy used for the adhesive bonded joint for systems with joint type 2. The normal and shear stiffness of the adhesive bonded joint are also large. This system shows many similarities with systems with joint type 2. However, this system has a very poor residual capacity at overloading caused by the eccentric in-plane load transfer between steel frame and glass pane. Through this, the adhesive bonded joint is also loaded in normal direction. The very large shear stiffness of the adhesive bonded joint and a small shear flexibility of the bolted connection between the outside beam and the beadwork used in the test set-up also lead to unfavourable distribution of the shear stresses in longitudinal and transversal direction at the ends of the adhesive bonded joint. Through this and in combination with the eccentric load transfer between glass pane and steel frame, the principle stresses rapidly increase at the corners of the glass panes. A shear stiffness of the adhesive bonded joint between 10 N/mm³ and 100 N/mm³ is also favourable in view of a mechanical and thermal point of view. However, the residual capacity is poor. Glass panes in few bays in the façade are sufficient to guarantee the stability of the building, but additional bays are needed for the required redundancy.

7.2 Conclusions

The main conclusions of each system, experiments, finite element simulations and parameter studies and the overall conclusions are drawn up below.

7.2.1 Systems with joint type 1

Joint type 1 is a flexible adhesive bonded joint across the full thickness of the glass pane and the following conclusions can be drawn:

- The relation between the horizontal in-plane load and the horizontal in-plane displacement at the RTC of the system has two stages for systems with square glass panes and three stages for systems with rectangular glass panes;
- Square glass panes only have one glass-steel contact at increasing horizontal in-plane load;

- Rectangular glass pane sizes have two glass-steel contacts at increasing horizontal in-plane load;
- The in-plane stiffness of the system is small in the first stage;
- The normal and shear stiffness of the adhesive bonded joint determines the in-plane stiffness of the system;
- The normal and shear stiffness of the adhesive bonded joint increases at increasing joint length and joint width which corresponds with the glass thickness;
- The shear flexibility of the bolted connection between the outside beam and the beadwork (clearance of the bolt holes) has no influence on the distribution of the normal and shear stresses of the adhesive bonded joint;
- At glass-steel contact(s), the in-plane load is mostly transferred through the compression diagonal in the glass pane between the LBC and the RTC;
- The glass pane starts cracking at glass-steel contact;
- The adhesive bonded joint is gradually pushed away in the compression zone and gradually torn off in the tension zone at larger horizontal in-plane displacements at the RTC of the system at the vicinity of the first stage;
- The slender transoms and mullions are susceptible for bending;
- The members of the steel frame are subjected to bending at glass-steel contact;
- The residual capacity of the system is good thanks to the choice of annealed float glass;
- The strength of the adhesive bonded joint and the in-plane displacement at the RTC of the system (serviceability) are the criteria at limited horizontal in-plane displacement at the RTC of the system;
- The critical plate buckling load for systems with slender glass panes is a criterion in the vicinity of first glass-steel contact.

7.2.2   Systems with joint type 2

Joint type 2 is a two-sided stiff adhesive bonded joint along the glass pane edges and the following conclusions can be drawn:

- The relation between the horizontal in-plane load and the horizontal in-plane displacement at the RTC of the system is a gradually and irregularly (cracks) declining curve;
- The in-plane stiffness of the system is large;
- The thickness of the glass pane, the shear stiffness of the adhesive bonded joint, bending of the members of the steel frame and the shear flexibility of the bolted connection between the outside beam and the beadwork contribute to the in-plane stiffness of the system;
- The very high shear stiffness of the adhesive bonded joint and the small shear flexibility of the bolted connection between the outside beam and the beadwork resulted in opposite shear stresses in longitudinal direction at the ends of the adhesive bonded joint and enlarge the shear stresses in transversal direction at the ends of the adhesive bonded joint;
- The distribution of the principle stresses corresponds with a pure shear wall except along the glass pane edges caused by the large shear stiffness of the adhesive bonded joint and the small shear flexibility of the bolted connection between the outside beam and the beadwork;

- Due to the large shear stiffness of the adhesive bonded joint and the small shear flexibility of the bolted connection between the outside beam and the beadwork the maximum and minimum principle stresses at the RBC and the LTC of the glass pane are both large tension stresses at which the glass pane cracks locally;
- Failure of the system is caused by a crack along the compression diagonal from the LBC to the RTC;
- The adhesive bonded joint is intact after failure of the system;
- The design criteria are strength of glass, strength of the adhesive and for slender glass panes the critical plate buckling load;
- The residual capacity of the system is very good thanks to the choice of annealed float glass;
- The proposed range of shear stiffnesses of the adhesive bonded joint results in an increase of the in-plane capacity of the system without loosing or even more in-plane stiffness of the system.

7.2.3 Systems with joint type 3

Joint type 3 is a one-sided stiff adhesive bonded joint along the glass pane edges. Systems with joint type 3 show many similarities with systems with joint type 2. So, the conclusions, given in the previous section, are similar for systems with joint type 3 and completed with:

- The residual capacity is very poor, because the glass pane instantaneously fails after the first crack caused by the eccentric load transfer between steel frame and glass pane.

7.2.4 Experiments

Tests were carried out on systems with square glass pane size of 1.0 m x 1.0 m and nominal glass thicknesses of 12 mm for each joint type. The tests actually showed the residual capacity of the systems which were certainly not found in finite element simulations. Furthermore, the choice for a replaceable beadwork (section 3.3.1) which is bolted to the outside beam has a large influence on the behaviour of the system viewed in retrospect.

7.2.5 Finite element simulations and parameter studies

It was possible to develop one finite element model for systems with joint types 1 and 3. Finite element simulations match well with the experiments up to the onset of the first crack. The strain gradients at the corners of the glass pane are described incorrectly for systems with joint type 1 at glass-steel contact and for systems with joint types 2 and 3 caused by the very large shear stiffness of the adhesive bonded joint and the small shear flexibility of the bolted connection between the outside beam and the beadwork. However, with an adhesive bonded joint having a smaller shear stiffness the strain gradients are described more correctly. Furthermore, finite element simulations behave stiffer for out-of-plane displacements at the centre of the glass pane than found in experiments. The parameter studies were needed to get more insight into the system behaviour by varying the nominal glass thickness and the glass pane size only. They are the main parameters in a design process.

7.2.6 Mechanical models

For systems with joint type 1 it was possible to set-up mechanical models. The mechanical models at limited horizontal in-plane displacement at the RTC of the system well predict: the in-plane stiffness of the system, the horizontal in-plane load, the maximum relative horizontal and vertical in-plane displacement in normal direction, the maximum relative horizontal and vertical in-plane displacement in longitudinal direction and the largest maximum principle stress. The mechanical models also predict well the residual capacity, namely the horizontal in-plane load and the horizontal in-plane displacement at the RTC of the system at first glass-steel contact. It is advisable to use finite element simulations for the prediction of the critical plate buckling load of the system. It is still premature to set-up design rules.

Systems with joint types 2 and 3 were difficult to capture in mechanical models, because the mutual relation between the large shear stiffness of the adhesive bonded joint and the small shear flexibility of the bolted connection between the outside beam and the beadwork. Therefore, it is advisable to use finite element simulations. An adhesive bonded joint with a moderate shear stiffness by a larger joint thickness (tolerances) and moderate shear modulus of the adhesive has a favourable effect on the distribution of the shear stresses of the adhesive bonded joint and the maximum principle stress without loosing of the in-plane stiffness of the system as found in this research project. The proposed mechanical models for systems with joint type 1 can be used. Moreover, in view of thermal reduction of stresses in the glass pane a small shear stiffness of the adhesive bonded joint is preferable.

7.2.7 Overall conclusions

Comparing systems with joint types 1 to 3 and considering the requirements for vertical stability systems of buildings, it can be concluded that systems with joint type 2 have a great potential to stabilize one-storey buildings. This conclusion is based on the large in-plane stiffness of the system, the fact that only few bays are needed for building stabilization as well as the necessary redundancy in stead of the entire façade and the very good residual capacity of the system. However, the capacity of this stability system increases if the shear stiffness of the adhesive bonded joint is chosen between the proposed values between 10 N/mm^3 and 100 N/mm^3.

7.3 Recommendations

The work in this thesis did not encompass all phenomena which are needed for bracing steel frames with glass panes for the use as vertical stability system of one-storey buildings. The mechanical behaviour of systems with joint types 1 to 3 appeared to be complex. Therefore, in order to improve and extend the work presented in this thesis, some suggestions can be given.

7.3.1 Glazing

Annealed float glass which is circumferentially adhesive bonded to a steel frame has good residual capacity. A good replacement of annealed float glass is heat-strengthened glass, because it also has a favourable crack pattern needed for the residual capacity after breakage (table 2.4). Moreover, the representative flexural tension strength of glass and the resistance against change of temperature increase (table 2.3). However, each structural glass application has to be laminated to deal with the brittleness of glass and safety (section 2.3.2). Furthermore, the out-of-plane imperfections of glass panes itself and the position of the adhesively bonded glass pane in the steel frame e.g. warping of the glass pane during making are main points for more specific research.

7.3.2 Loading

Systems with joint types 1 to 3 were only subjected to a short term horizontal in-plane load. Other considerable loadings are long term horizontal in-plane load e.g. geometrical imperfection of the building and a combination of in-plane loads and out-of-plane loads e.g. wind suction and cycle loading by wind. Another substantial loading are thermal loads.

7.3.3 Adhesives

Regarding systems with joint type 1, it is advisable to apply an adhesive with larger Young's modulus and shear modulus to increase the in-plane stiffness of the system. Furthermore, the effect of tolerances of the glass pane (table A.3) and steel frame on the joint thickness, which influences the in-plane stiffness of the system, has to be further investigated.

Regarding systems with joint types 2 and 3, the very large shear stiffness of the adhesive bonded joint and the small shear flexibility of the bolted connection between the outside beam and the beadwork resulted in an unfavourable distribution of the principle stresses at the corners of the glass pane (chapter 5). Nowadays, a wide range of structural adhesives is available. However, a proper structural adhesive has to be chosen which satisfies the requirements such as environmental conditions and mechanical properties at long-term duration. The proposed range of shear stiffnesses of the adhesive bonded joint in section 7.1.2 has great potential for circumferentially adhesive bonded glass panes in steel frames.

Literature

[Antonelli et al. 2008]   Antonelli, A.; Cagnacci, E.; Giordano, S.; Orlando, M.; Spinelli, P. (2008), Experimental and Theoretical Analysis of CFRP Reinforced Glass Beams, ISAAG 2008, pp. 171-182, Munich, Germany

[ASTM E 1300 2004]   ASTM E1300 (2004), Standard Practice for Determination Load Resistance of Glass in Buildings, American Society for Testing Materials

[Beason et al. 1984]   Beason, W.L.; Morgan, J.R. (1984), Glass Failure Prediction Model, Journal of Structural Engineering, Vol. 110, No 2, pp. 197-212

[Belis 2006]   Belis, J. (2006), Kipsterkte van monolitische en gelamineerde glazen liggers, thesis, University Ghent Laboratory for Research on Structural Models, Ghent, Belgium

[Bennison et al. 2002]   Bennison, S. J.; Smith, C.A.; Van Duser, A.; Jagota, A. (2002), Structural Performance of Laminated Glass Made with a 'stiff' Interlayer, Glass in Buildings, ASTM STP 1434, V. Block (editor)

[Bergmeister et al. 2007]   Bergmeister, K.; Englhardt, O. (2007), The Aesthetics of Transparency – Conceptual Design for an All-Glass Façade System, Proceedings of the 10th International Conference on Architectural and Automotive Glass (GPD), pp. 130-133, Tampere, Finland

[Blandini 2007]   Blandini, L. (2007), Structural Use of Adhesive for the Construction of Frameless Glass Shells, International Journal of Adhesion & Adhesive 27, p.p. 499-504, Elsevier

[Blandini 2008]   Blandini, L. (2008), Structural Use of Adhesives in Glass Shells, Challenging Glass, pp. 185-192, Delft, The Netherlands

[Born 2005]   Born, P. (2005), Modern design in Glazing – Glass Bonding in Automotive, Proceedings of the 9th International Conference on Architectural and Automotive Glass (GPD), pp. 679-680, Tampere, Finland

[Bos et al. 2007]   Bos, F.; Veer, F. (2007), Transparent polymer joints in glass structures, Proceedings of the 10th International Conference on Architectural and Automotive Glass (GPD), pp. 62-67, Tampere, Finland

[BS 6262-3 2005]   BS 6262-3:2005 (2005), Code of practise for glazing for buildings – Part 3: Code of practise for fire, security and wind loading, British Standards Institution (BSI)

[BS 6262-6 2005]   BS 6262-6:2005 (2005), Code of practise for glazing for buildings – Part 6: Code of practise for special applications, British Standards Institution (BSI)

[Bucak et al. 2006]   Bucak, Ö.; Hagl, A. (2006), Kleben im Bauwesen – gestern, heute, morgen, Stahlbau 75, Heft 6, p.p. 499-507, Berlin, Germany

[Callaghan O' 2007]   Callaghan O', J. (2007), An All Glass Cube in New York City, Proceedings of the 10th International Conference on Architectural and Automotive Glass (GPD), pp. 98-101, Tampere, Finland

[Carbary 2007]   Carbary, L.D. (2007), A review of the durability and performance of silicone structural glazing systems, Proceedings of the 10th International Conference on Architectural and Automotive Glass (GPD), pp. 190-193, Tampere, Finland

[CUR 2007]   CUR Bouw & Infra/Kenniscentrum Glas (2007), Construeren met glas, Rapport 2007-1, Gouda, The Netherlands

[Cruz et al. 2008a]   Cruz, P.; Pequeno, J. (2008), Structural Timber-Glass Adhesive Bonding, Challenging Glass, pp. 205-214, Delft, The Netherlands

[Cruz et al. 2008b]   Cruz, P.; Pequeno, J. (2008), Timber-Glass Composite Beams: Mechanical Behaviour & Architectural Solutions, Challenging Glass, pp. 439-448, Delft, The Netherlands

[CWCT 2004]   CWCT (2004), Safety & fragility of glazed roofing, Technical Note No. 42, Centre for Windows and Cladding Technology (CWCT), Bath, UK

[Diana 2005]   Diana finite element analyses (2005), Diana User's Manual Release 9, 1st edition, TNO Diana BV, Delft, the Netherlands

[Decliné et al. 2008]   Decliné, D.; Callewaert, D.; Belis, J.; van Impe, R. (2008), Post-breakage behaviour of laminated glass in structural applications, Challenging Glass, pp. 459-467, Delft, The Netherlands

[DIN 1249-10:1990]   DIN 1249-10 (1990), Flachglas im Bauwesen, Chemische und physikalische Eigenschaften, Teil 10, Ausgabe 1990-08, Berlin, Germany

[Doremus 1982]   Doremus, R.H. (1982), Fracture and Fatigue of Glass, Treatise on Materials Science and Technology, Vol. 22, pp. 169-237, Academic Press, New York, USA

[Dubois 2007]	Dubois, M. (2007), Glass Bearing Walls – a Case Study, Proceedings of the 10th International Conference on Architectural and Automotive Glass (GPD), pp. 130-133, Tampere, Finland
[Düster 2002]	Düster, H. (2002), Tragfähigkeit von Glasscheiben unter Schub- und Plattenbelastung, RWTH Aachen, Aachen, Germany
[EN 356 1999]	EN 356:1999 (1999), Glass in building – Security glazing – Testing and classification of resistance against manual attack, CEN, Brussels, Belgium
[EN 572-1 2004]	EN 572-1 (2004), Glass in building – Basic soda lime silicate glass products, part 1, Definitions and general physical and mechanical properties, CEN, Brussels, Belgium
[EN 572-8 2004]	EN 572-8 (2004), Glass in building – Basic soda lime silicate glass products, part 8, Supplied and final cut sizes, CEN, Brussels, Belgium
[EN 1748-1-1 2004]	EN 1748-1-1 (2004), Glass in building – Special basic products – Borosilicate glasses, part 1-1, Definitions and general physical and mechanical properties, CEN, Brussels, Belgium
[EN 1990 2002]	NEN-EN 1990:2002+NB:2007 nl, Eurocode - Basis of structural design, CEN, Brussels, Belgium
[EN 1991 2002]	NEN-EN 1991-1-2:2002+NB:2007 nl, Eurocode 1 - Actions on structures - Part 1-2: General actions - Actions on structures exposed to fire, CEN, Brussels, Belgium
[EN 12150-2 2004]	EN 12150-2:2004, Thermally toughened soda lime silicate safety glass – Part 2: Evaluation of conformity /Product Standard, CEN, Brussels, Belgium
[EN 12600 2003]	EN 12600:2003, Glass in building, Pendulum test, Impact test method and classification for flat glass, CEN, Brussels, Belgium
[Englhardt et al. 2007]	Englhardt, O.; Bergmeister, K. (2007), Hybrid Structural Elements – an Innovative High Filigree Glass-Steel-System, Proceedings of the 10th International Conference on Architectural and Automotive Glass (GPD), pp. 134-137, Tampere, Finland
[Englhardt 2008]	Englhardt, O. (2008), Transparent Surface Structures - Engineering to Architecture, Challenging Glass, pp. 341-351, Delft, The Netherlands

[ETAG 002 2003]   ETAG 002 (2003), Guideline for European Technical Approval of Structural Sealant Glazing Systems, European Organisation for Technical Approvals, Part 1: Supported and Unsupported Systems, Brussels, Belgium

[Feirabend et al. 2008]   Feirabend, S., Sobek, W. (2008), Reinforced Laminated Glass, Challenging Glass, pp. 469-477, Delft, The Netherlands

[Feldmann et al. 2006]   Feldmann, M.; Völling, B.; Geßler, A.; Wellershoff, F.; Geiß, P.; Wagner, A. (2006), Kleben im Stahlbau, Stahlbau 75, Heft 10, p.p. 834-846, Berlin, Germany

[Feldmann et al. 2008]   Feldmann, M.; Pilsl, M.; Segura, C. C. (2008), Tragfähigkeit von Lochleibungsverbindungen vorgespannter Glasscheiben zur Ausbildung von Anschlüssen im konstruktiven Glasbau, Stahlbau 77, Heft 1, p.p. 17-25, Berlin, Germany

[Fink 2000]   Fink, A. (2000), Mechanische Eigenschaften und Dauerstandverhalten von Flachglas für bauliche Anlagen, Bauen mit Glas, p.p. 603-616, VDI-Verlag, Düsseldorf, Germany

[Freytag 2004]   Freytag, B. (2004), Glass-Concrete Composite Technology, Structural Engineering Internal, Vol. 14, number 2, p.p. 111-117, IABSE, Zurich, Switzerland

[Güsgen 1998]   Güsgen, J. (1998), Bemessung tragender Bauteile aus Glas, Schriftenreihe Stahlbau RWTH Aachen, Shaker Verlag, Aachen

[Griffith 1920]   Griffith, A.A. (1920), The Phenomena of Rupture and Flow in Solids, Philosophical Transactions, Series A, Vol. 221, pp. 163-198, Royal Society of London, 1920

[Habenicht 2006]   Habenicht, G. (2006), Kleben, Grundlagen, Technologien, Anwendungen, 5., erweiterte und aktualisierte Auflage, Springer-Verlag, Berlin, Germany

[Hamm 2000]   Hamm, J. (2000), Tragverhalten von Holz und Holzwerkstoffen im statischen Verbund mit Glas, PhD thesis, EPFL, Thèse no 2065, Lausanne, Switzerland

[Hagl 2006]   Hagl, A. (2006), Die Innovation – Kleben, Stahlbau 75, p.p. 508-520, Heft 6, Berlin, Germany

[Hagl 2007]   Hagl, A. (2007), Bemessung von strukturellen Silikon-Klebungen, Stahlbau 76, Heft 8, p.p. 569-581, Berlin, Germany

[Hagl 2008]	Hagl, A. (2008), Understanding Complex Adhesive Behaviour: Case Study U-type Bonding Geometry, Challenging Glass, pp. 227-240, Delft, The Netherlands
[Haldimann 2006]	Haldimann, M. (2006), Fracture Strength of Structural Glass Elements – Analytical and Numerical Modelling, Testing and Design, PhD thesis, EPFL, Thèse no 3671, Lausanne, Switzerland
[Haldimann et al. 2008]	Haldimann, M.; Luible, A.; Overend, M. (2008), Structural use of Glass, Structural Engineering Documents 10, IABSE, Zurich, Switzerland
[Hanisch 2002]	Hanisch, V. (2002), Tragfähigkeit vorgespannter Floatgläser unter diagonaler Druckkraft in der Scheibenebene, Aachen, Germany
[Herwijnen et al. 2007]	Herwijnen, F. van; Hofmeyer, H.; Koggel B.A. (2007), The Behaviour of Flexibly Constrained Glass Panes subjected to Temperature Load, Proceedings of the 10th International Conference on Architectural and Automotive Glass (GPD), pp. 157-160, Tampere, Finland
[Hess 2004]	Hess, R (2004), Material Glass, Structural Engineering International, Vol. 14, number 2, p.p. 76-79, IABSE, Zurich, Switzerland
[Hildebrand et al. 2008]	Hildebrand, J.; Werner, F.; Zimmerer, K. (2008), Load-Bearing Glass-Plastic Hybrid Elements, ISAAG 2008, pp. 195-202, Munich, Germany
[Huveners et al. 2003]	Huveners, E.M.P.; Herwijnen, F. van; Soetens, F. (2005), Load Sharing in Insulated Double Glass Units, Heron, Vol. 48, No 2, pp. 99-122, Delft, The Netherlands
[Huveners et al. 2005]	Huveners, E.M.P.; Herwijnen, F. van; Soetens, F.; Hofmeyer, H. (2005), In-Plane Loaded Glass Pane in Façades, Temperature Loads in Fixed Bonded Glass Panes, Proceedings of the 9th International Conference on Architectural and Automotive Glass (GPD), pp. 284-286, Tampere, Finland
[Huveners et al. 2006]	Huveners, E.M.P.; Koggel, B.A. (2006), Tensile Shear Tests for the Determination of the Shear Strain Diagram of Several Adhesive Types, Report O-2006.11, Eindhoven University of Technology, Eindhoven, The Netherlands
[Huveners et al. 2007a]	Huveners, E.M.P.; Herwijnen, F. van; Soetens, F.; Hofmeyer, H. (2007), Glass Panes Acting as Shear Wall, Heron, Vol. 52, No 1/2, pp. 5-29, Delft, The Netherlands

[Huveners et al. 2007b] Huveners, E.M.P.; Herwijnen, F. van; Soetens, F.; Hofmeyer, H. (2007), In-Plane Loaded Glass Pane (Shear Wall), Proceedings of the 10th International Conference on Architectural and Automotive Glass (GPD), pp. 362-366, Tampere, Finland

[Huveners et al. 2007c] Huveners, E.M.P.; Herwijnen, F. van; Soetens, F.; Hofmeyer, H. (2007), Mechanical Shear Properties of Adhesives, Proceedings of the 10th International Conference on Architectural and Automotive Glass (GPD), pp. 367-370, Tampere, Finland

[Huveners et al. 2008a] Huveners, E.M.P.; Hofmeyer, H.; Herwijnen, F. van; Soetens, F. (2008), Numerical Research on Glass Panes Acting as a Shear Wall, Challenging Glass, pp. 359-368, Delft, The Netherlands

[Huveners et al. 2008b] Huveners, E.M.P.; Herwijnen, F. van; Soetens, F.; Hofmeyer, H. (2008), Parametric Studies on Bracing Steel Frames with Glued Glass Panes, ISAAG 2008, pp. 211-222, Munich, Germany

[Huveners et al. 2009] Huveners, E.M.P.; Herwijnen, F. van; Soetens, F.; Hofmeyer, H. (2009), Bracing Steel Frames with Adhesively Bonded Glass Panes - Mechanic Models, Proceedings of the 11th International Conference on Architectural and Automotive Glass (GPD), pp. 256-260, Tampere, Finland

[Inglis 1913] Inglis, C.E. (1913), Stresses in a plate due to the presence of cracks and sharp corners, Transactions of the Institution of Naval Architects, Vol. 60, p.p. 219-230, London, UK

[Irwin 1957] Irwin, G. (1957), Analysis of Stresses and Strains near the End of a Crack Traversing a Plate, Journal of Applied Mechanics, Vol. 24, p.p. 361-364, ASME

[Kasper 2005] Kasper, R. (2005), Tragverhalten von Glastagern, PhD thesis, RWTH Aachen, Aachen , Germany

[Koggel et al. 2006] Koggel, B.A.; Huveners, E.M.P. (2006), Tensile Shear Tests for the Determination of the Shear-Strain Diagram of Several Adhesive Types, report O-2006.11, Eindhoven University of Technology, Eindhoven, The Netherlands

[Kreher 2004] Kreher, K. (2004), Tragverhalten und Bemessung von Holz-Glas-Verbundträgern unter Berücksichtigung der Eigenspannungen in Glas, EPFL, Thèse no 2999, Lausanne, Switzerland

[Kreher et al. 2004] Kreher, K.; Natterer, J.; Natterer, J (2004), Timber-Glass-Composite Girders for a Hotel in Switzerland, Structural Engineering Internal, Vol. 14, number 2, p.p. 149-151, IABSE, Zurich, Switzerland

[Kutterer 2005] Kutterer, M. (2005), Verbundglasplatten – Schubverbund und Membrantragwirkung – Teil 1, Stahlbau, Vol 1, No. 74, pp. 28-35, Berlin, Germany

[Laufs et al. 2001] Laufs, W.; Mohren, R. (2001), Neuartige Stahl-Glas-Konstruktionen mit tragwirkung in Scheibenebene, Bautechnik, Vol. 78, Heft 10, p.p. 716-723

[Liess 2001a] Liess, J. (2001), Bemessung druckbeanspuchter Bauteile aus Glas, PhD thesis, Universität Kassel, Kassel, Germany

[Liess 2001b] Liess, J. (2001), Bemessung druckbeanspuchter Bauteile aus Glas, BoD, GmbH, Norderstedt, Germany

[Ludwig et al. 1998] Ludwig, J.J.; Weiler, H.U. (1998), Innovative Tragstrukturen aus Glas, Stahlbau, Vol. 4, No. 67, Ernst&Sohn, Berlin, Germany

[Louter 2007] Louter, P.C. (2007), Adhesively Bonded Reinforced Glass Beams, Heron, Vol. 52, No 1/2, pp. 31-58, Delft, The Netherlands

[Louter et al. 2008] Louter, Ch., Veer, F. Belis, J. (2008), Redundancy of reinforced glass beams; temperature, moisture and time dependent behaviour of the adhesive bond, Challenging Glass, pp. 479-490, Delft, The Netherlands

[Luible 2004] Luible, A. (2004), Stabilität von Tragelementen aus Glas, PhD thesis, EPFL, Thèse no 3014, Lausanne, Switzerland

[Maniatis et al. 2004] Maniatis, I; Albrecht G. (2004), Stress Distribution in Glass Drillings with In-plane Loads, International Symposium on the Application of architectural Glass 2004, Munich, Germany

[Menčik 1992] Menčik, J. (1992), Strength and Fracture of Glass and Ceramics, Glass Science and Technology, Vol.12

[Močibob et al. 2007] Močibob, D.: Crisinel, M. (2007), Glass Panel under In-Plane Shear Loading: Experimental Investigation on Structural Glass Panel Point Support, Proceedings of the 10th International Conference on Architectural and Automotive Glass (GPD), pp. 380-383, Tampere, Finland

[Močibob 2008] Močibob, D. (2008), Glass Panel under Shear Loading – Use of Glass Envelopes in Building Stabilization, PhD thesis, EPFL, Thèse no 4185, Lausanne, Switzerland

[Narayanan 1983] Narayanan, R. (1983), Plated Structures – Stability and Strength, Applied Science Publishers, Great Yarmouth, United Kingdom

[NEN 2608-1 2007]   NEN 2608:1997/C1:2007 nl, Glass in buildings - Resistance against wind load - Requirements and determination method, NNI, Delft, the Netherlands

[NEN 2608-2 2007]   NEN 2608-2:2007 nl, Glass in building - Part 2: Glazed installations non-vertical installed - Resistance against self-weight, wind load, snow load and isochore pressure - Requirements and determination method, NNI, Delft, the Netherlands

[NEN 3569 2001]   NEN 3569:2001 nl, Veiligheidsbeglazing in gebouwen, NNI, Delft, the Netherlands

[NEN 6700 2005]   NEN 6700:2005 nl, Technical Principles for Building Structures – TGB 1990 – General Principles, NNI, Delft, the Netherlands

[NEN 6702 2001]   NEN 6702:2001/A1:2005 nl, Technical Principles for Building Structures – TGB 1990 – Steel Structures, NNI, Delft, the Netherlands

[NEN 6770 1997]   NEN 6770:1997/A1:2005 nl, Technical Principles for Building Structures – TGB 1990 – Loadings and Deformations, NNI, Delft, the Netherlands

[Niedermaier 2003]   Niedermaier, P. (2003), Shear-Strength of Glass Panel Elements in Combination with Timber Frame Constructions, Proceedings of the 8th International Conference on Architectural and Automotive Glass (GPD), pp. 262-264, Tampere, Finland

[Norville 1998]   Norville, H. S.; King, K.W; Swofford, J.l. (1998), Behavior and Strength of Laminated Glass, Journal of Engineering Mechanics, Vol. 124, No 1, pp. 46-53, ASCE

[Nijsse 2004]   Nijsse, R. (2004), Special Steel and Adhesively Bonded Connections for Glass Structures, Structural Engineering International, Vol. 14, number 2, p.p. 104-106, IABSE, Zurich, Switzerland

[Ofner 2007]   Ofner, R. (2007), Leichtbau und Glasbau, S-5-01/2007, Institut für Stahlbau und Flächentragwerke, Technische Universität Graz, Graz, Austria

[Ølgaard et al. 2008] Ølgaard, A.B., Nielsen, J.H., Olesen, J.F. Stang, H. (2008), Properties of an Adhesive for Structural Glass Applications, Challenging Glass, pp. 263-272, Delft, The Netherlands

[Overend 2002]   Overend, M. (2002), The Appraisal of Structural Glass Assemblies, PhD thesis, University of Surrey, United Kingdom

[Overend et al. 2005]   Overend, M., Vassallo, C., Camillieri, K. (2005), The Design, Assembly & Performance of glass Columns, Proceedings of the 9th International Conference on Architectural and Automotive Glass (GPD), pp. 287-291, Tampere, Finland

[Palumbo et al. 2005]   Palumbo, D., Palumbo, M., Mazzuccheli, M. (2005), A New roof for the XIIIth Century "Loggia de Vicari" Based on Structural Glass Trusses - A Case Study, Proceedings of the 9th International Conference on Architectural and Automotive Glass (GPD), pp. 434-435, Tampere, Finland

[Porter 2001]   Porter, M. (2001), Aspects of Structural Design with Glass, PhD thesis, University of Oxford, Oxford, UK

[prEN 13474-1 1999]   NEN-EN 13474-1:1999 Ontw. En, Glass in building - Design of glass panes - Part 1: General basis of design, NNI, Delft, the Netherlands

[prEN 13474-2 2000]   NEN-EN 13474-2:2000 Ontw. En, Glass in building - Design of glass panes - Part 2: Design for uniformily distributed loads, NNI, Delft, the Netherlands

[Rusch et al. 2001]   Rusch, A.; Lindner, J. (2001), Zur Anwendung von Glas als druckbeanspruchtes Bauteil, Berichte aus dem konstruktiven Ingenieurbau, p.p. M1-M10, Technische Universität München, Munich, Germany

[Schober et al. 2004]   Schober, H; Schneider, J. (2004), Developments in Structural Glass and Glass Structures, Structural Engineering International, Vol. 14, number 2, p.p. 84-87, IABSE, Zurich, Switzerland

[Schober et al. 2006]   Schober, K.P., Leitl, D. Edl, T. (2006), Holz-Glas-verbundkonstruktionen zur Gebäudeaussteifung, Magazin für den Holzbereich, Heft 1, Holzforschung Austria, Vienna, Austria

[Schuler et al. 2004]   Schuler, Ch.; Bucak, Ö.; Sackmann, V.; Gräf, H.; Albrecht, G. (2004), Time and Temperature Dependent Mechanical Behaviour and Durability of Laminated Safety Glass, Structural Engineering International, Vol. 14, number 2, p.p. 80-83, IABSE, Zurich, Switzerland

[Sedlacek et al. 1999]   Sedlacek, G.; Blank, K.; Laufs, W.; Güsgens, J. (1999), Glas im konstruktiven Ingenieurbau, Ernst und Sohn, Berlin, Germany

[Sedlacek 2004]   Sedlacek, G.; Wellershoff, F.; Kasper. R. (2004), Basis of Design and Standard Codes for Glass Structures, International Symposium on the Application of Architectural Glass (ISAAG 2004), Munich, Germany

[Siebert 2004]   Siebert, G. (2004), Overhead Glazing: Regulations and Applications, International Symposium on the Application of Architectural Glass (ISAAG 2004), Munich, Germany

[Siebert et al. 2008]   Siebert, G.; Herrmann, T.; Maniatis, I. (2008), New German DIN Standard DIN 18008 for design of glass structures, Challenging Glass, pp. 413-418, Delft, The Netherlands

[Sika 2004]   Sikaflex-252 (2004), Sikaflex-252 – Constructielijm, Technical Data Sheet, version 04/2004, Sika Netherlands, Utrecht, The Netherlands

[Smulders 2009]   Smulders, C.D.J. (2009), M2-Glass, Master report O-2009.02, Eindhoven University of Technology, Eindhoven, The Netherlands

[Stutzki et al. 2004]   Stutzki, C.; Zande Van de, B.J.; Stahl, D. (2004), Versuche an Verbindungen für Glaskonstruktionen, Stahlbau 73, Heft 8, p.p. 588-494, Berlin, Germany

[Szilard 2004]   Szilard, R. (2004), Theories and Applications of Plate Analysis, Classical, Numerical and Engineering Methods, John Wiley & Sons, Hoboken, United States of America

[Timoshenko et al. 1970] Timoshenko, S.P., Goodier, J.N. (1970), Theory of Elasticity, McGraw-Hill, London, United Kingdom

[Timoshenko et al. 1990] Timoshenko, S.P., Gere, J.M. (1990), Mechanics of Materials, PWS Kent Publishing Company, Boston, United State of America

[TRAV 2003]   Technische Regeln für die Verwendung von absturzsichernden Verglasungen (2003), Deutsches Institut für Bautechnik (DIBt), Berlin, Germany

[TRVL 2006]   Technische Regeln für die Verwendung von linienförmig gelagerten Verglasungen (2006), Mitteilungen des Deutschen Instituts für Bautechnik (DIBt), Berlin, Germany

[Vallabhan 1983]   Vallabhan, C. V. G. (1983), Interactive Analyses of Nonlinear Glass Plates, Journal of Structural Engineering, Vol. 109, No 2, pp. 489-502, ASCE

[Vallabhan et al. 1990] Vallabhan, C. V. G.; Minor, J.E. (1990), Seal Forces in Structural Glazing Systems, Journal of Structural Engineering, Vol. 116, No 4, pp. 1080-1089, ASCE

[Veer 2007]   Veer, F.A. (2007), The Strength of Glass, a nontransparent value, Heron, Vol. 52, No 1/2, pp. 87-104, Delft, The Netherlands

[Vuolio 2003]   Vuolio, A. (2003), Structural Behaviour of Glass Structures in Facades, PhD Thesis, Helsinki University of Technology Laboratory of Steel Structures, TKK-TER-27, Helsinki, Finland

[Wagner 2002]   Wagner, E. (2002), Glasschäden - Oberflächenbeschädigungen Glasbrüche in Theorie und Praxis, Verlag Karl Hofmann, Schorndorf, Germany

[Weiler 2000]   Weiler, H.U. (2000), Versuchsergebnisse und Stand der Entwicklung eines Bemessungskonzepts für druckbeanspruchte Glasbauteile, Bauen mit Glas, VDI-Tagung in Baden-Baden, p.p. 161-184, Düsseldorf, Germany

[Weller 2005]   Weller, B.; Tasche, M. (2005), Adhesive Fixing in Glass Construction, Proceedings of the 9th International Conference on Architectural and Automotive Glass (GPD), pp. 267-270, Tampere, Finland

[Weller et al. 2006a]   Weller, B.; Tasche, M. (2006), Glashäuser im Osten Deutschlands, Stahlbau 75, Heft 6, Berlin, Germany

[Weller et al. 2006b]   Weller, B.; Prautzsch, V.; Tasche, S.; Vogt, I.; Jansen, I. (2006), Fügen und Verbinden mit UV- und lichthärtende Acrylaten, Stahlbau 75, Heft 6, p.p. 521-528, Berlin, Germany

[Weller 2007a]   Weller, B. (2007), Designing of Bonded Joints in Glas Structures, Proceedings of the 10th International Conference on Architectural and Automotive Glass (GPD), pp. 74-76, Tampere, Finland

[Weller 2007b]   Weller, B. (2007), Transparent Roofs as Space Grid Structures with Steel-Glass-Modules, Proceedings of the 10th International Conference on Architectural and Automotive Glass (GPD), pp. 77-80, Tampere, Finland

[Weller et al. 2008]   Weller, B.; Reich, S.; Ebert, J. (2008), Testing on Space Grid Structures with Glass as Compression Layer, Challenging Glass, pp. 155-162, Delft, The Netherlands

[Wellershoff et al. 2003] Wellershoff, F.; Sedlacek, G. (2003), Structural Use of Glass in Hybrid Elements: Steel-Glass-Beam, Glass-GFRP-Plates, Proceedings of the 8th International Conference on Architectural and Automotive Glass (GPD), pp. 268-270, Tampere, Finland

[Wellershoff et al. 2005] Wellershoff, F.; Sedlacek, G. (2005), Glued Connections for New Steel Glass Structures, Proceedings of the 9th International Conference on Architectural and Automotive Glass (GPD), pp. 340-343, Tampere, Finland

[Wellershoff 2006]   Wellershoff, F. (2006), Nutzung der Verglasung zur Aussteifung von Gebäudehüllen, PhD thesis, Schriftenreihe – Stahlbau RWTH Aachen, Heft 57, Shaker Verlag, Aachen, Germany

[Wellershoff et al. 2007]   Wellershoff, F.; Sedlacek, G. (2007), Glued Joints in Glass Structures, Glass & Interactive Building Envelopes, EU COST C13 Final report, Volume 1, p.p. 229-238, IOS Press, Amsterdam, The Netherlands

[Wiederhorn et al. 1970]   Wiederhorn, S.M., Bolz, L.H. (1970), Stress corrosion and static fatigue of glass, Journal of the American Ceramic Society, Vol. 50, p.p. 543-548

[Wigginton 1996]   Wigginton, M. (1996), Glass in Architecture, Phaidon Press Limited, London, UK

[Wörner et al. 1993]   Wörner, J.D.; Shen, X.; Sagmeister, B. (1993), Determination of Load Sharing in Insulating Glass Units, Journal of Engineering Mechanics, Vol. 119, No 2, pp. 386-392, ASCE

[Zachariasen 1932]   Zachariasen, W.H. (1932), The Atomic Arrangement in Glass, Journal of American Chemical Society, Vol. 54, pp. 3841-3851

[3M 1995]   3M Scotch Weld 9323 B/A (1995), Structural Adhesive, Product Data Sheet

A Supplementary data for the experiments

A.1 Specification of the steel frame

This appendix accurately describes the parts of the system which is discussed in chapter 3.

Steel grade	S235
Bolt grade	10.9
H7	diameter hole is 0.1 mm larger than the nominal diameter
h7	diameter hole is 0.1 mm smaller than the nominal diameter
ZGB 30X36X30-W(INA)	type of the applied sleeve-bearing bush used in the top and bottom transom with an internal diameter of 30 mm and an external diameter of 36 mm
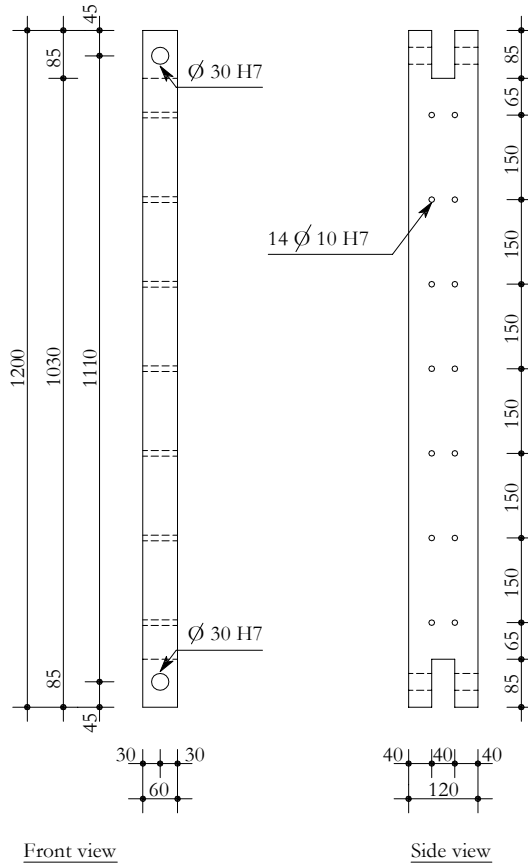
Figure A.1: *Outside beam of the left and right mullion*
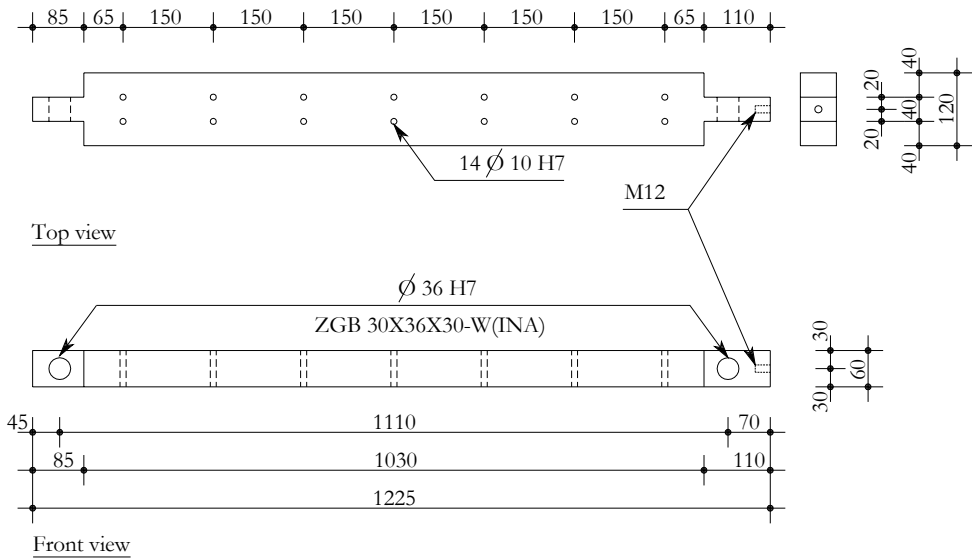
Figure A.2:   Outside beam of the top transom
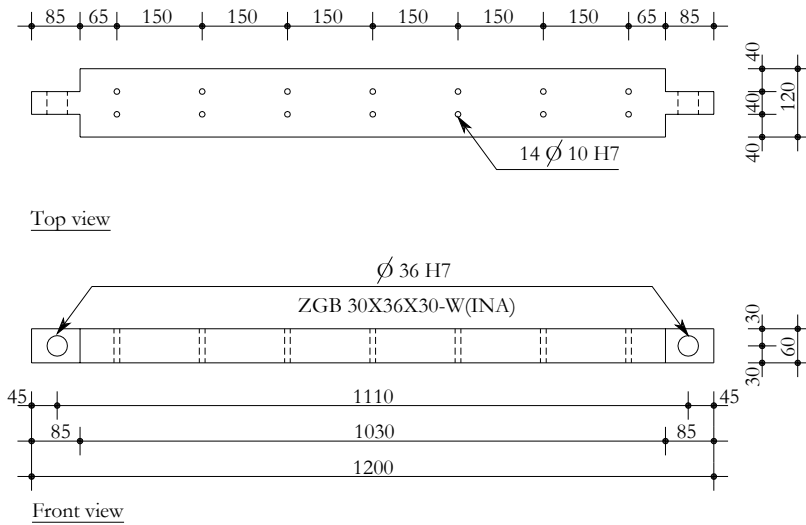
Figure A.3:   Outside beam of the bottom transom

2 Ø 30 H7

2 Ø 30 H7

welds a = 8 mm

Front view

Front view

4 Ø 26 H7

4 Ø 26 H7

Top view

Top view

Horizontal roller

Pinned connection

Ø 30 h7

250

Pin for internal hinges
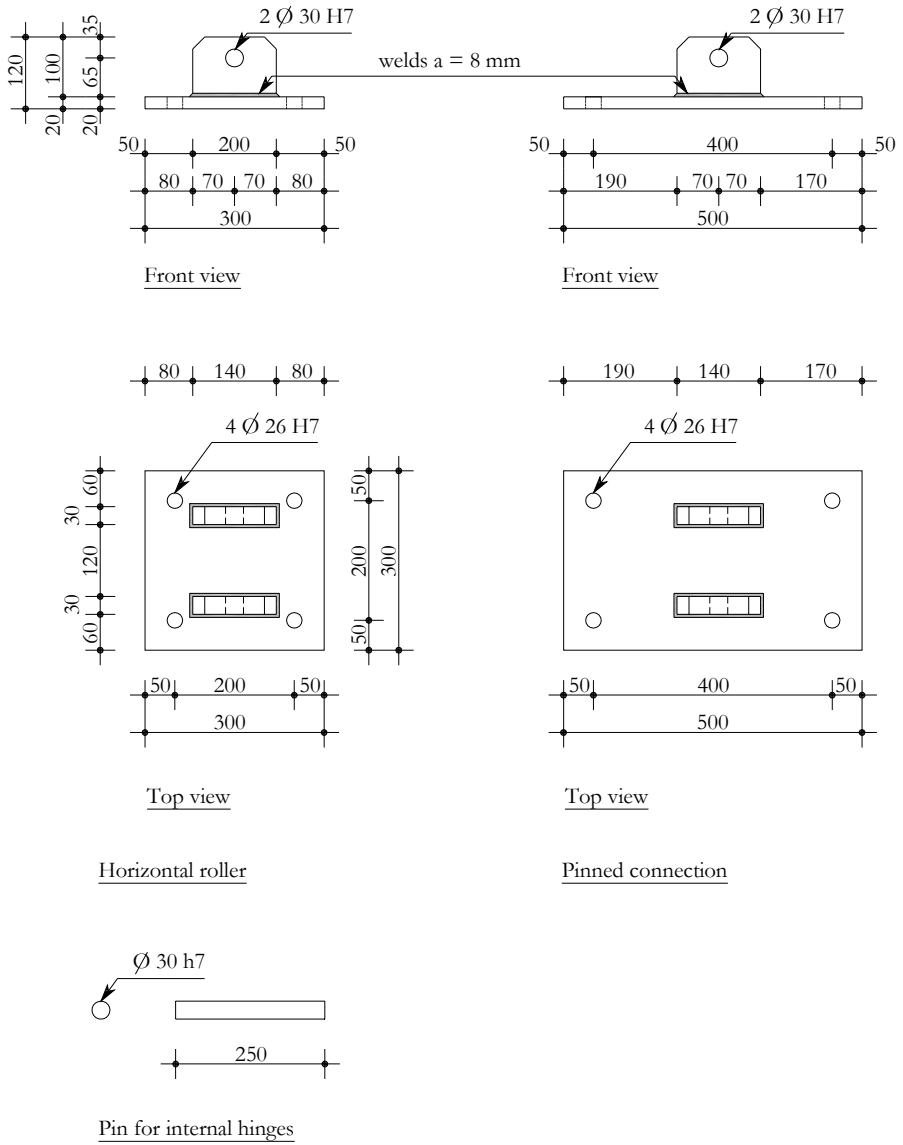
Figure A.4:   Horizontal roller, pinned connection and the pin for the internal hinges

175

1045

28   989   28

Side view

40-30
100
30

14 M10
internal thread

72.5   150   150   150   150   150   150   72.5

1045

Topview

22
13

1050   980

13
22
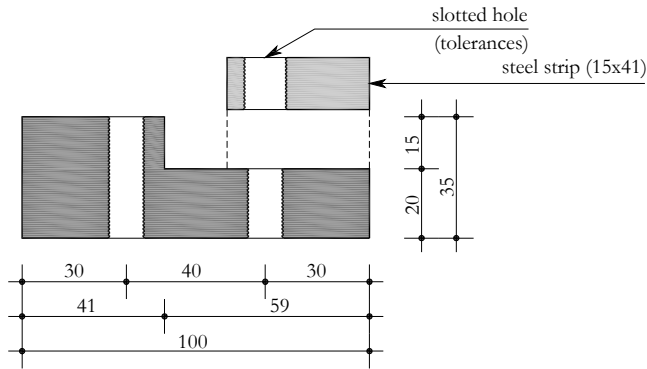
section A-A (figure A.6)

mitre

22   13   980   13   22

1050

Front view

Figure A.5:   *Beadwork*

176

Figure A.6:   Cross section of the beadwork for joint type 1 (top) and joint type 2 and 3 (bottom)

A.2 Application of the adhesive

A.2.1 Making the adhesive bonded joint for joint type 1

This section punctually describes the process of making the adhesive bonded joint for joint type 1 (figure A.7). The encircled numbers in figure A.7 indicate the step order which is explained textually below.

Step 1
The groove and the strip of the beadwork were made smooth by sandpaper to remove the burrs, the sharp edges and the small remainders of the adhesive of the previous test. The smooth bonding areas underwent the first cleaning to remove dust and grease with a clear

cloth. Then the beadwork was placed within the frame and bolted to the outside beam. After fastening the beadwork, the bonding areas underwent a second and more intensive cleaning. This cleaning consisted of rubbing the bonding area with a cloth provided with acetone. The cloth was regularly replaced by a new one. The cleaning was stopped when the last cloth was clean. The bonding area was provided with a primer (Sika Activator) to increase the adhesion. This was recommended by the supplier of the polyurethane adhesive (Sika).
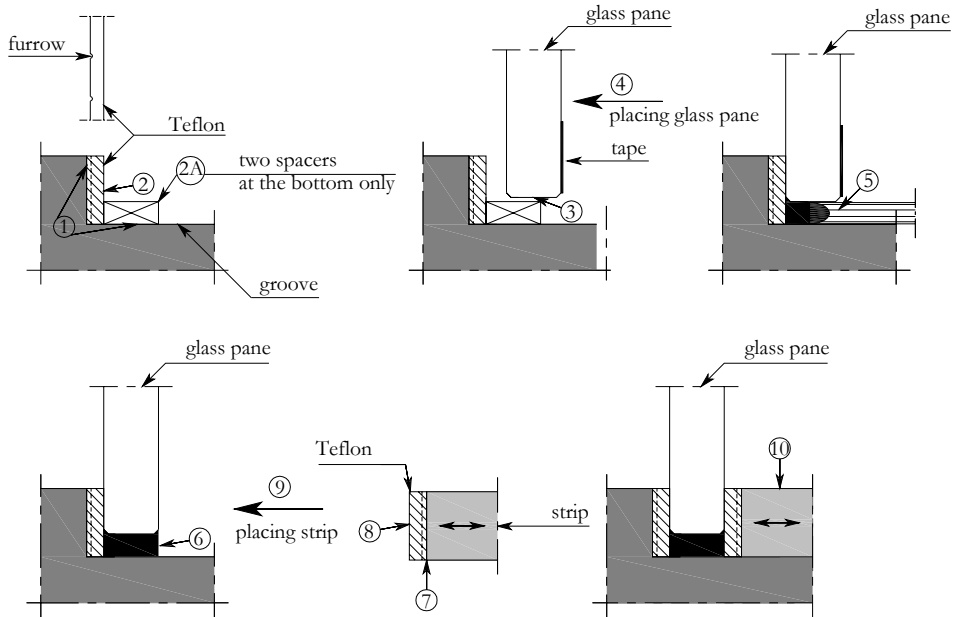
Figure A.7: Making the adhesive bonded joint for joint of type 1(drawn cross section of the bottom transom)

Step 2

A Teflon strip with a thickness of 3 mm and a height of 15 mm was placed against the groove of the beadwork. The Teflon strip was provided with small furrows to supply the adhesive with sufficient air, because the adhesive needs moisture from the ambient air for curing.

Step 2A

Two small Teflon spacers with a cross section of 5 mm x 5 mm and a length of 10 mm were placed on the bottom beadwork for two reasons. The first reason was to transfer the dead weight of the glass pane to the bottom beadwork. The second reason was to guarantee the joint thickness. By the way, the spacers were permanent, because removing of the spacers can lead to damage of the glass pane.

Step 3

The edges of the glass pane were also cleaned with a cloth provided with acetone. The front of the glass pane was provided with a tape along the edges. Then the bonding areas of the glass pane were also provided with a primer (Sika Activator).

Step 4
The glass pane was placed with suction cups into the frame and positioned carefully by sliding the glass pane over the two Teflon spacers on the bottom beadwork until the gaps at the left side and the right side of the glass pane were equal (measured).

Step 5
The adhesive was applied with a pneumatic squirt equipped with an adapted nozzle. The common nozzle has a cone like shape and partly fits between the glass pane and the frame resulting in a badly filled up joint with much air enclosures. The adapted nozzle had a prismatic tube with a diameter of 4 mm and a length of 60 mm. The end of the nozzle was placed in front of the Teflon strip and straightforwardly filled the gap with adhesive from corner to corner in a slowly continuous movement.

Step 6
After applying the adhesive, a synthetic spatula was used to wipe off the surplus and made the joint smooth followed by removing the tape on the front of the glass pane.

Steps 7 to 10
The steel strip was cleaned as described at step 1 and provided with a Teflon strip. The Teflon strip was also provided with small furrows at both sides to supply the adhesive with sufficient air. The strip was placed in the frame and bolted. The curing time of the adhesive was one week at the ambient temperature and relative humidity in the laboratory.

After each test the beadwork was disconnected from the test set-up and placed on a bench for cleaning. The polyurethane adhesive was removed by a solvent named Natufix. Then the preparations started for the new test with step 1 to 10.

A.2.2   Making the adhesive bonded joint for joint type 2 and 3

This section punctually describes the process of making of the adhesive bonded joint for joint type 2 as well as for joint type 3 (figure A.8). The encircled numbers in figure A.8 indicate the step order which is explained textually below.

Steps 1 to 3
The beadwork and the strip had the same treatment as described at making the adhesive bonded joint for joint type 1. The bonding areas were only cleaned with acetone and no primer was needed. Three small spacers (0.5 mm x 2 mm x 10 mm) were glued on the beadwork to guarantee the joint thickness. The component A (accelerator) and B (base) of epoxy were mixed manually in accordance with the handling prescription of the supplier. The epoxy was applied with a spatula on the cleaned beadwork within half an hour.

Step 4
The edges of the glass pane were cleaned with a cloth provided with acetone.

Step 5
The glass pane was placed with suction cups into the test set-up and positioned carefully by sliding the glass pane over the two Teflon spacers on the bottom beadwork until the gaps at

the left side and the right side of the glass pane were equal (measured). The two spacers transferred the dead weight of the glass pane to the bottom beadwork and guarantee a bottom gap of 3 mm. The glass pane was carefully pressed against the uncured adhesive.
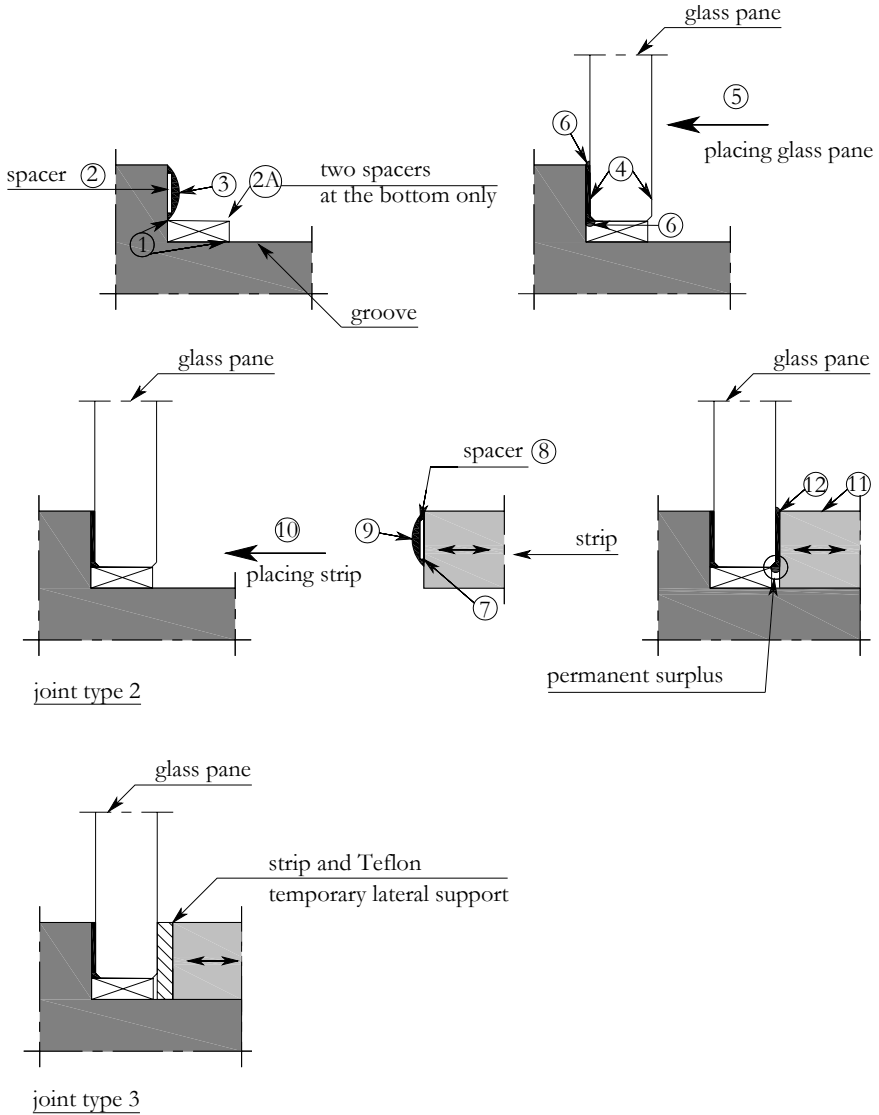
Figure A.8:   Making the adhesive bonded joint for joint of type 2 and 3 (drawn cross section of the bottom transom)

Step 6
After placing the glass pane, a small synthetic spatula was used to wipe off the surplus and made the joint smooth at once.

Steps 7 to 12

A cleaned strip provided with three spacers of 0.5 mm thick was applied with adhesive. Then the strip was placed and pushed carefully on the glass pane. The strip was bolted and the surplus at one side was removed by a small synthetic spatula at once. The adhesive at the gap side could not be removed anymore and the small surplus was permanent. The curing time of the adhesive was three days at the ambient temperature and relative humidity in the laboratory.

Making the adhesive bonded joint for joint type 3 was in accordance with the step order from 1 to 6 of making the adhesive bonded joint for joint type 2. The steel strip provided with a Teflon strip supported the glass pane laterally during curing of the adhesive. This strip was removed before testing.

After each test the beadwork was disconnected from the test set-up and placed on a bench for cleaning. The epoxy adhesive was removed by burning off in a well-ventilated room. Then the preparations started for the new test with step 1 to 12 for joint type 2 and step 1 to 6 for joint type 3.

A.3   Ambient conditions in the laboratory

The main ambient conditions in the laboratory for the adhesive bonded joint for systems with joint types 1 to 3 were the temperature and the relative humidity. Table A.1 gives an overview of the ambient temperature and the relative humidity in the laboratory obtained from the research project of Schoenmakers. These ambient conditions were measured each half an hour from 29 November 2006 till 10 March 2008. The experiments of systems with joint types 1 to 3 were carried out from July 2006 till January 2007.

Table A.1:   Ambient conditions in the laboratory

Laboratory conditions			Mean	Min	Max	St. dev
Temperature	T	[°C]	20.3	15.5	23.5	1.35
Relative humidity	RH	[%]	41.6	16.0	75.0	10.43

A.4   Measuring equipment

The measured quantities of the load cell, the LVDTs and the strain gauges were electrical signals and were sent to a data acquisition unit. Figure A.9 shows a schematic overview of the measuring equipment. The data acquisition unit can be divided into three chief units, namely the conditioners, the multiplexing unit and the A/D converter. The conditioners firstly received the signals. These signals were amplified and filtered. The electrical signals of the strain gauges were corrected by the K-factor given by the supplier of the strain gauges. The multiplex unit collected the data and sent them to the A/D converter. The A/D converter transformed the analog data into digital date. The digital data was sent with a standard serial

connection to the personal computer and wrote the data into an ASCII file. The tabulated data of the strain gauges represented the mechanical strain in µm/mm. The tabulated data of the load cell and the LVDT's represented the electric potential in Volt. The values had to be calibrated into load (kN) and displacements (mm).

A control loop was developed to guarantee a displacement of 1 mm/min at the RTC of the system. Next to jack A an LVDT measured the actual displacement of the RTC of the system. An electrical signal was sent via a conditioner to a subtractor. A generator dedicated a displacement of 1 mm/min by also sending an electrical signal to the subtractor. The subtractor calculated the difference between the signals and sent it to a PID controller. A negative outcome of the subtractor means that the displacement was larger than the dedicated displacement. A positive outcome means that the displacement was smaller than the dedicated displacement. The PID controller controlled the motor of the spindles of the test stand with the outcome of the subtractor. The spindles moved the rigid top plate on jack B up or down and activated jack A. At larger displacement the top plate moved from jack B (release). At smaller displacement the top plate moved to jack B (push in).
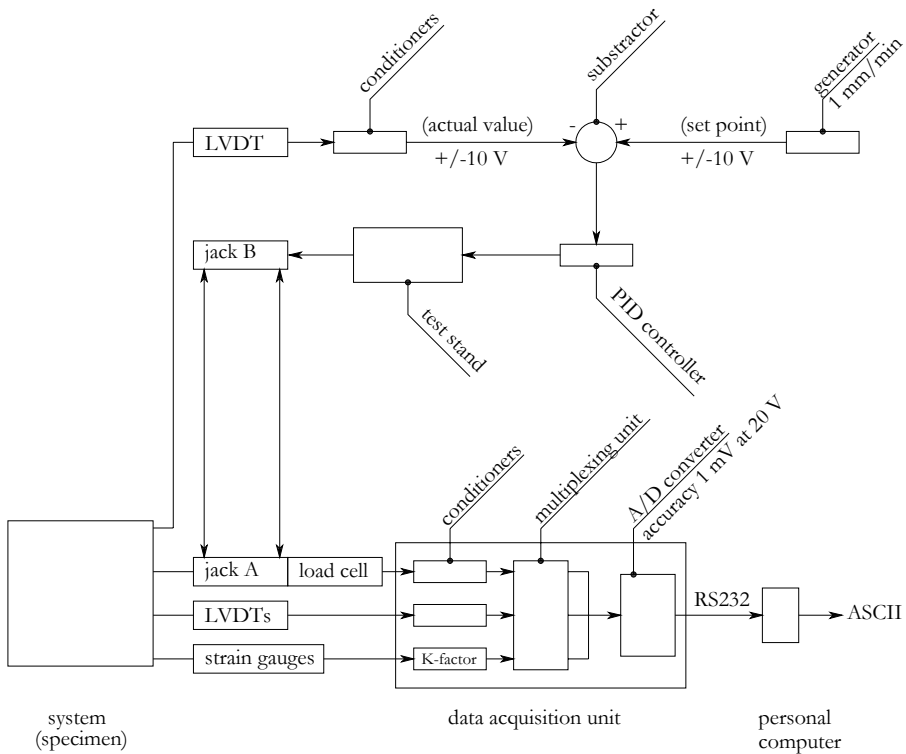
Figure A.9:   *Measuring equipment*

A.5 High-speed camera

During the test a high-speed camera constantly recorded the illuminated glass pane. The used high-speed camera was Redlake Motion Pro X3. The high-speed camera was used to record the crack initiation and the crack propagation in the glass pane. The image quality was adjusted on 100 dpi x 100 dpi. This image quality was sufficient to detect the crack initiation and to follow the crack propagation. The camera was adjusted to record 4000 images a second and was based on the crack velocity of the glass (see section 2.2.2). Actually, two to four images were needed to follow the first cracks after the crack initiation, but an observer pressed on the button at a considerable sound of cracking of the glass pane. This moment depended on the human audition and reaction time and therefore one second recording time is used. To save the memory of the camera the camera constantly overwrote the old image of one second ago by the actual image. The overwriting process stopped after pressing manually on a push button (a trigger). After triggering, the high speed camera digitally recorded 0.8 second (3200 images) before pressing and 0.2 second (800 images) after pressing. The images made in this second were stored in the memory of a computer.

A.6 Actual geometry of the glass pane

Table A.2:   Measured glass pane thickness in mm (accuracy 0.05 mm)

	Test	$t_{g;1}$	$t_{g;2}$	$t_{g;3}$	$t_{g;4}$	$t_{g;5}$	$t_{g;6}$	$t_{g;7}$	$t_{g;8}$	$t_{g;ave}$
System 1	18	11.95	11.95	11.95	12.00	11.90	11.90	11.90	11.95	*11.94*
	19	11.90	11.90	11.90	11.95	11.95	11.95	11.95	12.00	*11.94*
	20	11.90	11.90	11.90	11.95	11.95	11.95	11.95	11.95	*11.93*
System 2	2	11.85	11.85	11.85	11.85	11.90	11.90	11.90	11.85	*11.87*
	3	11.90	11.90	11.90	11.90	11.90	11.90	11.90	11.90	*11.90*
	17	11.90	11.90	11.90	11.95	11.95	11.95	11.95	12.00	*11.94*
System 3	5	11.95	11.95	11.90	11.90	11.90	11.95	11.95	11.95	*11.93*
	6	11.95	11.95	11.95	12.05	11.90	11.90	11.90	12.00	*11.95*
	7	11.95	11.95	11.95	12.00	11.90	11.90	11.90	12.00	*11.94*
	8	11.90	11.90	11.90	11.90	11.90	11.90	11.90	11.90	*11.90*

Table A.3:   *Measured glass pane size in mm (accuracy 1.00 mm)*

	Test	$w_{g;1}$	$w_{g;2}$	$h_{g;1}$	$h_{g;2}$
System 1	18	1002	1002	1001	1001
	19	1001	1002	1001	1001
	20	1002	1002	1001	1001
System 2	2	1002	1001	1002	1002
	3	1002	1001	1002	1002
	17	1002	1002	1001	1001
System 3	5	1002	1002	1001	1001
	6	1002	1002	1001	1001
	7	1002	1002	1001	1001
	8	1002	1002	1002	1002

The width between the groove of the left mullion and the right mullion is 1012 mm and the height between the groove of the bottom transom and the top transom is 1012 mm, because of the outside beam is planed at the inside.

B Additional measurements of the system

B.1 Boundary conditions of the supporting structures

The boundary conditions of the supporting structures can have influence on the induced horizontal in-plane displacement (u_{RTC}) at the top of the system. The additional horizontal in-plane displacements are a horizontal in-plane displacement of the pinned connection at the RBC of the system and the vertical in-plane displacement of the supporting structures resulting in an in-plane rotation of the entire system. In an additional experiment the in-plane displacements of the horizontal roller and the pinned connection were verified whether they complied with the assumed boundary conditions of the supporting structure.
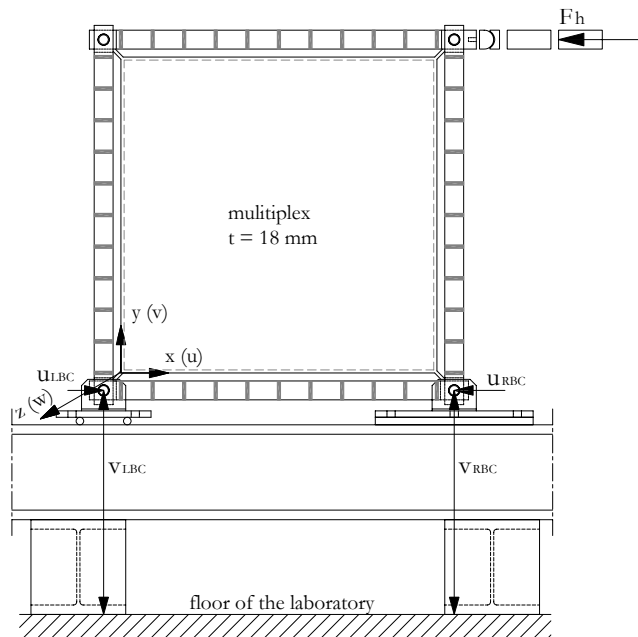
Figure B.1:   Test set-up for the measurement of the in-plane displacements of the horizontal roller and the pinned connection

The test set-up is given in figure B.1 and was the same as the test set-up as described in chapter 3. However, the glass pane was replaced by an 18 mm thick adhesively bonded multiplex sheet for transferring the in-plane load to the supporting structure. The adhesive bonded joint was based on joint type 2 and epoxy adhesive was used. So, the horizontal roller and the pinned connection were loaded on the same way. The in-plane load introduction was also displacement controlled (1 mm/min). The horizontal in-plane displacements (u_{LBC} and u_{RBC}) and the vertical in-plane displacements (v_{LBC} and v_{RBC}) were measured at the centre of the

horizontal roller and at the centre of the pinned connection with respect to the floor of the laboratory.
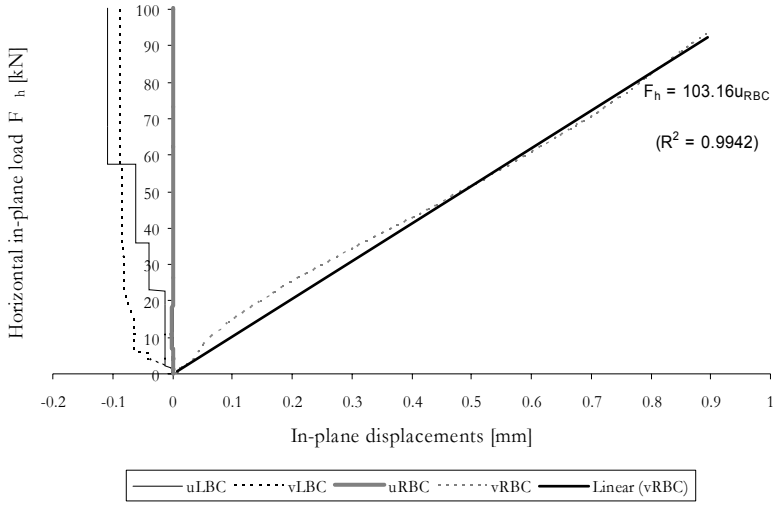
Figure B.2:   The relation between the horizontal in-plane load and the in-plane displacements of the horizontal roller and the pinned connection

Figure B.2 shows the relation between the horizontal in-plane load and the horizontal and the vertical in-plane displacements of the supporting structure of the system until a horizontal in-plane load of 100 kN. For the horizontal roller at the LBC of the system, the horizontal in-plane displacements (u_{LBC}) were small. The irregular relation was the result of the contact friction between the steel rollers, the steel plate and the steel beam of the test rig at increasing compression load. The vertical in-plane displacements (v_{LBC}) were also small. At the beginning the relation rapidly increased by impressing the plays of the rollers between the steel paltes. For the pinned connection at the RBC of the system, the horizontal in-plane displacements (u_{RBC}) were negligible small. On the other hand, the vertical in-plane displacements (v_{RBC}) were large in comparison to the other in-plane displacements. This was caused by the vertical in-plane displacements of the bottom plate of the pinned connection, because the largest distance between the bolts was 400 mm resulting in bending of the plate (figure A.4). Therefore, the pinned connection can not be considered as very stiff in the y-axis. Figure B.2 also shows a linear approximation of the relation between the horizontal in-plane load (F_{h}) and the vertical in-plane displacements (v_{RBC}) of the pinned connection at the RBC of the system.

It can be concluded that the boundary conditions of the supporting structures complied with the assumed boundary conditions except for the pinned connection in vertical in-plane direction. Therefore, the boundary condition of the pinned connection in the y-axis had to be adapted with a vertical spring with a discrete normal stiffness of $K_{y;RBC} = 103.16$ kN/mm[1]. The discrete normal stiffness of the vertical spring was valid till a horizontal in-plane load of 100 kN.

B.2 Shear flexibility of the bolted connection between the outside beam and the beadwork

The transoms and mullions of the steel frame were built up of a beadwork connected with bolts to the outside beam. The bolted connection consisted of 14 bolts M10 placed in slightly larger holes of the outside beam (figures A.1 and A.2 denoted to H7 means +0.1 mm) and screwed in the beadwork (figure A.6). So, every bolt had a clearance which made a small sliding possibly between the outside beam and the beadwork. Moreover, flexural stiffness of the transoms and the mullions was reduced. The degree of collaboration of the outside beam and the beadwork was the point of interest. The shear flexibility of the bolted connection was determined experimentally. A four-point-bending test was carried out to determine the flexural stiffness of the mullions and the transoms. Then the mullions and the transoms were simulated in a finite element programme to find the shear flexibility of the bolted connection (try and error). Exactly, the shear flexibility of the bolted connection between the outside beam and the beadwork simulated the clearance of the holes as well as the contact friction between the steel outside beam and the steel beadwork.

The test set-up is showed in figure B.3. The used supporting structures were originating from the system. The pinned connection was placed at the left side and the horizontal roller was placed at the right side. The vertical in-plane load (*2F*) was displacement controlled with a speed of 0.5 mm/min and distributed the vertical in-plane load to the specimen at 370 mm (point 2) and 740 mm (point 4) from the origin. The vertical in-plane displacements were measured at five points (point 1 to 5), namely at 0 mm, 370 mm, 555 mm, 740 mm and 1110 mm from the origin. The relative horizontal in-plane displacements between the outside beam and the beadwork were measured at four points (points 6 to 9), namely at 105 mm and 1005 mm on the front and the rear.

In section B.1 was found that the pinned connection was actually a vertical spring. Therefore, the vertical in-plane displacements of the pinned connection had to be eliminated from the measured vertical in-plane displacements using equation B.1.

$$v_i = v_{i;m} - \frac{\left(v_{5;m} - v_{1;m}\right)x}{l} + v_{5;m} \qquad \text{(Equation B.1)}$$

In which:
v_i	is the corrected vertical in-plane displacement in point i mm
$v_{i;m}$	is the measured vertical in-plane displacement in point i mm
$v_{1;m}$	is the measured vertical in-plane displacement at point 1 (pinned) in mm
$v_{5;m}$	is the measured vertical in-plane displacement at point 5 (roller) in mm
x	is the position of the vertical in-plane displacement in point i with respect to its origin in mm
l	is the length of the transom or mullion between the hinges in mm
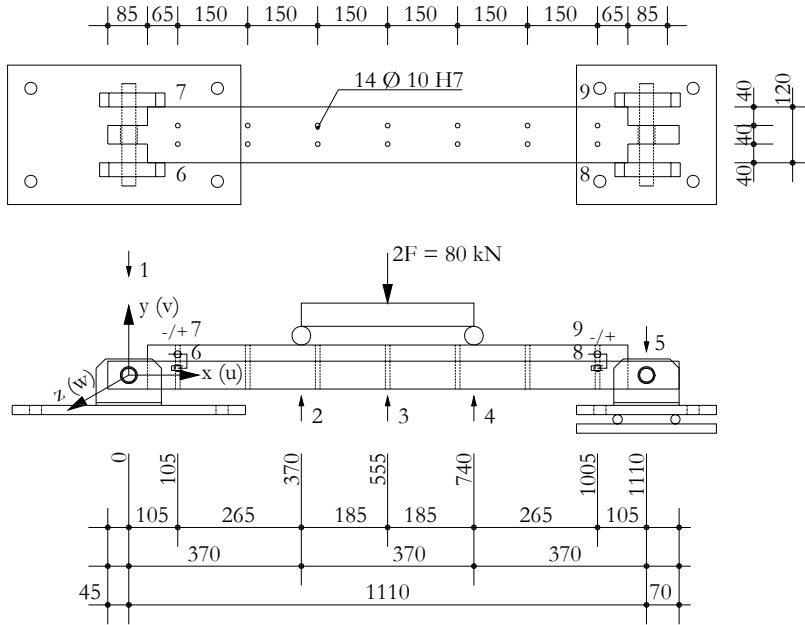
Figure B.3: Four point bending test for the determination of the flexural stiffness of the transoms and the mullions
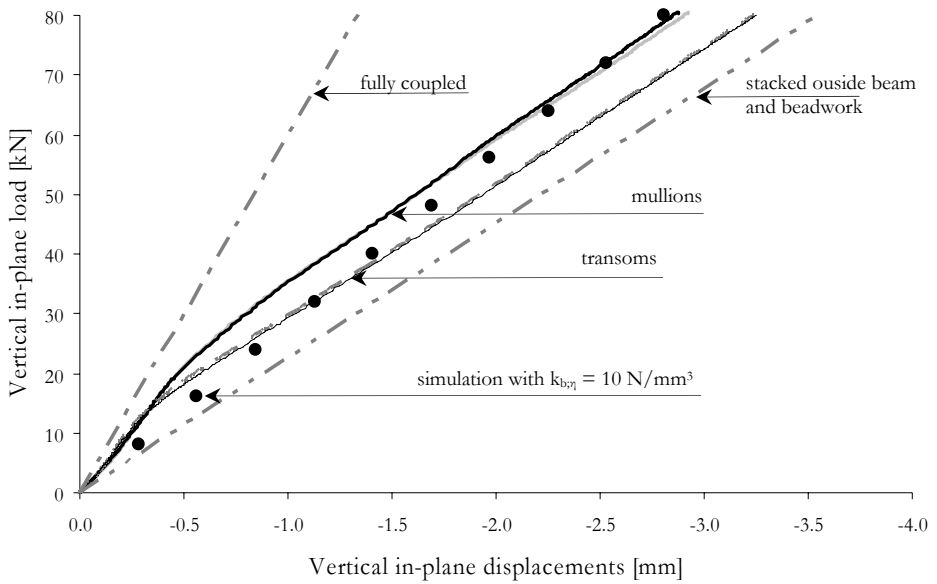
Figure B.4: Relation between the vertical in-plane load and the vertical displacement at points 2 and 4
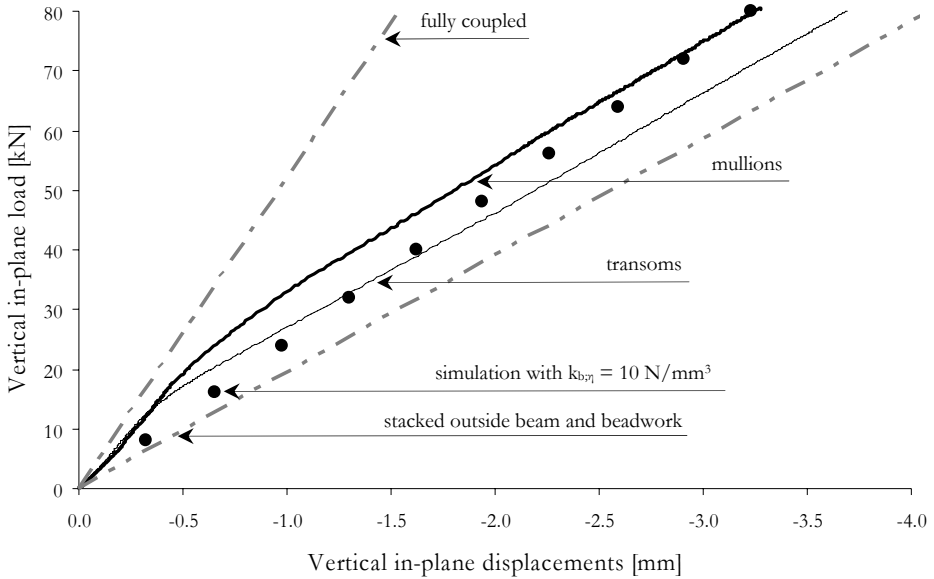
Figure B.5:   Relation between the vertical in-plane load and the vertical displacement at point 3

Figures B.4 shows the relation between the vertical in-plane load and the vertical in-plane displacements at points 2 and 4 of the transoms and the mullions. Figure B.5 shows the relation between the vertical in-plane load and the vertical in-plane displacements at point 3 of the transoms and the mullions. The measured vertical in-plane displacements lay between the fully coupled connection (dash-dot line) and the stacked outside beam and beadwork (dash-double dot-line). The relation showed two stages. The first stage tends to follow the fully coupled connection, but the slope is less steep. This was caused by the contact friction between the steel outside beam and steel beadwork which dominated and enlarged the flexural stiffness. The second stage was parallel to the stacked outside beam and beadwork. This indicated that the contact fiction between the steel outside beam and the beadwork still existed, which slightly enlarged the flexural stiffness of the transoms and the mullions.

Figure B.6 shows the relation between the vertical in-plane load and the relative horizontal in-plane displacements between the outside beam and the beadwork of the transoms (continuous line) and the mullions (dashed line) at points 6 to 9. At the beginning the relative horizontal in-plane displacements of all points of the transoms and the mullions were close to zero followed by an increase of the relative horizontal in-plane displacement in which the beadwork more displaced horizontally in-plane than the outside beam. The bead work had a horizontal displacement to the negative x-axis at the side of the pinned connection and to the positive x-axis at the side of the horizontal roller.

At the beginning of the relation the contact friction between the outside beam and the beadwork predominated and then the contact friction was overcome resulting in sliding of the

beadwork over the outside beam. The irregularly relative horizontal in-plane displacement at the side of the horizontal roller was the result of overcoming the contact friction between the rollers and the steel plates.
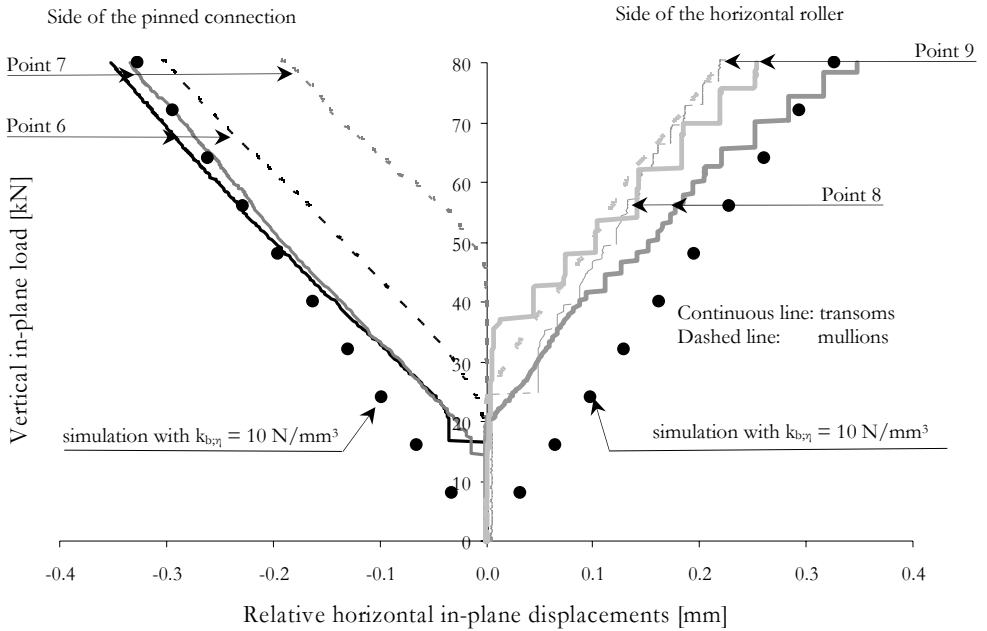
Figure B.6:   Relation between the vertical in-plane load and the relative horizontal in-plane displacements between the outside beam and the beadwork at points 6 to 9

Figures B.4 to B.6 also shows the results of the simulated four point bending test of the modeled transoms and mullions (bolt dots) in the finite element programme DIANA and had the same geometry as described in chapter 4 (figures 4.1 and 4.2). Figure B.7 shows the results the finite element model for the horizontal in-plane displacements only. The value for the shear flexibility for the bolted connection between the outside beam and the beadwork which simulated the contact friction and the clearance of the holes was a linear shear stiffness $k_{b;\eta} = 10 \text{ N/mm}^3$.

It can be concluded that the bolted connection between the outside beam and the beadwork showed shear flexibility. The shear flexibility consisted of clearance of the holes and the contact friction between the steel outside beam and the steel beadwork resulting in a reduction of the flexural bending stiffness of the transoms and mullions.
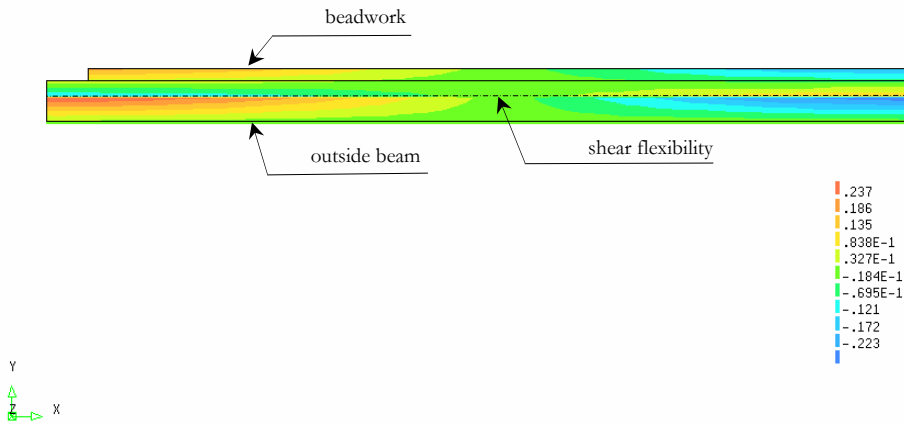
Figure B.7: *Simulation of the shear flexibility of the bolted connection between the outside beam and the beadwork (horizontal in-plane displacements)*

C Determination of mechanical properties of the adhesives

Two types of adhesive were applied for the adhesive bonded joint between the steel frame and the glass pane (see section 3.3.3). Sikaflex-252 [Sikaflex 2004] is a polyurethane adhesive and was used for joint type 1. 3M Scotch Weld 9323 B/A [3M 1995] is an epoxy adhesive and was used for joint type 2 and 3. The mechanical properties of the adhesives are well-documented, but the relations between the normal stress and the strain and the shear stress and the strain are absented. These relations are needed for the simulation of the experiments (chapter 3) in the finite element programme DIANA (chapter 4). DIANA offers a non linear material input for interface element which represents the adhesive bonded joint. Therefore, tests were carried out to find these relations. The first series were to find the relation between the average shear stress and the average shear strain and the second series were to find the relation between the average normal compression/tension stress and the average strain.

C.1 Shear stress – shear strain/relative in-plane displacement relations

C.1.1 Test set-up

The determination of the relation between the average shear stress and the average shear strain were carried out in conformity with the German code DIN 54 451 [DIN 54 451 1979] and completed with ETAG 002 [ETAG 2003]. The preparations, the storing, the testing of the specimens and the results were documented in a report of Eindhoven University of Technology [Koggel et al. 2006]. This section is a brief summary of the report.

Figure C.1 shows the geometry of the test specimens and table C.1 gives additional specifications for the batch with the polyurethane adhesive (batch 03 [Koggel et al. 2006]) and the batch with the epoxy adhesive (batch 10 [Koggel et al. 2006]). The specimens consisted of two aluminum blocks (part 1 and part 2) provided with a lip for a single overlap. The geometry of the test specimens for polyurethane deviated from the code, namely the overlap length was enlarged from 5 mm to 18 mm, because of the expected large shear deformation. The joint thickness of polyurethane specimens was smaller than in the experiments (table 3.1), because a large joint thickness leads to eccentricities. The bonding area of the lips were pre-treated to increase the adhesion in conformity with DIN 53 281 [DIN 53 281 1979]. The pre-treatments of the bonding area were degreasing in an immersion bath of acetone, rinsing with clean acetone, staining in a chemical immersion bath with chromium sulphuric acid at 65°C for 30 minutes, rinsing with distillate water and drying in a dust free kiln at 65°C. After the pre-treatments part 2 was fixed on a template and the adhesive was applied followed by placing part 1 on the adhesive after which the adhesive bonded joint was finished off. These activities were carried out at room temperature. The fixed test specimens on the template were stored in a climate room. The test specimens were cardanic connected at the top and at the bottom in

the tension bench. The tension bench measured the load and two displacement gauges (LVDT) were placed at both sides of the specimens to measure the relative displacements of the adhesive bonded joint. The tests were carried out in a climate chamber. The code DIN 54 451 prescribed a load control of 5000 N/min, but was replaced by a displacement control, to measure the softening of the adhesive bonded joint.

Figure C.1:   Test specimens

The average shear stress (equation C.1) is the quotient of the measured load divided by the initial length and width of the adhesive bonded joint. The average shear strain (equation C.2) is the arctangent of the quotient of the average relative displacement of two displacement gauges divided by the initial thickness of the adhesive bonded joint (figure C.2).

$$\tau_{ave} = \frac{F_t}{l_j \cdot w_j} \qquad\qquad \text{(Equation C.1)}$$

$$\gamma_{ave} = \arctan\left(\frac{u_{j;rel;ave}}{t_j}\right) \qquad\qquad \text{(Equation C.2)}$$

In which:
F_t is the load in N
$u_{j;rel;ave}$ is the average relative displacement of the adhesive bonded joint in the line of action
            in mm

Table C.1:   Geometry of the adhesive bonded joint, storing and test conditions of the specimens

Adhesive			Polyurethane	Epoxy
Geometry joint	Thickness (t_j)	[mm]	1	0.5
	Width (w_j)	[mm]	18	5
	Length (l_j)	[mm]	25	25
Storing conditions	Temperature	[°C]	23	23
	Relative humidity	[%]	60	60
	Curing time	[Days]	23	7
Test conditions	Temperature	[°C]	23	23
	Relative humidity	[%]	60	60
	Velocity of displacement control	[mm/min]	2.5	2.5
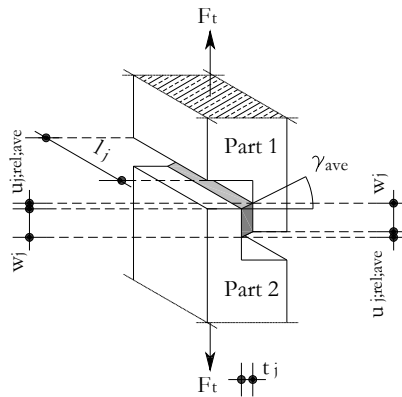
Figure C.2:   Test specimen with deformed adhesive bonded joint

C.1.2   Polyurethane adhesive

Figure C.3 shows the relation between the average shear stress and the average shear strain of the polyurethane adhesive under the test conditions given in table C.1. The relation shows that the increment of the average shear stress increases with increasing average shear strain. The graph was truncated at the moment of the first fracture of the specimen, because the parts of the test specimen started rotating in plane by locally tearing off of the adhesive bonded joint.

This non-linear relation between the average shear stress and the average shear strain is typical for a sealant-like adhesive in the rubber state [Habenicht 2006]. The testing temperature was 23°C (±2°C) and was higher than the glass transition temperature of this adhesive (T_g = -40°C). The glass transition temperature is defined as a transitional stage in which a rubber-like

polymer becomes a glassy-like polymer (stiff and brittle) by decrease of temperature. In a rubber state, the chains of the polymer were entangled and were able to move (restructuring the chains of the polymer) resulting in large average shear strain increment at the initial stage. After the restructuring of the chains of the polymer, they were positioned in the line of action resulting in smaller average shear strain increment with larger average shear stresses. The local tearing off of the adhesive bonded joint was the result of adhesion problems.

Figure C.4 shows the relation between the average shear stress and the average relative in-plane displacement of the polyurethane adhesive with a joint thickness of 5 mm. The relation between the average shear stress and the average shear strain (figure C.3) and equation C.2 are used for the conversion from a joint thickness of 1 mm to 5 mm. The relation between the negative average shear stress and the negative average relative in-plane displacement is assumed to be the same as the relation between the positive average shear stress and the positive average relative in-plane displacement. In the experiments (section 3.7.1) the adhesive bonded joint in the compression zone was gradually pushed away till the glass-steel contact at a relative in-plane displacement of 5 mm. The adhesive bonded joint in the tension zone was gradually torn off at a relative in-plane displacement of 5 mm. The adhesive bonded joint can not transfer shear load anymore and this was simulated in the non linear material input with a small average shear stress and large average relative in-plane displacement (very small shear stiffness). The numerical values for the material input in DIANA are given in the table of figure C.4.

Figure C.3: *Relation between average shear stress and average shear strain of the polyurethane adhesive under the test conditions given in table C.1*

TAUDIS ($\tau_{j;\eta;ave}$ $u_{j;\eta\ ;rel;ave}$)	-0.1 -10^9; -0.44 -5.00; -0.16 -1.55; -0.01 -0.25; 0.00 0.00; 0.01 0.25; 0.16 1.55; 0.44 5.00; 0.1 10^9

Figure C.4:   Relation between average shear stress and average relative in-plane displacement of polyurethane adhesive with joint thickness of 5 mm and numerical values for the material input in DIANA

C.1.3   Epoxy adhesive

Figure C.5 shows the relation between the average shear stress and the average shear strain of epoxy adhesive under the test conditions given in table C.1. The relation is bi-linear. The first stage is linear with small average shear strain increment and large average shear stresses till an average shear strain of 0.10 and an average shear stress of 24.40 N/mm². The second stage shows a gradually decline of the average shear stress at increasing average shear strains. The graph was truncated at the moment of the first fracture of the specimen, because the parts of the test specimen started rotating in plane by locally tearing off of the adhesive bonded joint.

The relation between the average shear stress and the average shear strain of epoxy shows a stiff linear behaviour in the first stage followed by a plastic like behaviour (toughened) in the second stage. The epoxy behaves like a solid material, because the testing temperature was lower than the glass transition temperature ($T_g = 50°C$).
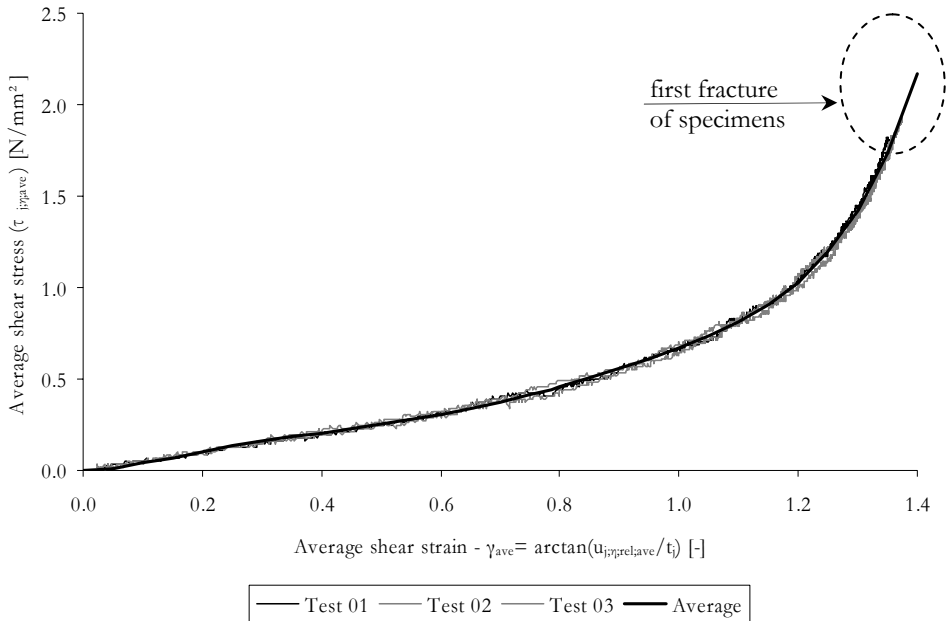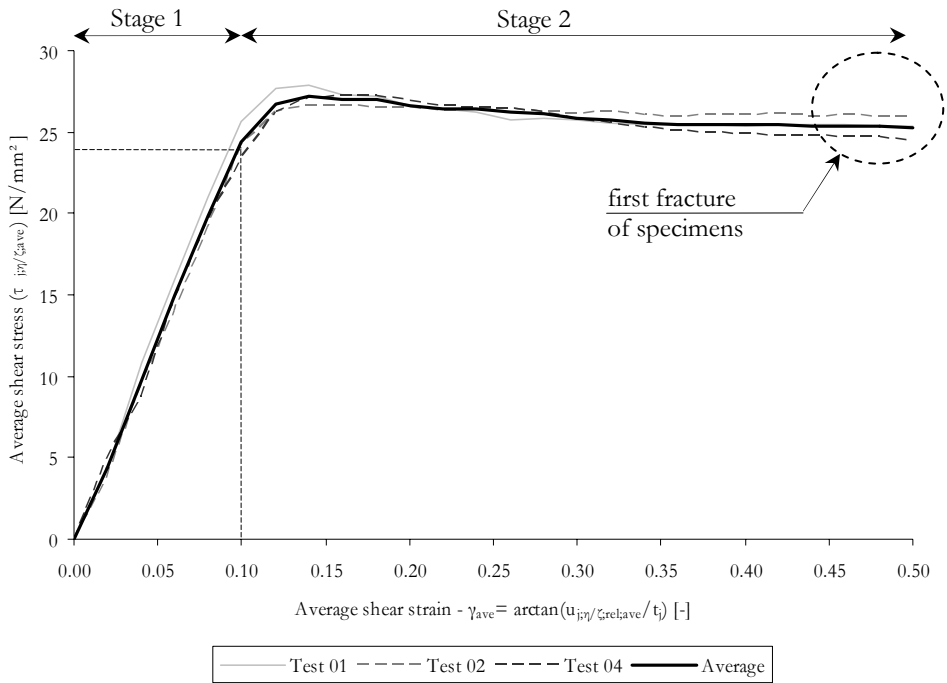
Figure C.5: *Relation between average shear stress and average shear strain of the epoxy adhesive under the test conditions given in table C.1*

Figure C.6 shows the relation between the average shear stress and the average relative in-plane displacement for a joint thickness of 0.5 mm converted from the relation between the average shear stress and average shear strain of figure C.5 with equation C.2. The relation between the negative average shear stress and the negative average relative in-plane displacement is assumed to be the same as the relation between the positive average shear stress and the positive average relative in-plane displacement. The relation was extrapolated, because at large horizontal in-plane displacement at the RTC of the system the average relative in-plane displacements exceeded the maximum measured average relative in-plane displacements. For the extrapolation was assumed that the gradually decline of the average shear stress continued till an average relative in-plane displacement of 1.0 mm. This extrapolation can be justified, because the adhesive bonded joint of systems with joint type 2 and 3 were intact in the experiments (sections 3.7.2 and 3.7.3). Moreover, the relation between the horizontal in-plane load and the horizontal in-plane displacement at the RTC of the system of the non-cracked glass pane for systems with joint type 2 (figure 3.13) also gradually declined. The numerical values for the material input in DIANA are given in the table of figure C.6.

The initial shear modulus and the initial Young's modulus of the epoxy adhesive were calculated with equations C.3 and C.4. These equations can be used, because the adhesive bonded joint behaved like a solid material. The Poisson's ratio is 0.30 [3M 1995]. The initial normal stiffness and the initial shear stiffness of the adhesive bonded joint were calculated with equations C.5 and C.6. The assumption was that the Young's modulus and also the normal

stiffness were constant in systems with joint type 2 and 3, because the adhesive bonded joint was loaded by in-plane shear. These values are tabulated in table C.2.

$$G_{a;ini} = \frac{\tau_{ave;ini}}{\gamma_{ave;ini}} \qquad \text{(Equation C.3)}$$

$$E_{a;ini} = 2G_{a;ini}(1 + \nu_a) \qquad \text{(Equation C.4)}$$

$$k_{j;\xi;ini} = \frac{E_{a;ini}}{t_j} \qquad \text{(Equation C.5)}$$

$$k_{j;\eta/\zeta} = \frac{G_{a;ini}}{t_j} \qquad \text{(Equation C.6)}$$
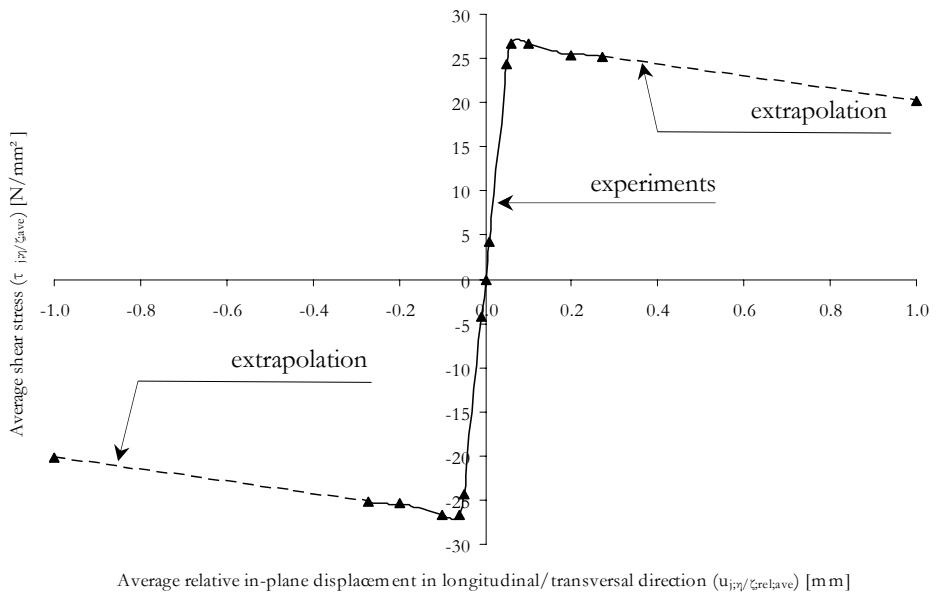
TAUDIS ($\tau_{j;\eta/\zeta;ave}$ $u_{j;\eta/\zeta;rel;ave}$)   -20.22 1.00; -25.39 -0.20; -26.65 -0.10; -26.71 -0.06; -24.40 -0.05; -4.32 -0.01; 0.00 0.00; 4.32 0.01; 24.40 0.05; 26.71 0.06; 26.65 0.10; 25.39 0.20; 20.22 1.00

Figure C.6:   Relation between average shear stress and average relative in-plane displacement of epoxy adhesive with joint thickness of 0.5 mm and numerical values for the material input in DIANA

Table C.2:   Overview of the linear behaviour of the adhesive bonded joint of epoxy

γ_{ave} [--]	τ_{ave} [N/mm²]	$G_{a;ini}$ [N/mm²]	t_j [mm]	$k_{j;\eta/\zeta}$ [N/mm³]	$E_{a;ini}$ [N/mm²]	$k_{j;\xi}$ [N/mm³]
0.10	24.40	246	0.5	492	640	1280

C.2 Normal stress - relative in-plane displacement relations of polyurethane adhesive

The polyurethane adhesive bonded joint was tested for the determination of the relation between the average normal stress and the average relative in-plane displacement by means of compression tension tests. The adhesive bonded joint of polyurethane adhesive under compression and under tension showed a different behaviour, because the adhesive bonded joint was in a rubber state at room temperature (section C.1.2). Furthermore, the adhesive bonded joint was four-sided enclosed which had influence on the relation between the average compression stress and the average relative in-plane displacement.

C.2.1   Test set-up

Test specimens are not prescribed by a code. The adhesive bonded joint of the test specimen represented a small piece of the adhesive bonded joint used in the systems with joint type 1. The relation between the average normal stress and the average in-plane displacement was needed to simulate the behaviour of the adhesive bonded joint subjected by a compression load or tension load between the rigid glass pane and the steel frame.

Figure C.7 shows the geometry of the test specimens and table C.3 gives additional specifications of batch T (tension tests) and batch C (compression tests). The test specimens consisted of two aluminium blocks (part 1 and part 2). Part 1 of the aluminium block had a groove with an internal width of 13 mm and an internal length of 110 mm. Part 2 of the aluminium block had an upright partition with a width of 12 mm and a length of 100 mm. The internal width of part 1 of the aluminum block was larger to provide air around the adhesive bonded joint, because the polyurethane adhesive is a moisture curing adhesive. The space filled up with Teflon with a thickness of 0.5 mm. The pre-treatments of the bonding area to increase the adhesion were similar to the pre-treatments of the bonding area for the shear tests (section C.1.1). After the pre-treatments part 2 of the aluminium block was fixed on a template and the adhesive was applied on the upright partition at once. Part 1 of the aluminium block with the Teflon strips was placed on the adhesive. The surplus of the adhesive was pushed away at the ends. Then the adhesive bonded joint was finished off by pulling out the Teflon strips carefully. These activities were carried out at room temperature. The fixed test specimens on the template were stored in a climate room.

Front view	**Cross section**

⊕ position of the
displacement gauges (LVDT)

Figure C.7:   Test specimens

The space between the adhesive bonded joint and the internal groove of part 1 of the aluminium block was filled up with a Teflon strip of 0.5 mm before testing (figure C.8). So, the freely out-of-plane displacement of the adhesive bonded joint (bulging) was prevented. The test specimens were clamped in the tension bench. The clamped connection was needed for a centric load introduction, but especially for stable compression tests (pushing away laterally at large compression load). The load was displacement controlled and was measured by the tension bench. Four displacement gauges (LVDTs) were placed at each corner (figure C.7) to measure the relative in-plane displacement between part 1 and part 2.

Table C.3:   *Geometry of the polyurethane joint, storing and test conditions of the specimens*

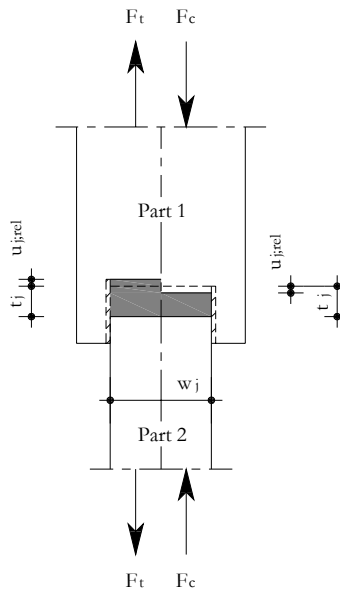| Batch number			T	C
Type of test			Tension	Compression
Number			4	4
Geometry joint	Thickness (t_j)	[mm]	5	5
	Width (w_j)	[mm]	12	12
	Length (l_j)	[mm]	100	100
Storing conditions	Temperature	[°C]	23	23
	Relative humidity	[%]	60	60
	Time	[Days]	23	23
Test conditions	Temperature	[°C]	23	23
	Relative humidity	[%]	60	60
	Velocity of displacement control	[mm/min]	2.5	2.5

Figure C.8:   *Schematic representation of the test specimen*

The measured relative in-plane displacements were calculated to an average relative in-plane displacement with equation C.7. The average tension and compression stress were calculated with equations C.8.1 and C.8.2. These stresses were the quotient of the measured tension or compression load divided by the measured initial joint length and joint width.

$$u_{j;rel;ave} = \tfrac{1}{4} \left(u_{j;1;rel} + u_{j;2;rel} + u_{j;3;rel} + u_{j;4;rel} \right) \qquad \text{(Equation C.7)}$$

$$\sigma_{t;ave} = \frac{F_t}{l_j \cdot w_j} \qquad \text{(Equation C.8.1)}$$

$$\sigma_{c;ave} = \frac{F_c}{l_j \cdot w_j} \qquad \text{(Equation C.8.2)}$$

In which:

$u_{j;rel;ave}$ is the average relative in-plane displacement of the adhesive bonded joint in the line of action in mm

$u_{j1/4;rel}$ are the measured relative in-plane displacements of the adhesive bonded joint at point 1 to 4 in mm

F_t, F_c is the measured tension load or compression load in N

$\sigma_{t;ave}$ is the average tension stress in N/mm²

$\sigma_{c;ave}$ is the average compression stress in N/mm²

C.2.2 Relation between tension stress and relative in-plane displacement

Figure C.9 shows the relation between the average tension stress and the average relative in-plane displacement under the test conditions given in table C.3. The relation has two stages. The first stage has a larger increment of the average tension stress than the second stage. The second stage has larger increment of the average relative in-plane displacement than the first stage. The graph was truncated at the moment of the first fracture of the specimen, because the adhesive bonded joint started tearing off from the aluminium blocks.

The non-linear relation between the average tension stress and the average relative in-plane displacement is typical for a sealant-like adhesive in the rubber state, because the testing temperature was 23°C (±2°C) and it was above the glass transition temperature (section C.1.2). The first stage is an initially linear relation at small average tension stress. The second stage is the restructuring of the chains of the polymer from entangled state to an arrangement of the chains of the polymer in the line of action (section C.1.2). The local tearing off of the adhesive bonded joint was the result of adhesion problems.
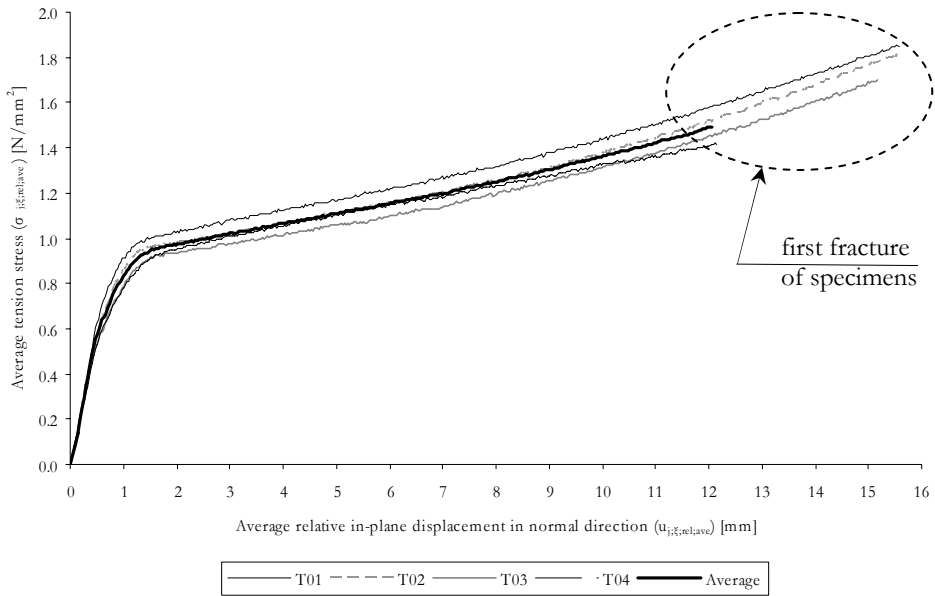
Figure C.9: *Relation between average tension stress and average relative in-plane displacement of polyurethane adhesive under the test conditions given in table C.3*

C.2.3 Relation between compression stress and relative in-plane displacement

Figure C.10 shows the relation between the average compression stress and the average relative in-plane displacement under the test conditions given in table C.3. The relation shows an increase of the average compression stresses at increasing relative in-plane displacements. At larger compression stresses the tests showed much more dispersal than before. The graph was truncated at the moment of rapid increase of the compression load. The adhesive bonded joint was not pressed out only at the end of the adhesive bonded joint. Furthermore, aluminium-aluminium contact was not reached.

The non-linear relation between the average compression stress and the average relative in-plane displacement is also typical for a sealant-like adhesive in the rubber state (section C.1.2). The adhesive bonded joint was easy pushed in resulting in an increase of the average compression stress. The pushed in adhesive bonded joint became stiffer, because the four-sided enclosed adhesive bonded joint can not displace laterally resulting a larger increase of the compression stress. At larger relative in-plane displacements, the adhesive bonded joint was pushed in and not pushed out resulting in a rapidly increase of the compression load. Therefore, no aluminium-aluminium contact was reached.
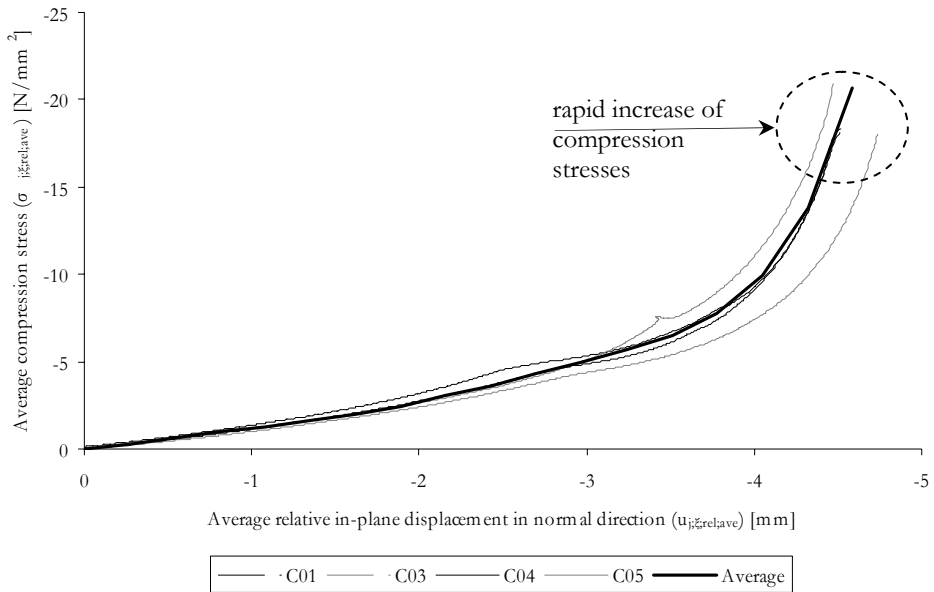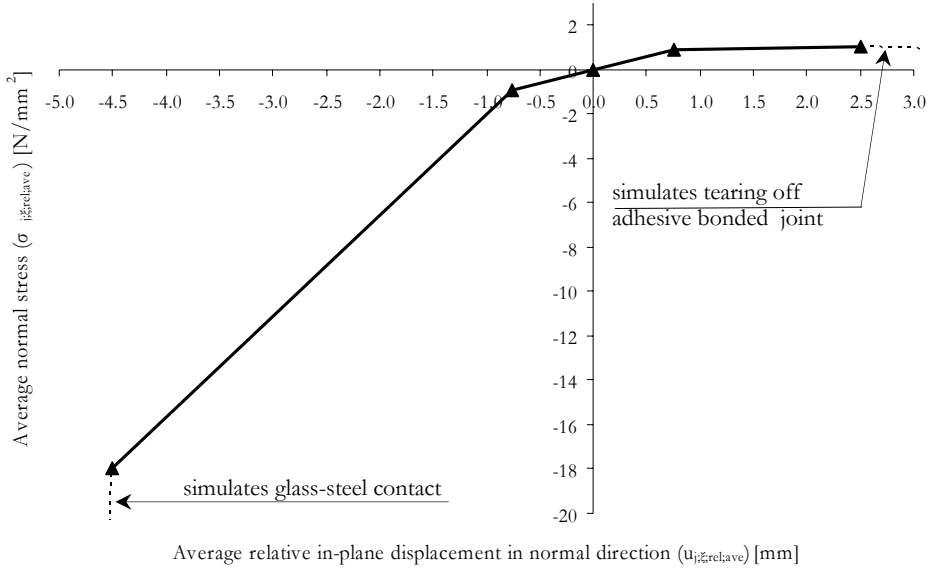
Figure C.10: Relation between average compression stress and average relative in-plane displacement of polyurethane adhesive under the test conditions given in table C.3

C.2.4 Relation between normal stress and relative in-plane displacement

Figure C.11 shows the relation between the average normal stress and the average relative in-plane displacement for a joint thickness of 5 mm which is used in the material input for systems with joint type 1 in DIANA. The adhesive bonded joint under compression is given at the left side of the graph and under tension is given at the right side of the graph. The relation starts at the left side of the graph with a very high compression stress at a relative in-plane displacement of -20 mm. Glass-steel contact was assumed to occur at a relative in-plane displacement of -5 mm with a compression stress of 18 N/mm² (figure C.10). Between a relative in-plane displacement of -5 mm and -20 mm the stiffness in normal direction is very large and simulates glass-steel contact. Between a relative in-plane displacement of -0.76 mm and -5 mm the relation was simplified, namely linear in stead of a gradual curve. This simplification can be justified, because at small relative in-plane displacements the simplification matches with the experimentally found relation (simulating the local behaviour of the system) and at glass-steel contact the relative in-plane displacement of 5 mm and the horizontal in-plane load are the point of interest (simulating the global behaviour of the system). The initial stiffness in normal direction of the adhesive bonded joint lay between a relative in-plane displacement of -0.76 mm and 0.76 mm. Then the tension stresses slightly increase till a relative in-plane displacement of 2.5 mm followed by a very small normal stiffness which simulates tearing off/adhesion problems of the adhesive bonded joint under

tension. The relative in-plane displacement of 2.5 mm of the adhesive bonded joint is based on the observation of the experiments (section 3.7.1). The numerical values for the material input in DIANA are given in the table of figure C.11.

Average relative in-plane displacement in normal direction ($u_{j;\xi;rel;ave}$) [mm]

SIGDIS ($\sigma_{j;\xi;rel;ave}$ $u_{j;\xi;rel;ave}$) -10^9 -20; -18 -5; -0.9 -0.76; 0 0; 0.9 0.76; 1.06 2.50; 0.1 10^9

Figure C.11: Relation between average normal stress and average relative in-plane displacement of polyurethane adhesive with joint thickness of 5.0 mm and numerical values for the material input in DIANA

D Modelling steel frame

Figure D.1 gives the geometry of the real and modelled cross section of the outside beam and the beadwork. The cross sectional data of the real cross section, the modelled outside beam and of the modelled beadwork are given in table D.1 to D.3 respectively. The values between the brackets in tables D.2 and D.3 are the deviation with regard to the real cross sectional data.
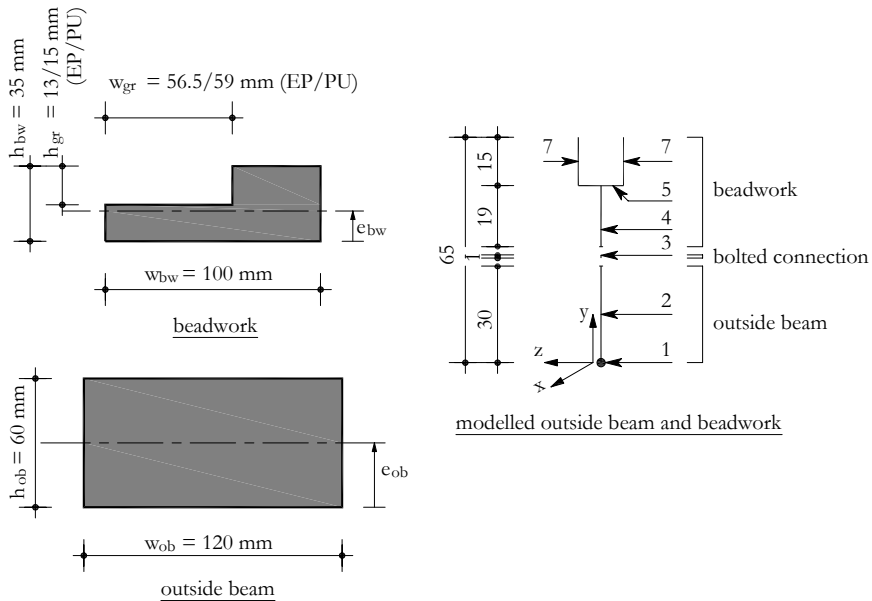
Figure D.1:   Real (left) and modelled (right) cross section of the outside beam and the beadwork

Table D.1:   Cross sectional data of the real outside beam and beadwork

Part	e_{ob} [mm]	A_{ob} [mm^2]	I_{ob} [mm^4]
Outside beam	30.00	7200	2160000
Beadwork for polyurethane joint (PU)	14.11	2615	192314
Beadwork for polyurethane joint (EP)	14.58	2766	210584

Table D.2:   *Cross sectional data of the modelled outside beam*

Number	Width [mm]	Height [mm]	e_{ob} [mm]	A_{ob} [mm^2]	I_{ob} [mm^4]
1	118	60	30.19	7170	2150746
2	3	30	(+0.63%)	(-0.42%)	(-0.46%)

Table D.3:   *Cross sectional data of the modelled beadwork*

Number	Width [mm]	Height [mm]	e_{bw} [mm]	A_{bw} [mm^2]	I_{bw} [mm^4]
4	98	19	13.89	2627	201972
5	13	15	PU(-1.53%)	PU(+0.46%)	PU(+5.02%)
6	19	15	EP(-5.01%)	EP(-4.71%)	EP(-4.09%)

E Critical plate buckling load for each system

Table E.1 shows an overview of the critical plate buckling loads of four-sided simply supported and four-sided clamped supported glass panes (equations 3.5 and 3.6) and the critical plate buckling loads adopted from the finite element models for systems with joint type 2 and 3. The mesh density is given in table 4.2.

Table E.1: Overview of critical plate buckling loads (F$_{b;crit}$) for four-sided simply supported glass panes (theory), four-sided clamped supported glass panes (theory), systems with joint type 2 (FEM) and systems with joint type 3 (FEM) for three nominal glass thicknesses and six glass pane sizes

Nominal glass thickness [mm]	Glass pane size [m]	Four-sided simply supported [kN]	Four-sided clamped supported [kN]	FEM System with joint type 2 [kN]	FEM System with joint type 3 [kN]
4	1.0 x 1.0	31.5	49.1	47.0	46.5
	1.5 x 1.5	20.9	32.6	33.4	33.0
	1.0 x 1.5	23.9	38.6	39.0	38.3
	1.0 x 3.0	19.5	32.3	27.6	35.3
	1.5 x 1.0	36.0	58.1	56.2	55.5
	3.0 x 1.0	58.8	97.6	99.5	99.1
8	1.0 x 1.0	261.8	408.7	374.0	363.0
	1.5 x 1.5	174.0	271.6	267.0	263.0
	1.0 x 1.5	199.2	321.0	308.0	299.0
	1.0 x 3.0	162.0	268.9	278.0	273.0
	1.5 x 1.0	299.8	483.2	447.0	434.0
	3.0 x 1.0	489.2	812.3	780.0	767.0
12	1.0 x 1.0	918.5	1433.8	1260.0	1190
	1.5 x 1.5	610.3	952.7	991.0	873.0
	1.0 x 1.5	698.8	1126.2	1040.0	973.0
	1.0 x 3.0	568.3	943.5	933.0	887.0
	1.5 x 1.0	1051.8	1695.1	1510.0	1410.0
	3.0 x 1.0	1716.3	2849.5	2620.0	2490.0

Table E.2 shows an overview of the critical plate buckling loads for four-sided simply supported glass panes adopted from finite element models for systems with joint type 1. However, other finite element models are used for the determination of the critical plate buckling loads. The critical plate buckling load is a linear calculation (eigenvalue). In this linear calculation the system behaves stiffer, because the Teflon strips for lateral support of the glass pane (figure 3.3) transfers compression and tension load and the adhesive bonded joint is intact at glass-steel contact. The finite element model for the determination of the critical plate buckling load is a four-sided simply supported glass pane with a compression load at the RTC of the glass pane (figure E.1). This is a safe approach, because the finite element model yields smaller critical plate buckling loads.

Table E.2: *Overview of critical plate buckling loads ($F_{h;crit}$) [kN] for systems with joint type 1 (FEM) for three nominal glass thicknesses and six glass pane sizes*

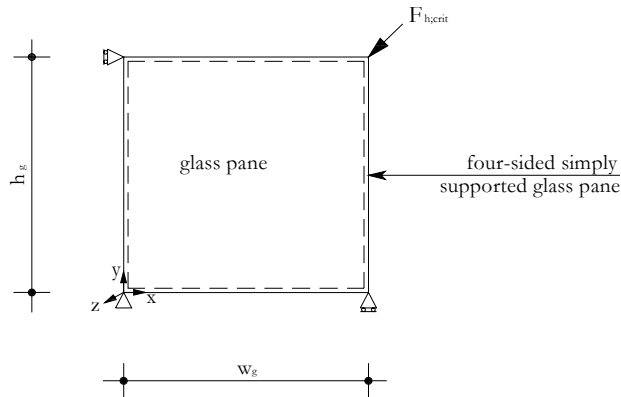| Glass pane size [m]	$t_{g;n}$ = 4 mm	$t_{g;n}$ = 8 mm	$t_{g;n}$ = 12 mm
1.0 x 1.0	14.4	120.1	420.0
1.5 x 1.5	9.7	80.3	281.4
1.0 x 1.5	13.8	114.1	398.4
1.0 x 3.0	13.1	108.5	379.5
1.5 x 1.0	13.7	114.1	398.4
3.0 x 1.0	13.1	108.5	379.5

Figure E.1: *Finite element model for the determination of the critical plate buckling load*

F Supplementary data for the mechanical models

F.1 Equivalent continuous normal stiffness of the adhesive bonded joint

Equation 6.23 needs an equivalent continuous normal stiffness of the adhesive bonded joint to avoid non linear calculations using equation 6.11. Figure F.1 shows the linear distribution of the relative vertical in-plane displacements in normal direction of the bottom and top adhesive bonded joint and the accompanying non-linear distribution of the normal stresses for a non-failed adhesive bonded joint (left side) and a partly torn off adhesive bonded joint (right side). This also concerns for the equivalent continuous normal stiffness of the left and right adhesive bonded joint. The distributions given in figure F.1 are applicable for the chosen polyurethane adhesive (section 3.3.3 and figure 4.9 right bottom).
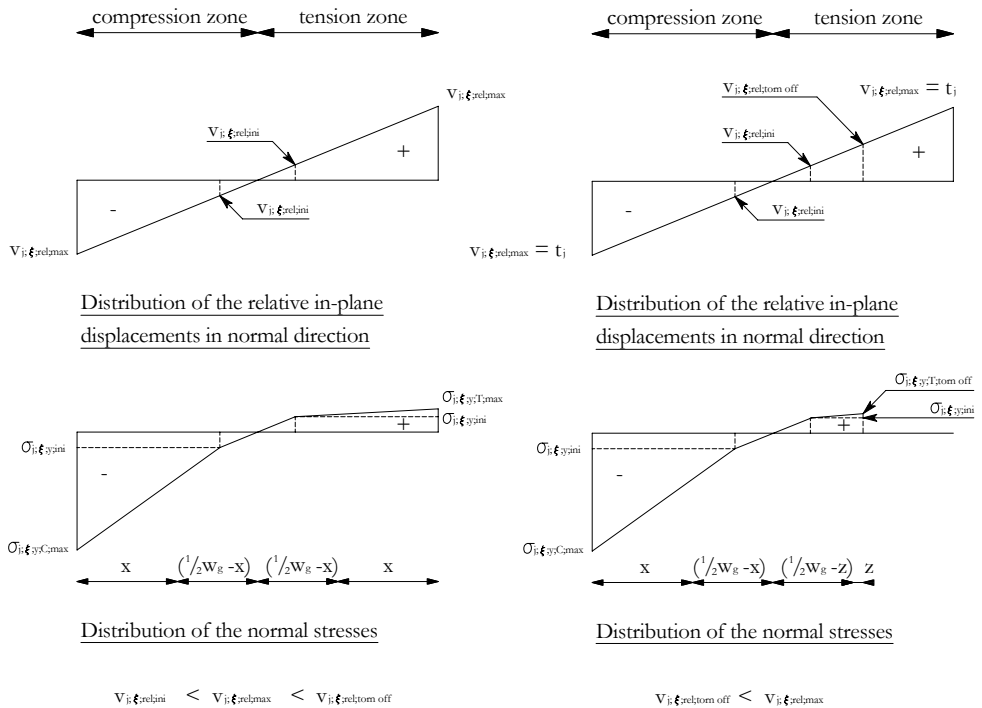

Figure F.1: *Distributions of the relative vertical in-plane displacements in normal direction and the non linear normal stresses of the non-failed adhesive bonded joint (left side) and the distributions of the relative vertical in-plane displacements in normal direction and the non linear normal stresses of a partly torn off adhesive bonded joint (right side)*

211

If the maximum relative vertical in-plane displacement in normal direction is larger than the initial relative vertical in-plane displacement in normal direction and smaller than the relative vertical in-plane displacement in normal direction at which the adhesive bonded joint starts tearing off, equations F.1 to F.6 have to be used.

$$\kappa = \frac{\sigma_{j;\xi;y;ini}}{\sigma_{j;\xi;y;C;max}}$$
(Equation F.1)

$$\lambda = \frac{\sigma_{j;\xi;y;T;max}}{\sigma_{j;\xi;y;C;max}}$$
(Equation F.2)

$$\rho = \frac{v_{j;\xi;rel;ini}}{v_{j;\xi;rel;max}}$$
(Equation F.3)

In which:

κ is the ratio between the initial normal stress and the maximum compression stress.
λ is the ratio between the maximum tension and compression stress.
ρ is the ratio between the initial relative vertical in-plane displacement in normal direction and the maximum relative vertical in-plane displacement in normal direction.

Equations F.4 and F.5 gives the distance x and $(\frac{1}{2}w_g\text{-}x)$ respectively expressed in the ratio ρ given in equation F.3.

$$x = \frac{(v_{j;\xi;rel;max} - v_{j;\xi;rel;ini})w_g}{2v_{j;\xi;rel;max}} = \tfrac{1}{2}(1-\rho)w_g$$
(Equation F.4)

$$(\tfrac{1}{2}w_g - x) = \frac{v_{j;\xi;rel;ini}w_g}{2v_{j;\xi;rel;max}} = \tfrac{1}{2}\rho w_g$$
(Equation F.5)

The sum of the moments around the centre of the adhesive bonded joint of the non-linear distribution of the normal stresses (equation F.6 left expression) is equated with the moment belonging to a linear distribution of the normal stresses (equation F.6 right expression) from which the equivalent continuous normal stiffness is isolated (equitation F.6). The equivalent continuous normal stiffnesses of the non-failed adhesive bonded joint are given in table F.1 at the left side.

$$\frac{\sigma_{j;\xi;C;max}w_g^2[2\kappa(1+\rho)+(1+\lambda)(1-\rho-\rho^2)]}{24} = \tfrac{1}{6}k_{j;\xi;eq}v_{j;\xi;rel;max}w_g^2$$

$$k_{j;\xi;eq} = \frac{\sigma_{j;\xi;C;\max}}{4v_{j;\xi;rel;\max}}[2\kappa(1+\rho)+(\lambda+1)(2-\rho-\rho^2)]$$ (Equation F.6)

If the maximum relative vertical in-plane displacement in normal direction is larger than the relative vertical in-plane displacement in normal direction at which the adhesive bonded joint starts tearing off, equations F.1 to F.3, F.7 and F.8 have to be used. Equation F.7 gives the distance z expressed in the ratio ρ given in equation F.3. The equivalent continuous normal stiffness of the adhesive bonded joint is determined in the same way as described above and is given in equation F.8. The equivalent continuous normal stiffnesses belonging to a partly torn off adhesive bonded joint are given in table F.1 at the right side.

$$z = \frac{(v_{j;\xi;rel;\max} - 2v_{j;\xi;rel;ini})w_g}{4v_{j;\xi;rel;\max}} = \tfrac{1}{4}(1-2\rho)w_g$$ (Equation F.7)

$$k_{j;\xi;eq} = \frac{\sigma_{j;\xi;\max;C}}{4v_{j;\xi;rel;\max}}[\tfrac{1}{4}\kappa(5+6\rho)+\tfrac{1}{2}\lambda(1-\rho-2\rho^2)+(2-\rho-\rho^2)]$$

(Equation F.8)

Table F.1:   *Overview of the equivalent continuous normal stiffness of a non-failed adhesive bonded joint (left side) and a partly torn off adhesive bonded joint (right side) based on joint thickness of 5 mm (figure 4.9 right bottom)*

$v_{j;\xi;rel;\max}$ [mm]	$\sigma_{\xi;\max;C}$ [N/mm²]	$\sigma_{\xi;\max;T}$ [N/mm²]	$k_{j;\xi;eq}$ [N/mm³]	$v_{j;\xi;rel;\max}$ [mm]	$\sigma_{\xi;\max;C}$ [N/mm²]	$\sigma_{\xi;\max;T}$ [N/mm²]	$k_{j;\xi;eq}$ [N/mm³]
0.76	0.90	0.90	1.18	2.60	8.32	1.06	1.48
0.80	1.06	0.90	1.19	2.80	9.13	1.06	1.51
1.00	1.87	0.92	1.25	3.00	9.93	1.06	1.55
1.20	2.67	0.94	1.34	3.20	10.74	1.06	1.58
1.40	3.48	0.96	1.42	3.40	11.55	1.06	1.60
1.60	4.29	0.98	1.48	3.60	12.35	1.06	1.62
1.80	5.09	1.00	1.54	3.80	13.16	1.06	1.65
2.00	5.90	1.01	1.59	4.00	13.97	1.06	1.66
2.20	6.71	1.03	1.63	4.20	14.77	1.06	1.68
2.40	7.51	1.05	1.66	4.40	15.58	1.06	1.70
2.50	7.92	1.06	1.67	4.60	16.39	1.06	1.71
				4.80	17.19	1.06	1.72
				5.00	18.00	1.06	1.73

F.2 Maximum allowable relative in-plane displacement in normal and longitudinal direction

According to the specification of the supplier of the polyurethane adhesive [Sika 2004] is the maximum allowable relative in-plane displacement in normal direction 20% of the joint thickness (t_j = 5 mm; $u/v_{j;\xi;rel;per}$ = 1 mm) and the maximum allowable relative in-plane displacement in longitudinal direction is 50% of the joint thickness (t_j = 5 mm; $u/v_{j;\eta;rel;per}$ = 2.5 mm).

Curriculum Vitae

Personal data

Name: Edwin Michel Pierre Huveners

Born: April 5th, 1974 in Maastricht, The Netherlands

Address: Keilruwe 32
6218 RG Maastricht, The Netherlands

Education

1986-1990:   Lower General Secondary School (MAVO) Maria Immaculata, Maastricht

1990-1994:   Intermediate Technical School (MTS), department of Architecture and Building Technology, Maastricht

1994-1997:   Technical College (HTS), Hogeschool Limburg, department of Civil Engineering and Environmentology, Heerlen (B.Sc. level)

1998-2002:   Eindhoven University of Technology, department of Architecture, Building and Planning, unit Structural Design and Construction Technology, Eindhoven (M.Sc. level)

Work

1997-1998:   Structural designer, department of Concrete and Steel Structures, engineering office Gemeentewerken Rotterdam, Rotterdam

2002-2007:   Part-time structural designer, engineering office Volantis-TEMA Ingenieurs, Maastricht

2002-2009:   Part-time PhD-researcher, Eindhoven University of Technology, department of Architecture, Building and Planning, unit Structural Design and Construction Technology, Eindhoven

2009-now: Specialist/advisor, unit Building Structures, engineering office Volantis, Maastricht